2011

Cell-Type Specific Translational Profiling in Huntington's Disease Mouse Models

Robert J. Fenster

CELL-TYPE SPECIFIC TRANSLATIONAL PROFILING IN HUNTINGTON'S DISEASE MOUSE MODELS

A Thesis Presented to the Faculty of

The Rockefeller University

in Partial Fulfillment of the Requirements for

the degree of Doctor of Philosophy

by

Robert Jonathan Fenster

June 2011

CELL-TYPE SPECIFIC TRANSLATIONAL PROFILING IN HUNTINGTON'S DISEASE MOUSE MODELS

Robert Jonathan Fenster, Ph.D.

The Rockefeller University 2011

Medium spiny neurons (MSNs) are among the most vulnerable cell populations in Huntington's Disease (HD). Within this population, striatopallidal MSNs are more vulnerable than striatonigral MSNs, which may explain the typical progression in HD of chorea to hypokinesis. The biological basis for this differential vulnerability is unknown, although differences in transcriptional dysfunction caused by mutant *huntingtin* (*mhtt*) have been proposed as a possible mechanism. In order to determine the differences in gene expression caused by *mhtt* in these two populations, we selectively isolated translated mRNAs from striatopallidal and striatonigral MSNs in the R6-2 and YAC128 HD mouse models at pre- and post-symptomatic time points using the BACTRAP technique (Heiman et al, 2008).

We re-characterized the behavioral phenotype of the HD model mice on the D1 and D2 TRAP backgrounds and found many changes in the translated mRNA profiles of these two classes of medium spiny neurons, including known changes in the literature as well as novel pathways. One novel pathway was sphingosine-1-phosphate (S1P) signaling.

Because the S1P-receptor G-protein coupled receptor 6 (GPR6) is enriched in striatopallidal cells, we hypothesized that changes in this pathway might play a role in striatopallidal medium spiny neuron vulnerability. Using mass spectrometry, we have shown that S1P levels, as well as other complex sphingolipid species, are decreased in the striatum of R6-2 mice early in disease progression. We have preliminary evidence to suggest Sphk2 and Sgpl1, the enzymes responsible for the production and degradation of S1P, are altered in HD mouse models in patterns that might explain the changes in S1P levels. We have shown that S1P can have pro-survival effects in an *in vitro* model of striatal origin. Together, these results implicate alterations in S1P signaling in the pathogenesis of Huntington's Disease and offer an approach for moving from clinical observations of a disease toward the beginning of a mechanistic understanding of the underlying causes of specific cell vulnerability in other diseases.

Acknowledgments

What a whirlwind three-and-a-half years it's been! I would first like to thank Dr. Paul Greengard, my adviser, who continually surprises and inspires me with his scientific dedication, wit, generosity, and grace. I am grateful for this opportunity you have given me.

Next, I wish to thank (the newly) Professor Myriam Heiman. I have been honored to learn from you, train with you, work alongside you, and become your friend. I could not have asked for a better mentor. I wish you every possible future success, and I will miss you when I return to medical school.

I thank Ruth Kulicke for help with many of the experiments in this work. Her technical expertise is remarkable—I hope one day you will listen to my goading, and become the path-breaking surgeon you were meant to be.

I would like to thank all of the members of the Greengard Lab and office staff for their support. A few special thanks to Jean-Pierre Roussarie for scientific discussion and for putting up with my messy bench; to Chan Lek Tan for his friendship; to Anne Schaefer and Lars Brichta for their scientific advice and humor; to Yotam Sagi for help with viruses and sage advice and to Marc Flajolet for cloning help and general support.

My committee members: Dr. Cori Bargmann, Dr. Nat Heintz, and Dr. Hugh Hemmings have all provided valuable advice and guidance along the way.

I wish to acknowledge the hard work of Dr. Jeff Moore at Avanti Polar Lipids who did all of the mass spectrometry experiments.

Thanks go to Max Heiman for critical reading of this thesis and for being a hero when computers crashed and all was falling apart.

I wish to thank my parents and sister for their love and support. And, finally, I thank my wife Sarah: I love you more than I can say.

TABLE OF CONTENTS

LIST OF FIGURES

Introduction

Most neurological diseases do not affect the brain diffusely, killing all cell types indiscriminately, but rather attack certain classes of neurons with precision. For example, Parkinson's Disease affects dopamine-producing cells of the substantia nigra *pars compacta,* but not nearby dopamine-producing cells of the ventral tegmental area. Amyotrophic Lateral Sclerosis kills upper and lower motor neurons, but not afferent sensory neurons. The pathology of Alzheimer's Disease, although eventually widespread, begins with a stereotyped progression of amyloid plaques in layer II of the entorhinal cortex, but the disease never affects neurons in the visual cortex. It is this selectivity that creates each disease's unique presentation: the pathognomonic akinesia of Parkinson's Disease is caused by the damage to the substantia nigra; the slow onset paralysis that is the hallmark of ALS results from the gradual destruction of motor neurons.

In all of these diseases, selective vulnerability is poorly understood. Investigation of this question has been hindered by technological limitations. The cellular heterogeneity of brain tissue, which underlies the richness of the brain's many functions, makes it difficult to detect changes in a single cell type among networks of vast complexity. But the potential rewards of answering this question are great: if we can understand why some cells succumb while others do not, we may learn a great deal

about how to protect vulnerable neurons and thereby treat disease.

The Polyglutamine Diseases

The conundrum of selective vulnerability is well illustrated by a group of diseases collectively known as the polyglutamine diseases. Unlike the examples mentioned above, which are all complex, polygenic diseases, the polyglutamine disorders are monogenic neurological diseases of known genetic cause. There are nine known polyglutamine diseases: Huntington's Disease (HD), dentatorubralpallidoluysian atrophy (DRPLA), spinal and bulbar muscular atrophy (SBMA), and the spinocerebellar ataxias (SCAs) 1, 2, 3, 6, 7, and 17 (for review, see (Bates, Harper et al. 2002); (Gatchel and Zoghbi 2005)). The nine polyglutamine diseases are caused by a germline expansion of CAG repeats in different genes, and they all follow a typical course of mid-life onset followed by unrelenting, progressive deterioration. These diseases have a heterogeneous clinical presentation, with some distinct, and some overlapping, features, but they are best distinguished through genetic means.

Despite a shared genetic lesion and overlapping clinical manifestations, five polyglutamine diseases can be distinguished by distinct patterns of cell death (see

Figure 1). For most of these diseases, with the exception of SBMA, the CAG expansion leads to the expression of extra glutamines in a protein, conferring a toxic gain-of-function that leads to cell death. Studies from model organisms demonstrate that these polyglutamine-expanded proteins can be toxic even in non-neuronal cells: when expressed in yeast, human mutant *huntingtin* (*mhtt*) forms aggregates and causes cellular toxicity (Muchowski, Schaffar et al. 2000; Meriin, Zhang et al. 2002). These two observations present a paradox, namely: how can ubiquitously expressed proteins, which can be toxic even in yeast, create differential patterns of cell death in the human central nervous system?

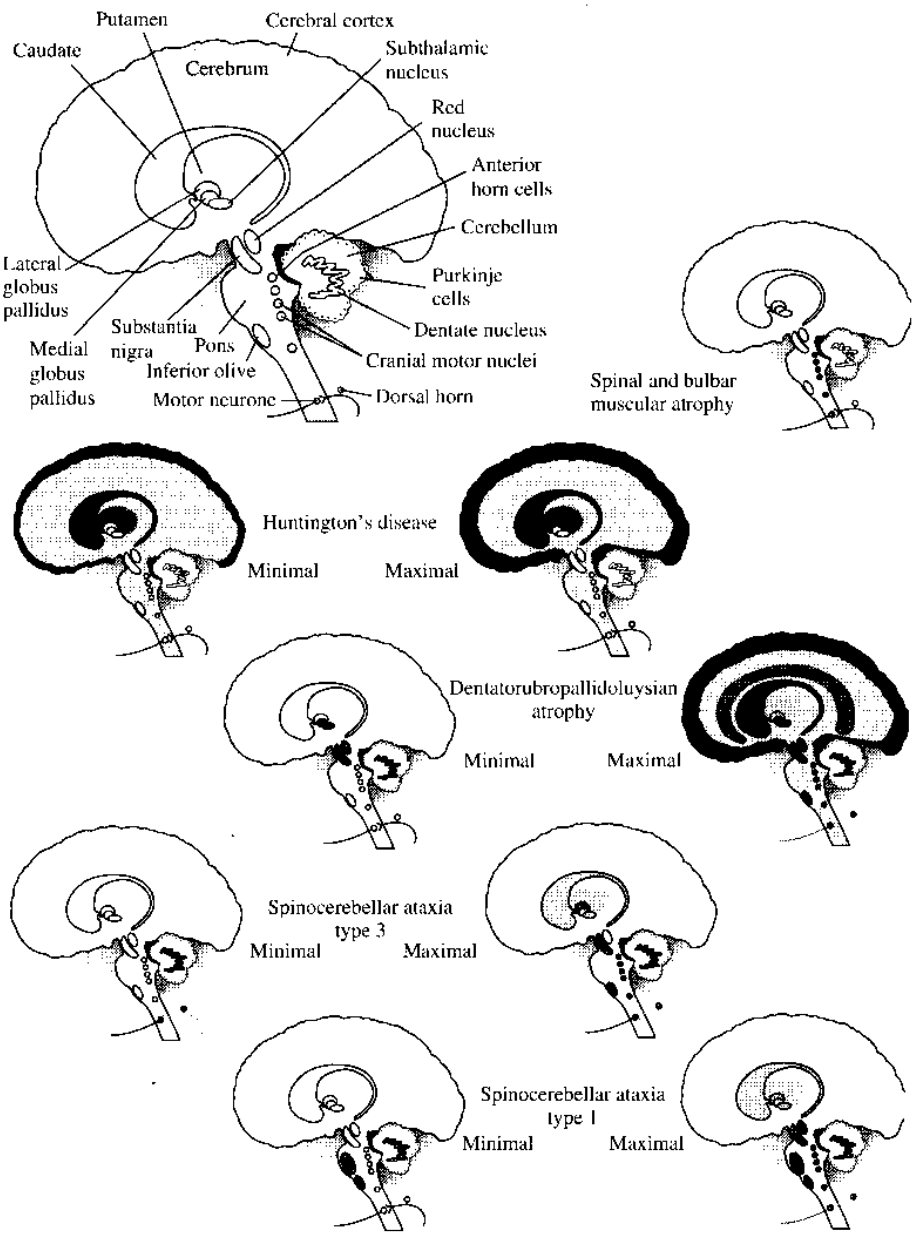

Figure 1: Selective vulnerability in polyglutamine diseases. Despite a shared genetic lesion, polyglutamine disorders have distinct patterns of vulnerability. Figure originally from (Bates, Harper et al. 2002). Shaded areas represent regions where the most cell death occurs in each disease.

Huntington's Disease

Huntington's Disease (HD) is the most prevalent of the polyglutamine disorders. Like the others, it is a progressive genetic neurodegenerative disorder. The disease typically presents during middle age with cognitive changes and the development of dance-like uncontrolled movements, termed "Huntington's chorea." These symptoms worsen over a period of ten to fifteen years and eventually progress to hypokinesis and rigidity. Patients slowly and inevitably succumb to complications from this loss of movement, frequently dying from causes such as aspiration pneumonia or starvation due to dysphagia (for review, see (Bates, Harper et al. 2002)).

Pathological studies of brains from HD patients reveal a selective degeneration of the striatum with a resultant widening of the lateral ventricles. Cell loss in the striatum progresses dorsolaterally to ventromedially, usually preserving the nucleus accumbens (Vonsattel 1985). While the greatest cell loss occurs earliest in the striatum, neuronal death has also been observed in several other brain regions, most notably the cortex, particularly in pyramidal projection neurons of layers III, V, and VI (Rosas, Liu et al. 2002; Rosas 2008).

Histologically, the striatum is composed of an almost-uniform population of projection neurons called "medium-spiny neurons" (MSNs), named for their characteristic

dendritic spine morphology. Two distinct but closely related subpopulations of neurons can be found within the MSNs that express different neurochemical markers, project to different brain regions, and have different functions (see Figure 2). The striatonigral cells express dopamine-1 receptors (D1Rs), which are coupled to Gαs, and project to the output nuclei of the basal ganglia—the internal segment of the globus pallidus in humans or the endopeduncular nucleus and substantia nigra pars reticulata in mice, which in turn project to the thalamus and then the cortex. Activation of striatonigral cells leads to a loss of inhibition of the thalamus, and the initiation of cortical movement pattern generators. In contrast, the striatopallidal cells express dopamine-2 receptors (D2Rs), which are coupled to Gi subunits, and first project to the globus pallidus externa, which inhibits movement by enhancing thalamic inhibition. MSNs are defined by several other neurochemical markers, including opioid peptides substance P (striatonigral) and enkephalin (striatopallidal). Besides these few differences, however, striatonigral and striatopallidal MSNs have similar origins, innervation, morphologies, and, to a large degree, gene expression profiles (Steiner H 1998) for review).

Despite the many similarities of striatonigral and striatopallidal cells, human pathological studies have suggested that D2-expressing striatopallidal MSNs die first

in Huntington's disease (see Figure 3 and, (Reiner A 1988);(Albin, Reiner et al. 1992) ; (Sapp, Ge et al. 1995). One small-scale recent study showed increased firing in GPe and decreased firing in GPi in an HD patient undergoing deep-brain stimulation, which is consistent with a selective loss of striatopallidal neurons (Starr, Kang et al. 2008). This observation fits with the clinical picture of HD, in which uncontrolled movements, caused by the dysfunction of indirect pathway cells, is followed by hypokinesis after loss of the direct pathway neurons. Understanding the molecular basis for this selective vulnerability could offer tremendous therapeutic potential, by both enhancing our knowledge of HD pathophysiology and also providing potential drug targets.

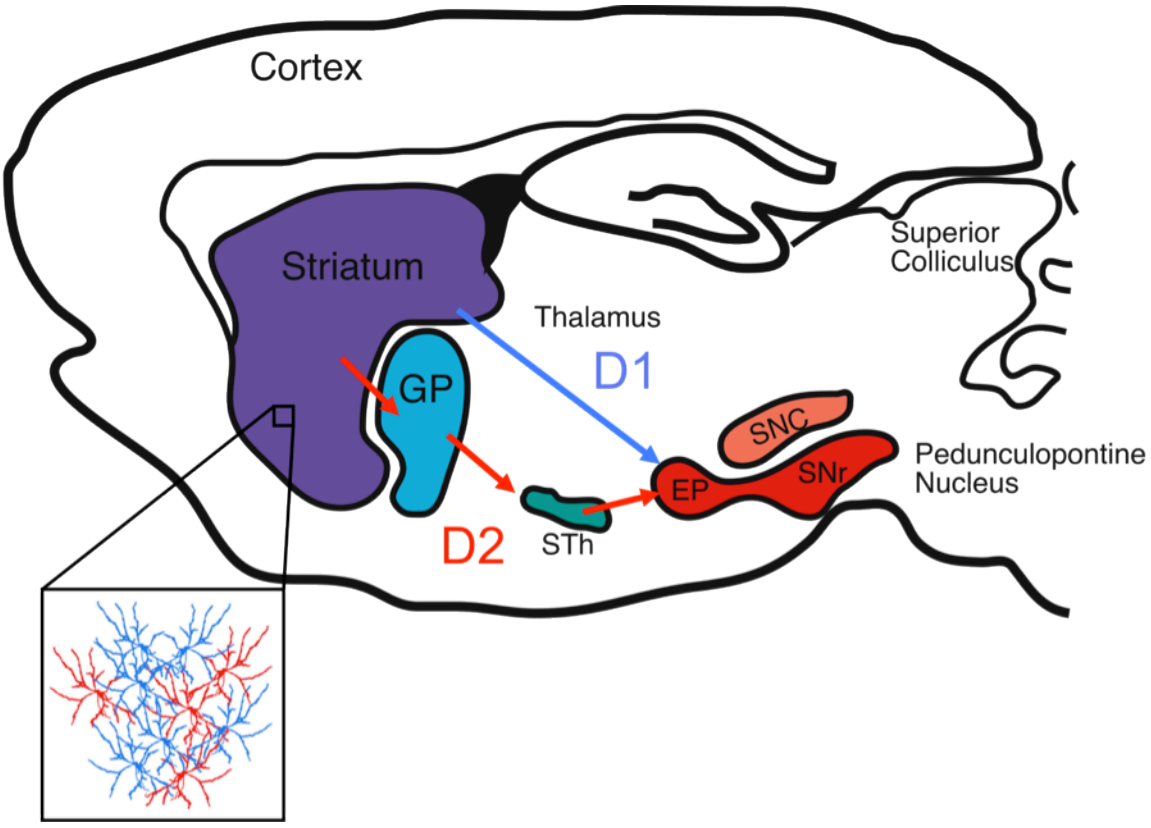

Figure 2: Mouse Basal Ganglia Circuitry. Glutamatergic input from the cortex to the striatum is processed by MSNs of the striatum (inset) through two parallel pathways, with opposing function and distinct, though related, gene expression signatures. Striatonigral (blue) MSNs project directly to the output nuclei of the basal ganglia, whereas striatopallidal MSNs (red), project first to the globus pallidum and subthalamic nucleus before projecting to the output nuclei. These two MSN populations are anatomically intermixed and morphologically indistinguishable, but it is the striatopallidal MSNs that are most vulnerable in HD. Adapted from Gerfen, 1992

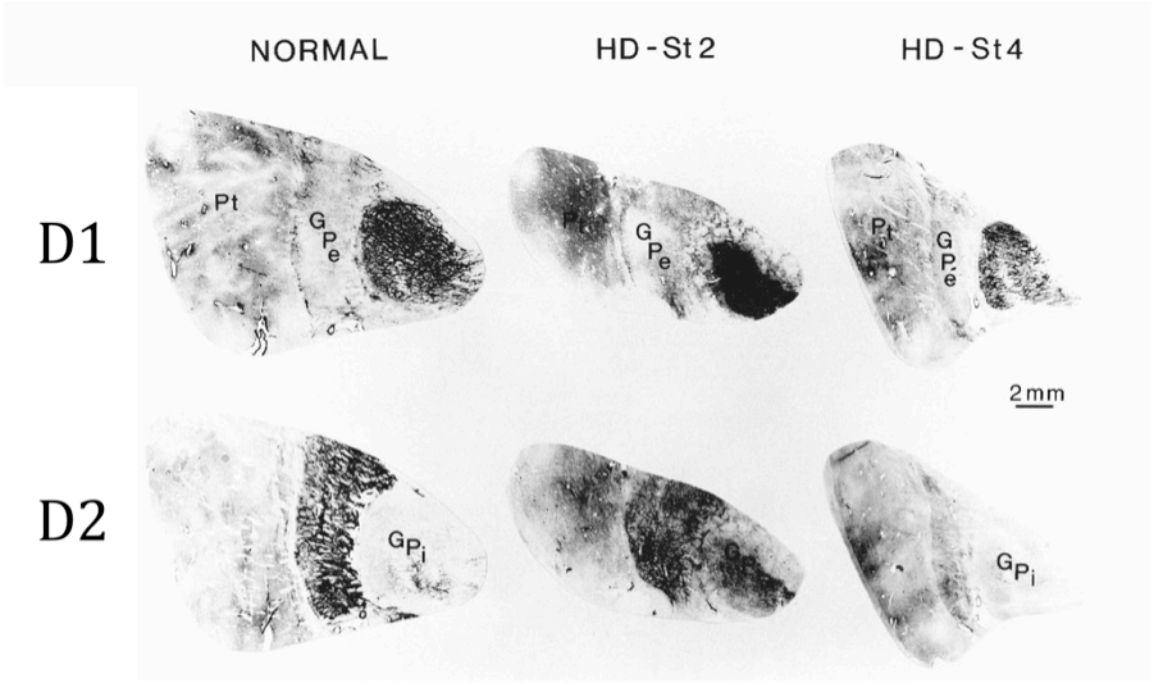

Figure 3: Striatopallidal fibers are selectively vulnerable in human HD post-mortem tissue. Immunohistochemistry for substance P (striatonigral marker) and enkephalin (striatopallidal marker) in human post-mortem tissue at worsening stages of HD. In early stage HD, striatopallidal fibers degenerate, while striatonigral fibers remain intact. In late stage HD, both striatonigral and striatopallidal fibers degenerate. Figure adapted from (Reiner, Albin et al. 1988).

HD mouse models

Human HD studies have yielded tremendous insight into the pathophysiology of the disease. A large-scale collaborative effort twenty years ago in Venezuela, led by the Huntington's Disease Collaborative Research Group, resulted in the identification of the CAG repeat expansion in the *htt* gene as the causative genetic factor in the disease (Gusella, Wexler et al. 1983; Group 1993). Post-mortem pathological studies have provided a wealth of information that has given rise to the current understanding of selective vulnerability. To further dissect the cellular pathways underlying disease, however, it is necessary to turn to model systems. HD research in simple model organisms has resulted in many insights into the direct toxicities of mutant *huntingtin* and provides good model systems for pharmacological screens. (Willingham, Outeiro et al. 2003), (Voisine, Varma et al. 2007). Work in simple model organisms cannot address the question of selective vulnerability, however, because these organisms do not share the neuronal circuitry of the striatum found in mammals. For this reason, many groups have turned to mouse models, which do offer the opportunity to study the effects of *mhtt* in the conserved circuitry of the basal ganglia.

A variety of HD mouse models have been developed, each model recapitulating different aspects of the disease. The

models differ by the strategy of their construction (knock-in vs. transgenic) the portion of *htt* gene expressed (full-length vs. truncation), their expression of human *htt* versus mouse *htt*, and the number of CAG repeats included (from about 90-250). These strategies produce mice with varying phenotypic severity. This study will focus on two of the most commonly used models, the R6-2 and the YAC128 mice, which correspond to a more severe and a milder phenotype, respectively (see Figure 4 for schematic and Table 1 for phenotype summary).

The R6-2 transgene, as originally published, was created in the laboratory of Dr. Gillian Bates, and is composed of ~1 kb of the 5′ UTR of the human htt gene, htt exon 1, 150 CAG repeats, and the first 262 bp of intron 1 (Mangiarini, Sathasivam et al. 1996). R6-2 mice appear normal at the time of weaning, but quickly develop a behavioral phenotype that includes gait disturbances, resting tremor, and hind-limb clasping. On gross pathology, the mice demonstrate decreased brain size; histopathologically, the mice develop both cytoplasmic and nuclear huntingtin aggregates in neurons (Mangiarini et al. 1997). Surprisingly, typical markers of apoptotic cell death are not observed in these animals, although a histologically novel neurodegenerative cellular phenotype has been observed in the anterior cingulate cortex, the dorsal striatum, and in Purkinje neurons of the cerebellum

(Turmaine et al. 2000). The advantages of the R6-2 mouse include its rapid phenotypic development, its wide use, and its thorough characterization.

The YAC128 model was constructed in Dr. Michael Hayden's laboratory by inserting 128 CAG repeats through homologous recombination into a yeast artificial chromosome that expressed human htt with full regulatory sequences. The mice express mutant human *htt* in a similar tissue distribution pattern and at similar levels to that observed for mouse *htt*. Disease progression in this model is much slower than in the R6-2 model. At 3 months of age, the mice display slight hyperactivity in an open field and gradually develop a hypokinesis at 6 months that worsens at 9 and 12 months (Slow et al., 2003); (Van Raamsdonk, Pearson et al. 2005). On the rotarod, the mice demonstrate a motor learning phenotype at 2 months, without any gross motor deficits. A true motor deficit on the rotarod emerges at 6 months of age, and worsens with time. The mice have a normal life expectancy, unlike human patients with HD. In pathological studies, the mice develop a specific cell loss in the striatum, losing 15% of striatal volume by 12 months of age. The mice also develop nuclear aggregates of huntingtin, mostly in the striatum and cortex by 2 months of age (Van Raamsdonk, Pearson et al. 2005).

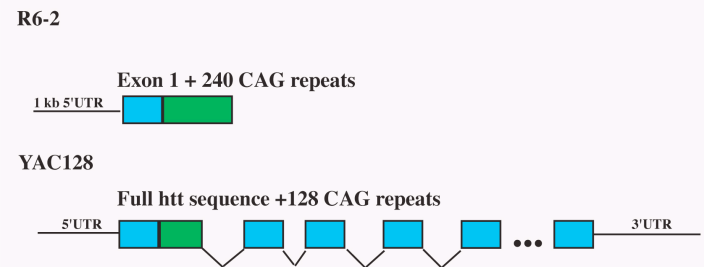

Figure 4: HD transgenic mouse models contain varying portions of htt and different numbers of CAG repeats. The R6-2 mouse was created by transgenic expression of a construct that included 1kb of the 5'UTR, exon 1 of human htt, and 150 CAG repeats. The YAC128 model includes the entire human *htt* gene, including introns and regulatory elements.

Table 1: Summary of Mouse Model Phenotypes

Feature of human HD	R6-2 B6/CBA background	YAC128 FVB/N
Motor Dysfunction	Tremor – 6 weeks Possible hyperactivity– 6-12 weeks Worsening rotarod deficits beginning at 6 weeks	No tremor Hyperactivity at 3 months Worsening rotarod deficits beginning at 6 months, severe by 1 year
Hypokinesis	By 12 weeks	By 1 year
Dystonias	Hind-limb clasping – 6 weeks	Not reported
Neuronal degeneration	"Dark body" degeneration primarily in anterior cingulate (Turmaine, 2000)	Cell loss in striatum found by neurostereological approaches
Life span	10-13 weeks	Normal

Endogenous function of *htt*

While most proposed mechanisms of neurodegeneration in HD assume that the initial insult results from a toxic gain-of-function mutation in *mhtt*, several groups propose a contributory loss-of-function pathway as well, through a dominant-negative effect. A thorough understanding of the physiological role of *htt* remains elusive because constitutive knockout of the mouse *huntingtin* disease gene homologue (hdh) leads to an early embryological death. In mouse embryos lacking Hdh, extra-embryonic tissues fail to develop properly, leading to an early developmental arrest of the embryo (Dragatsis et al., 1998). Conditional knockout of hdh in post-mitotic neurons using the Cre/lox system causes an adult-onset neurodegeneration, implicating a functional role for Hdh in maintenance of cell survival (Dragatsis et al., 2000).

Htt is a very large protein, nearly 350 kDA, with several HEAT repeat domains. One theory is that the protein serves as a molecular scaffold that allows the binding of many proteins in a complex (Seong et al., 2009) A great number of endogenous functions for *htt* have been proposed, but the best-described functions concern transcriptional regulation and vesicular transport. As mentioned above, htt binds to many transcription factors, and it may bind

DNA itself. Seong et al. have also shown that Hdh binds to Polycomb Repressor Complex 2 (PRC2), a histone methyltransferase responsible for regulating developmental gene networks. Knockout of Hdh closely mimics loss of function of PRC2, further suggesting a complementary role for the two genes— but a true genetic rescue experiment between the two genes has not been described.

The evidence implicating *htt* in vesicular transport is fairly robust. In isolated rat sciatic nerves, *htt* is transported in both anterograde and retrograde directions (Block-Galarza et al., 1997). Htt binds dynein and facilitates microtubule transport *in vitro* (Caviston et al., 2007). Mutant *htt* impairs fast axonal transport in isolated squid axoplasm (Trushina et al., 2004; Morfini et al., 2009). Yeast-two hybrid screens have shown myriad binding partners of *htt* in vesicular transport, including HAP1, which is involved in clathrin-mediated endocytosis of BDNF (Gauthier et al., 2004).

Existing Hypotheses

Investigation of HD mouse models, combined with data from human *post mortem* studies, has led to several hypotheses in the field to explain the differential vulnerability of MSNs in HD (for review, see (Han, You et al.2010).

Neurochemical Specificity

A longstanding hypothesis in the field, which predates the identification of the CAG expansion in huntingtin as the causative mutation in HD, is that neurochemical differences in MSNs underlie their selective vulnerablility. The striatum receives two major sources of neurochemical input: glutamate from the cortex and thalamus, and dopamine from the substantia nigra *pars compacta*. Both of these neurotransmitters have been considered as a possible precipitant of toxicity: excess glutamate can cause cell death through "excitotoxicity," a term coined by John Olney in 1969 to explain a phenomenon in which over-stimulation of neurons, usually via glutamate receptors, can lead to altered calcium homeostasis, mitochondrial dysfunction, and activation of apoptotic cascades. Early pharmacological models of HD, such as the stereotactic injection of glutamate receptor agonists kainic or quinolinic acid into the striatum, created lesions that resembled those of HD (Coyle and Schwarcz 1976). However, there have been few convincing arguments

linking these pharmacological models to the genetic cause of the disease. In genetic HD models, there have been reports of electrophysiological changes at the glutamatergic-corticostriatal synapse in genetic HD mouse models (Cepeda, Hurst et al. 2003). Transcriptional changes of the levels of NMDA receptor subunits have also been reported; however, there has been no mechanism shown to explain why striatal glutamate transmission would be altered over other strongly glutamatergic non-vulnerable regions, like the hippocampus or olfactory bulb (Han, You et al. 2010).

The arguments in favor of alterations in dopamine signaling causing pathology in HD also have a long history in the field. After Arvid Carlsson published his studies on the use of L-dopa to treat Parkinson's Disease in the 1960s, it was hypothesized that HD could be the "mirror image" of PD, where an excess of dopamine was responsible for uncontrolled movements. Pathological studies, however, revealed no differences in the amount of tyrosine hydroxylase, the enzyme that produces dopamine, in the substantia nigra (McGeer and McGeer 1976). On the other hand, tetrabenazine, recently approved by the FDA for the symptomatic treatment of HD chorea, acts by inhibiting vesicular monoamine transporter 2, which actively transports dopamine into synaptic vesicles.

Symptomatically, dopamine depletion seems to have benefit for the chorea of some HD patients.

While the pre-synaptic production of dopamine does not seem to change in HD, there is ample evidence for alterations in dopamine signaling post-synaptically. As mentioned previously, the expression of dopamine receptors changes dramatically early in the disease, in the pattern explained above, in which loss of Drd2 receptors precede Drd1a receptor changes. Other critical components of dopamine signaling are changed early in HD mouse models, including loss of DARRP-32 (Bibb, Yan et al. 2000). Further studies into the significance of changes in dopamine signaling in HD are warranted.

Aggregation of mhtt

Several years after the publication of the R6-2 mouse, Gillian Bates's group discovered that immunohistochemical staining of the R6-2 mouse brain revealed the presence of aggregate structures in the neuropil, cell bodies, and nuclei of neurons, but not glia (Davies, Turmaine et al. 1997). Subsequent work showed that these aggregates were also present in *post mortem* tissue from human HD patients (Davies, Turmaine et al.; DiFiglia, Sapp et al. 1997; Gutekunst, Li et al. 1999). While initial studies suggested that the appearance of aggregates correlated with vulnerability to disease, subsequent careful analysis

suggested that the two processes are not so easily linked. Aggregates appear early in the disease course of HD, but their appearance does not correlate strongly with pathology; for example, in human tissue, the great preponderance of aggregates are found in the cortex, not the striatum. Furthermore, in a mouse model of HD in which *mhtt* is expressed only in MSNs, striatal aggregates occur in the absence of motor symptoms or other pathology (Gray, Shirasaki et al. 2008). These results have lead some to argue that the presence of aggregates may actually protect cells from a more toxic fibrillar form of *mhtt*.

Somatic CAG repeat instability

One intriguing hypothesis to explain selective vulnerability relates to the instability of CAG repeats. Since 1988, when Ridley and coworkers analyzed the U.S. National Huntington's Disease Roster, HD has been known to display anticipation, a phenomenon whereby the age of onset decreases in successive generations (Ridley, Frith et al. 1988). For HD, anticipation only occurs through paternal inheritance. The molecular underpinning of anticipation is an expansion in the number of CAG repeats in huntingtin. The mechanism by which the CAG expansion occurs in the male germline is still not understood, but may involve DNA repair pathways (Dragileva, Hendricks et al. 2009). Recent work has shown that the number of CAG repeats in HD patients is unstable somatically, and more suggestively,

the CAG repeats are longest in vulnerable brain regions (Shelbourne, Keller-McGandy et al. 2007); (Swami, Hendricks et al. 2009). These observations lead to the hypothesis that the most vulnerable neurons are those that have the longest somatic expansion of CAG repeats. Work in HD mouse models seemed to support this hypothesis, as crossing the HD knock-in mouse to a constitutive knockout of the gene *Msh2* abrogated somatic CAG expansion and delayed symptom onset (Wheeler, Lebel et al. 2003). This experiment showed that Msh2 is necessary for somatic CAG expansion to occur, and suggested that this loss of somatic CAG expansion could interfere with the disease process. This model suffered a strong setback, however, when Gray et al. showed that mice containing a Bacterial Artificial Chromosome (BAC) with alternating CAA-CAG repeats, which are stable in somatic tissues, still develop selective striatal and cortical pathology (Gray, Shirasaki et al. 2008).

Axonal Transport

Another hypothesis, advocated by Han et al. in their review of the huntingtin literature, is *mhtt*'s interference of axonal transport. All of the most vulnerable cells in HD are projection neurons, or neurons that send axons to brain regions that are relatively far away. The interneurons of the striatum and cortex are unaffected. Additionally, the cell death that occurs in HD seems to occur via a "dying back" process, in which there is a loss of axon fibers and

synaptic proteins before outright cell body loss. Furthermore, *mhtt* has been shown to interfere with axonal transport in preparations of isolated squid axoplasm, suggesting that deficits in transport are independent of effects in the cell body, including transcription (Morfini et al., 2009). The proposed pathway through which mhtt exerts these effects is through alteration of phosphorylation of microtubule motor proteins, acting through the JNK pathways.

While these initial findings are intriguing, they do not explain why other projection neurons, which also express *mhtt,* are not as vulnerable in HD. Indeed, neurons of the corticospinal tract, which extend from the cortex to the very base of the spinal column and are vulnerable in ALS, are not vulnerable in HD. If deficits in axonal transport are responsible for the selective vulnerability of MSNs, then they must first reside in differences upstream of transport itself, most likely in differences of gene expression between different projection neuron populations.

Transcriptional Dysfunction

The literature implicating transcriptional dysfunction in HD is extensive (for review, see Cha 2007). Early pathological studies of *post mortem* human tissue from HD patients demonstrated decreased expression of many genes in

Grade 0 and Grade 1 HD cases measure by *in situ* hybridization, before overt cell loss is observed (Albin et al. 1991). These genes included markers of striatopallidal MSN identity, such as Drd2 and enkephalin (Reiner et al., 1998), as well as glutamate receptors (Arzberger et al., 1997), and cannabinoid receptors (Glass et al., 1993). Although the decreased expression of these genes was thought to precede cell loss, definitive proof that this loss of expression was due to transcriptional changes instead of cell loss was difficult to obtain in human pathological studies. However, many of these same gene expression changes also occur in mouse models of HD, and in the mice, gene expression changes are not confounded by cell death, because in all mouse models of HD, very little or no actual cell loss occurs (Cha et al., 1998, 1999).

Despite the lack of overt cell death in HD mouse models, transcriptional changes abound. Transcriptional changes in HD mouse models were first measured at the single gene level, and then with genome-wide approaches, once microarray technology became available (Cha et al., 1998, Luthi-Carter, 2000; Strand et al., 2007; Brochier et al., 2008). In a microarray study of whole mouse striatum of R6-2 mice, Luthi-Carter et al. found that 1.7% of all genes were changed by 12 weeks of age. The genes fell into

many functional categories possibly related to neurodegeneration including neurotransmitter receptors and genes involved in signal transduction, calcium homeostasis, and regulation of nuclear hormones (Luthi-Carter et al., 2000). Interestingly, the vast majority of gene changes were loss-of-expression: very few genes were found to be upregulated.

Several mechanisms have been proposed to explain *mhtt*'s effects on transcription. One theory is that the polyglutamine-rich region that causes *mhtt* to aggregate inappropriately binds and sequesters other proteins, including transcription factors, which thereby changes gene expression. Mutant *huntingtin* has been shown to preferentially bind CBP, Sp1, p53, and NCoR (Kazantsev et al., 1999; McCampbell et al., 1999; Stefan et al., 2000; Dunah et al., 2002; Boutell et al., 1999). Differences in transcription factor expression or aggregate formation in vulnerable and non-vulnerable cell-types could then explain differences in cell vulnerability. There has not yet been a systematic meta-analysis of all gene-expression studies in the HD literature to search for conserved patterns of promoter elements common to the most highly affected genes — such an unbiased approach might reveal novel pathways for transcriptional dysregulation in HD.

Htt's proposed regulation of BDNF transcription represents a slight variation on these ideas. Instead of proposing that *mhtt* inappropriately sequesters transcription factors in the cytosol, Zuccato et al., proposed that one of wild-type htt's roles is to sequester a powerful transcriptional repressor outside of the nucleus. They have shown that wt *htt* binds to transcriptional repressor element-1 transcription factor/neuron restrictive silencer factor (REST/NRSF) in an *in vitro* system and that *mhtt* fails to perform this function adequately. The failure to sequester REST was then shown to decrease the expression of BDNF. Thus, the theory postulates a dominant-negative effect of *mhtt* on wt *htt* function.

Benn et al. have proposed a third mechanism through which *mhtt* could alter transcription: by binding directly to DNA itself (Benn et al., 2008). Using chromatin immuno-precipitation in several *in vitro* systems, Benn et al. show that *htt* and *mhtt* bind differentially to promoters. Using a micrococcal nuclease assay in the STHdh cell-line, Benn et al. show that *mhtt* opens DNA conformation in the cells, making it more accessible to cleavage by the nuclease, and, perhaps, by extension, explaining observed changes in transcription.

All cell types share the same DNA, so their differences reside in how they express genes. Neurons acquire their identity through the expression of a series of transcription factors, and they differentiate further into neuronal subtypes through the actions of a series of more specialized signals. While these processes are incompletely understood, it is now possible to differentiate stem cells into dopaminergic neurons (Studer 2001).

In HD, medium spiny neurons seem to lose markers that define their identity before they die. As mentioned previously, markers for striatopallidal MSNs, Drd2 and preproenkaphlin, disappear in early disease stages, well before disappearance of striatonigral markers Drd1a and substance P. These losses of markers are recapitulated in HD mouse models, in the absence of overt cell death. *Mhtt* aggregates in the nucleus of neurons, can bind directly to DNA, and has been shown to alter gene expression very early in the disease process (Benn, Sun et al. 2008); (Cha 2007). These observations have lead to the hypothesis that gene expression changes are responsible for the selective cell death in HD.

Many groups have attempted to characterize HD gene expression changes in both human post-mortem tissue and in HD mouse models without separating cellular populations.

Hodges and coworkers performed a large-scale microarray study with 44 post-mortem HD brains and 36 age-and sex-matched controls (Hodges, Strand et al. 2006). While this exhaustive study confirmed that the greatest gene expression changes corresponded to regions with the greatest pathology (caudate and cortex), the insights into the pathophysiology of HD from this work have been limited. Studies using human tissue have many obstacles: samples are often from advanced disease, so it is difficult to know whether changes are secondary or initial insults; there are rarely perfectly-matched controls available; differences in post-mortem handling of tissue can lead to the appearance of artifacts in the data; and there is a great degree of variability between samples.

Microarray studies of whole striatum from HD transgenic mouse models have been somewhat consistent with human data, but have also yielded disappointingly few therapeutic leads (Luthi-Carter, Strand et al. 2000);(Chan, Luthi-Carter et al. 2002) ; (Ferrante, Kubilus et al. 2003); (Benn, Landles et al. 2005), (Kuhn, Goldstein et al. 2007), see (Cha 2007)for review. Some of these studies have found decreases in known striatopallidal markers Drd2 and enkephalin (Luthi-Carter, Strand et al. 2000); (Menalled, Zanjani et al. 2000), while others have shown primary decreases in striatonigral markers, like Drd1a (Cha 2000). The time of harvesting these mRNAs was often quite

late in the disease process, however, making it difficult to isolate any initial insults. Pathways found to be altered in HD from these studies include changes in: neurotransmission (receptors, second-messengers, neurotransmitter synthesis), synaptic structural proteins, mitochondrial proteins, calcium homeostasis, proteasomal regulation, inflammatory pathways, and many others (Cha 2007). In addition to their focus upon late-stage disease, these studies have been limited by the cellular heterogeneity of the striatum. Studies in the Greengard lab have shown that signaling within striatonigral and striatopallidal cells is frequently divergent, and sometimes opposite in nature (Bateup, Svenningsson et al. 2008); (Heiman, Schaefer et al. 2008). Thus, gene expression changes in one population may mask changes in the other. In addition to these different striatonigral and striatopallidal MSN populations, the striatum is composed of interneurons, glia, and many other supporting cells. This heterogeneity introduces noise into the data that makes it difficult to identify important early changes from secondary or tertiary effects.

The BACTRAP technology

Until recently, there have been few ways of separating mRNAs from distinct cellular populations to reduce noise from heterogeneity. Existing methods are not perfect, and FACS sorting can suffer from long periods of tissue

disruption, during which loss of intrinsic signals can lead to major changes in gene expression and a loss of sensitivity.

A new technology developed in the Heintz and Greengard laboratories takes a complementary approach by using a genetic approach to mRNA isolation. The "BACTRAP" technology utilizes a GFP-tagged ribosomal protein to co-immunoprecipitate mRNAs incorporated into polysomes (see Figure 5). This GFP-tagged ribosomal protein can be genetically driven in a cell population of interest – in striatopallidal cells, for example – by inserting the GFP-tagged ribosomal protein within a large swath of DNA regulatory sequences for the gene of interest in a bacterial artificial chromosome (BAC). (Gong, Zheng et al. 2003). These modified BACs can then be inserted into the mouse genome, and expression of the transgene of interest is controlled by endogenous regulatory elements, independent of the point of insertion. Because the tagged ribosomal protein is expressed only in striatonigral or striatopallidal neurons, mRNAs can be selectively isolated from one population. These mRNAs can then be analyzed to monitor changes in gene translation. The BACTRAP technique (abbreviated as "TRAP") thus provides a snapshot of all the messages being translated in a given cell population at one time.

In this study, we have used the TRAP technique to investigate differences between striatopallidal and striatonigral medium spiny neurons in HD mouse models. We have found that these two closely related neuronal populations, with varying susceptibility to the toxic insult of mutant *huntingtin*, have different gene expression responses to this perturbation. Correlating gene expression changes to behavioral phenotypes, we have observed that increasing phenotypic severity of the mouse models is mirrored by increasing numbers of changes in translational profiles. Choosing from the changes we have observed in these cell types, we have followed those in sphingosine-1-phosphate (S1P) signaling. We have seen that S1P levels are decreased in HD mouse models, and we have shown that S1P can exert pro-survival effects on striatal-derived cell lines. Changes in S1P signaling may therefore affect disease progression in HD. The following chapters detail the results that have led to these conclusions.

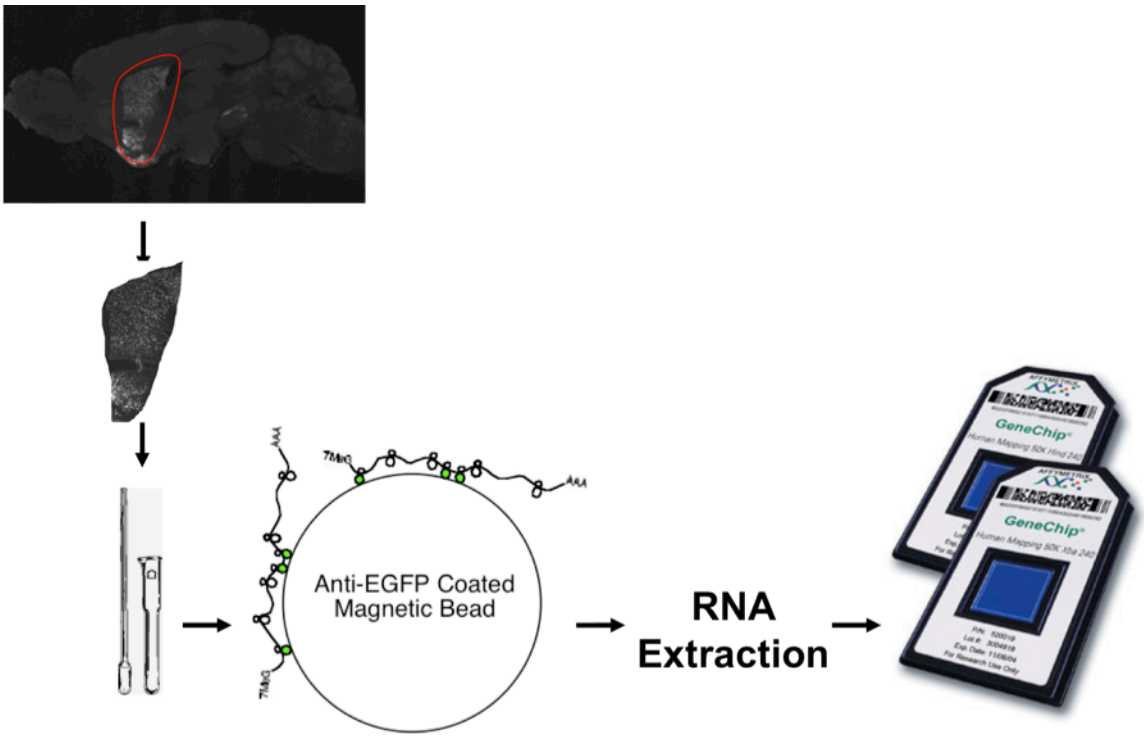

Figure 5: BACTRAP technology allows isolation of translated mRNAs from genetically defined cell populations. Striatal tissue is dissected from brain tissue, immediately homogenized, and mRNAs are co-immunoprecipitated with tagged ribosomal proteins. mRNAs are extracted and analyzed by Affymetrix GeneChip microarrays.

Results

Section 1: Behavioral and Phenotypic Characterization of HD/TRAP Models

Background

We wanted to correlate gene expression changes to behavioral deficits, because we reasoned that changes in translational profiles immediately preceding behavioral symptom onset would be most relevant to disease pathology. Mouse behavior assays are highly sensitive to experimental variation, including, in our case, mouse strain, CAG repeat number, and possible unknown variables. Indeed, striking variability has even been seen when mouse behavior assays were performed at the same time in three different geographic testing locations, despite controlling for numerous environmental parameters (Crabbe, Wahlsten et al. 1999). For these reasons, and because our strains contained the D1 and D2 TRAP transgenes, it was critical to re-characterize the behavior of the established HD models under our testing regime and after having crossed them to the D1 and D2 TRAP lines, to ensure that we could select behaviorally relevant time-points for harvesting mRNAs.

Mouse strain and behavior

The behavior of the R6-2 mouse has been extensively characterized, which made it an attractive model for study (Mangiarini, Sathasivam et al. 1996; Menalled, El-Khodor et al. 2009). The R6-2 line was originally derived with 144

CAG repeats and maintained on a hybrid F1 C57BL/6 x CBA background in order to maximize litter size (Mangiarini, Sathasivam et al. 1996). On this background, the R6-2 mice exhibit resting tremor, weight loss, diabetes, and spontaneous epileptic seizures. They develop progressively worsening motor impairments early in life, measurable on the rotarod as early as 4 weeks of age and a hypokinesis in the open field beginning at 6 weeks of age (Menalled, El-Khodor et al. 2009).

The D1 and D2 TRAP lines are maintained on a C57Bl/6J inbred background. To avoid confounds in the data due to strain differences between animals, a version of the R6-2 model congenic on the line C57Bl6/J was obtained from Dr. Gillian Bates and from Dr. David Howland of the HighQ Foundation. These mice originally had 240 CAG repeats and were reported to have a later age of onset than the published line (G. Bates, personal communication). Over the course of the experiments presented here, Menalled et al. published a thorough behavioral characterization of the R6-2 line on the C57Bl/6 background. Consistent with the observation that the C57Bl/6 background delays phenotype onset, they found a progressively worsening phenotype on the rotarod beginning at 8 weeks of age and a worsening hypoactive locomotor behavior at 6 weeks in females and 8 weeks in males (Menalled, El-Khodor et al. 2009). R6-2 C57BL/6 mice also showed reduced grip strength, reduced

body weight, abnormalities in gait analysis, as well as deficits in pre-pulse inhibition and light-dark choice.

The phenotype of the YAC128 mice has also been characterized, and its phenotype is also strain-dependent. The YAC128 model was created on an FVB/N background, and was shown to exhibit a rotarod deficit beginning at 6 months of age that was constant with respect to wild-type performance over time. In the open field, YAC128 mice were hyperkinetic at 3 months of age, but then gradually exhibited an increasing hypokinetic phenotype that became statistically significant at 12 months of age (Slow, van Raamsdonk et al. 2003). However, in an extensive study characterizing YAC128 mice on three different inbred strain backgrounds (FVB/N, C57BL/6, and 129), van Raamsdonk and co-workers show significant differences in the extent and timing of these phenotypes, with the most severe phenotypes observed on an FVB/N background, and the mildest phenotype on the C57Bl/6 background (Van Raamsdonk, Metzler et al. 2007). Menalled et al. attempted to reproduce these results in both the FVB/N and C57Bl/6J backgrounds: their results confirmed the rotarod results from the Slow study, but they found no statistically significant locomotor changes in the open field.

As the D1 and D2 TRAP mice were not available on the FVB/N background, we used the Swiss-Webster background instead. Although outbred Swiss-Webster mice and the

inbred FVB/N strain are related – the FVB/N line was derived from the Swiss-Webster background in the 1970s at the NIH (Taketo, Schroeder et al. 1991) – the progeny of this cross are no longer inbred. For all these reasons, we paid special attention to establishing baseline behavioral testing in our experimental strain background.

Behavioral Tests

In our study, we hoped to identify differences between D1 and D2 MSN gene expression that would mirror behavioral deficits caused by dysfunction of these two neuronal cell types. As mentioned earlier, stimulation of D1 MSNs is thought to stimulate locomotion, whereas activation of D2 MSNs is thought to inhibit movement. Direct evidence in support of this model was recently shown in mice by using light to selectively activate D1 or D2 MSNs that had been engineered to express a channelrhodopsin construct (Kravitz, Freeze et al. 2010). Upon activation of D2 MSNs with light, the mice exhibited freezing behaviors and a loss of movement reminiscent of Parkinsonism. In contrast, activating D1 MSNs lead to increased locomotion and fewer instances of freezing.

Several assays are widely used to characterize motor behaviors that reflect striatal function (for review, see

(Crawley 2000). The rotarod is the most commonly used assay to monitor changes in motor coordination and balance. Essentially a mouse treadmill, the rotarod apparatus consists of a motorized plastic cylinder raised to a standard height that is then rotated. Mice walk on the rotating cylinder until they fall off. The time to fall off, or fall latency, is measured. Rotarods can be driven at constant or accelerating speeds; the latter is thought to add a component of motor learning to the task. The rotarod task is thought to depend on several circuits: mice with cerebellar deficits show impaired rotarod performance (Lalonde, Filali et al. 1996), (Schaefer, O'Carroll et al. 2007), but the task depends on striatal function as well. For example, one radio-ligand imaging study found that rats exercised consistently on a rotarod showed increased metabolic activity in cerebellar-thalamic circuits and decreased activity in basal ganglia-thalamic-cortical circuits compared to rats exposed only once to the rotarod (Holschneider, Yang et al. 2007). The authors argue that during training phases, basal ganglia control is important, whereas after training, cerebellar-thalamic loops become more prominent in controlling the behavior.

The rotarod is advantageous as a behavioral test because it produces quantifiable results that are reproducible, computer-controlled, and easily scaled to larger cohorts of animals. Its wide use in the field allows

for comparison of results across laboratories, to the degree that behavioral results can be compared. On the other hand, it is not a specific readout of striatal function, and it cannot differentiate between D1 and D2 MSN deficits.

To complement the data from the rotarod, we therefore also chose to test the mice for locomotor deficits in the open field. Like the rotarod, open field tests are easily automated. Commercially available photocell-equipped boxes are often used, which track mice through breaks in infrared light beams. Measured parameters include total distance traveled over a given time period, number of beam breaks, and time spent moving or resting. The open field can also illustrate anxiety behaviors by measuring thigmotaxis, or the time spend on the edges of the open field versus the center. Unlike the rotarod, the open field would be capable of detecting a hyperkinetic locomotor phenotype as expected in selective D2 MSN dysfunction. We hypothesized that the published hyperkinesis in the YAC128 model at 3 months reflected a period when D2 MSN tone was lower than D1 MSN output, leading to an overall hyperkinesis in the animal's locomotor behavior.

R6-2 C57Bl/6J Behavioral results

R6-2 TRAP lines exhibit profound behavioral phenotypes at 12 weeks

For the R6-2 C57Bl/6J line, open field behavior was tested as early as three weeks of age, immediately upon weaning the mice. Mice were left in the open field for one hour, during which total distance and horizontal activity were measured in 10-min bins. At 3 weeks of age, there were no statistically significant differences among any of the groups tested at any point in the hour-long test (Figure 6). Motor coordination was initially tested on the rotarod at 4 weeks of age, one week after weaning and genotyping, using an accelerating protocol from 4 rpm to 40 rpm over 5 min on five consecutive days, after three initial training trials on the first testing day. As with the open field test, there were no significant differences in rotarod fall latency between double transgenic mice (carrying both the R6-2 and D2-TRAP construct) versus single-transgenic controls (carrying the D2-TRAP construct alone) at this early time point, (N=10 each group) (Figure 7).

Motor behaviors were again tested later in the disease course, at 6, 9 (Dr. Wenjie Luo, personal communication), 12 and 14 weeks of age. By the 12 and 14 week timepoints, there was a statistically significant hypokinesis in both the R6-2 D1 and R6-2 D2 TRAP mice compared to TRAP alone in total distance traveled in the open field test (Figure 7).

There was also a significant impairment in the R6-2 D2 TRAP mice on the rotarod (Figure 8). These deficits were present on the first day of testing and persisted throughout the week. The exact age of onset at which behavioral deficits are detectable in the R6-2 is about 6-8 weeks of age for the open field, and 10-12 weeks for the rotarod. These results are consistent with the phenotype published for this line by Menalled et al., although our line had a slightly later age of onset, and open field deficits could be detected prior to rotarod deficits. For a complete list of ages tested and results, see Table 2.

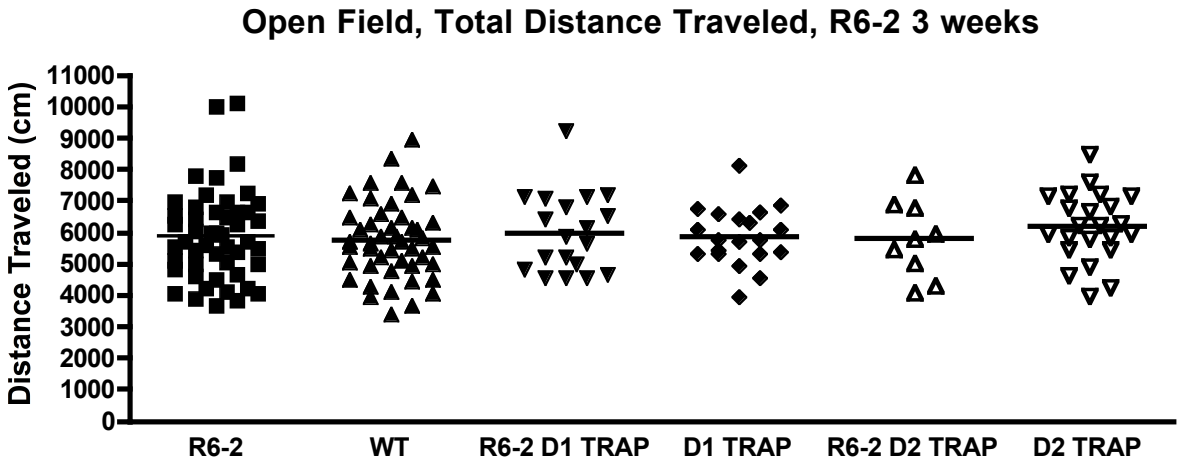

Figure 6: R6-2 movement at 3 weeks of age in the open field. At 3 weeks of age, there were no locomotor differences found among R6-2, WT, or TRAP mice in any groups. Data represents total distance traveled in open field in 1 hour (R6-2 group n=49, WT n=46, R6-2 D1 TRAP n=19, D1 TRAP n=20, R6-2 D2 TRAP n= 10, D2 TRAP n=23; 1-Way ANOVA, p=0.81).

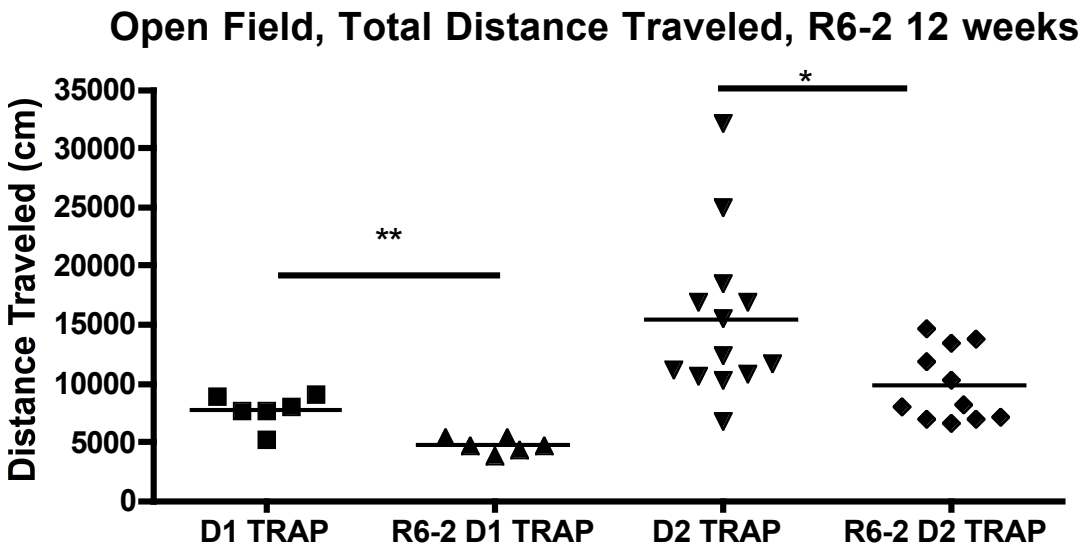

Figure 7: R6-2 12 week Open Field Behavior. At 12 weeks of age, both R6-2 D1 TRAP and R6-2 D2 TRAP mice exhibit hypokinesis with respect to their controls (D1 TRAP n=6, R6-2 D1 TRAP n=6, D2 TRAP n= 13, R6-2 D2 TRAP n=11, Two-tailed Unpaired Student's T-test p=.006 (D1) and p=.02 (D2).

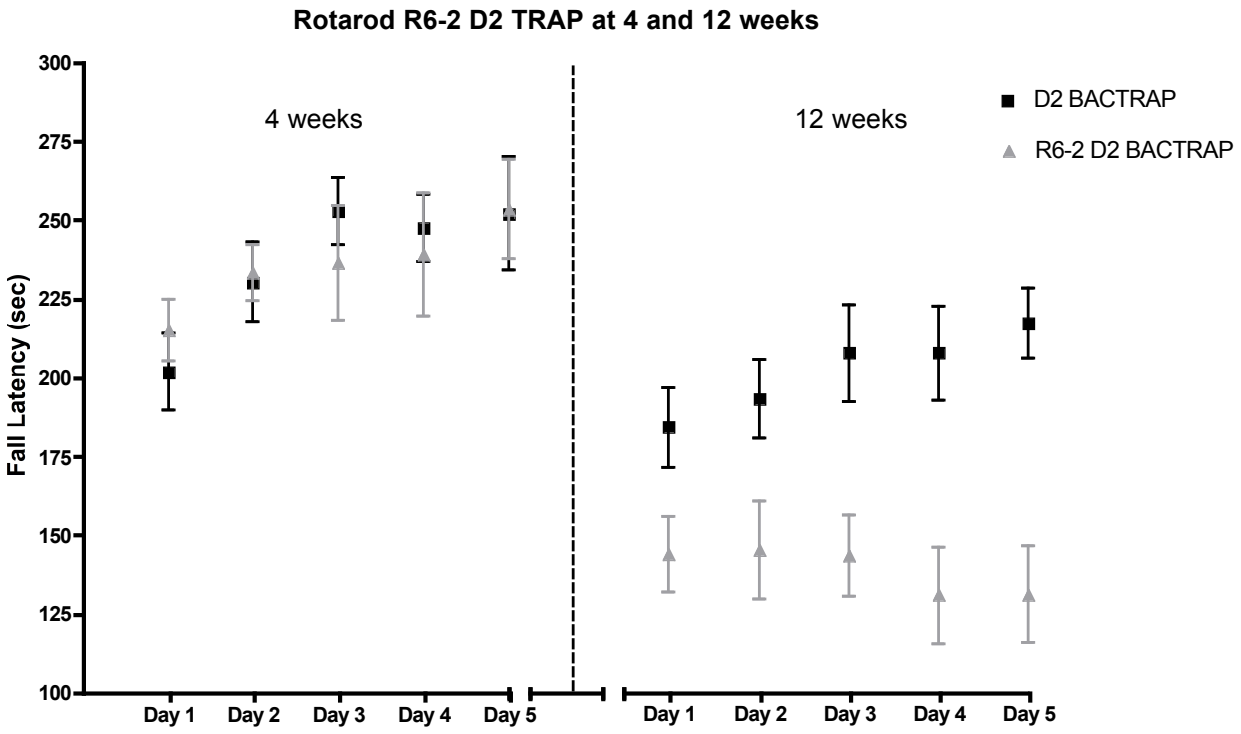

Figure 8: R6-2 D2 TRAP rotarod behavior: At 4 weeks of age, R6-2 D2 TRAP mice perform as well as D2 TRAP littermates on the accelerating rotarod task. At 12 weeks of age, R6-2 mice have a profound motor deficit (Repeated Measures Two-Way ANOVA p=.91 and p=.0006, respectively, n=9 per group).

Table 2: Behavioral Time-points tested in R6-2 model

Model	Age	Open Field Tested?	Significance?	Rotarod Tested?	Significance?
R6-2	2.5 weeks	Yes	No	No	N/A
R6-2	3.5 weeks	Yes	No	Yes	No
R6-2	4.5 weeks	Yes D2 only	No	Yes	No
R6-2	6 weeks	Yes D1 only	No	No	N/A
R6-2	9 weeks	Yes * data from Dr. Wenjie Luo, personal communication	Yes	Yes *Dr. Luo, personal communication	No
R6-2	12 weeks	Yes	Yes	Yes	Yes
R6-2	14 weeks	Yes	Yes	Yes	Yes

YAC128 TRAP lines exhibit a variable late-onset behavioral phenotype

On the rotarod, YAC128 D1 and D2 TRAP animals exhibited a constant deficit that appeared at 15 weeks of age and remained as the mice aged (Figure 9), although this difference is only statistically significant in the D1 TRAP line; this difference is largely in agreement with the results of Slow et al. and Menalled et al. For the YAC128 D1 TRAP mice, latency to fall was significantly less than D1 TRAP controls on all days tested (Two-way ANOVA, repeated measures, genotype $p<.001$). In the D2 TRAP line, the results were more variable: the effects due to genotype were not statistically significant on any day tested, although they approach significance on Day 3 (Two-way ANOVA, repeated measures, genotype $p=0.053$). The data shown in Figure 9 represents the average score of all mice in a cohort at each time point.

YAC128 mice have been reported to initially exhibit hyperkinesis in the open field beginning at 3 months of age and then a gradually worsening hypokinesis beginning at 6 months of age (Slow, van Raamsdonk et al. 2003). To confirm this phenotype in the hybrid background, two cohorts of YAC128 mice were crossed to D1 and D2 TRAP mice (~n=8 mice per group) and were tested approximately every 3 weeks from 7 weeks of age through 13 months of age. The behavior in these mice in the open field was variable and not statistically significant until 13 months of age, when the

interaction term between age and genotype reached significance (Repeated measures ANOVA, $F=3.2$; $p=.01$, Figure 10). Although one cohort of YAC D2 TRAP mice exhibited a statistically significant hyperkinesis at 12 weeks (data not shown), this result was not reproducible across other cohorts.

Baseline TRAP phenotype

Also of note upon analysis of the data, there was a highly significant hyperkinesis, nearly two-fold the distance traveled during an hour, present in both the D2 TRAP and YAC D2 TRAP animals in comparison to the D1 TRAP lines (Figure 10, Two-Way ANOVA, $p<.001$). The onset of this hyperkinesis began as early as 12 weeks and persisted throughout testing. Similar hyperactive phenotypes have been communicated to us from investigators using other D2 BAC lines, and we have seen a similar effect in the D2 BAC GFP and D2 BAC CRE lines (Myriam Heiman, personal communication; data not shown). As these lines involve independent integration events, the phenotype likely results from sequences present on the BAC itself. Seen in both strain backgrounds used (BL/6, mixed), and worsens with age.

The hyperkinesis in the D2 TRAP lines is consistent with reduced activity of D2 MSNs in these lines. This baseline hypo-function, present in both control and HD

groups, may have obscured a period of selective vulnerability of the D2 MSNs in the HD models by reducing the background against which the deficit would have been measured. The presence of the TRAP transgene in both control and HD populations limits confounding effects of the transgene.

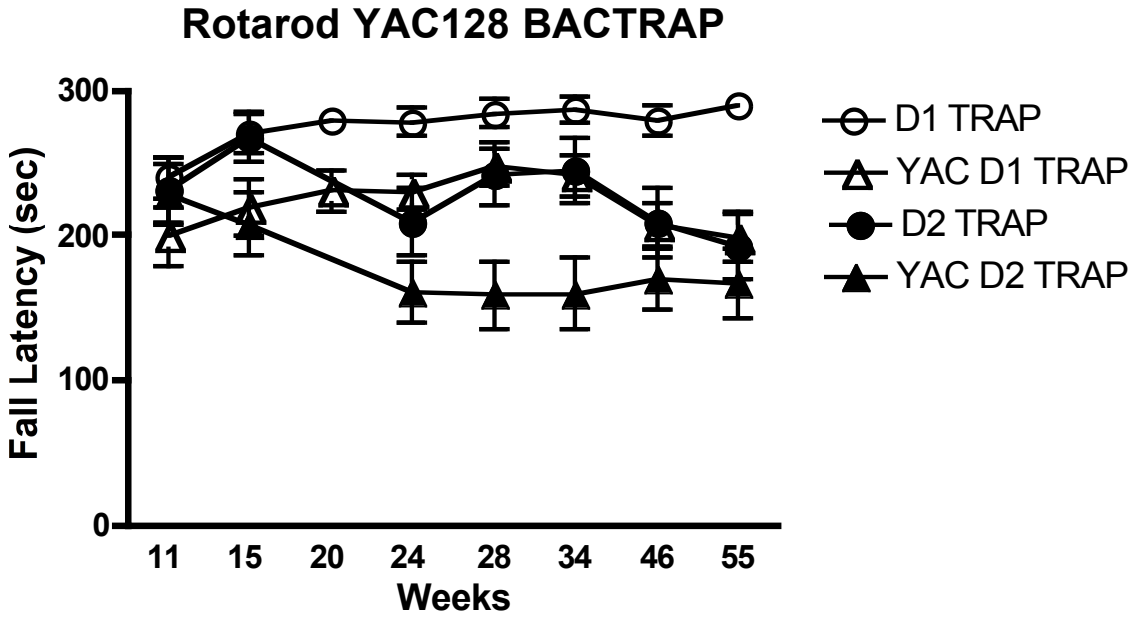

Figure 9: YAC128 TRAP rotarod data. YAC128 mice exhibit constant deficit on rotarod from 11 (D1) or 15 (D2) weeks of age—this result is significant in D1 TRAP line (D1 TRAP n=9, YAC D1 TRAP n=10, Two-way ANOVA, repeated measures, genotype $p<.001$), but just misses significance in D2 TRAP (D2 TRAP n=7, YAC D2 TRAP n=10, Two-way ANOVA, repeated measures Day 3, genotype $p=0.053$). Data plotted represent average taken from all mice over all trials over all days, error bars represent +/- standard deviation over all days.

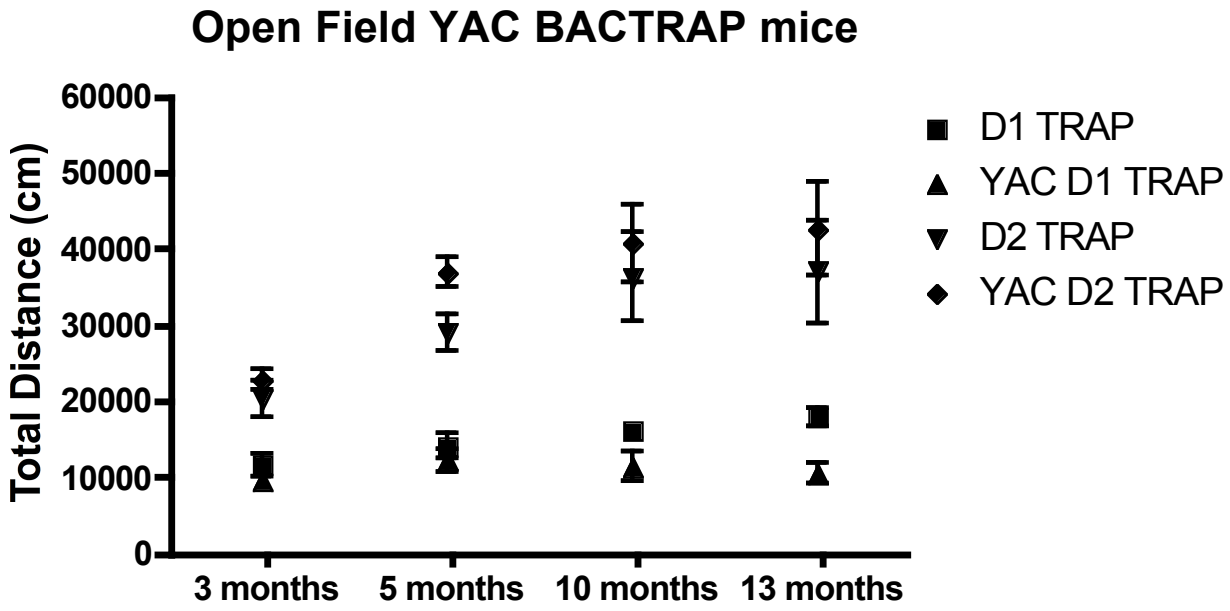

Figure 10: YAC128 Open field behavior (selected time points). YAC mice do not exhibit a behavioral phenotype in the open field until 13 months, when YAC D1 TRAP mice have a significant hypokinesis (D1 TRAP n=7, YAC D1 TRAP n=7, D2 TRAP n=9, YAC D2 TRAP n=8. Repeated measures ANOVA, F=3.2; p=.01). Error bars represent mean +/- standard error.

Gross Pathological studies

In order to characterize the gross pathology of R6-2 mice on the C57Bl/6J background, we sent 12-week-old animals (n=7 transgenic, n=5 wild-type littermates) for gross and microscopic pathological analysis at the MSKCC Laboratory of Comparative Pathology, directed by Dr. Julie White. For the analysis, tissue from skeletal muscle, heart, lungs, esophagus, kidney, salivary glands, lymph nodes, stomach, small and large intestine, pancreas, spleen, liver, gallbladder, genitourinary tract, and skin were compared at gross and microscopic levels. The laboratory found that, like the R6-2 mice on the hybrid strain background, the C57Bl/6J mice all had elevated blood glucose, indicative of diabetes. The pancreatic islet cells were shrunken in the mice, but there was no TUNEL staining present. There were no gross abnormalities in the brain, and no staining by TUNEL or GFAP.

Although there has been an extensive characterization of the diabetes phenotype in mouse models of Huntington's Disease (Andreassen, Dedeoglu et al. 2002), there are conflicting reports about whether there is actually an increased incidence of diabetes in human patients with HD (Farrer 1985).

A cohort of YAC128 mice was also sent for analysis (n=6 transgenic, n=6 wild-type controls) and showed no gross pathological phenotypes.

Thus, consistent with previous observations, we found that these models display HD-like behavioral deficits without the concomitant cell death observed in human patients. While this distinction highlights the limits of the mouse model, it also may open the door to dissecting the cellular events underlying the specific motor dysfunctions of the disease without the confounding effects on the tissue that would be produced by cell death.

CAG Repeat Expansion in the R6-2 Line

Since the year after the R6-2 model was first reported, it was known that the CAG repeats in the model are unstable, particularly when passed through the male germ line (Mangiarini, Sathasivam et al. 1996). The molecular basis of this instability is unknown, although in somatic cells, CAG expansion may depend on the protein OGG1 (Kovtun, Liu et al. 2007). It has also been shown that, as in humans, changes in CAG repeat length can affect phenotype (Morton et al, 2009).

To monitor the number of CAG repeats in our mouse colony, we attempted several strategies. First, we attempted to develop PCR genotyping protocols that contained the CAG repeat region. Due to the highly repetitive nature of the sequence, this technique requires special modifications. We used genotyping primers based on

sequences found on The Jackson Laboratory website, and attempted to optimize the PCR protocol for G-C rich regions: we separately, and in combination, adjusted concentrations of MgCl2, dNTPs, added stabilizing agents DMSO and/or BSA, adjusted annealing temperatures, and used a polymerase specialized for amplifying GC rich regions. We also applied the "Slowdown PCR" technique published in (Frey, Bachmann et al. 2008), which was specially designed for amplification of GC-rich and repetitive sequences. Thus, there may be additional barriers to PCR amplification of the CAG repeats than their GC-rich nature.

We were unable to obtain reproducible genotyping of CAG repeat number with any of these approaches, and therefore decided to outsource the CAG repeat sizing to the Laragen Corporation. Laragen has optimized a protocol for CAG repeat sequencing using fluorescently-labeled PCR products and an Applied Biosystems GeneMapper electrophoresis system. We sent them tail clippings from mice that had been born over the course of two years in the colony. During this time, the R6-2 mice in the colony began living longer, from an average of 6 months to as much as a year. It is known that, paradoxically, very long stretches of CAG repeats can ameliorate the phenotype in the R6-2 mice (Dragatsis, Goldowitz et al. 2009); (Morton, Glynn et al. 2009). In accordance with this observation, the results show that the number of CAG repeats had

expanded linearly over the course of the life of the colony by over 100 CAG repeats (Figure 11). This phenomenon is specific to the R6-2 line, as the CAG repeat number remained constant at 128 repeats in all YAC128 mice tested (n=20, data not shown).

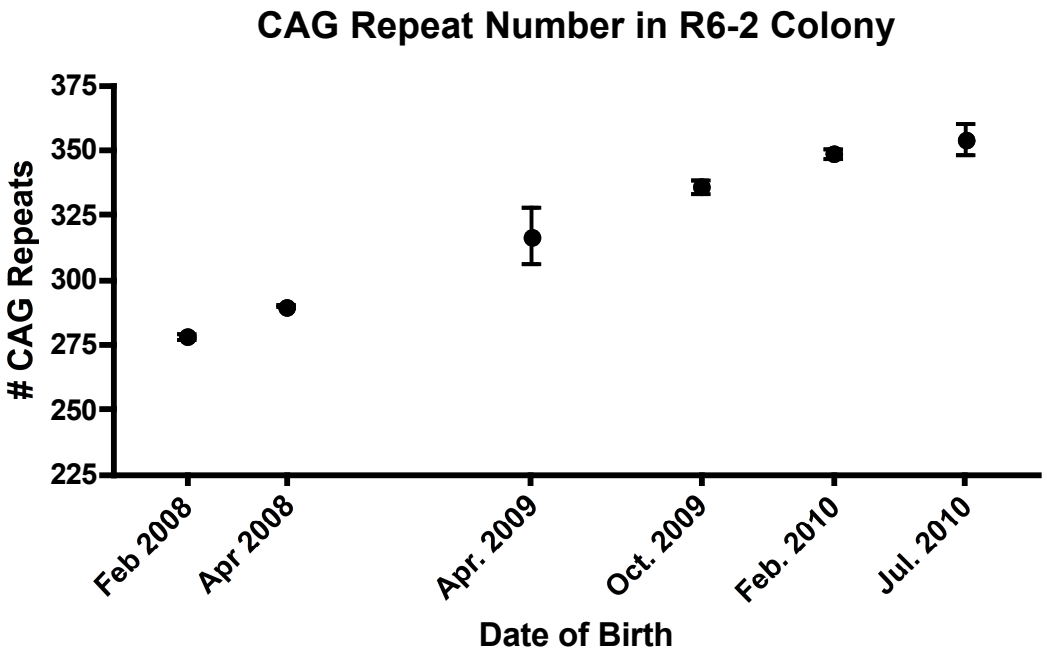

Figure 11: CAG repeat sizing in R6-2 colony. Tail clips from R6-2 mice born at different points in the colony were sent to Laragen Inc. for CAG repeat sizing. Repeats have expanded by nearly 100 repeats since colony originated.

YAC128 Aggression

Over the course of the longitudinal behavioral studies in the YAC128 lines, we observed an increased incidence of littermate fighting in the males in the D2 TRAP line. Severe fights occurred in nearly half of the cages of males being aged for the study. Thus, we decided to separate and single-house all males. Because social isolation can have a profound affect on behavior (Crawley 2000), we placed an ovarectomized female (to prevent breeding), with each male. This phenotype was specific for the D2 TRAP line, but for consistency, we also separated D1 TRAP males as well. This phenotype was specific to the YAC line, as we never observed this phenotype in the R6-2 mice but may be due to strain differences, as we have not yet tested whether the aggression was predominant in mice of any particular genotype.

Discussion

Human patients with Huntington's Disease typically live several decades of normal life before showing any symptoms of their disease. This period of normalcy is both a blessing and a curse for these patients: on the one hand, they can live disease-free for many years, but on the other hand, the late onset of symptoms means that the disease is often passed to the next generation. The two HD mouse models chosen for this study are imperfect reflections of the full disease state they were designed to mirror; however, these models both share with human HD a period of normal behavior that precedes symptom onset. This shared characteristic is not trivial: it suggests that to a large degree, normal development of the nervous system has occurred and that accumulation of some form of toxic damage must happen to create the behavioral syndrome.

In HD patients, the appearance of symptoms is often experienced as abrupt: one day a patient will fall down a flight of stairs, but the cellular pathology has most likely burned slowly for many years before this day of onset. Prospective imaging studies of patients at risk for developing HD demonstrates that there are volumetric changes in the striatum and cortex that precede overt symptom development by years (Tabrizi, Scahill et al. 2010). Likewise in the mice, many biochemical changes have been shown to take place before symptom onset.

Therapeutic interventions for HD have the best chance to be viable if they target changes that occur early in the disease course. One hypothesis about disease progression in HD is that the disease begins with an early insult or set of insults caused directly by the mutant htt (*mhtt*), which are then followed by a series of secondary and tertiary effects as the cell attempts to compensate to its stressed state (for review, (Cha 2007)). But to isolate these early insults, it would be necessary to harvest the gene expression profile of the MSNs before and after the initial insults occur.

Since there is no *a priori* way to determine the correct time to harvest mRNAs to identify these primary insults, and because this time most likely varies between HD models and among strains, the development of behavioral symptoms informed the timepoints chosen for mRNA collection. There were several reasons to justify this choice. First, by the time of symptom onset, sufficient changes should have occurred within MSNs to be detectable by molecular assays. Second, changes that are reflected by behavioral symptoms are likely to be relevant to human disease. Third, correlations with a behavioral phenotype would allow for future experiments to link candidate genes causatively to the phenotype. Thus, an mRNA collection timepoint before and after behavioral symptoms emerge were

chosen to reveal early, relevant pathological changes within these neurons.

Because we introduced a new transgene into the HD mouse models and changed the mouse strain background upon which they were characterized, we re-tested their behavior, in order to find the time of symptom onset in the mice.

The R6-2 model exhibited a robust behavioral phenotype with an onset of approximately 9 weeks in the open field and 12 weeks on the rotarod. The mice steadily declined in health, becoming moribund and cachetic by 5-6 months of age and dying soon after. This phenotype follows a similar course to the R6-2 on the B6/CBA background; it just takes approximately twice as long to develop. Our results largely agree with those of Menalled who also characterized the R6-2 mice on the C57Bl/6 background; however, they found that females were slightly more susceptible to disease, with open field deficits at 6 weeks. In our colony, females typically showed a less severe phenotype and lived longer than males (data not shown).

In agreement to the findings of other groups, we have found a constant expansion of the number of CAG repeats in our R6-2 colony over time. Similar to the results in Dragatsis et al. and Morton et al, we have seen a paradoxical amelioration of the phenotype with this CAG expansion. Whereas R6-2 mice from early generations in the

colony would die at approximately 5-6 months of age, R6-2 mice born 2 years later could live up to 1 year of age or longer (Morton, Glynn et al. 2009); (Dragatsis, Goldowitz et al. 2009). As suggested by both of these groups, this delay in phenotype onset may result from a difference in the ability of *mhtt* with very long polyglutamine repeats to traffic to the nucleus, where it exerts some of its deleterious effects.

The YAC128 model exhibits a late onset phenotype that exhibits more variability between individuals. We aged two cohorts of mice and found that, in the open field, the hypokinesis of the model only became statistically significant at 13 months and only in the D1 TRAP background. The YAC D2 TRAP mice did not exhibit hypokinesis even as late as 23 months (data not shown). On the rotarod, we observed a statistically significant constant deficit in the D1 TRAP background beginning at 15 weeks of age: in the D2 TRAP line, a similar pattern was observed, but the repeated measures ANOVA test failed to reach significance ($p=.08$), perhaps owing to the premature death of three of the D2 TRAP mice prior to the completion of the study. The CAG repeats were stable in the YAC128 line.

Our results agree with the phenotype in the published literature with the exception of the subtle hyperkinesis published in Slow et al., although Menalled et al. also

failed to reproduce this result (Menalled, El-Khodor et al. 2009). The variability of the behavior in these mice may be due to their hybrid background, but this complication was unavoidable, as the YAC128 phenotype on the C57Bl/6 phenotype is almost completely silent (Van Raamsdonk, Metzler et al. 2007; Menalled, El-Khodor et al.). The basis of these strain modifier effects would be interesting to unravel in future studies.

Section 2: RNA collection and Microarray Analysis

Background

Improvements to the TRAP Protocol

Once the behavioral decline of the models had been mapped, we began harvesting RNA from both D1 and D2 TRAP animals. When this project began, we used the co-immunoprecipitation protocol published in Heiman et al. 2008. Using this version of the TRAP methodology, it was necessary to pool groups of 8 animals to achieve a sufficient yield for subsequent amplification and hybridization to microarrays. The large number of animals required for a single replicate made longitudinal aging studies very challenging, as the R6-2 model has very small litters and the YAC128 line, as mentioned previously, is prone to aggression and fighting. Many of these males needed to be single-housed with ovarectomized females, and the numbers of animals required for the study quickly became space and cost limiting. Additionally, due to the inherent variability of age-related phenotypes, pooling individuals risks diluting out otherwise statistically significant changes occurring at the individual level.

Fortunately, during the course of this study, Dr. Myriam Heiman continued to make improvements to the TRAP technique. By substituting Protein L, an immunoglobulin-binding protein produced by *Peptostreptococcus*, for the

Protein G that had been used in the original protocol, and introducing a blocking step with BSA, signal-to-noise ratio was greatly enhanced (see Figure 12). As a result, the immunoprecipitation reaction could occur for much longer, allowing for higher yields, and analysis of translational profiles for individual animals. The possibility of single-animal analysis allowed for larger sample sizes, reducing noise in the array data, and for the inclusion of timepoints far later in the disease process than would otherwise have been possible.

In selecting the timepoints for RNA harvest, we wanted to start as early in the disease process as possible, particularly for the R6-2 line, which has a rapid-onset phenotype. We chose to harvest from 3-4 week old mice, as we had not identified any behavioral deficits in the mice at this age. We also harvested animals at the post-symptomatic timepoint of 12 weeks and at an intermediate timepoint of 8 weeks. For a complete list of harvested timepoints, with IP protocol used and downstream applications tested, see Table 3.

For the YAC128 mice, we harvested one cohort of mice at 13 weeks, the period during which we had initially observed hyperkinesis. We also harvested mice at 13 months, when the hypokinesis in the D1 TRAP line became significant. We aged the remaining mice and harvested them

at 23 months. For a full detailed listing of all cohorts harvested see Table 3.

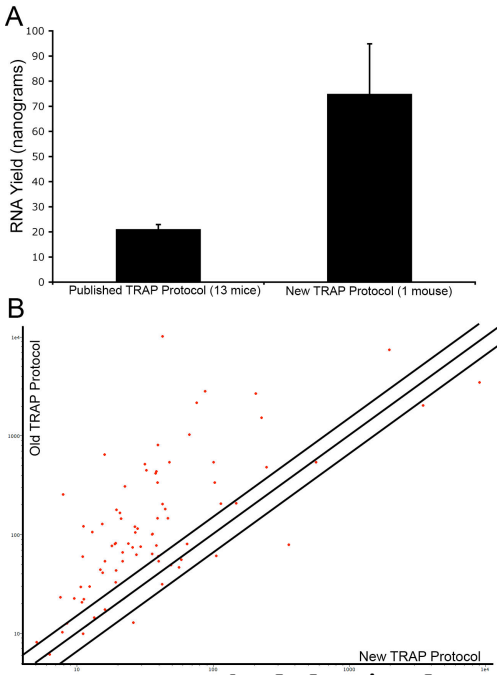

Figure 12. TRAP methodological improvements. A. Average RNA yield from D1-expressing MSNs, using our published and newly refined TRAP protocol (± S.D.). 13 mice were used in the previous protocol, compared to 1 mouse with the new protocol. **B.** The expression values of astrocyte-enriched genes (Cahoy, Emery et al. 2008) (red dots; should be background signal in our purifications) are compared in our new protocol TRAP D1 samples (X-axis) versus our old protocol TRAP D1 samples (Y-axis). Middle line represents equal expression; lines to each side represent 1.5-fold enrichment.

Table 3: Summary of IP timepoints collected, with protocol and downstream application. CAG repeats are included when available.

Model	Cell-Type	Age	Gender	IP Protocol	Number of animals	Amplification method	Analysis used	CAG repeats
R6-2	D1	4 weeks	Mixed	Pooled	3 groups of n= 8 mice	Affymetrix Two cycle	Array	
R6-2	D2	4 weeks	Mixed	Pooled	3 groups of n=8 mice	Affymetrix Two-cycle	Array	
R6-2	D1	4 weeks	Mixed	Pooled	2 groups n=5	NuGen WT-Ovation	qPCR	
R6-2	D2	4 weeks	Mixed	Pooled	1 group n=5	NuGen WT-Ovation	qPCR	
R6-2	D2	12 weeks	Mixed	Pooled	3 groups; n=10 (2)	Affymetrix, Two cycle	Array	
R6-2	D2	14 weeks	Mixed	Pooled	1 group n=6	NuGen WT-Ovation	qPCR	
R6-2	D1	3 weeks	Male	Single	R6-2 D1 n=8, WT D1 n=6, WT D2, n=5	NuGen Ovation-Pico	Array, qPCR	339 (could not recover enough DNA for most samples)
R6-2	D2	3 weeks	Male	Single	R6-2 D2 n=4; WT D2, n=5	NuGen Ovation-Pico	Array, qPCR	327-343
R6-2	D2	4.5 weeks	Male	Single	n=3	NuGen Ovation-Pico	qPCR	341-364
R6-2	D1	8 weeks	Male	Single	n=4	NuGen Ovation-Pico	Array	347-356
R6-2	D2	8 weeks	Male	Single	n=4	NuGen Ovation-Pico	Array	341-353
R6-2	D1	13 weeks	Male	Single	n=3	NuGen Ovation-Pico	Array	328-367
R6-2	D2	13 weeks	Male	Single	n=3	NuGen Ovation-Pico	Array	302-315
R6-2	D1	14 weeks	Mixed	Single	n=10	Not yet Amplified		
YAC128	D1	13 weeks	Mixed	Pooled	3 groups of n=8 mice	Affymetrix Two-cycle	Array	
YAC128	D2	13 weeks	Mixed	Pooled	3 groups of n=8 mice	Affymetrix Two-cycle (on different days)	Array	
YAC128	D1	10 month	Male	Single	N=6	Not yet Amplified		
YAC128	D2	10 month	Male	Single	n=6	Not yet Amplified		
YAC128	D1	13 months	Male and Female, separate	Single	WT D1 M n=5;YAC D1 M n=4; WT D1 F n=6; YAC D1 F n=6	Affymetrix Two-cycle AND NuGEN Ovation Pico (qPCR)	Array, qPCR	101 and 127
YAC128	D2	13 months	Male and Female, separate	Single	WT D2 M n=5; YAC D2 M n=5; WT D2 F n=6; YAC D2 F n=6	Affymetrix Two Cycle (array) AND NuGEN Ovation Pico (qPCR)	Array. qPCR	101 and 127
YAC128	D1	19.5 month	Male	Single	N=4	NuGen Ovation-Pico	qPCR	

YAC128	D2	19.5 month	Male	Single	N=4	NuGen Ovation-Pico	qPCR	
YAC128	D1	23 month	Male	Single	n=3	NuGen Ovation-Pico	Array, qPCR	101 and 127
YAC128	D2	23 month	Male	Single	n=3	NuGen Ovation-Pico	Array, qPCR	101 and 127

Results:

The RNA yield from striatopallidal neurons but not striatonigral neurons decreases over time in R6-2 model

One observation that we made prior to microarray analysis was that the relative amount of RNA that we could immunoprecipitate from individual mice declined with age in the R6-2 D2 TRAP line. While there was no significant difference in the amount of RNA collected from the 3-week-old R6-2 cohort or age-matched controls, there was a six-fold decrease in the amount of RNA harvested on average from 12-week-old striatopallidal cells (Student's t-test, p=.003 see Figure 13). This decline was not observed in the R6-2 D1 TRAP line or in the YAC model (data not shown).

To investigate the mechanism of this decline, we verified that there were no changes in copy number of the TRAP transgene at the DNA level using qPCR (data not shown). Because Drd2 expression is known to decrease in the R6-2 model and because the D2 TRAP promoter is driven by the Drd2 promoter, we next measured changes in the expression of the transgene at the RNA level, using qPCR from the amplified mRNAs that had been immunoprecipitated. At the RNA level, we saw differences of slightly more than two-fold at 14 weeks in D2 cells. This effect was age-dependent, as no difference was observed at 4 weeks (qPCR from pooled sample; see summary table). Finally, at the protein level, we found a dramatic decrease—a near absence of transgene expresed—in the amount of GFP detected in the

striatum by Western blot in a 6-month-old end-stage R6-2 D2 TRAP animal (data not shown). This decrease in Drd2 expression could reflect a general loss of D2 cell identity or a specific downregulation of dopamine signaling pathways in this cell type.

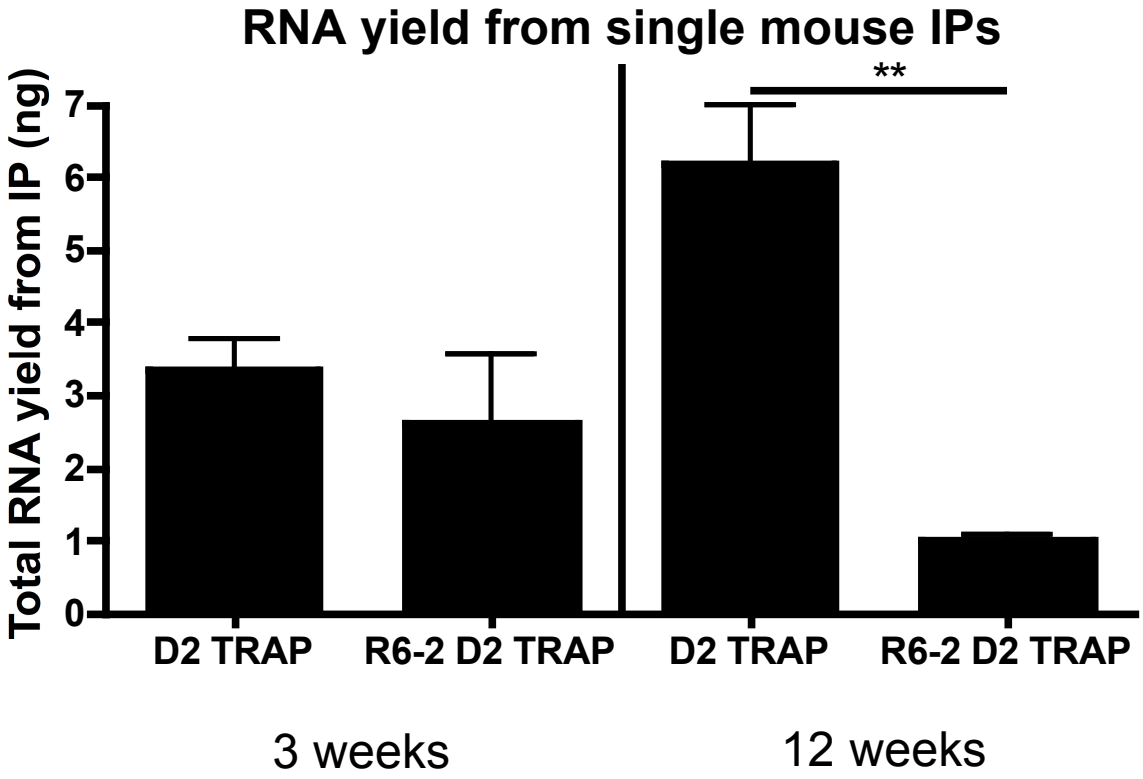

Figure 13: RNA yield decreases in R6-2 D2 TRAP mice over time. RNA was co-immunoprecipitated from single R6-2 D2 TRAP mice and D2 TRAP littermate controls. At 12 weeks, RNA yield in the R6-2 striatum was significantly decreased compared to controls (Student's Two-tailed t-test, p=.003). Yield was measured using Invitrogen Quant-It Ribogreen reagent.

Array results recapitulate known changes from the literature

In order to confirm that we had indeed harvested cell-type specific messages from our animals, all groups were first analyzed for the expression of known markers for striatonigral and striatopallidal MSNs. In all cases, D1 and D2 samples cluster separately upon Principal Components Analysis (PCA) (data not shown). We then examined the expression of known D1 and D2 markers in the wild-type samples (HD groups were excluded from this analysis, as these markers are known to decrease at later stages of the disease). WT D2 samples were enriched for known striatopallidal markers: Drd2 (63-116 fold), Gpr6 (25-50-fold), Adora2a (41-fold), and Penk (7.2-fold); WT D1 samples were enriched for Drd1a (11 fold); Pdyn (15-fold), and Eya1 (50-fold). These values are consistent with previous studies performed by other members of the laboratory (Heiman, Schaefer et al. 2008).

We next wanted to see whether our data from the HD models recapitulated any known changes from the literature. Phosphodiesterase10a (Pde10a) has been shown to decrease by ~3 fold in late-stage R6-2 mice (Hu, McCaw et al. 2004); (Hebb, Robertson et al. 2004). In the R6-2 12 week timepoint, which is a symptomatic timepoint, Pde10a was decreased by ~6.5 in D2 cells and 1.75 in D1 MSNs. Preproenkephalin (Cahoy, Emery et al.), which has been found to be downregulated 2-fold in the R6-2 B6/CBA line

was downregulated by 1.7 fold in D2 cells and 1.5 fold in D1 cells at the 12 week timepoint.

To address this question more comprehensively, cell-type specific data sets were compared with microarray data files from whole striatum of 12 week-old R6-2 B6/CBA mice and controls from (Kuhn, Goldstein et al. 2007). Microarray .CEL files were downloaded from the Gene Expression Omnibus Database (www.ncbi.nlm.nih.gov/**geo**/) and were analyzed in parallel with R6-2 12 week C57Bl6/J D1 and D2 MSN changes. There were 51 gene expression changes of fold change > 1.5 and $p<.05$ present in all three datasets. Of these, 96% changed in the same direction, indicating a high concordance with previous results. The two genes which were not concordant were Chdh and Abcc12. The former was found to be upregulated 1.8 fold in whole striatum in the Kuhn data set: in our data, it was 3 fold up-regulated in D2 cells and 1.7 fold down-regulated in D1 cells. It is possible that the average of the D1 and D2 fold changes would lead to an overall fold change of 1.8 up-regulation. For Abcc12, the down-regulation of 1.8-fold in whole striatum is not easily explained by a combination of 2-fold up in D1 cells and 1.6 fold down in D2 cells, but it is possible that changes in expression level of this protein in the glia could help explain the observed discrepancy.

There were many genes that were found in the Kuhn et al. study that were not found in either of the D1 or D2

changes in our data sets. Pathway analysis of these changes using the Ingenuity Pathway Analysis algorithm yields highest significance in pathways of G-protein coupled receptor signaling, calcium signaling, and glutamate receptor signaling. These pathways are driven by the loss of several key genes, including known MSN markers Drd1 and Adora2a, as well as non-neuronal genes such as Slc1a2. The discrepancies are due to differences in disease progression on the two strain backgrounds — 12 weeks on the B6/CBA background from the Kuhn study is far more advanced in disease progression that our mice on the C57B/6J background, as well as the inclusion of changes in non-neuronal cell types in the whole striatum Kuhn study.

For the YAC128 mice, several gene changes from the literature were confirmed in the datasets. Three of the four changes confirmed by qPCR identified in Becanovic at the 24 month time point—Wilms Tumor 1 (WT1), DNA-damage induced transcript 4-like (Ddit4l), Gsg1l—are changed in D1 MSNs at 23 months. A similar GEO parallel analysis with datasets from Becanovic et al. for the YAC128 13 month timepoint showed less overlap: only 5 gene changes were present in all sets. But 100% of the gene changes identified in Becanovic et al. shared directional concordance with the data from our results.

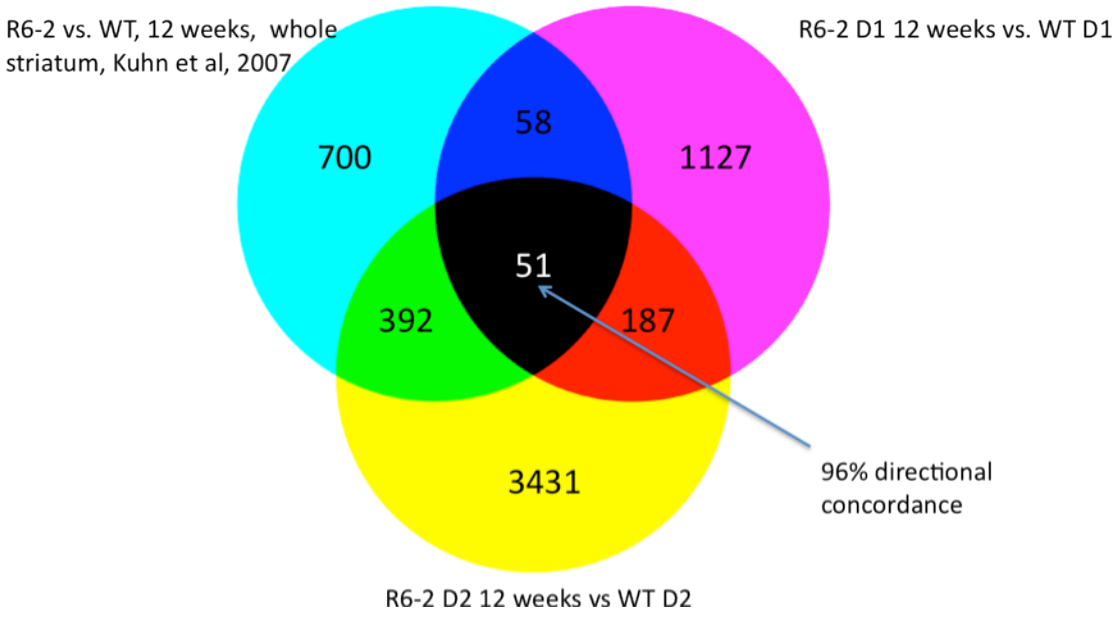

Figure 14: Comparison of cell-type specific changes with microarray datasets downloaded from the Gene Omnibus Database. .CEL files from total striatum of R6-2 12 week mice from Kuhn et al., 2007 were downloaded from GEO and analyzed together in Genespring with data from R6-2 12 week D1 and D2 BACTRAP data. Overlapping gene changes are shown.

The magnitude of gene expression changes correlates with progressive behavioral phenotype

In both the R6-2 and YAC128 models, the number of genes that are differentially translated increases with time. This change happens dramatically in D2 MSNs in the R6-2 model between 4 and 12 weeks of age when symptom-onset occurs. During this period, the number of gene changes increases from 156 probesets at 4 weeks to 5913 at 12 weeks (f.c.>1.5 and p<.05; see Figure 15 for scatter plots of the data). In the YAC128 model, in D2 MSNs, there were 183 gene changes at 13 months of age, and 538 changes by 23 months. (For these comparisons, sample sizes were kept constant by randomly selecting 3 replicates from the YAC128 13 month group; this adjustment was necessary as larger sample sizes reduce noise in the data, and this can lower the number of observed changes).

Comparisons of D1 and D2 changes within any one timepoint revealed many more differences than similarities. At 3 weeks of age in the R6-2 mice, there were 584 gene changes in R6-2 D1 MSNs compared to WT D1 MSNs and 781 changes in D2 MSNs at this stringency. Surprisingly, only 22 of these changes overlap (see Figure 16 for tables of changes with overlap). Similarly, at 8 weeks of age, there were 572 gene changes in D1 cells, 716 changes in D2 cells, with 34 overlapping changes. By the 12 week timepoint, many more changes have occurred in both cell types, with 1423 changes in D1 cells and 4061 changes in D2 cells, with

238 overlapping changes (all listed results have f.c.>1.5 and p<.05, without multiple testing corrections). These results indicate that the toxic effects of *mhtt* are progressive and differential between D1 and D2 subtypes, with the greater changes occurring in D2 MSNs.

While there were fewer translational changes observed in the YAC128 model at all times tested, the number of overlapping gene changes between D1 and D2 cells was similar. At 13 months of age, there were 139 changes observed in D1 cells, 69 in D2 cells, and 22 overlapping changes. At 23 months, there were 590 changes in D1 cells, 538 in D2 cells, and 25 overlapping gene changes (all lists f.c.>1.5; p<.05). Thus, the striking differences observed in the R6-2 model are borne out in miniature in the milder YAC128 model. However, on the single gene level, there are few overlapping changes between models at the time points tested and notably more changes in D1 cells at early timepoints.

An important caveat regarding these numbers is that they do not factor in correction for multiple testing. Microarrays allow the parallel interrogation of thousands of probesets at one time. While this powerful tool can provide a snapshot of all genes expressed at a given time, the large number of statistical tests asked at one time raises the likelihood of false-positive tests. In the most stringent analyses of microarray data, the p-values for

each statistically significant gene need to be adjusted by the number of comparisons made. There are several different methods for making this correction – the results from Benjamini-Hochberg FDR, one of the more commonly used multiple testing corrections, is shown in Table 4. For most of the comparisons made, no genes were found to be statistically significant after multiple testing correction. This result is most likely due to the small sample sizes – in the YAC 13 month timepoint, which had the largest sample sizes (see Table 3), there are several genes that remain statistically significant after multiple testing corrections. Because so few genes came through with multiple testing corrections in the other experiments, however, the remainder of the analysis was performed without the correction. The risk of false positive results increases without the correction, but as the microarrays were being used a screening tool to find candidates for further analysis, the less stringent filtering was used.

Experimental Comparison	# genes with fold change >1.5, p<.05 without multiple testing correction	# genes with fold change >1.5, p<.05 WITH Benjamini-Hochberg correction
3 weeks R6-2 D1 vs. D1 WT	594	0
3 weeks R6-2 D2 vs. D2 WT	781	0
8 weeks R6-2 D1 vs. D1 WT	572	0
8 weeks R6-2 D2 vs. D2 WT	716	0
12 weeks R6-2 D1 vs. D1 WT	1423	0
12 weeks R6-2 D2 vs. D2 WT	4061	637
13 month YAC D1 vs. D1 WT	139	120
13 month YAC D2 vs. D2 WT	69	32
23 month YAC D1 vs. D1 WT	590	1
23 month YAC D2 vs. D2 WT	538	0

Table 4: Number of genes that remain statistically significant after Benjamini-Hochberg FDR multiple testing correction, using fold change > 1.5 and p-value < .05.

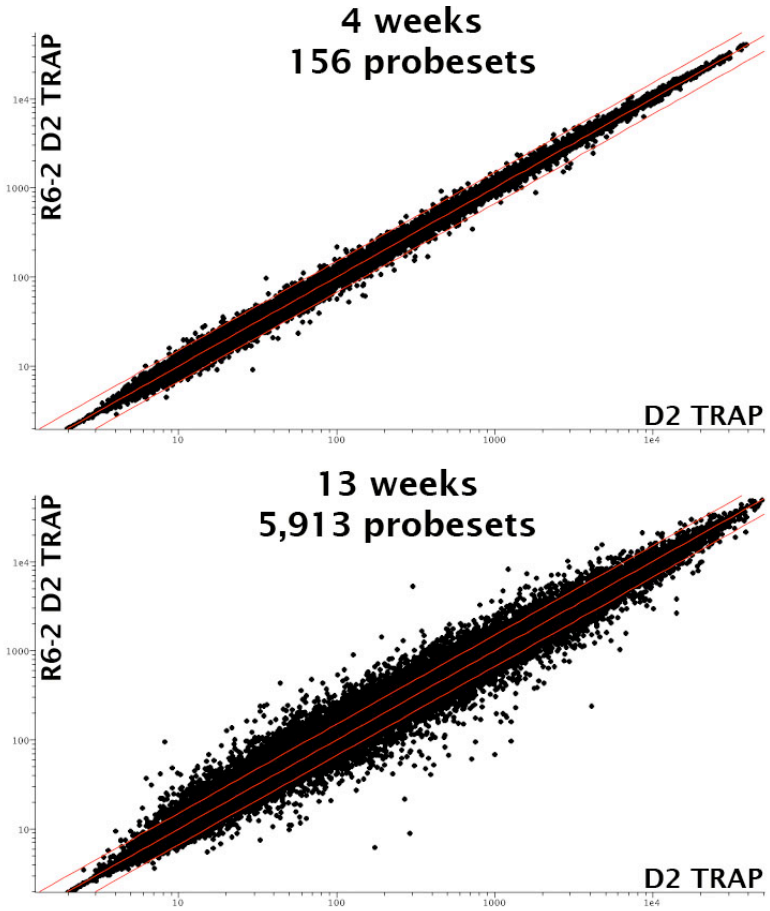

Figure 15: Gene expression scatter plots for R6-2 striatopallidal neurons (Top Panel) Normalized expression values from Affymetrix Mouse Genome 430 2.0 arrays are plotted for 4-week old R6-2 D2 TRAP mice (y-axis) and 4-week-old D2 TRAP littermate controls (x-axis). The middle diagonal line represents probe sets with equal expression in both groups, and the outer diagonal lines delineate probe sets with 1.5 fold difference in either group. Total number of probesets with greater or less than 1.5 fold difference between groups is indicated. (Bottom Panel) Same as in above for 13-week old mice.

3 week R6-2 D1 vs D1 WT gene changes fold change >1.5, p<.05 594	3 week R6-2 D2 vs D2 WT gene changes fold change >1.5, p<.05 781	Overlap 22
8 week R6-2 D1 vs D1 WT gene changes fold change >1.5, p<.05 572	8 week R6-2 D2 vs D2 WT gene changes fold change >1.5, p<.05 716	Overlap 34
12 week R6-2 D1 vs D1 WT gene changes fold change >1.5, p<.05 1423	12 week R6-2 D2 vs D2 WT gene changes fold change >1.5, p<.05 4061	Overlap 238
13 month YAC D1 vs D1 WT gene changes fold change >1.5, p<.05 139	13 month YAC D2 vs D2 WT gene changes fold change >1.5, p<.05 69	Overlap 22
23 month YAC D1 vs D1 WT gene changes fold change >1.5, p<.05 590	23 month YAC D2 vs D2 WT gene changes fold change >1.5, p<.05 538	Overlap 25

Figure 16: Comparison of single-gene changes shared between cell-types at different time points in the R6-2 and YAC128 models. All data represent lists generated at fold change >1.5, p<.05, with no multiple testing corrections.

Pathway analysis reveals recurring patterns of cellular dysfunction

In order to gain a better functional understanding of the gene changes observed across different models, cell types, and time-points, we grouped the observed changes by Gene Ontology Analysis and analyzed the data using Ingenuity Pathway Analysis. Gene Ontology analysis groups genes according to known molecular function, biological process, and subcellular localization. In the R6-2 3 week time point, we found enrichment in GO pathways only in D2 MSNs. The analysis revealed that the changes were enriched in the cellular compartment of the nucleus (p=.005), where *mhtt* is known to exert toxic effects, and the biological pathways enriched for RNA processing, metabolism, and rRNA transcription (p=.01, .01, and .07 respectively). This last pathway is intriguing given a very recent paper showing that the overexpression of rRNA processing genes can suppress *mhtt* toxicity in yeast (Tauber, Miller-Fleming et al.), implicating broader dysfunction in translation very early in the pathology. At the R6-2 D2 12 week timepoint, there are many more GO terms represented, with the most stringently enriched pathways occurring in various forms of carbohydrate metabolism (see Appendix). There is a long literature regarding changes of metabolism and mitochondrial function in HD, beginning with the 3-nitropropionic acid pharmacological model of the disease, but it is unclear whether these changes are specific to the

toxic insult of *mhtt* or are more general indicators of cell stress. In the YAC model, many fewer GO changes were observed. There was no representation of GO terms in D2 cells at either the 13 or 23 month timepoints, and only 3 in the D1 YAC 13 month timepoint. These changes pertained to G-protein signaling, driven by increases in the expression of the G-proteins Gng4 and Gng5 in the D1 MSNs at both these times, but very little is known about the function of these genes.

To examine whether we could find any biological pathways that had a statistically significant enrichment in the datasets, we analyzed the gene changes using Ingenuity Pathway Analysis (IPA). IPA works by mapping gene changes to a library of canonical pathways obtained from reports of gene interactions in the literature. The ratio of the number of changes in a pathway to the total number of genes contained in a pathway is used to rank an order of the most to least enriched pathways in a dataset. A Fisher's exact t-test is then used to determine the likelihood that the pattern of enrichment in each pathway could be due to chance alone.

Several pathways emerged consistently at different timepoints in the analysis, and some pathways appeared in both models. A summary table with the most commonly represented pathways is listed in Table 4. Some of these pathways, such as PPAR activation (appearing 6 times), IGF-

1 signaling (5 times), and DNA damage pathways (4 times, combining p53 and ATM signaling) have been previously implicated in HD. We took this enrichment of previously described changes as a further validation of our approach. In addition to these known pathways, our analysis uncovered several pathways previously unpublished with respect to Huntington's Disease.

Ingenuity Canonical Pathways	Appearances
Axonal Guidance Signaling	6
*PPARα/RXRα Activation	6
*IGF-1 Signaling	5
*Role of NFAT in Cardiac Hypertrophy	4
RANK Signaling in Osteoclasts	4
*Molecular Mechanisms of Cancer	4
*Inositol Phosphate Metabolism	3
Relaxin Signaling	3
Thrombin Signaling	3
CXCR4 Signaling	3
4-1BB Signaling in T Lymphocytes	3
*Protein Kinase A Signaling	3
*NRF2-mediated Oxidative Stress Response	3
Integrin Signaling	3
Breast Cancer Regulation by Stathmin1	2
*Nicotinate and Nicotinamide Metabolism	2
Ephrin Receptor Signaling	2
*Androgen Signaling	2
Sphingosine-1-phosphate Signaling	2
*Endoplasmic Reticulum Stress Pathway	2
*Type I Diabetes Mellitus Signaling	2
*ATM Signaling	2
*p53 Signaling	2
*Purine Metabolism	2
Chronic Myeloid Leukemia Signaling	2

*IL-1 Signaling	2
*cAMP-mediated Signaling	2
Small Cell Lung Cancer Signaling	2
CD27 Signaling in Lymphocytes	2
Cardiac Hypertrophy Signaling	2
*14-3-3-mediated Signaling	2
Semaphorin Signaling in Neurons	2
Germ Cell-Sertoli Cell Junction Signaling	2
Wnt/β-catenin Signaling	2
*Calcium Signaling	2
*Synaptic Long Term Potentiation	2
Glioma Signaling	2
RAR Activation	2
*Huntington's Disease Signaling	2
Leukocyte Extravasation Signaling	2
Notch Signaling	2
Aryl Hydrocarbon Receptor Signaling	2
Phospholipase C Signaling	2
LPS/IL-1 Mediated Inhibition of RXR Function	2
*GABA Receptor Signaling	2

Table 4: Pathway with multiple appearances in Top 15 pathways at different time-points

Gene lists (f.c.>1.5, p<.05) from all time points for both R6-2 and YAC128 models were analyzed with the Ingenuity Pathway Analysis algorithm. This program lists molecular pathways enriched in the datasets by testing how many genes in a pathway would be expected to change by chance alone. Pathways with multiple appearances in different models or at different times are listed in the table. Pathways that return hits when included in a PubMed search with “Huntington’s Disease” are marked with an asterisk.

Novel Pathway Changes from Cell-Type Specific Data

In analyzing the many pathway changes, we established a set of priorities for thinking about the data. First, because we were interested in cell-type specific changes, we looked for any pathways that contained changes in genes with known differences between D1 and D2 MSNs. Second, we looked for pathways that changed early in the time course of the disease—these changes could worsen with time, but they should be present before large number of secondary pathological effects. Third, we prioritized pathways that were shared at some point between models, as any model can have individual artifacts. Lastly, because D2 MSNs are more vulnerable than D1 MSNs, we preferred changes that occurred first in D2 cells and then later in D1 cells. These criteria were not meant as strict filters, but rather as guidelines for analyzing the data.

One pathway that fits many of these criteria is endoplasmic-reticulum (ER) stress signaling. ER stress is the top-ranked pathway in D2 MSNs in the R6-2 model. It is also enriched in YAC D1 MSNs at 14 weeks (p=.005). In the R6-2 3-week time point this enrichment is due to an increase in Eif2ak3 (f.c. 2.8, probeset 1449278_at), also known as PERK; where as in the YAC128 D1 gene set, it is driven by an increase in Hspa5 (f.c. 1.6; probeset 1427264_at). Both of these genes play critical roles in the regulation of this pathway (for review, see (Rutkowski

and Hegde)). These changes happen early in the pathological progression of the disease, before aggregates of mhtt are typically seen (typically 3 weeks in the cortex, 4-6 weeks in the striatum in the B6/CBA background). It is not immediately clear why *mhtt*, a cytosolic protein that aggregates both in the cytosol and in the nucleus would disrupts protein folding in the ER, but one possibility is that MSNs benefit from the chaperones induced by the unfolded protein response initiated by ER-stress. Another possibility is that misregulation of sphingolipid synthesis, (to be discussed in Section 3) which takes place in the ER, is causing this activation of ER stress. The yeast mutants Orm1 and Orm2, two proteins which regulate membrane biogenesis in yeast, exhibit abnormal sphingolipid profiles and constitutively upregulate the UPR (Han, Lone et al.).

Another pathway that is highly enriched in both models, which exhibits increasing enrichment with progression of phenotype is axonal guidance signaling. Axonal guidance signaling is the ninth top-ranked pathway in R6-2 D1 cells at 3 weeks, and the 16th pathway in D2 cells; by 12 weeks, it is the second most enriched pathway in both D1 and D2 cells. This pathway also makes several appearances in the YAC128 model, in D1 cells at 13 months and 23 months, where is the second-most enriched pathway. At many of these timepoints, various isoforms of

semaphorins, ephins, netrins, and slit proteins are changed. These proteins play canonical roles in the regulation of axonal growth cone guidance during development, but they have also recently been implicated through genome-wide association studies to Parkinson's Disease (for review, see (Lin, Lesnick et al. 2009)). It is not known whether this association is due to developmental abnormalities that occur many years before the degenerative disease is seen (i.e. mis-wiring patterns), or if there are synaptic remodeling events occurring in adulthood that use developmental pathway in different ways.

Another possible reason for observing the prevalence of axonal guidance signaling enrichment in our datasets is the loss of BDNF that occurs in HD mouse models. In HD, MSNs lose the trophic support of BDNF secreted from the cortex (Zuccato, Ciammola et al. 2001). BDNF exerts many roles on neurons, including the promotion of axon-branching (Cohen-Cory and Fraser 1995), which is mediated in cortical neurons by MKP-1 (Jeanneteau et al., 2010). MKP-1 is downregulated in D2 MSNs at the R6-2 12 week time point. The loss of BDNF-induced signaling might disturb axon guidance signaling pathways in the MSNs as a compensatory response, although a complete absence of BDNF seems to have a greater role to play in dendritic structure (Rauskolb, Zagrebelsky et al. 2010).

A third novel pathway is inositol phosphate metabolism. Inositol phosphate metabolism was ranked first in R6-2 D1 MSNs at 3 weeks and second in R6-2 D2 MSNs at the same time point. It is significantly enriched in D2 MSNs at the 8 week time point (p=.01), and it remains enriched in both cell types at 12 weeks. It is selectively enriched in D2 MSNs in the YAC128 model at 14 weeks. This pathway is intriguing given the important role that inositol 1,4,5 triphosphate plays as a second messenger in glutamatergic signaling, and the hypothesis that glutamatergic excitotoxicity might play an important role in HD pathology. One gene in this pathway that is oppositely regulated in D1 and D2 cells at this early timepoint is Ipmk (1.8 up in D1; 1.5 down in D2). Ipmk has been shown to play critical roles in nervous system development, as constitutive knockouts of this gene are embryonic lethal, displaying abnormal neural tube closure (Frederick, Mattiske et al. 2005). This gene is thought to participate in the generation of complex inositol second messengers.

Besides inositol metabolism, another lipid signaling pathway altered in the models was sphingolipid metabolism. S1P metabolism will be discussed in detail in Section 3. A comprehensive list of pathways found from the IPA analysis can be found in the Appendix.

Quantitative PCR confirms many cell-type specific changes

Microarrays allow for massively parallel interrogations of amplified cRNA. The large number of probes contained on each array, however, increases the probability of false positive results due to noise in probe hybridization, plate reading, or other experimental handling. As a result, it is standard practice to confirm gene changes of biological interest with another, independent methodology. We attempted to use immunohistochemistry (IHC) to detect differential cell-type specific changes at the protein level. However, due to limitations in the availability of commercial antibodies compatible with IHC, we could only test a small subset of targets and in all cases any cell-type specific change was obscured by high background signals in the tissue. We therefore turned instead to qPCR.

We chose to use Taqman Expression real-time PCR assays from Applied Biosystems for their wide availability and ease of use. In the R6-2 model, because so many genes change their expression at various points in the disease, several of the housekeeping genes typically used to normalize qPCR results, such as beta-actin or glyceraldehyde-3-phosphate dehydrogenase (GAPDH), cannot be used for normalization because their level of expression changes in late stage disease. Benn et al. characterized 12 candidate housekeeping genes from whole striatum in R6-2 at 15 weeks, a late timepoint in disease. In the striatum,

they found the least variation in Eif4a2 and Atp5b. We have used Eif4a2 as the reference gene for most of the studies, in both models.

We confirmed a range of genes at both low and high levels of expression from the arrays, and also focused upon particular genes and pathways of interest. Changes were confirmed with independent amplifications of mRNA, using a different amplification kit. In some instances when samples were available, changes were confirmed with independent biological replicates. A subset of confirmed changes is shown for the YAC 13 month timepoint (Figure 17), and a full list of confirmed and unconfirmed gene changes is available in the Appendix.

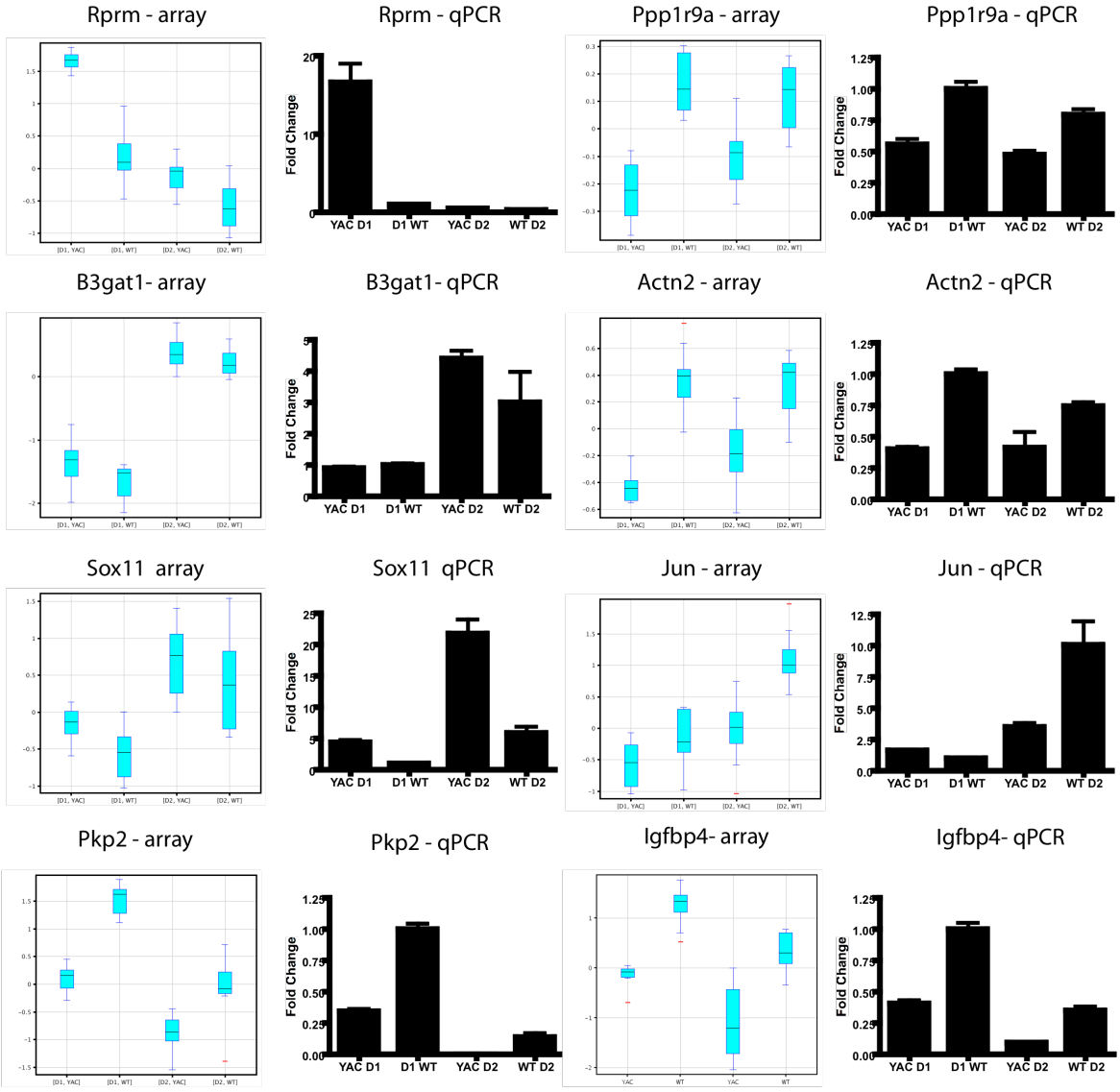

Figure 17: Confirmation of selected genes from YAC128 13 month time point by qPCR. Some of the most robust changes at the YAC128 13 month time point are compared by their expression on microarray (box-whisker graphs) and by qPCR (bar graphs). Experiments were performed using independent amplification methods on same biological samples, n=3-4 mice per group.

Discussion

For the first time, we have collected cell-type specific gene expression changes from vulnerable cell types in HD mouse models. Previous studies have attempted to track gene expression changes in HD models in whole tissue, which can obscure relevant gene expression changes in noise from interneurons, glia, and other cell types. By excluding messages from these other cell types, the TRAP technique allows for increased sensitivity in detecting cell-specific gene changes. Our results both confirm changes in pathways previously reported as implicated in HD pathogenesis, such as PPAR activation, IGF-1 signaling, and the p53 pathway, while also revealing changes in novel pathways, such as sphingosine-1-phosphate signaling, ER stress response, axonal guidance, and inositol phosphate metabolism, which may contribute to MSN vulnerability and warrant further investigation. Even within previously identified pathways, our analysis implicates novel genes, and the full publication of our microarray results in the Gene Expression Omnibus Database will serve as a resource for the HD community.

Our early observation that RNA yields from D2 MSNs decreased over time in the R6-2 model may reflect the selective vulnerability of this cell type in the model. Our data suggest that the downregulation of the D2 TRAP construct occurs at the transcriptional, and possibly,

post-transcriptional levels. It is known that transcription of the Drd2 gene is altered in the R6-2 model, so it is unsurprising that the D2 TRAP construct, which is under control of the Drd2 promoter would also be affected. At the timepoints we harvested, we did not see any reduction in the RNA yields from the D1 MSNs. Drd2 expression has been shown to be either mildly reduced (Xie, Hayden et al. 2010) or unchanged (Benn, Slow et al. 2007) in the YAC128 line. In agreement with these results, we did not see a loss in RNA yield in the YAC128 mice.

Our analysis of the microarray results indicates that the number of translational changes in striatonigral and striatopallidal cells increased with age in both models. This result fits with the model that *mhtt* exerts primary insults in cells which are further amplified by secondary compensatory changes as cells struggle to maintain homeostasis. For this reason, we chose to focus our analysis on gene expression changes from earlier time points in the disease process, as these changes are more likely to represent primary toxic insults of *mhtt*.

It is somewhat surprising that the number of changes common to D1 and D2 MSNs is as low as it is. At baseline, the two groups of neurons share 80% of their genes in common, but a very small percentage of total changes are shared between cell types at any one timepoint. The apparent discrepancy could be due to either biological

interference with genes that determine MSN identity, or to mathematical noise in the data. To test the latter hypothesis, we filtered all of the data sets with Benjamini-Hochberg multiple testing corrections. With this highest stringency filtering, only the YAC128 13-month cohort still had detectable changes, most likely because of its very large sample size (n=9 in the smallest group compared with an average of n=4 for the other time points). Without applying the highest stringency filter, 13% of the total changes overlap between the two cell types; with the stringency filter applied, that number remains 13%. This result suggests that the differences between the two cell types are unlikely to be an artifact of low stringency filters.

We used several tools to gain deeper biological insight into the function of the observed changes. Our pathway analysis returned many pathways previously implicated in HD pathogenesis. One of the two most commonly represented pathways, PPAR/RXR signaling (6 appearances), has received considerable attention in the HD community. One major regulator of this pathway, PPARGC1alpha, has been shown to be downregulated in HD knock-in mice, and overexpression of this protein can rescue some toxicity in an in vitro system (Cui, Jeong et al. 2006). Moreover, subsequent genetic analysis has identified the same gene as

modifier of age of onset in human patients (Weydt, Soyal et al. 2009).

A number of groups have also studied the role of the IGF-1 signaling pathway in HD. Humbert et al. have shown *in vitro* that activation of the IGF-1 pathway leads to an AKT-mediated reduction in nuclear inclusions (Humbert, Bryson et al. 2002). Pouladi has shown that the large weight gain present in the YAC128 model, which we have also observed, correlates to circulating plasma levels of IGF-1 and that perturbation of IGF-1 levels leads to a weight-decrease (Pouladi, Xie et al. 2010). We have seen in the arrays and confirmed by qPCR a downregulation in Igfbp4 in the YAC128 model, one of the most robust changes present in all timepoints tested. Interestingly, Gatchel et al. identified Igfbp5 as a misregulated gene in a screen to identify polyglutamine-induced changes between two spinocerebellar ataxias in the cerebellum (Gatchel and Zoghbi 2005). This downregulation of Igfbp4 that we have observed could be a striatal response to polyglutamine expression.

Thirdly, the high number of cancer and DNA-damage pathways fits with other studies in the HD field. One very recent study has shown that *mhtt* increases the number of double-strand breaks in DNA in the R6-2 striatum and also interferes with Ku70-mediated DNA repair (Enokido, Tamura et al.). Other groups have shown that mhtt binds to DNA

directly, changing its confirmation (Benn, Slow et al. 2007). Still other groups have demonstrated a major relationship between mhtt and p53 signaling. Mutant htt binds to p53, and more importantly, knockdown of p53 improves longevity in several HD mouse models (Bae, Xu et al. 2005).

Because of the greater likelihood of identifying primary pathogenic insults, we chose to focus our attention on the changes that occurred very early in the disease process. One pathway in particular, sphingolipid metabolism, caught our attention, and became the subject of further study, to be described in the next section.

Section 3: Sphingolipid Metabolism

Background

In preliminary studies, one of the most altered pathways in R6-2 mice at the presymptomatic timepoint was sphingolipid metabolism. This result was intriguing for several reasons. First, several groups, including ours, have recently described GPR6, a sphingosine-1-phosphate (S1P) receptor, as a highly specific marker for striatopallidal neurons (Lobo et. al, 2007; (Heiman, Schaefer et al. 2008). Second, in gene expression studies from human HD pathological specimens, GPR6 was found to be the third most significantly downregulated gene in human striatum, although it is not yet clear whether this loss of GPR6 is due to downregulation of GPR6 in striatopallidal neurons or death of GPR6-expressing striatopallidal neurons overall (Hodges, Strand et al. 2006). Third, S1P has recently been appreciated as an important signaling molecule in the nervous system, for neurite extension and retraction, neuronal survival, and neurotransmitter release (for review, see (Milstien, Gude et al. 2007); (Okada, Kajimoto et al. 2009)). Fourth, S1P has recently been implicated in neurodegenerative disease: in an Alzheimer's Disease study, GPR3, an S1P receptor, was found in an RNAi screen to increase the amounts of toxic ABeta produced in cell culture (Thathiah, Spittaels et al. 2009).

S1P is a bioactive lipid with diverse cellular functions both within and outside of the central nervous system. It has been implicated in numerous cellular processes, including proliferation, migration, and survival. S1P's functions have historically been understood in terms of signaling through a series of G-protein coupled receptors (GPCRs) S1PRs 1-5, although more recently, S1P has been suggested to exert direct intracellular effects in diverse processes including chromatin remodeling, mitochondrial function, and ubiquitination (Strub, 2010;) (Hait, Allegood et al. 2009); (Alvarez, Harikumar et al. 2010). In the nervous system, S1P is thought to regulate glutamatergic neurotransmission, and injection of S1P directly into the brain leads to catalepsy, suggesting possible direct modulation of striatopallidal signaling (Sim-Selley, Goforth et al. 2009). S1P is made from sphingosine by two different kinases, sphingosine kinase 1 (Sphk1) and sphingosine kinase 2 (Sphk2). It can be dephosphorylated by sphingosine-1-phosphate phosphatase (Sgpp1) or irreversibly cleaved to phosphoethanolamine by sphingosine-1-phosphate lyase (Sgpl1) (Maceyka, Milstien et al. 2007).

Together with ceramide, S1P is thought to regulate a cell-survival "rheostat," in which S1P exerts pro-survival effects and ceramide stimulates apoptosis (Hannun and Obeid). S1P, sphingosine, and ceramide can also be

converted to wide range of other more complex sphingolipid species (see Figure 18). There are a great diversity of complex sphingolipid species, but much is unknown about their individual biological functions. Some of these molecules, like S1P and ceramide, can influence protein-signaling pathways by binding to receptors or second messengers. Others may signal through still-unknown mechanisms. But these bioactive molecules also serve as building blocks for two classes of lipids that are known to play fundamental roles in the nervous system—sphingomyelin, a major component of the myelin sheath around neurons, and gangliosides, lipids for which defects in metabolism lead to a series of severe neurological disorders, including Tay-Sachs and Gaucher's Disease.

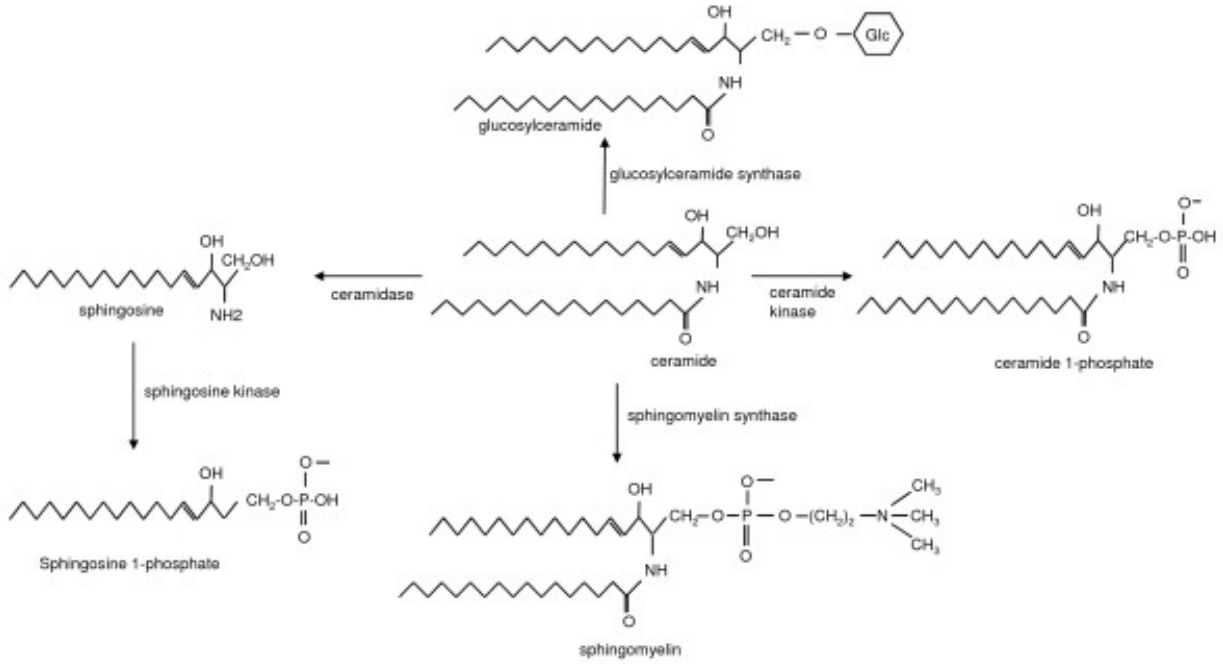

Figure 18 (Fuller et al 2010). Schematic representation of metabolic relationships between sphingolipid bases. Sphingosine can be created *de novo* from serine and palmitoyl CoA, or it can be made by cleavage of ceramide by ceramidase. Sphingosine can then in turn be phosphorylated by one of two sphingosine kinases to make sphingosine-1-phosphate (S1P). S1P can be reversibly dephosphorylated or it can be irreversibly metabolized by the enzyme Sgpl1.

Quantification of S1P and sphingoid bases in HD mouse models and post-mortem tissue

For all of the reasons above, the S1P pathway was chosen as a candidate pathway for further analysis. We attempted several different methods for measuring S1P in the R6-2 mice, including immunohistochemistry (Cosmo Bio), and ELISA (Echelon Biosciences). However, both of these assays failed quality control experiments. The antibody from Cosmo Bio was found to cross-react with sphingomyelin in a dot-blot assay (data not shown), and the colorimetric assay used in the Echelon Biosciences ELISA kit was inhibited by a component of the recommended homogenization buffer (data not shown). Thus, the highly related nature of these sphingolipid species makes study of individual components in the pathway difficult, and many reagents are not specific enough to detect changes in single molecules.

We therefore attempted to quantify S1P by mass spectrometry, the gold standard for detection and quantification of complex lipids. For these experiments we collaborated with Dr. Jeff Moore of Avanti Polar Lipids, who was involved in the establishment of protocols for the use of mass spectrometry for complex sphingolipid analysis. We analyzed striatal homogenates, normalized to total amounts of protein, from R6-2 C57Bl6/J mice and WT controls at 3, 6, and 24 weeks (n=3-5 animals for each group), as well as 6-week-old R6-2 B6/CBA mice and WT controls from the Jackson Laboratory (to control for CAG repeat

expansion) (n=5). There were statistically significant decreases in several complex sphingolipid species in the striatum. Most sphingolipids in mammals are 18 or 20 carbon chains, with differing placement of double bonds along the chain. This property affects the classification and naming of the species: thus, there are two known forms of S1P detectable by mass spec, differing in length by two carbons, and they each have a double bond on the first carbon, hence they are named d18:1 and d20:1 S1P. We observed changes in d:20:1 S1P (significant at 6 weeks and 24 weeks $p<.05$; $p<.005$ respectively). There were also statistically significant decreases in d18:1 sphingosine-1-phosphate, d18:0 sphinganine, d20:1 sphingosine, d18:0 sphinganine-1-phosphate, d20:0 sphinganine-1-phosphate and d20:1 sphinganine-1-phosphate, although at different time points. All statistically significant differences are displayed in Figure 19. There were no changes observed in any of the 25 ceramide species tested or in the other complex sphingolipids. There were no changes observed in the cerebellum from 6-week and 24-week-old R6-2 C57Bl6/J, with the exception of d:18:0 sphinganine, which was decreased by 40%, $p=.03$, and there were no changes observed from 6-month-old YAC128 mouse striatum or cerebellum.

We next asked whether levels of S1P would be decreased in post-mortem tissue from human patients with Huntington's Disease. We obtained one sample each of striatum and

cerebellum from an early stage HD case (Grade 2 on the Vonsattel neuropathological scale), a late stage HD case (Vonsattel Grade 4), and a control patient who had no known neurological history. We observed very large fluctuations in several complex lipids between HD cases and control. There were undetectable levels of d18:1 S1P in Grade 2 HD striatum, and then a large increase in the level of d18:1 S1P in Grade 4 HD post mortem tissue (Figure 20). This same pattern occurred with other lipid species, particularly with several of the ceramide moieties—sometimes with an order of magnitude difference (Figure 20). However, given the small sample size, it is difficult to make any conclusions from these observations. Future experiments will require larger sample sizes.

Figure 19: Summary of mass spectrometry quantification for complex sphingolipids in the R6-2 mouse striatum. Lipids are normalized to total protein in sample, as measured by BCA assay. All R6-2 mice are on C57Bl/6 background except "JAX" mice, which are maintained on B6/CBA background (see Introduction for details). **A.** d20:1 Sphingosine-1-phosphate is decreased in R6-2 striatum at 6 weeks in B6/CBA background (Students t-test p=.03) and at 24 weeks on C57Bl/6J background (p=.005), n=3-5 per group. **B.** d18:1 Sphinsogine-1-phosphate is decreased in R6-2 striatum on C57Bl/6 background at 6 weeks (Student's t-test p=.03). **C.** Mass spectrometric quantification of d20:1 Sphingosine, which is decreased at 6 weeks on B6/CBA background and at 24 weeks on C57Bl/6J (Students two-tailed t-test, p=.004 and p=.03). **D.** d18:0 sphingosine is decreased at 6 weeks in B6/CBA background (p=.03). **E.** d18:1 sphinganine-1-phosphate is decreased at 6 weeks in B6/CBA background (p=.01). **F.** d20:1 sphinganine-1-phosphate is decreased at 6 weeks on B6/CBA background (p=.01).

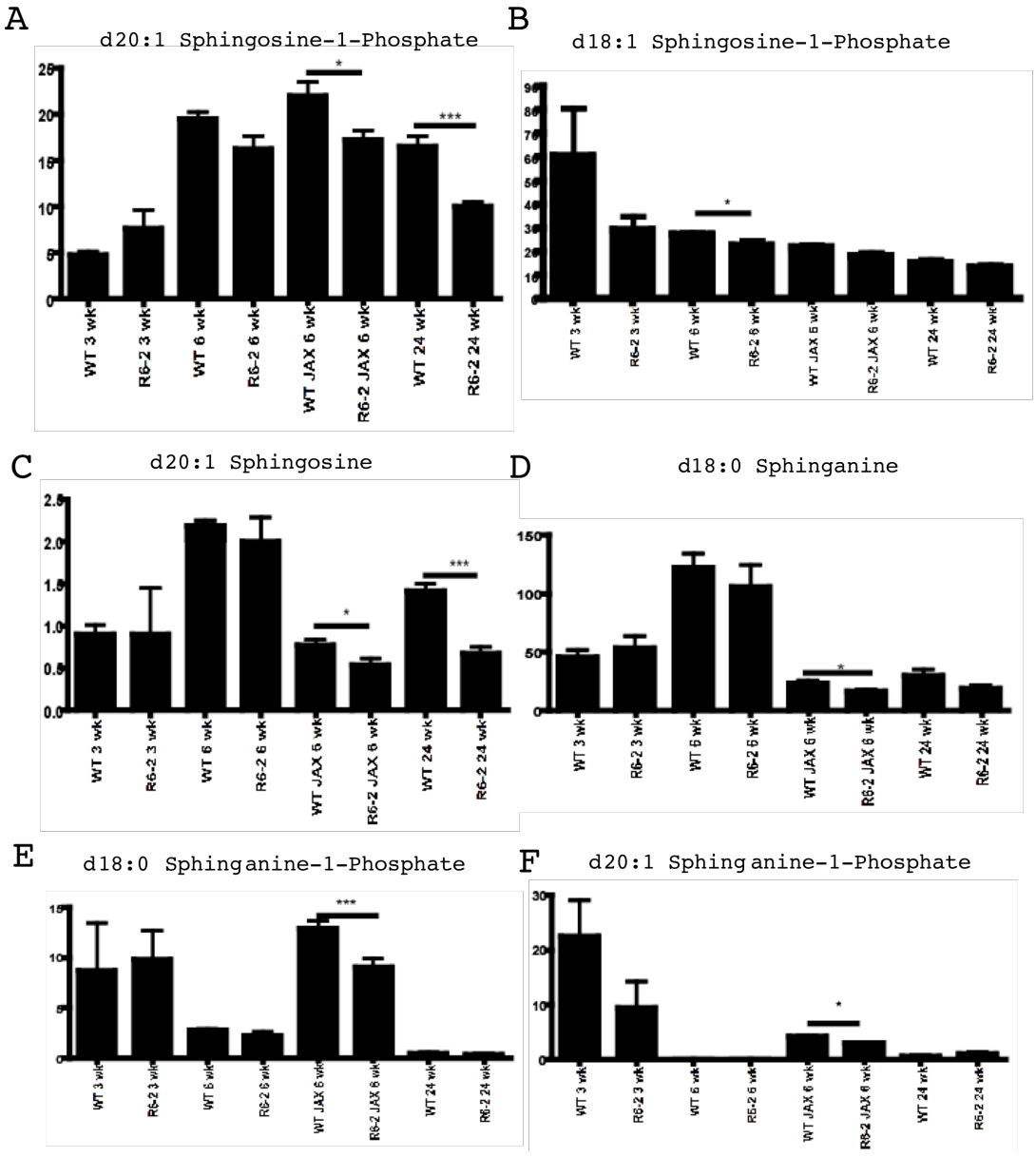
A
d20:1 Sphingosine-1-Phosphate
B
d18:1 Sphingosine-1-Phosphate
C
d20:1 Sphingosine
D
d18:0 Sphinganine
E
d18:0 Sphinganine-1-Phosphate
F
d20:1 Sphinganine-1-Phosphate
WT 3 wk
R6-2 3 wk
WT 6 wk
R6-2 6 wk
WT JAX 6 wk
R6-2 JAX 6 wk
WT 24 wk
R6-2 24 wk

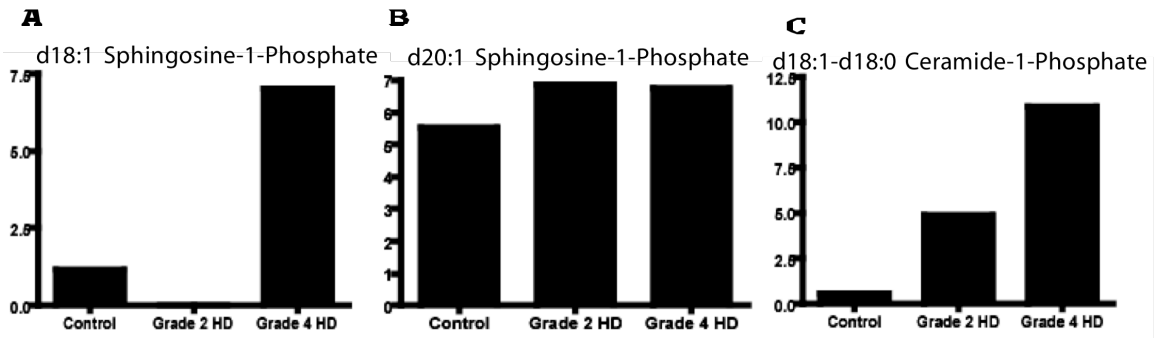

Figure 20: Preliminary mass spectrometric quantification of complex sphingolipids in human caudate. A pilot experiment to compare levels of complex sphingolipids and ceramides was conducted in human caudate from a control, Grade 2, and Grade 4 HD patient (n=1 per group). Levels of sphingosine-1-phosphate were variable, but there were large increases in the amounts of some complex ceramide moieties-at times, almost an order of magnitude.

Mechanism of Changes in S1P abundance

In the microarrays, Sgpl1 exhibited low, variable levels of expression, but it was increased at several timepoints in the R6-2 model and in both cell types. It was increased 1.3 fold in the 4-week R6-2 D2 pooled animals, 1.4 fold (in one probe) in the R6-2 3-week D1 cells, and 2-fold in R6-2 D1 cells at 12 weeks (data not shown). In contrast, Sphk2 was expressed at intermediate levels and was downregulated by 1.4 fold in both R6-2 D1 and D2 cells at 12 weeks compared to WT TRAP levels alone (data not shown). Sphk1 levels were very low and unchanged at all times and Sgpp1 did not change at any timepoint.

Although these results were variable, we attempted to investigate the changes by qPCR. At 3 weeks, in the R6-2 line, Sgpl1 expression was too low in any of the WT animals, either D1 (n=4) or D2 (n=4) to be detected by qPCR; however, in the R6-2 mice, Sgpl1 was present in 3/5 R6-2 D1 mice tested and 2/4 R6-2 D2 mice tested, at variable levels ranging from 7 cycles above Eif4a2 to 17 cycles. In the same animals, Sphk2 was decreased by 2-fold in D1 cells and 34-fold in D2 cells (Figure 21). Sphk1 was not detected in two separate assays.

Eight months later, however, in an independent cohort of R6-2 D2 TRAP 4.5 week animals, with a different number

of CAG repeats, expression levels of both Sgpl1 and Sphk2 were highly variable (data in qPCR supplemental table).

To settle this discrepancy, we attempted to investigate Sphk2 and Sgpl1 with *in situ* hybridization, an independent technique. Although *in situ* hybridization is less sensitive and less quantitative than qPCR, we reasoned that if the large differences observed were present, they would be detectable by the technique. In addition, because of the instability of the CAG repeats in the R6-2 colony, we performed the *in situ* experiment in R6-2 animals on the B6/CBA background from the Jackson Laboratory colony, where CAG repeats are monitored and maintained at constant levels through periodic resuscitation of the line from frozen embryos. Unfortunately, preliminary results from this study were inconclusive, as sense and anti-sense probes for both genes gave similar low-level patterns of expression.

While incomplete, these studies offer a preliminary hypothesis for the mechanism by which S1P levels might decrease in HD models, and possibly in HD patients, namely by transcriptional downregulation of the kinase that converts sphingosine to S1P and upregulation of the lyase that degrades S1P.

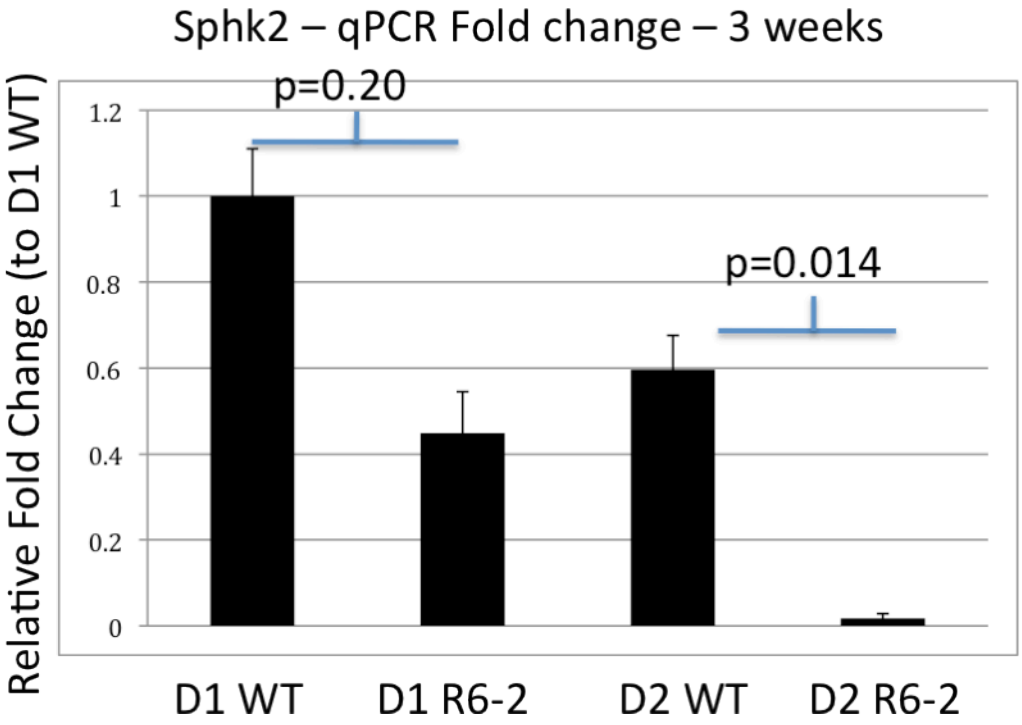

Figure 21: Sphk2 mRNA is downregulated in D2 MSNs in pre-symptomatic R6-2 mice. Quantitative PCR was performed on amplified immunoprecipitated mRNA from D1 or D2 MSNs. Sphk2 is statistically decreased in R6-2 D2 MSNs at 3 weeks of age. Data represents 4 technical replicates from n=3 biological replicates.

S1P exerts a modest pro-survival effect in striatal cell culture lines

To gain insight into the function of S1P in MSNs in Huntington's Disease, we turned to an *in vitro* model, the ST14A cell line (Cattaneo and Conti, 1998). The ST14A line was established by transducing rat embryonic striatal cells with a temperature sensitive allele of the large T40 antigen oncogene. At the permissive temperature of 33°C, these cells grow indefinitely, but when shifted to 39°C in serum-deprived conditions, the non-permissive temperature, the activity of the T40 antigen is reduced, and the cells differentiate into neuronal-like cells (expressing NeuN, Map2, and low levels of DARPP-32), and then die due to loss of growth factor stimulation. We received three lines of these cells: the parental ST14A line; the N548 line, which is stably transfected with the first 548 amino acids of *mhtt* with 128 CAG repeats; and the ST12.7 line, which places the same N548 transgene under the control of a Tet-on promoter, allowing the doxycycline-inducible control of the *mhtt* transgene (Rigamonti, Bauer et al. 2000); (Sipione, Rigamonti et al. 2002).

We performed a dose-response experiment with S1P in the ST12.7 cell line, with or without doxycycline. Cells were plated at high-density and grown for two days at 33°C days in serum-containing media in the presence or absence of doxycycline and with various concentrations of S1P. The

cells were then changed to serum-free media, to which the same concentrations of S1P were added, and then shifted to 39°C. In the absence of S1P, after temperature shift, cells quickly begin to die, and by 24 hours after shifting, there is 46.8% cell toxicity, as measured by an LDH release assay. In the presence of S1P at 2.5 uM, the cell toxicity was 37.2% (Figure 22). The result was statistically significant (2-WAY ANOVA, Bonferroni post-test $p<.001$). This effect was specific, as an identical protocol substituting S1P treatment with BDNF, a neurotrophin that is thought to contribute to MSN survival, failed to produce any statistically significant effect on survival (Figure 23). Importantly, ST14A cells express low levels of TrkB at both 33˚C and 39˚C (Cattaneo et al, 1998). BDNF exerts its cell-survival effects by signaling through the TrkB receptor. Thus, we cannot exclude that the lack of effect on cell survival by increasing BDNF concentrations might reflect the low TrkB expression in the cell line. This experiment also shows that the induction of mhtt by doxycycline does not accelerate cell death in this line ($p=.44$).

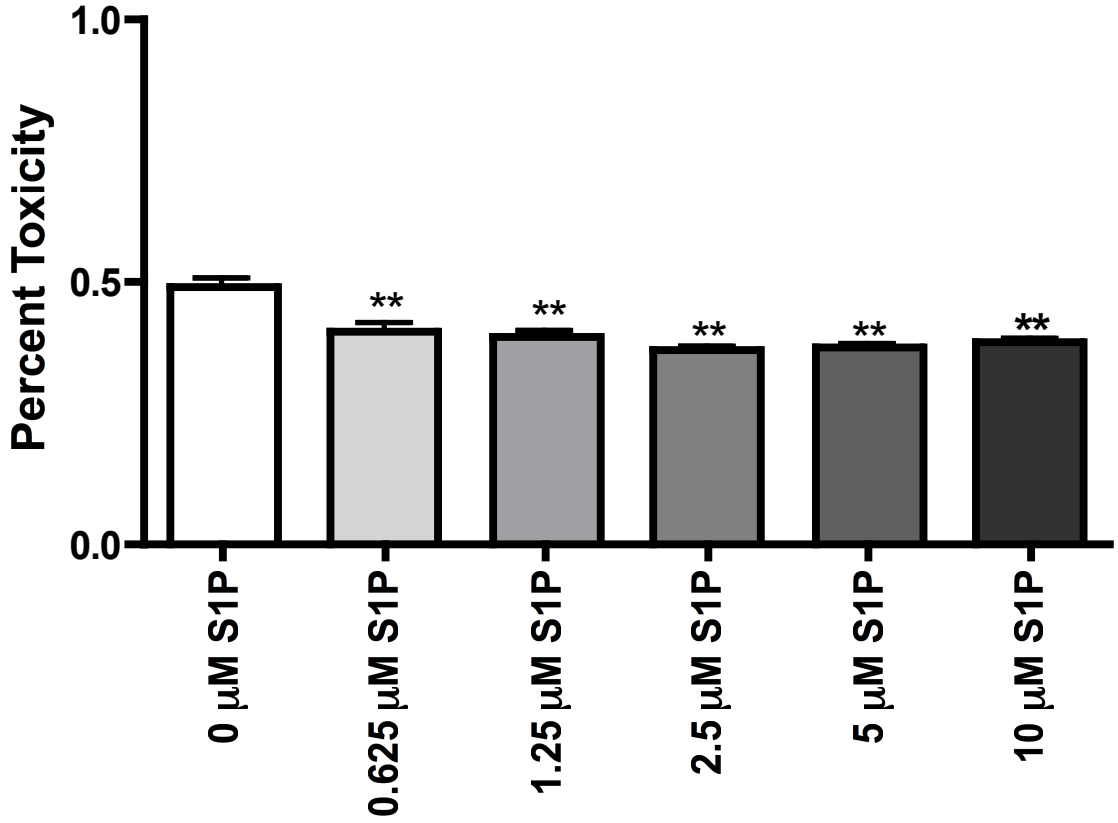

Figure 22: S1P protects ST12.7 cells from cell death after serum deprivation and temperature shift. Cell death was measured using LDH-release assay 24 hours after temperature shift, without *mhtt* induction using doxycline. Data represent replicates from n=16 separate wells. One-Way ANOVA with Tukey's post-hoc comparison, $p<.001$ for each concentration of S1P as compared to control condition.

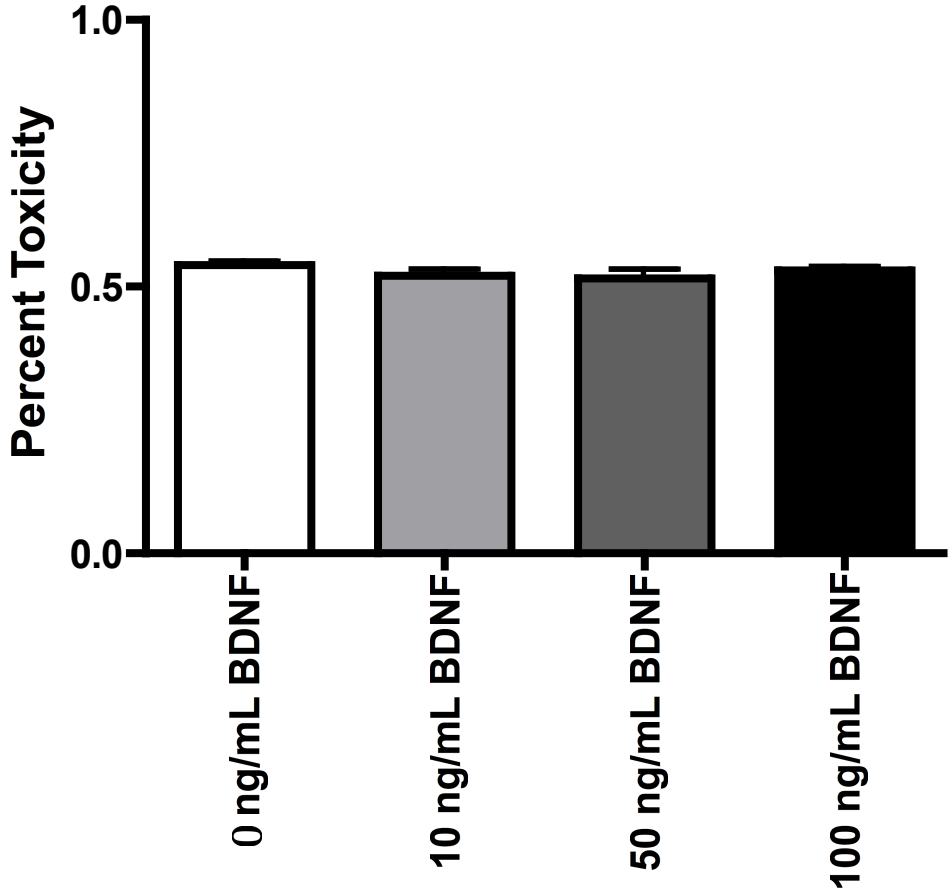

Figure 23: BDNF exerts no cell-survival effect on ST12.7 cell line. Cell death was measured with an LDH-release assay, without *mhtt* induction using doxycline. Data represent n=16 well replicates. Statistical analysis was performed using a one-way ANOVA test.

Because the doxycycline-induced mhtt in the ST12.7 cell line has no effect on cell death, we could not determine the effects of S1P upon *mhtt* toxicity in this model. Instead, we turned to the constitutively-expressing N548 line to investigate the effect of S1P on mhtt-induced cell death. Rigamonti et al. show a strong acceleration of cell death at 39°C with serum deprivation in the N548 line using an MTT assay. We have subsequently acquired the N548 line from the Cattaneo lab and have reproduced the accelerated cell death phenotype due to mhtt using Trypan Blue staining (see Figure 24). We will next use this cell line to test S1P's ability to mitigate against *mhtt* toxicity in this line. At this time, however, we do not yet have results for the effects of S1P treatment of the N548 line.

We also tested the effect of a dose response of S1P with or without BDNF in primary culture from wild-type animals on the expression of DARRP-32. We found a variable trend toward an increase of DARPP-32 expression in primary culture at 2.5 uM S1P treatment that failed to reach statistical significance (Figure 25 n=5 separate experiments, p=.1)

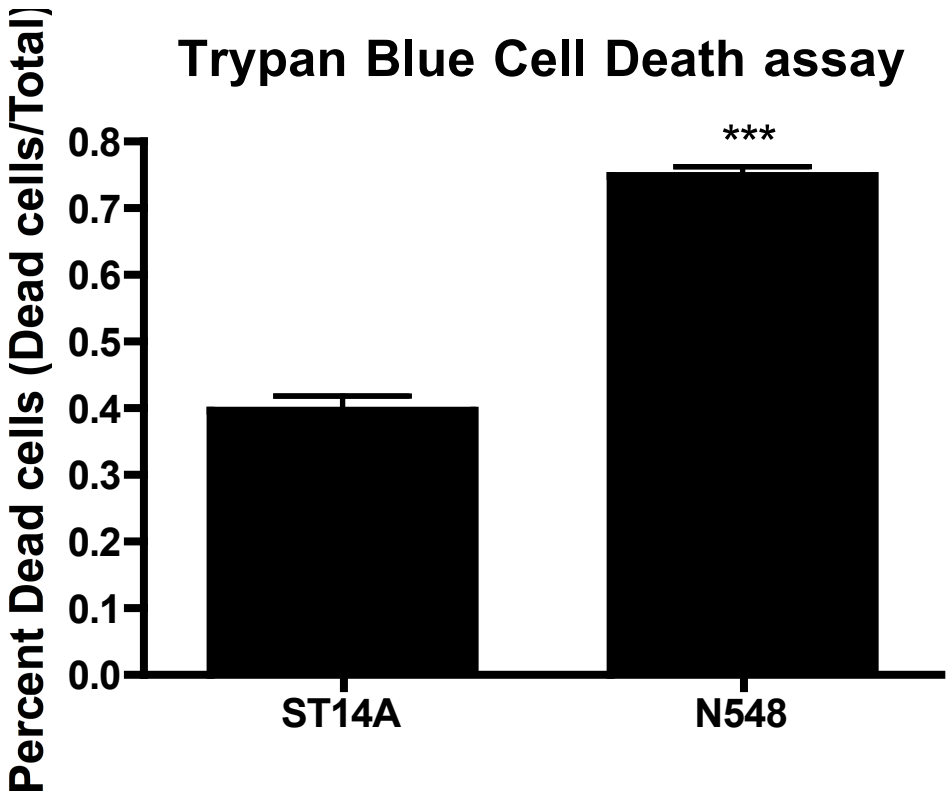

Figure 24: Stably transfected N548 cell line (ST14A transfected with *mhtt* with 128 repeats) has an accelerated cell death phenotype at 24 hours when measured with Trypan Blue staining. Cells were stained with Trypan blue and counted with a hemocytometer. Results represent 3 independent biological replicates each counted four times. Students Two-tailed t-test, $p<.0001$.

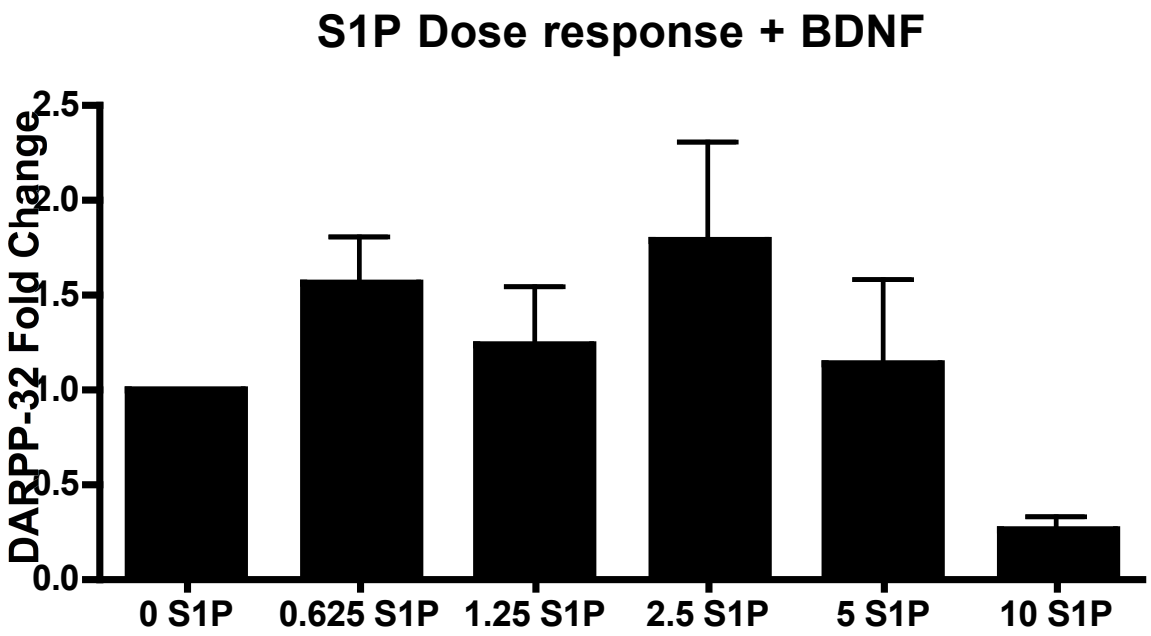

Figure 25: S1P may promote differentiation in striatal primary culture. Primary culture started from striata of E15-E17 C57Bl/6 embryos and treated with S1P for 7 days. Protein lysates from cells were run on a Western blot and detected with rabbit anti-DARPP32. Quantification of blots was performed with ImageJ software. Data are not statistically significant (One-Way ANOVA p=0.25), n=5 independent experiments with 3 well replicates in each experiment.

Production of S1P Modifying Viruses

In order to assess the effects of altering S1P levels on the HD phenotype *in vivo*, we produced Adeno-associated viruses (AAV) to overexpress Sphk2 and Sphk1, and an shRNA virus to knockdown expression levels of Sphk2. Plasmids for over-expression and shRNA were tested prior to packaging by transfection into HEK293T cells. We saw robust expression of Sphk2 by Western blot, and we were then able to knockdown this overexpressed protein by ~80%, using the viral plasmid encoding for the shRNA against Sphk2 (Figure 26). Viruses were then packaged by Vector Biolabs. In future work, viruses will be injected into the striatum of R6-2 mice using stereotactic guidance (see Figure 27 picture of dye injection).

***In Vitro* Functional Screen of Additional Candidates**

The genes and pathways identified from the interrogation of microarrays in Section 2 might play a role in HD pathogenesis. In order to identify candidates within these gene changes that have functional relevance, we performed a preliminary *in vitro* functional screen by over-expressing candidates in N548 cells and assaying their ability to protect against serum-deprivation death at 39°C. A list of gene candidates was chosen for their robust differences at early time-points. Of the 16 candidates

tested, 4 have shown modest protection of ~3-5% with Trypan Blue counting. These candidates, Sox11, Pea15a, Bcl11a, and Mrpl22, await further confirmation (see Figure 28). None of the other candidates, except Anxa5, which worsened cell death, showed any effect (data not shown).

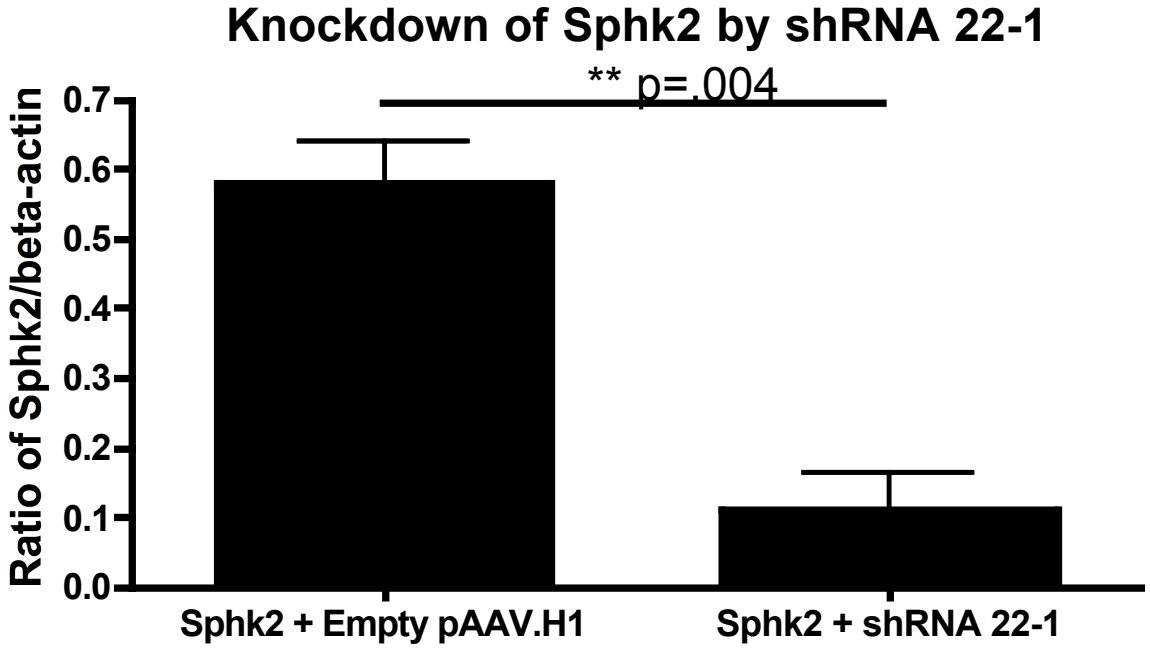

Figure 26: Knockdown of Sphk2 with shRNA. Sphk2 overexpression virus plasmid and Sphk2 shRNA plasmids were co-transfected into HEK293T cells. Protein lysates were analyzed by Western blot and quantified with LiCor Odyssey Imaging System. Results represent mean of 3 independent biological replicates.

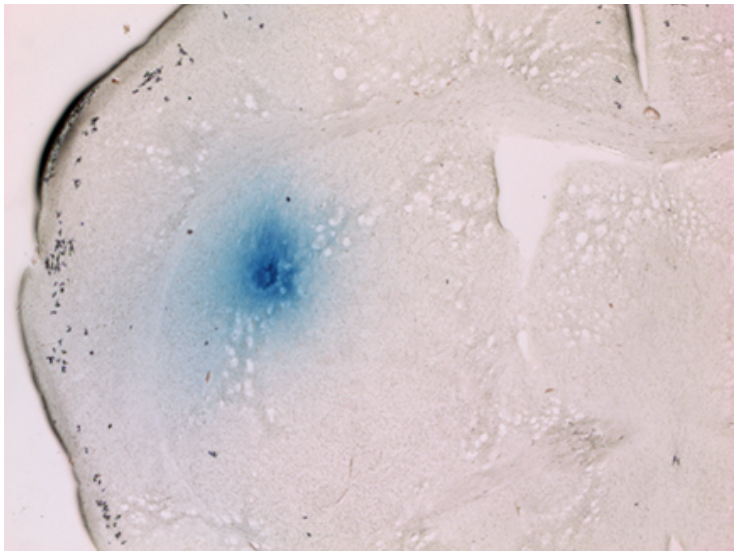

Figure 27: Dye injection into striatum. 2 ul of Nile Blue dye (10%) was injected stereotactically with a Hamilton syringe and microinjecting pump. The same method will be used to deliver AAV viruses to the dorsal striatum.

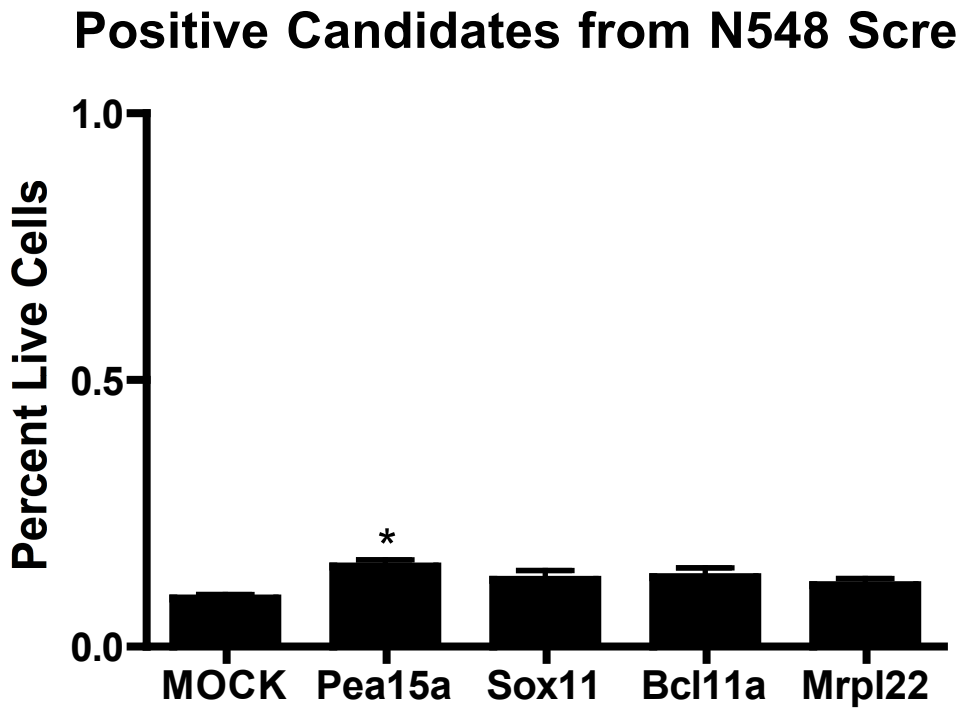

Figure 28: Candidates from preliminary screen in N548 cells for rescue of cell death. Gene candidates found from microarrays were transfected into N548 cells and then shifted to 39˚C in serum-deprived conditions. Trypan blue staining was used to count live cells remaining after 48 hours. Data represent average of 3 independent wells, each counted 4 times. Statistical analysis performed using one-way ANOVA ($p=.0002$ overall difference due to chance. * represents Tukey post-hoc test which shows Pea15a compared to Mock $p<.001$.)

Discussion

We have conducted preliminary investigations into alterations in the sphingosine-1-phosphate signaling pathway in HD mouse models, human *post mortem* tissue, and *in vitro* systems. We focused our interest on this pathway because of the strong D2 enrichment (~50 fold) of GPR6, a putative S1P receptor, alterations in sphingolipid metabolism at the pre-symptomatic timepoint in the R6-2 model, and because of S1P's role in cell-survival signaling. We have shown that S1P and other complex sphingolipid levels are altered at an early symptomatic timepoint in the R6-2 model and that S1P can exert a modest pro-survival effect on the striatally-derived ST12.7 line *in vitro*.

As mentioned previously, S1P is a powerful signaling molecule that exerts effects through both extracellular signal transduction cascades through GPCRs as well as intracellular pathways by binding to a series of protein partners. S1P levels are maintained at low levels in the tissue and are tightly regulated by both sphingosine kinases, lipid phosphatase Sgpp1, as well as Sgpl1, which irreversibly cleaves S1P into phosphoethanolamine. Sphingolipid signaling is remarkably complex, involving many categories of distinct, biologically active signaling lipids, such as ceramides, ceramide-phosphates, and complex glycosphingolipids. In their review of sphingolipid

signaling, Hannun emphasize the interconnectivity of these lipid species and suggest that alterations of any one enzyme in the pathway may result in more widespread changes than simple changes of the sphingolipid immediately downstream of the effect.

For this reason, we cast a wide net when analyzing mouse striatum samples by mass spectrometry to look at the levels of many complex sphingolipids. We found many changes in different sphingoid base species in the R6-2 mouse striatum, including two forms of S1P, d:18:1 and d:20:1 S1P, which differ by two carbon atoms. There has been some evidence to suggest that d:20 sphingoid bases are more CNS specific (Sonnino and Chigorno 2000), but there is not very much information in the literature about differences in biological activity between these two molecules. We observed many other changes in these complex lipids, but the changes were specific to the sphingolipids—the closely related ceramide species, which can send potent apoptotic signals themselves, were unchanged. These changes were also specific to the striatum: in the cerebellum, with the exception of a decrease in d18:0 sphinganine, we observed no changes in any of the sphingolipids tested, at either 6 or 24 weeks of age.

In the human samples, S1P levels varied between control and HD subjects—it was increased in Grade 2 and decreased in Grade 4 tissue. There were also very large

changes—sometimes an order of magnitude—difference in the levels of several ceramide species between HD tissue and control tissue. It is too early to make any conclusions about these trends, because of the small sample size, but these promising data warrant further study with larger cohorts.

One of the challenges in this investigation was the variability of Sgpl1 and Sphk2 levels as measured by qPCR. This variability was seen in both HD and WT animals at different ages, and was not attributable to technical variability, as the standard deviation of the technical replicates for each sample was within the range of 0.05-0.1 cycles, which is within the typically acceptable range of <.1 cycles. Furthermore, other genes tested in parallel, from the same samples on the same plates, did not show this variability.

There are some possible biological explanations to explain this variability. One possibility is that these genes are highly susceptible to environmental signals, such as stress. Sgpl1 might function as an immediate early gene in the striatum, subject to quick alterations in translation. There is some precedence for this in the literature: Sgpl1 was found in an unbiased screen for immediate early genes stimulated by PDGF (Chen, Delrow et al. 2004). If Sgpl1 levels are regulated in such a way as

to produce rapid changes in translation of the protein, it might vary widely between individual animals.

To gain insight into the functional consequences of these observed changes in sphingolipid levels and regulating enzymes, we took a parallel approach to study the effects of perturbations in S1P signaling in both *in vivo* and *in vitro* systems. For our *in vitro* studies, we chose to use the ST14A cell line. The ST14A cell line established in Elena Cattaneo's lab has been used by several groups in the HD community to investigate the role of BDNF in HD (Zuccato, Ciammola et al. 2001), to study cell death pathways in HD (Wang, Zhu et al. 2003), and for pharmacological screens of natural products to protect against HD-indued cell death (Varma, Cheng et al. 2007). We chose this cell line because it is derived from rat embryonic striatum and expresses markers of MSN identity, including Map2 and DARPP-32 (Ehrlich, Conti et al. 2001), and because it has a measurable acceleration of cell death pathways when stably transfected with mhtt (Rigamonti, Bauer et al. 2000).

We were originally sent a version of this cell line, the ST12.7 line, in which mhtt expression is controlled by a Tet/on promoter. When exposed to doxycycline, the ST12.7 cells are induced to express a truncated mhtt construct with exon 1 of the gene and 128 CAG repeats. We performed S1P dose response experiments with this line and saw a

consistent, modest rescue of ~10% upon temperature shift and serum deprivation without doxycycline. This result was consistent with many studies that have shown S1P to have pro-survival effects in many cell lines (Edsall, Pirianov et al. 1997; Olivera, Kohama et al. 1999 2000, Karliner et al, 2001).

Because the transformation process of immortalized cell lines can introduce artifacts in cell behavior, we complemented our studies in the ST14A system with a primary culture model. The induction of DARPP-32 upon S1P stimulation suggests that S1P may promote MSN differentiation. Taken together, like many neurotrophic factors, such as BDNF, S1P may play a role in MSN survival and differentiation.

Conclusions and Future Directions

The brain is composed of hundreds of different neuronal cell types, possessing distinct morphologies, gene expression profiles, connectivity, and functions. This heterogeneity allows for the manifestation of the vast array of behaviors of which the brain is capable, but it also produces complex disease syndromes when particular parts in the machine become damaged. Given the extraordinary diversity of cell types in the brain and the highly specialized, divergent functions each type has been evolutionarily selected to carry out, it is unsurprising that these cell types might respond differently to disease. Indeed, one of the unifying properties of the many neurological disorders that affect the brain is their specificity: Parkinson's Disease affects the substantia nigra; ALS damages motor neurons, Alzheimer's Disease first affects the entorhinal cortex. Indeed, the classical definitions of these neurological diseases are based on their differing clinical symptoms, which are themselves a result of damage to distinct neuronal populations.

The polyglutamine disorders in general and Huntington's Disease in particular offer an opportunity to investigate the molecular mechanisms responsible for selective vulnerability in genetically defined systems. HD is a monogenic disease of known cause with a well-characterized and highly specific pattern of neuronal

pathology. It is a disease that has been modeled in a wide range of systems, from single-celled organisms to primates. The mouse models of HD, although imperfect, reproduce many of the behavioral aspects of the human disease and recapitulate features of human selective vulnerability.

Until recently, however, the question of selective vulnerability of striatopallidal MSNs in HD was severely limited by technological constraints. The complexity and heterogeneity of cell types in the brain, which facilitates the brain's rich complement of behaviors and make it fascinating to study, obscure changes in one cell type within noise from the messages present in surrounding types. Even in the striatum, which is a relatively homogeneous brain structure, there are glia, endothelial cells, and interneurons, in addition to the presence of the two major classes of MSNs, which prevented whole tissue studies from identifying many gene changes that could specifically be assigned to one cell type or another. A recent study using microarray profiling from whole striatal tissues in the YAC128 model was able to identify only a handful of changes at the tissue level, and these changes could not be attributed to any particular cell type (Becanovic, Pouladi et al. 2010).

The development of the BACTRAP technique allows this question of selective vulnerability to be addressed for the first time. Among the techniques that allow study of cell-

type specific messages, such as laser-capture microdissection (LCM) and fluorescence-activated cell sorting (FACS), TRAP provides the highest sensitivity and most faithful reflection of endogenous messages by avoiding loss of tissue-intrinsic signals and loss of messages from within neurites.

We have taken the previously characterized D1 and D2 TRAP lines (Heiman, Schaefer et al. 2008) and applied this system to the problem of selective vulnerability in HD. We chose to study HD because it affects MSN function generally and striatopallidal MSN biology specifically. We hypothesized that differences in the gene expression patterns that characterize these two cell types would contribute to their selective vulnerability and that by following changes in the translational profiles of these cell types over time, we might learn something about the underlying basis of their susceptibility.

To address this question, we chose two HD mouse models to study, the R6-2 and YAC128 models. We chose these models because they reflect complementary properties of human HD: whereas the R6-2 mouse phenotype is rapid, robust, but less specific, the YAC128 phenotype is specific, but more protracted. The YAC128 model is often thought be the better model of HD, because one of the defining characteristics of human HD is its late onset: even though *mhtt* is expressed in development, the nervous

system of HD patients seems to develop normally. The reasons for the late onset of the disease are not entirely known but are thought to relate to the slow build-up over time of post-translational modifications to *mhtt*, including phosphorylations, sumoylations, and cleavages that enhance or diminish the toxicity of the protein. These modified pieces of *mhtt* aggregate, which may protect or hurt the cell. The end result of this long process may be the gradual accumulation of insults that become too much for the cell to handle. The R6-2 transgene, which truncates the *mhtt* protein, may not undergo any of these protective modifications.

Because this experiment introduced a novel transgene into the models and because we wished to account for differences due to mouse strain and variability between laboratories, we re-characterized the behavior of the HD TRAP mice. The R6-2 model exhibited a robust behavioral phenotype in both the open field and on the rotarod. The YAC128 model exhibited a variable behavioral phenotype, which reached significance at only a very late age. The more variable, milder YAC128 phenotype fits with the model that the processing of full-length *mhtt* is subject to more stochastic biochemical modifications, and hence leads to more varied disease presentation. It is somewhat surprising that deficits in the R6-2 appeared earlier in the open field, while the YAC128 model showed earlier deficits on

the rotarod. It is difficult to provide a satisfying answer to this question without more careful studies mapping the neural circuits required for the rotarod task, which might then allow investigation into the differential vulnerability of these cell types. The TRAP technique gives us access to cell-type specific translational information, but there are very few known behavioral outputs that respond to deficits in one particular cell type in the mouse: hyperlocomotion in the open field would have been one such example, but we did not observe it in our experiments.

We harvested mRNAs separately from both cell types first using the original published TRAP protocol and then, when it became available, an improved TRAP co-immunoprecipitation methodology that allowed single-animal analysis. Our results both confirmed pathways, such as PPAR signaling and DNA damage responses, which had previously been implicated in HD pathology, as well as uncovered new pathways and genes, such as sphingosine-1-phosphate signaling, which may provide new avenues for research. At the pathway level, we did not observe a great deal of cell-type specificity: most of the pathways seemed specific to the model, rather than the cell-type. However, we do observe the preferential loss of D2 MSN markers—at the 12 week time point in the R6-2, Drd2, Penk, and Gpr6 are all decreased by ~2-fold, whereas D1 MSN markers Drd1a

and Pdyn are changed only slightly (~1.2 fold down). One possible explanation for the loss of D2 markers is that *mhtt* is interfering with the action of a transcription factor responsible for coordinating levels of these genes.

There are a few major conclusions one can make about the data. We began these experiments with the hypothesis that gene expression changes opposite in direction in D1 and D2 MSNs were being lost in studies of transcriptional changes in whole striatal tissue. Our data show that this hypothesis was incorrect: the most statistically significant gene changes are shared in D1 and D2 MSNs. We did, however, identify some gene changes of high statistical significance and low magnitude, like Igfbp4, that were previously unreported in the literature. These changes may have been obscured by noise from other cell types besides MSNs in the tissue. Future studies might use TRAP to profile glia in the striatum, to see whether the changes found in this study but not whole tissue are reflected by opposing changes in non-neuronal cell types. Second, we hypothesized that differences in D1 and D2 MSNs could explain the variability observed in most previous studies. However, our cell-type specific data also showed high variability and gene changes of low magnitude. The high variability seems to be a problem intrinsic to the HD models themselves. We are in discussions with a biostatistician from Yale about trying to account for some

of this variability in our data sets by breaking the mice into phenotypic sub-groups.

Interestingly, biochemically, the R6-2 model seems better able to recapitulate the differential vulnerability of D1 and D2 MSNs. In this model, the loss of D2 markers Gpr6, Adora2a, and Penk all occur before loss of D1 markers. We also saw this result reflected in the fact that at all timepoints tested in the R6-2 model, there were more changes in D2 MSNs than D1 MSNs. Furthermore, in this model, we saw the loss of the TRAP transgene selectively in D2 MSNs, which was another indication we had that there were differential responses of these two cell populations to *mhtt*. Despite these biochemical indications of D2 MSN vulnerability, however, we have seen no phenotypic hyperkinesis in the R6-2 model that would reflect this preferential D2 vulnerability.

In contrast, the YAC128 model, which we expected to have a more cell-specific phenotype given its inclusion of *mhtt*'s full regulatory elements, had *fewer* changes in D2 cells compared to D1 cells. In this model we also did not see hyperkinesis, but we did eventually see a hypokinesis. This result raises the question of whether it is true that D2 MSNs are more vulnerable in the YAC128 model. We performed a very thorough behavioral characterization of these mice, so it is unlikely that we missed a hyperkinetic phenotype, so it may be that these mice are a better model

for D1 MSN dysfunction than D2 vulnerability. Thus, we saw the opposite pattern from what we expected: the R6-2 model, with a less specific transgene, gave a better recapitulation of D2 MSN vulnerability than the YAC128 model.

There is an ongoing debate in the HD community about which of the models best recapitulates human disease. As many others have found as well, we show than neither model is perfect. The R6-2 model has a more robust behavioral phenotype, and it displays features of D2 MSN vulnerability, but it suffers from a very rapid phenotypic progression and a steady expansion of CAG repeats that modifies the phenotype in successive generations. The YAC128 model has a more variable behavioral phenotype, but it offers a long enough time window to see early pathological changes.

We have performed the most detailed follow-up on a significant difference observed in the arrays for the S1P pathway. We saw statistically significant decreases in striatal S1P levels at early timepoints in the R6-2 model by mass spectrometry, and we have some indication that levels of sphingolipids are variable in human HD as well. We have shown that this decrease in S1P may be caused by increases in Sgpl1 expression and decreases in Sphk2 expression, but these differences were variable. Finally,

we have shown that S1P can exert pro-survival effects on a striatally-derived cell culture line *in vitro*.

We do not know why the levels of Sphk2 and Sgpl1 are so variable in MSNs, but one possibility is that the observed changes in sphingolipids are being caused by changes in expression of these enzymes in coordination with other cell types. Endothelial cells are known to express high levels of S1P regulating enzymes, so the changes we observe in sphingolipids in the striatum may be due to regulation by other cell types in the striatum (Lucke and Levkau, 2010). This uncertainty reflects a larger question in the sphingosine-1-phosphate field about whether S1P's signaling is primarily autocrine or paracrine in nature. Future studies will require TRAP lines in other striatal cell types to provide the necessary resolution to parse where the changes in sphingolipids are coming from.

Future Directions

Short-term

There are a number of experiments which will be done in the immediate short-term to clarify points of uncertainty in the data for publication. First, the *in situ* hybridization experiments will be repeated with tissue that is already available using lower hybridization temperatures and lower stringency washes in order to amplify signal-to-noise ratios in the assay. Second, S1P

dose-response experiments will be performed in the N548 cell lines to observe the effect of S1P on rescuing cell death in a model where there is a clear acceleration of cell-death caused by mhtt. Third, viral injections to overexpress and knockdown levels of Sphk2 will be initiated in R6-2 mice. These experiments will be performed with Ruth Kulicke, a technician in the laboratory, who is proficient in all of the techniques needed to perform these experiments. These mice will be analyzed for behavioral phenotypes, development of nuclear inclusions, DARPP-32 expression, and other markers of D1 and D2 MSN identity. We will expand our mass spectrometry studies of human samples, if we can procure more *post-mortem* tissue: we are currently requesting more tissue. We will complete our more sophisticated microarray analysis, and we will expand our preliminary screen of robust gene changes in N548 cells to include some of the changes seen in pathway analysis.

Longer-term

Taking the long view of the experiments presented here, there are a number of possible directions to take future work.

Development of a cell-type specific *in vitro* system

One of the challenges posed by the exciting wealth of data afforded by the BACTRAP technique is how to investigate the functional relevance of the gene candidates

identified by the screen. The establishment of immortalized *in vitro* systems that reflected D1 or D2 MSN properties would allow for high-throughput functional analysis of the gene changes observed *in vivo*. Stephen Finkbeiner's group at UCSF has had success in developing *in vitro* primary cultures from D1 and D2 BAC GFP mice (Miller et al., 2010), but these cultures are not immortalized, and therefore cannot be used for high throughput studies.

A potential approach toward solving this problem would be to find a protocol to differentiate embryonic stem cells into D1 or D2 MSNs. Currently, the transcription factors needed to create D1 or D2 MSN identity are unknown; however, these genes are most likely those that are differentially expressed at high levels in these two cell populations. In fact, a number of the genes that are most divergent in their expression patterns between these two cell types are transcription factors: we could employ an approach like the one used by Shinya Yamanaka to identify factors to restore pluripotency to determine which transcription factors are necessary and sufficient to confer D1 and/or D2 identity. We could then use this model system to screen the gene changes from the TRAP analysis for survival and the expression of cell-specific identity traits.

<u>Mapping loci of modifier genetic mouse strain differences</u>

There is a very clear effect of mouse strain on phenotype in both of these models. In particular, the C57Bl/6 background seems to afford protection against pathology in both models. One possible future project would be to attempt to map genetic loci that could explain these differences in strain background. One could then take these candidate loci and compare them to modifier effects of age of onset from human HD patients. These studies could also be complemented with more careful clinical analysis of patients to see whether any of the effects could be correlated with specificity of disease presentation.

Development of techniques to investigate cell-type specific post-translational modifications

There is considerable evidence that *mhtt* exerts many toxic cellular effects at the post-translational level and that mhtt itself can be post-translationally modified in ways that affect its toxicity (Morfini, Burns et al. 2009; Subramaniam, Sixt et al. 2009; Thompson, Aiken et al. 2009). One of the limitations of the BACTRAP approach is that it cannot help identify these post-translational effects. While there are approaches for studying the cell-type specific post-translational modifications of particular proteins, such as the work of Helen Bateup, a former graduate student in the Greengard Lab who pioneered an approach for studying the phosphorylation state of

DARRP-32 selectively in D1 or D2 MSNs, current methods for analyzing all post-translational modifications in an unbiased fashion do not provide cell-type specific information.

To begin to address this question, one could use the protocol developed in Kriaucionis et al. to sort nuclei from HD/BACTRAP animals and perform mass spectrometry upon proteins found in the nuclei of D1 and D2 MSNs (Kriaucionis et al, 2009). This study would allow a comprehensive analysis of post-translational modifications that occur in nuclear proteins. It would also allow the identification of any differences in the composition of nuclear inclusions that may exist between these two cell populations. This study is immediately feasible, as members of our laboratory and the Heintz laboratory are currently using this technique to identify baseline differences in DARPP-32 phosphorylation in D1 and D2 MSNs and changes in response to psychostimulants.

Materials and Methods

All procedures involving animals were performed in accordance with the National Institutes of Health Guide for the Care and Use of Laboratory Animals and were approved by The Rockefeller University Institutional Animal Care and Use Committee.

Behavioral Analysis

Open Field Test

Mice were brought into the behavioral testing room at least 30 minutes before beginning of the test. Open field testing was conducted using the AccuScan activity monitoring system (AccuScan Instruments; Columbus, Ohio). The arenas were each 40 cm x 40 cm x 30 cm and made from clear Plexiglass. Light in the room was measured with a luminometer and maintained between 100 and 200 Lux, tested in 5 points in each arena so that light was evenly distributed across arenas +/- 10 Lux. Before each round of testing, arenas were disinfected with Clidox for 5 minutes and washed twice with distilled water.

The mice were tested in groups of 8 in identical home cage environments. Each testing session lasted one hour, during which mouse activity was quantified through breaks in a grid of infrared beams. Activity was analyzed for total activity and grouped into 10 minute bins for analysis of habituation to the novel environment.

Rotarod Test

Mouse balance and motor function were tested with a standard accelerating rotarod test protocol in which the rotarod speeds from 4 rpm to 40 rpm over a period of 5 minutes (Med Associates St. Albans, Vermont). Mice were trained on the machine on the first day with three successive trials, during which they were continually placed onto the rotarod if they fell off, until 100 seconds had passed. These three training runs were followed by a rest interval of at least 2 hours before the first day test. Mice were tested on consecutive days with three trials of the accelerated protocol on each day. The time it took for the mouse to fall off the bar (latency to fall) was recorded in seconds. If a mouse clung passively to the rod for two consecutive rotations without moving, it was scored as a fall.

CAG repeat analysis

1 cm tail-clips of mice were immediately placed upon biopsy in 200 ul Direct Lysis reagent (Viagen Biotech) with a 1:50 dilution of Proteinase K (Viagen Biotech). Tail samples were incubated overnight at 55 °C. Samples were vortexed thoroughly to ensure complete disgestion of the tissue and then centrifuged and heat-inactivated for 45 minutes at 85 °C. 100 ul of the lysate were sent to Laragen Inc. for analysis.

Immunoprecipitation of mRNA

For pooled-animal IPs, purifications were performed as described in Heiman et al., 2008.

For single-animal IPs, mice were anesthetized with CO_2, decapitated, and striata were quickly dissected. Tissue was immediately homogenized 12 times at 900 rpm in ice-cold polysome extraction buffer (10 mM HEPES [pH 7.4]. 150 mM KCl, 5 mM MgCl2, 0.5 mM dithiothreitol, 100 ug/mL cycloheximide, protease inhibitors, and recombinant RNase inhibitors) with a motor-driven Teflon glass homogenizer (Lab Stirrer LT-400, Yamato-USA, Santa Clara, CA). Homogenates were centrifuged for 10 minutes at 2000 x g, 4 C to pellet large cell debris, and NP-40 (EMD Biosciences, San Diego, CA) and 1,2-Diheptanoyl-sn-Glycero-3-Phosphocholine (DHPC, Avanti Polar Lipids, Alabaster, AL) were added to the supernatant at a final concentration of 1% and 30 mM, respectively. After incubation on ice for 5 minutes, samples were centrifuged for 10 minutes at 20,000 x g, 4 C. Supernatant was added to Streptavidin MyOne T1 magnetic beads (Invitrogen, Carlsbad, CA), which were coupled to biotinylated Protein L (Pierce, Rockford, IL) and anti-GFP antibody (custom-made). Beads were prepared as follows: beads were resuspended, aliquoted 300 ul per IP and washed once with PBS. Biotinylated Protein L (Pierce # 29997) was resuspended to a concentration of 1 ug/ul in PBS and was added to beads, 120 ul per IP. Tubes were

incubated for 35 minutes at room temperature with end-over-end mixing. Beads were collected on a magnetic rack and blocked by washing 5 times with 3% BSA (w/v; Jackson Immunoresearch, West Grove, PA). Beads were then resuspended in low salt wash buffer (20 mM HEPES, 150 mM KCl, 5 mM MgCl2, 1% NP-40) and incubated with mouse monoclonal anti-GFP antibody for 1 hour. After antibody-binding, beads were washed three times with low-salt wash buffer, resuspended in 100 ul low-salt wash buffer per IP and then added to samples as described above.

Beads and samples were incubated at 4 °C for 18 hours with end-over-end mixing. Tubes were centrifuged briefly to collect beads, and beads were washed 4 times with high-salt wash buffer, containing 350 mM KCl. Beads were resuspended in lysis buffer from the Absolutely RNA Nanoprep kit from Agilent (Santa Clara, CA), incubated for 5 minutes at room temperature, and then lysis buffer containing the eluted RNA was removed from beads. RNA was processed according to the Nanoprep kit protocol. RNA quantity was measured using Quant-it RiboGreen reagent (Invitrogen, Carlsbad, CA) and quality was measured with a Bioanalyzer (Agilent, Santa Clara, CA).

Gene Expression Analysis

Purified mRNAs were amplified with either the Affymetrix Two-Cycle cDNA synthesis kit (Affymetrix, Santa Clara, CA) or NuGen WT-Ovation Pico kit (NuGen, San Carlos, CA) according to the manufacturer's instructions. Amplified cDNA was hybridized to Affymetrix Mouse Genome 430 2.0 microarrays and scanned at The Rockefeller University Genomics Center.

Microarray .CEL files were imported into the GeneSpring GX software. RMA normalization was performed on the data and genes were normalized to that chips 50^{th} percentile. Quality control analysis was performed by calculating Pearson correlation coefficients for replicate arrays and by performing Principal Components Analysis to scan for outlier gene chips. Data were filtered to select genes with expression levels above the 20^{th} percentile. Genes were then filtered using a volcano plot analysis with a student's unpaired t-test. Fold change value was set at 1.5 and a significance level of $p<.05$ was selected. For Venn diagram plots, data were reanalyzed with equal sample sizes. Gene ontology analysis was performed on these lists within GeneSpring. Lists were also exported and analyzed using Ingenuity Pathway Analysis.

Quantitative PCR

Quantitative PCR was performed using cDNA amplified from NuGen WT-Ovation kit. Reaction were performed with 20

ng of cDNA in triplicate or quadruplicate. The Taqman Gene Expression assays used included: Eif4a2 Mm01343573_gH, Sphk2 Mm00445020_m1, Actb Mm00607939_s1, Sgpl1 Mm01149898_m1, Sphk1 Mm00448841_g1, Mm01252544_m1, GPR6 Mm01701705_s1, Tmem183a Mm00508045_m1, Pea15a Mm01293295_m1, Rprm Mm00469773_s1, B3gat1 Mm00661499_m1, Thtpa Mm00462068_m1, Agfg2 Mm00523929_m1, Igfbp4 Mm00494922_m1, Sox11 Mm01281943_s1, Gpr56 Mm00457581_m1, Bcl11a Mm00479358_m1, Anxa5 Mm00477537_m1, Mrpl13 Mm00452782_m1, Mrpl22 Mm00838506_g1, Hexb Mm00599880_m1, Spata5 Mm00502400_m1, Pcdh20 Mm00724499_m1, Mgst1 Mm00498294_m1, Jun Mm00495062_s1, Phyh Mm00477734_m1, Pkp2 Mm00503159_m1, WT1 Mm00460570_m1, Ppp1r9a Mm00725102_m1, Actn2 Mm00473657_m1, Mapkbp1 Mm00522025_m1, Lsm10 Mm00522588_m1, trnamt6 Mm01278146_m1, tbc1d24 Mm00557451_m1, Ntrk3 Mm00456222_m1, Fxc1 Mm00727252_s1, Igfbp5 Mm00516037_m1, Mtap1a Mm01330378_m1

Immunohistochemistry and immunofluorescence

IHC and IF were performed as described in (Heiman, Schaefer et al. 2008) with the following antibodies: Abcam Chicken anti-GFP (ab13970) 1:1000, Abcam Rabbit anti Map2 ab32454 1:200; Cell Signaling Rabbit anti-DARPP-32 1:1000; Abcam Rabbit anti PPARalpha ab8934 1:1000; Cosmo Bio Mouse anti-S1P 1:100; Santa Cruz Goat anti IGFBP4 1:100; Abcam Sheep anti-prealbumin (transthyretin) ab9015 1:1000; Abcam mouse anti-desmoplakin ab16434 1:100; Novozymes Rabbit anti

Igfbp4 1:250; Santa Cruz goat anti Sph2 1:100; Abcam rabbit anti-Sphk2 ab37978 1:100; Millipore anti-NeuN; Millipore anti-htt EM48 ; Abcam Rabbit anti-Sox11 1:1000; Abcam anti-WT1 ab96792 1:200; Origene rabbit anti-Actn2 1:100

Mass Spectrometric Analysis

Mice were stunned with CO_2 and immediately decapitated. Striata or cerebella were quickly dissected and placed into cell lysis buffer ((10 mM HEPES [pH 7.4]. 150 mM KCl, 5 mM MgCl2). Tissue was homogenized as above and then sonicated with 2 x 15 sec pulses. A 50 ul aliquot of homogenate was saved for BCA analysis, which was performed with Pierce BCA detection kit. Samples were immediately frozen in liquid nitrogen and stored at -80 C, until they were shipped on dry ice to Avanti Polar Lipids. Samples were coded so that analysis was performed in a blind fashion. Extraction and LC/MS/MS analysis were performed according to protocol in Merrill et al. 2005, with optimization by Dr. Jeff Moore.

Human samples were provided by the New York Brain Bank, and the study was approved as being exempt from IRB regulation.

Cell Culture

ST12.7, ST14A, and N548 were provided by the Cattaneo lab. Cells were grown in DMEM + 10% FBS (Sigma-Aldrich, heat inactivated), and 1X penicillin/streptomycin/glutamine

and split every 2-3 days. For S1P experiments, cells were plated at density of 30,000 cells/well in a 24 well dish. They were left to grow overnight, and then washed two times in serum-free media (DMEM + F12 supplement +N2 supplement) and then left in serum-free media with S1P diluted at test concentrations. Fatty-acid free BSA (4 mg/mL), which is used as a carrier to dilute S1P, was used as control. Cells were transferred to 39 ℃, where they were allowed to grow for 24 hours. Media was then harvested for Promega lactate dehydrogenase (LDH) assay. Fresh media was added to the cells, which were then lysed at -80 ℃ for at least 30 minutes and used for LDH kit to control for total cell numbers. Cell toxicity represents fraction of released LDH over total LDH in the sample.

Primary Culture

Pregnant C57Bl/6 females were ordered from Charles River. At embryonic day E15-E17, a dam was sacrificed, the uterus was removed, and embryos quickly dissected into PBS + 0.6% glucose (filtered sterilized). Striata from embryos were dissected and treated with trypsin for 30 minutes. Trypsin was inactivated by adding Neurobasal medium + 10% FBS and DNase was added. Cells were triturated using a P1000 pipette tip until no tissue clumps remained. Cells were pelleted and resuspended in DMEM +10% FBS, + penicillin-streptomycin-glutamine and counted. Cells were then plated on wells at density of 500,000 cells/well in a

24-well-dish with coverslips that had been coated with polyornithine. Cells were grown at 37 C +10% CO2 for 2 hours. After attaching, cells were washed 2 x with neurobasal media and fresh neurobasal medium with S1P and BDNF were applied. Cells were grown for 7 days in vitro, changing media every other day. On final day, NuPage sample buffer was applied directly to wells.

Western Blots

Protein lysates were prepared in 1X NuPage Sample Buffer with 100 mM DTT. Samples were heated to 70 C for 5 minutes and then centrifuged at maximum speed for 1 minute to pellet debris. Samples were loaded onto NuPage 4-12% Bis-Tris gels and run at 120 mV for 1.5 hours. Proteins were transferred for 2 hours at 30 mV onto PVDF membranes that had been activated with 1 methanol wash for 30 seconds, followed by 3 washes with PBS, and a 5 minute incubation in 1X NuPage Transfer Buffer. After transfer, membranes were allowed to dry completely and then were re-activated with a 30 second methanol wash, followed by 3 x 5 min PBS washes. Membranes were blocked with 10% non-fat evaporated milk dissolved in PBS-T, and then incubated overnight at 4 °C with rabbit anti-DARPP-32 antibody (Cell Signaling) dissolved in blocking buffer 1:1000. Membranes were washed 3 x 10 minutes with PBS-T and then incubated in HRP-coupled secondary antibody for 1 hour. Membranes were washed 3 x in PBS-T, then once in PBS and developed using

Western Lightning Detection method. Membranes were exposed to film, and bands were quantified using Image J software.

In situ Hybridization

6-week-old R6-2 mice and WT littermates from Jackson laboratory were stunned with CO_2 and decapitated. Brains were rapidly dissected and placed on dry ice for 30 minutes, before storing at -80°C. Brains were cut on a cryostat in 12 uM sagittal sections. Slides were fixed for 15 minutes in 4% paraformaldehyde at 4 °C. Slices on slides were washed 1 min in 1XPBS, then for 1 min in 0.1 M triethanolamine (TEA). Sections were aceylated for 15 minutes in 0.1M TEA + .25% acetic anhydride. Sections were washed 2 X 2 min in 2X SSC, then washed in 30%, 75%, and 100% ethanol, each for 2 minutes. Sections were air-dried for 20 minutes and then incubated 1 hour in prehybridization buffer (50% formamide/5XSSC/5X Denhart's solution/250 ug/mL yeast RNA/500 u/mL sonicated DNA). The hybridization solution was heated 15 minutes at 80 °C, RNA probes were added, and the mixture was then heated an additional 5 minutes at 80°C. Hybridization buffer with probes was applied to sections and slides were incubated overnight at 58 °C Slides were washed in 5X SSC for 30 minutes at 65 °C and then washed twice for 20 minutes each in 2X SSC/50% formamide. Slides were washed in 2XSSC, 0.2X SSC, and 0.1X SSC and then 2 times in PBS. Slides were then incubated 30 minutes in 0.2% H_20_2. Slides were washed 2 x 10

minutes in PBS, 1 x 10 min in PBS-T and blocked for 1 hour in PBS-T + 2% heat-inactivated donkey serum + 0.1% fish gelatin. Slides were incubated at 4 C overnight with Roche mouse-anti-DIG at 1:250. Slides were washed 3 x 10 minutes in PBST and then incubated with mouse Superpicture reagent (Invitrogen) for 2 hours at room temperature. Slides were washed 3 x in PBS-T for 10 minutes and then incubated with Tyramide –AlexaFluor 546 for 10 minutes (Invitrogen). Slides were washed 3 x 10 minutes in PBST and mounted with ProLong Gold Anti-fade.

Appendix I: GO analysis R6-2 3 wk D2

GO Term	Ontology	p value	Adjusted p value	Total genes in GO class	Genes present
RNA metabolic process	BP	3.13E-06	0.011	647	Sart3, Cpeb1, Trdmt1, LOC639633 /// Npm3 /// Npm3-ps1, Ddx41, Cugbp1, LOC433064 /// Ppih, Hnrpdl, Cpsf4, Tcof1, Cugbp1, Trp53, Dicer1, Prpf39, Elac2, Aqr, Aqr, Bxdc5, Exosc10, Adarb1, Tfb1m, Sfrs7, Trmt1, Eif4g1, Plrg1, Hars2, Smad3, Gemin8, Nova1, Rbm22, Sf3a2, Tardbp, Exosc8, Smg1, Trmt6, Gemin5, Mettl1, Tdrd3, Lcor, Sf3a1, Hif3a, Mettl1, Elac1, Zfc3h1, Zhx2, Utp23, Dgcr8, Ppwd1
RNA processing	BP	3.98E-06	0.012	466	Sart3, Cpeb1, Trdmt1, LOC639633 /// Npm3 /// Npm3-ps1, Ddx41, Cugbp1, LOC433064 /// Ppih, Cpsf4, Cugbp1, Dicer1, Prpf39, Elac2, Aqr, Aqr, Bxdc5, Exosc10, Adarb1, Tfb1m, Sfrs7, Trmt1, Plrg1, Gemin8, Nova1, Rbm22, Sf3a2, Tardbp, Exosc8, Trmt6, Gemin5, Mettl1, Tdrd3, Sf3a1, Mettl1, Elac1, Zfc3h1, Utp23, Dgcr8, Ppwd1

biopolymer metabolic process	BP	8.97E-07	0.006	2988	Mcm5, Aurkaip1, Mcm6, Ptprn, Ube3a, Gys1, Tyk2, Sart3, Cpeb1, Ufd1l, Csnk1d, Acvr2b, Stk39, Trdmt1, Cul2, Suz12, Gbe1, B3gnt2, Traf6, Wsb2, Nr3c1, Pdgfra, Mapk11, Uty, Xpc, Stk17b, Riok2, LOC639633 /// Npm3 /// Npm3-ps1, Ddx41, Cugbp1, Suv420h2, LOC433064 /// Ppih, Hnrpdl, Cpsf4, Tcof1, Hemk1, Ube3a, Polb, Mark1, Nmnat1, Hltf, Mlh3, Park2, Ryk, Cugbp1, Trp53, Ptprz1, Mdm2, EG665955, LOC100045866 /// Tceb1, Dicer1, Prpf39, Elac2, Cand1, Fbxo45, Otud7b, Aqr, Aqr, Agk, Uba3, Bxdc5, Exosc10, Mul1, Tbl1x, Adarb1, Parp1, LOC100048362 /// Rimklb, Tfb1m, Sfrs7, Trmt1, Mcm7, Eif4g1, Mcm7, Rlim, Plrg1, Irak1, Ube2j1, Afg3l1, Eif2ak3 /// LOC100047634, Hars2, Grk5, Suz12, Ptprt, Lnx1, Smad3, C1galt1, Kat2b, Prkx, Pomt2, Gemin8, Setdb1, Nova1, 0610007P08Rik, Kdm5d, Zdhhc2, Rbm22, Cad, 2810408M09Rik, Vrk2, BC057552, Dusp11, Sf3a2, Tardbp, Nsmce1, Pxn, Ndst1, Irak1, Exosc8, B3galt5, Smg1, Senp5, Fem1c, Ttll4, Senp7, Cdyl2, Trmt6, Stk32b, Cbx7, Mapk4, Ccdc88a, Gemin5, Rtel1, Bmpr1b, Rrm2b, Ntrk2, Ipmk, Mettl1, Map3k5, March1, Med12l, Socs2, Tdrd3, Ercc1, B230120H23Rik, Tbl1xr1, Lcor, Rad51l3, Pak6, Sf3a1, Hif3a, Mettl1, Spop, Usp15, Fbxl20, Cdc2l5, Elac1, Ep400, Zfc3h1, Zhx2, Utp23, Dgcr8, Zdhhc17, Cdkl3, Ssh2, Ppwd1, LOC100046241 /// Tlk1, Tnks, Ttll10

intracellular membrane-bound organelle	CC	1.26E-05	0.031	7500	Mcm5, Klf10, Sec61a1, Aurkaip1, Mcm6, Ap3m1, Mrpl4, Eif3a, Ube3a, Sigmar1, Cpt2, Tia1, Cisd1, Bet1, Nt5c, Plekha2, Sorbs1, S100a1, Sart3, Sfxn1, Sdc4, Zfp35, Ndst2, Hmgxb3, Ufd1l, Lhx2, Wdr33, Mtx1, Etv3, Rfxap, Bcl10, Invs, Stk39, Tmem9, Trdmt1, Hdgf, Suz12, Myh9, Phf7, B3gnt2, Hccs, Mef2c, Vps25, Zbtb33, Myo7a, Zfp318, Tmem49, Acer2, Txnrd1, Sytl2, Nr3c1, Elk1, Mrpl19, LOC100045442 /// Stag1, Ccdc123, Pex5, Khdrbs2, Uty, Chrac1, Ccnf, Xpc, Yy1, Dgat2, Gyk, Sypl, Sfmbt1, Sc4mol, Tomm20, Npc1, Gnpnat1, Pole4, Plbd2, Stk17b, LOC100048299 /// Max, LOC639633 /// Npm3 /// Npm3-ps1, Ddx41, Cugbp1, Suv420h2, LOC433064 /// Ppih, Hnrpdl, Pet112l, Gart, Cpsf4, Tmem70, Tcof1, Cux1, Tmed10, Zkscan5, Sox10, Zfp472, Ddx19a /// Ddx19b, Ube3a, Mllt6, Polb, Nmnat1, B4galt4, Hltf, Mlh3, Park2, Scmh1, B4galt7, Far1, Cugbp1, Tmem43, Trp53, Me2, Acbd3, Apbb2, Rpap1, Mtmr7, Smo, Ascc2, Ryr1, Mdm2, LOC100045866 /// Tceb1, Dicer1, Pcgf1, Prpf39, Elac2, Mrpl41, Cand1, Cytsb, Mapre1, Otud7b, Klf3 /// LOC100046855, Aqr, Aqr, Mbtps1, Ica1, Agk, 9030409G11Rik, Bxdc5, Exosc10, Rab3c, Nup54, Fubp1, Mul1, Zfp574, Tbl2, Agpat5, Crebzf, Tbl1x, Sema5a, Adarb1, Pip5k1a, Tom1, Id2, Baz2b, Parp1, Bcl2l11, 2310008H09Rik, Tfb1m, Mrpl13, Mrpl22, Sfrs7, Rab2b, Lpp, Serinc1, Cux1, Mcm7, Timm17b, Son, Mcm7, Bach1, Plrg1, Tpp1, Timm22, Cox4nb, Mcm3ap, Ciz1, Ube2j1, Afg3l1, Zfp148, Eif2ak3 /// LOC100047634, Eps15l1, Hars2, Zfx, Suz12, Commd5, Nkx3-1, Ngfr, Tef, Kif5a /// Kif5c, Lnx1, Smad3, Chst11, Surf1, Smpd3, Kat2b, Synpo2, Gadd45b, Oxa1l, Zscan12, Vps36, Ergic2, Pex26, Pomt2, Gemin8, Nop16, Zfp451, Setdb1, Agfg1, Nova1, Phf20, Med26, 0610007P08Rik, Kdm5d, Rab2b, Rbm22, Cad, 2810408M09Rik, 0610038F07Rik, Vrk2, Nr2c2, Wasf2, LOC100047324 /// Sesn1, Dusp11, AU021838, Sf3a2, Tardbp, Unc45a, Nsmce1, Fuca1, Agxt2l2, Syn2, Ppp4c, Tm9sf2, Mrpl13, Ccdc117, Ndst1, Ap2a1, Ing4, Exosc8, Ip6k2, B3galt5, Smg1, Senp5, Ttll4, Hexim2 /// LOC100044959, Cdyl2, Trmt6, Rabl2a, Cbx7, Zfp367, Hspa13, Pknox2, Gtpbp10, Epm2aip1, Csrnp1, Bbs4, Zfp715, Ebf4, Arl4a, Taf5, Mrps5, Ikbkg, Optn, Pphln1, 5730455O13Rik, Ccdc88a, Nfkbid, Pcyt1b, Nmnat2, Gemin5, Rtel1, Mbtps2, Mex3b, Rrm2b, 5430432N15Rik, Ipmk, Zfp799, Npas3, Ddx11, Mllt10, Sept10, Mettl1, Zfp827, Zfp708, Klf12, 4933407N01Rik, Atxn3, Rora, Med12l, Zfp39, Tdrd3, Ercc1, B230120H23Rik, Tbl1xr1, Mga, Zfp827, BC031441, Lcor, Dgkd, Rad51l3, 2700050L05Rik, Yipf5, Pdia3, Sf3a1, Hif3a, Mettl1, Ripply2, Spop, Spred1, Elac1, Ep400, 5730507C01Rik, Rabgap1l, Ccnt2, Cgrrf1, 1110020G09Rik, 2810002N01Rik, Gmeb2, Zfc3h1, Zhx2, Utp23, Dgcr8, Zdhhc17, Cdkl3, Adamts5 /// LOC100048332, LOC100046241 /// Tlk1, Tmem38b, Rbm12, Tia1, 4930422I07Rik, Mtdh, Tmed5, Nup54, Tnks, Zfp592

kinase activity	MF	1.70E-05	0.036	830	Aurkaip1, Tyk2, Csnk1d, Mpp3, Acvr2b, Stk39, Pdgfra, Mapk11, Gyk, Stk17b, Riok2, Rbks, Mark1, Crk, Ryk, Fastkd1, Dscaml1, Pip5kl1, Agk, Etnk1, Pip5k1a, 2010111I01Rik, Irak1, Nrp1, Akap2, Eif2ak3 /// LOC100047634, Grk5, Pip5k1c, Prkx, Cad, 2810408M09Rik, Vrk2, AU021838, Ppp4c, Irak1, Ip6k2, Smg1, Stk32b, Mapk4, Ikbkg, Kcnh1, Bmpr1b, Ntrk2, Ipmk, Dgke, Map3k5, Med12l, B230120H23Rik, Dgkd, Pak6, Cdc2l5, 1110020G09Rik, Sephs1, Cdkl3, LOC100046241 /// Tlk1

					Mcm5, Klf10, Sec61a1, Aurkaip1, Mcm6, Ap3m1, Mrpl4, Eif3a, Ube3a, Sigmar1, Cpt2, Tia1, Cisd1, Bet1, Nt5c, Plekha2, Sorbs1, S100a1, Sart3, Sfxn1, Sdc4, Zfp35, Ndst2, Hmgxb3, Ufd1l, Lhx2, Wdr33, Mtx1, Etv3, Rfxap, Bcl10, Invs, Stk39, Tmem9, Trdmt1, Hdgf, Suz12, Myh9, Phf7, B3gnt2, Hccs, Mef2c, Vps25, Zbtb33, Myo7a, Zfp318, Tmem49, Acer2, Txnrd1, Sytl2, Nr3c1, Elk1, Mrpl19, LOC100045442 /// Stag1, Ccdc123, Pex5, Khdrbs2, Uty, Chrac1, Ccnf, Xpc, Yy1, Dgat2, Gyk, Sypl, Sfmbt1, Sc4mol, Tomm20, Npc1, Gnpnat1, Pole4, Plbd2, Stk17b, LOC100048299 /// Max, LOC639633 /// Npm3 /// Npm3-ps1, Ddx41, Cugbp1, Suv420h2, LOC433064 /// Ppih, Hnrpdl, Pet112l, Gart, Cpsf4, Tmem70, Tcof1, Cux1, Tmed10, Zkscan5, Sox10, Zfp472, Ddx19a /// Ddx19b, Ube3a, Mllt6, Polb, Nmnat1, B4galt4, Hltf, Mlh3, Park2, Scmh1, B4galt7, Far1, Cugbp1, Tmem43, Trp53, Me2, Acbd3, Apbb2, Rpap1, Mtmr7, Smo, Ascc2, Ryr1, Mdm2, LOC100045866 /// Tceb1, Dicer1, Pcgf1, Prpf39, Elac2, Mrpl41, Cand1, Cytsb, Mapre1, Otud7b, Klf3 /// LOC100046855, Aqr, Aqr, Mbtps1, Ica1, Agk, 9030409G11Rik, Bxdc5, Exosc10, Rab3c, Nup54, Fubp1, Mul1, Zfp574, Tbl2, Agpat5, Crebzf, Tbl1x, Sema5a, Adarb1, Pip5k1a, Tom1, Id2, Baz2b, Parp1, Bcl2l11, 2310008H09Rik, Tfb1m, Mrpl13, Mrpl22, Sfrs7, Rab2b, Lpp, Serinc1, Cux1, Mcm7, Timm17b, Son, Mcm7, Bach1, Plrg1, Tpp1, Timm22, Cox4nb, Mcm3ap, Ciz1, Ube2j1, Afg3l1, Zfp148, Eif2ak3 /// LOC100047634, Eps15l1, Hars2, Zfx, Suz12, Commd5, Nkx3-1, Ngfr, Tef, Kif5a /// Kif5c, Lnx1, Smad3, Chst11, Surf1, Smpd3, Kat2b, Synpo2, Gadd45b, Oxa1l, Zscan12, Vps36, Ergic2, Pex26, Pomt2, Gemin8, Nop16, Zfp451, Setdb1, Agfg1, Nova1, Phf20, Med26, 0610007P08Rik, Kdm5d, Rab2b, Rbm22, Cad, 2810408M09Rik, 0610038F07Rik, Vrk2, Nr2c2, Wasf2, LOC100047324 /// Sesn1, Dusp11, AU021838, Sf3a2, Tardbp, Unc45a, Nsmce1, Fuca1, Agxt2l2, Syn2, Ppp4c, Tm9sf2, Mrpl13, Ccdc117, Ndst1, Ap2a1, Ing4, Exosc8, Ip6k2, B3galt5, Smg1, Senp5, Ttll4, Hexim2 /// LOC100044959, Cdyl2, Trmt6, Rabl2a, Cbx7, Zfp367, Hspa13, Pknox2, Gtpbp10, Epm2aip1, Csrnp1, Bbs4, Zfp715, Ebf4, Arl4a, Taf5, Mrps5, Ikbkg, Optn, Pphln1, 5730455O13Rik, Ccdc88a, Nfkbid, Pcyt1b, Nmnat2, Gemin5, Rtel1, Mbtps2, Mex3b, Rrm2b, 5430432N15Rik, Ipmk, Zfp799, Npas3, Ddx11, Mllt10, Sept10, Mettl1, Zfp827, Zfp708, Klf12, 4933407N01Rik, Atxn3, Rora, Med12l, Zfp39, Tdrd3, Ercc1, B230120H23Rik, Tbl1xr1, Mga, Zfp827, BC031441, Lcor, Dgkd, Rad51l3, 2700050L05Rik, Yipf5, Pdia3, Sf3a1, Hif3a, Mettl1, Ripply2, Spop, Spred1, Elac1, Ep400, 5730507C01Rik, Rabgap1l, Ccnt2, Cgrrf1, 1110020G09Rik, 2810002N01Rik, Gmeb2, Zfc3h1, Zhx2, Utp23, Dgcr8, Zdhhc17, Cdkl3, Adamts5 /// LOC100048332, LOC100046241 /// Tlk1, Tmem38b, Rbm12, Tia1, 4930422I07Rik, Mtdh, Tmed5, Nup54, Tnks, Zfp592
membrane-bound organelle	CC	1.31E-05	0.031	7503	

nucleobase, nucleoside, nucleotide and nucleic acid metabolic process	CC	1.64E-06	0.007	3089	Impdh2, Mcm5, Klf10, Mcm6, Atp6v0e, Nt5c, Sart3, Zfp35, Cpeb1, Lhx2, Etv3, Trdmt1, Hdgf, Suz12, Mef2c, Vps25, Zbtb33, Zfp318, Nr3c1, Elk1, Khdrbs2, Uty, Xpc, Yy1, Gnpnat1, LOC100048299 /// Max, LOC639633 /// Npm3 /// Npm3-ps1, Ddx41, Cugbp1, Suv420h2, LOC433064 /// Ppih, Hnrpdl, Gart, Cpsf4, Tcof1, Cux1, Zkscan5, Sox10, Zfp472, Polb, Nmnat1, Hltf, Mlh3, Scmh1, Cugbp1, Trp53, Rpap1, Ascc2, Dscaml1, EG665955, LOC100045866 /// Tceb1, Dicer1, Pcgf1, Prpf39, St5, Elac2, Cand1, Klf3 /// LOC100046855, Aqr, Aqr, Bxdc5, Exosc10, Fubp1, Zfp574, Crebzf, Tbl1x, Adarb1, Parp1, Tfb1m, Sfrs7, Trmt1, Cux1, Mcm7, Eif4g1, Mcm7, Rlim, Bach1, Plrg1, Zfp148, Hars2, Zfx, Suz12, Nkx3-1, Tef, Smad3, Kat2b, Zscan12, Vps36, Gemin8, Zfp451, Setdb1, Nova1, Phf20, Med26, 0610007P08Rik, Kdm5d, Rbm22, Cad, Nr2c2, AU021838, Sf3a2, Tardbp, Nsmce1, Exosc8, Smg1, Hexim2 /// LOC100044959, Fpgt, Cdyl2, Trmt6, Cbx7, Zfp367, Csrnp1, Zfp715, Ebf4, Taf5, Ikbkg, Ccdc88a, Nmnat2, Gemin5, Rtel1, Mbtps2, Rrm2b, 5430432N15Rik, Zfp799, Npas3, Ddx11, Mettl1, Zfp827, Zfp708, Klf12, Atxn3, Rora, Med12l, Zfp39, Tdrd3, Ercc1, Tbl1xr1, Mga, Zfp827, BC031441, Lcor, Rad51l3, 2700050L05Rik, Sf3a1, Hif3a, Mettl1, Elac1, Ep400, 5730507C01Rik, Gmeb2, Zfc3h1, Gmps, Zhx2, Utp23, Dgcr8, Ppwd1, LOC100046241 /// Tlk1, 4930422I07Rik, Zfp592

nucleus	CC	4.45E-07	0.005	4706	Mcm5, Klf10, Aurkaip1, Mcm6, Eif3a, Ube3a, Sigmar1, Tia1, Nt5c, Plekha2, Sorbs1, Sart3, Zfp35, Hmgxb3, Ufd1l, Lhx2, Wdr33, Etv3, Rfxap, Bcl10, Invs, Stk39, Trdmt1, Hdgf, Suz12, Myh9, Phf7, Mef2c, Vps25, Zbtb33, Zfp318, Txnrd1, Nr3c1, Elk1, Mrpl19, LOC100045442 /// Stag1, Khdrbs2, Uty, Chrac1, Ccnf, Xpc, Yy1, Sfmbt1, Pole4, Stk17b, LOC100048299 /// Max, LOC639633 /// Npm3 /// Npm3-ps1, Ddx41, Cugbp1, Suv420h2, LOC433064 /// Ppih, Hnrpdl, Gart, Cpsf4, Tcof1, Cux1, Zkscan5, Sox10, Zfp472, Ddx19a /// Ddx19b, Ube3a, Polb, Nmnat1, Hltf, Mlh3, Park2, Scmh1, Cugbp1, Tmem43, Trp53, Apbb2, Rpap1, Mtmr7, Ascc2, Mdm2, LOC100045866 /// Tceb1, Dicer1, Pcgf1, Prpf39, Elac2, Cand1, Cytsb, Otud7b, Klf3 /// LOC100046855, Aqr, Aqr, Mbtps1, 9030409G11Rik, Bxdc5, Exosc10, Nup54, Fubp1, Zfp574, Crebzf, Tbl1x, Adarb1, Id2, Baz2b, Parp1, 2310008H09Rik, Sfrs7, Lpp, Cux1, Mcm7, Son, Mcm7, Bach1, Plrg1, Mcm3ap, Ciz1, Zfp148, Eps15l1, Zfx, Suz12, Commd5, Nkx3-1, Ngfr, Tef, Kif5a /// Kif5c, Lnx1, Smad3, Kat2b, Synpo2, Gadd45b, Zscan12, Vps36, Ergic2, Gemin8, Nop16, Zfp451, Setdb1, Agfg1, Nova1, Phf20, Med26, 0610007P08Rik, Kdm5d, Rbm22, Cad, 2810408M09Rik, Nr2c2, LOC100047324 /// Sesn1, Dusp11, AU021838, Sf3a2, Tardbp, Unc45a, Nsmce1, Ppp4c, Ccdc117, Ing4, Exosc8, Ip6k2, Smg1, Senp5, Hexim2 /// LOC100044959, Cdyl2, Trmt6, Rabl2a, Cbx7, Zfp367, Pknox2, Gtpbp10, Csrnp1, Zfp715, Ebf4, Arl4a, Taf5, Ikbkg, Pphln1, 5730455O13Rik, Nfkbid, Gemin5, Rtel1, Mbtps2, Mex3b, Rrm2b, 5430432N15Rik, Ipmk, Zfp799, Npas3, Ddx11, Mllt10, Sept10, Mettl1, Zfp827, Zfp708, Klf12, Atxn3, Rora, Med12l, Zfp39, Tdrd3, Ercc1, B230120H23Rik, Tbl1xr1, Mga, Zfp827, BC031441, Lcor, Rad51l3, 2700050L05Rik, Sf3a1, Hif3a, Mettl1, Ripply2, Spop, Spred1, Elac1, Ep400, 5730507C01Rik, Rabgap1l, Ccnt2, Cgrrf1, Gmeb2, Zfc3h1, Zhx2, Utp23, Dgcr8, Cdkl3, Adamts5 /// LOC100048332, LOC100046241 /// Tlk1, Rbm12, Tia1, 4930422I07Rik, Mtdh, Nup54, Tnks, Zfp592

phosphotransferase activity, alcohol group as acceptor	MF	2.33E-05	0.044	678	Tyk2, Csnk1d, Acvr2b, Stk39, Pdgfra, Mapk11, Gyk, Stk17b, Riok2, Rbks, Mark1, Ryk, Fastkd1, Pip5kl1, Agk, Etnk1, Pip5k1a, 2010111I01Rik, Irak1, Nrp1, Eif2ak3 /// LOC100047634, Grk5, Pip5k1c, Prkx, Cad, 2810408M09Rik, Vrk2, Ppp4c, Irak1, Ip6k2, Smg1, Stk32b, Mapk4, Kcnh1, Bmpr1b, Ntrk2, Ipmk, Dgke, Map3k5, Med12l, B230120H23Rik, Dgkd, Pak6, Cdc2l5, 1110020G09Rik, Cdkl3, LOC100046241 /// Tlk1
rRNA transcription	BP	4.22E-05	0.074	12	LOC639633 /// Npm3 /// Npm3-ps1, Tcof1, Trp53
transferase activity, transferring phosphorus-containing groups	MF	1.73E-06	0.007	967	Aurkaip1, Tyk2, Csnk1d, Mpp3, Acvr2b, Stk39, Pdgfra, Mapk11, Chrac1, Gyk, Pole4, Stk17b, Riok2, Rbks, Polb, Mark1, Nmnat1, Crk, Ryk, Rpap1, Fastkd1, Dscaml1, EG665955, Pip5kl1, Agk, Etnk1, Ugp2, Pip5k1a, 2010111I01Rik, Irak1, Nrp1, Akap2, Eif2ak3 /// LOC100047634, Grk5, Pip5k1c, Prkx, Ugp2, Cad, 2810408M09Rik, Vrk2, AU021838, Ppp4c, Irak1, Ip6k2, Smg1, Fpgt, Stk32b, Mapk4, Ikbkg, Kcnh1, Pcyt1b, Nmnat2, Bmpr1b, Ntrk2, Ipmk, Dgke, Map3k5, Med12l, B230120H23Rik, Dgkd, Pak6, Cdc2l5, 1110020G09Rik, Sephs1, Cdkl3, LOC100046241 /// Tlk1

R6-2 8 weeks D1 GO analysis

GO Term	Ontology	p value	Adjusted p value	Genes present
integrase activity	MF	7.64E-14	1.88E-09	100039204 /// 100039345 /// 100040790 /// 100041175 /// 100041416 /// 100042151 /// 100042787 /// 100043211 /// 100043258 /// 100043316 /// 434166 /// Bzw2 /// OTTMUSG00000017752

R6-2 8 weeks D2 GO analysis

GO Term	Ontology	p value	Adjusted p value	Genes present
interleukin-11 binding	MF	5.62E-06	0.074	100038993 /// Il11ra1 /// Il11ra2 /// OTTMUSG00000011351
interleukin-11 receptor activity	MF	5.62E-06	0.074	100038993 /// Il11ra1 /// Il11ra2 /// OTTMUSG00000011351

R6-2 12 weeks D1 GO analysis

GO Term	Ontology	p value	Adjusted p value	Total genes in GO class	Genes present
protein binding	MF	1.43E-06	0.034	6998	Fryl, Creg1, LOC100048726 /// Sec23b, Efr3a, Olig1, Vcl, Sec61a1, Crk, Il2rg, Shcbp1, Wwox, Ap3m1, Dpf2, Ezh2, Ptprn, Acvr1, C1d, Tsn, Psme1, Gipc2, Ppm1a, Il16, Nap1l5, Arid1a, Cap1, Ctnnbip1, Thumpd3, Cplx1, Ccna2, Pak3, Ncapg2, Apoa2, Tnfrsf1b, Hey2, Ezh1, Kif5b, Stx7, Yes1, Cenpo, Sf3b1, Limk2, Avpr1a, Kcnj1, Rgs9, Fech, Ccl25, F10, Nagk, Vsx2, Efnb2, Trp53rk, Asgr2, Cul2, Arap3, Nfkbia, Sntb2, Pcdhb19, Pglyrp2, Ccdc50, Sgce, Dach1, Ppp3cc, Ccndbp1, Pcdha1 /// Pcdha10 /// Pcdha11 /// Pcdha12 /// Pcdha2 /// Pcdha3 /// Pcdha4 /// Pcdha5 /// Pcdha6 /// Pcdha7 /// Pcdha8 /// Pcdha9 /// Pcdhac1 /// Pcdhac2, Hdac7, Ywhag, Ywhaq, Itga9, Tgfbr1, Cnot4, 2610028A01Rik, Itsn1, Chrna4, Rnf144a, Irf9, Csf2rb, Mynn, Gria4, Trim34, Adrb3, Tnfrsf8, Cacna1e, Eya1, Nr5a1, Stag2, Tcf12, Faah, Eif4e2, Strn, Ntn3, Khdrbs2, LOC100047606 /// Ntrk3, Hist1h1e, Krt1, Cpox, Cask, Rprm, Yy1, Exoc4, Ttyh1, Pmepa1, Inha, Mapre1, Fstl3, Prkcd, Ctbp2, Fgf3, Pcdhb6, Txndc17, Tmod3, Irs1, Shoc2, Sfrs5, Id4 /// LOC100045546, Nedd4l, Stmn2, Hyou1, Pnn, Ergic1, Orc4l, Wnt7a, Psmd9, Phip, Kptn, Rad54l2, LOC100048299 /// Max, Tagln, Cct6a, Tram1, Ddx41, Prpf6, Ppp5c, Gprin1, Nup93, Camkk2, Camkk2, Elmo1, Frag1, Cstf3, Rasgrf1, Zbtb1, Ric8, Ptbp1, Baiap2l1, Vrk1, Ephb2, Cdh10, Ace2, Epb4.1l5, Tcf7l2, Trim31, Polb, Parn, Il12a, H2-D1, Klc4, Edil3, Cep290, Lepr, Eps8 /// LOC632638, Recql, Csrp1, Hpca, Limk1, Nek6, Htt, Wt1, Rabggta, Trib3, Tor1aip1, Syt6, Kcnj9, Gipc3, Kitl, Shmt2, Gphn, Rasa1, Ckap4, Hipk3, Cln5, Crim1, Myh4, Zbed4, Zbtb3, Sfrs12, Hnrpll, Palld, Mll1, Ryr1, Dab1, Dapk1, Odc1, Mdm2, Ids, Myh1, Pold4, Mycbp, Hist1h4h, Synj2bp, Ptcd3, Ebf3, Cand1, Hopx, Zbtb46, 2610524H06Rik, Csnk2a2, Styx, Clasp2, Myl6b, Slc9a3r2, Myo5a, Scara5, Gas7, Slc4a1, Il34, Stambp, Sh3kbp1, Cbx3, Cd80, Derl1, Cdc37l1, Sox4, S100pbp, Pla2g1b, Rcan3, Tle1, Kat2b, Ibtk, Adipor2, S100b, Ncoa1, Ero1lb, Coro2b, Iqgap3, Sec61a1, Pip5k1a, Limch1, Sod1, Pim1, Pacs1, Actr10, Itsn1, Atp1a1, Rab3gap2, Kazald1, Sptlc1, D0H4S114, Sh3bgrl, Usp39, Akap9, Rpa1, EG620521 /// Hnrnpr, Apex1, Pax6, Nupl1, Hexb, Bat1a, Eea1, Vim, Rbm39, Id4, Srr, Srr, Masp1, Foxp1, Nup54, Dtx2, Syt2, Bach1, Fgf3, Ankib1, Rnf2, Wwp2, Cul1, Fkbp5, Rdx, Lgals3bp, Myh6 /// Myh7, Ralbp1, Smc2, Eed, Arhgdig, Rpp25, Nfat5, Syn2, Crem, Mapk8ip2, Cdh2, B2m, Hsf2, Zfp53, Qpctl, Trps1, Coro1c, Map3k6, Ctnnb1, Pard6g, Itga9, Stat1, Gopc, H2-D1, Ngfr, Cbx5, Ccl24, Gli3, Ing3, Zfp191, Cbx1, Sgcd, D0H4S114, Wdr1, Rqcd1, Bcl2l2, LOC100047651 /// Zfpm1, Atp1a1, Cmtm6, Pias3, Edem1, Lamb1-1, Ppp5c, Ctsl, Spon1, Racgap1, Angptl7, Mtss1, Rhobtb2, H2-D1, H2-D1, Mib1, Setdb1, H2-L, Txnrd2, Trdn, Dyrk1a, Dlat, Actr1b, Rrp1b, Phf17, Ahnak, Fxr1,

Shprh, Rnf20, Atp2a2, Coro2a, Mll1, Actn1, LOC100046932 /// Taf4a, H2-D1 /// H2-T18 /// H2-T3 /// H2-T3-like /// H2-Tw3 /// LOC674370, Pcbd2, Tubb2b, Itgav, Ppfia4, Apaf1, Gna13, Serinc1, Ckap4, Pip5k1a, Vps18, Ccnd2, Itgb5, Trib3, Fgf17, Lasp1, Mat2a, Hexb, Phyh, Cmtm7, Dusp7, Brpf1, 100039786 /// OTTMUSG00000014597 /// Ywhaq, Ap2a1, Cltb /// LOC100046457, Pramef12, LOC676870 /// Pbx1, Tns1, Pfn4, Otud7b, Smurf2, Tln2, Nradd, Gapvd1, 2310057M21Rik, Dab2, Cdc73, Fcnb, Klf5, Sdcbp, Cmtm5, Lrrc28, Rassf4, Dnajc8, 2310061N02Rik, Mllt4, Dock8, Parp14, Pde3b, Gcn1l1, Ntf3, Irak3, Prmt8, Taf4b, Sarm1, Htr2c, Atl2, Nufip2, Klhl12, Ppm1l, Aph1b, Ppfia1, Lrrc15, Rnf24, Dock4, Metap2, Rgs7bp, Lsm6, Peli2, Zbtb7a, Pak3, Nedd4l, Plec1, Nek2, Lrrtm2, Tgfb2, Shc2, Parvb, Hnrnpr, Fras1, 627912 /// Mllt4 /// Zfp160, Klhl4, Zbtb16, Dnajb4, Hrk, Ank2, Dynll1, Rxfp1, Lrp8, Strn3, Wnt8b, Socs2, Kctd8, Kcnj5, Atp8b2, Zfp467, Fgf3, Lynx1, Zfp295, Usp4, Top2a, Lrch1, Pdzrn3, Atp2a2, Utf1, Ppp4r4, Tbc1d5, Agrn, Rgnef, Epb4.1, Thrsp, Cep135, Tm2d1, Adcy1, Chn1, Ostf1, Akap9, Cd84, Atox1, Dnajc17 /// EG621763, Tbc1d5, Snx6, Srrm1, Ripply2, Spop, Hist2h2be, Zbtb7a, Med13, Fam175a, Pdzd11, Mpp7, Fnbp1, Senp8, Mpp7, Mif, Cep97, Mapt, Phf16, Pak6, Frem1, Abl2, Vangl2, Ssh1, Ltbp3, Emx2, Ints10, Clspn, Pag1, Fbxo41, Paip1, Ppfia2, Garnl1, Snx19, Tcf4, Kdm2a, Vapb, Matr3, Ston2, Adam23, Nup54, Hecw1

R6-2 D2 TRAP GO Analysis

GO Term	Ontology	p value	Adjusted p value	Total genes in GO class	Genes present
cell morphogenesis	BP	3.51E-13	5.21E-10	311	Gja1, Stmn1, Tbr1, Cap1, Chl1, Gas7, Dcx, Dcx, Lhx2, Notch1, Atp7a, Drd2, Cnp, Pdpn, Rgnef, Rgnef, Ect2, Myh9, Myh9, Atp2b2, 100039963 /// Sema3a, Add1, Apc, Plxna3, Myo7a, Etv1, Shroom3, Isl1, Ift172, Dclk1, Dst, Slit2, Enah, Enah, Ndel1, Mapk8ip3, Hnrnpab, Slc1a3, Apbb2, Ptprz1, Sox6, Egr2, Pafah1b1, Apoe, Cdk5r1, Mycbp2, Sod1, Hmgb1, Atp7a, Cnp, Gja1, Gja1, 100042515 /// EG545555 /// EG546331 /// EG665056 /// ENSMUSG00000060128 /// Hmg1l1 /// Hmgb1 /// LOC100045972 /// LOC100046019 /// LOC637733, EG623112 /// Stmn1, Hnrnpab, Hif1a, 100039943 /// 100040234 /// 100041386 /// 100041667 /// 100042549 /// 100043683 /// 4932431P20Rik /// EG432959 /// EG545506 /// EG545555 /// EG546331 /// EG666011 /// EG666969 /// Hmg1l1 /// Hmgb1 /// Hmgb1l /// LOC100045876 /// LOC637733 /// OTTMUSG00000007611 /// OTTMUSG00000015121, Ulk1, Pafah1b1, Dscam, Klf7, B3gnt2, Arx /// LOC100044440, Kif5a /// Kif5c, Onecut1, Isl1, Nr4a2, Dclk1, Tgfb2, Ephb3, Ptprz1, Hnrnpab, Ablim1, Ntn1, Gli2, Pafah1b1, Nrn1, Dync2h1, Pcnt, Kif5a, Nr2e1, Chl1, Apc, Dnaic2, Sema6a, Efna5, Bmpr1b, Sema5a, Prox1, Bcl11b, Slitrk3, Onecut2, Dcc, Evl /// LOC100047333, Dscam, Enah, Rgnef, Pcdh15, Onecut2, Sox6, Nr4a2, Col4a3bp, Ablim1, Mycbp2, Nr4a2, Onecut2
cell projection organization	BP	1.10E-15	2.77E-12	344	Gja1, Stmn1, Cd24a, Rdx, Rdx, Tbr1, Vav3, Lpar1, Frap1, Chl1, Gas7, Dcx, Dcx, Lhx2, Notch1, Atp7a, Drd2, Cnp, Rgnef, Rgnef, Myh9, Myh9, Atp2b2, 100039963 /// Sema3a, Apc, Plxna3, Myo7a, Itga6, Itga6, Lima1, Etv1, Isl1, Ift172, Ube2b, Dclk1, Rock1, Rock1, Dst, Fgfr1, Lamb1-1, Gprin1, Slit2, Enah, Enah, Ndel1, Klc3, Baiap2, Mapk8ip3, Cit, Lpin1, EG666036 /// EG666422 /// EG666875 /// EG668576 /// Phgdh, Apbb2, Wasl, Ptprz1, Egr2, Pafah1b1, Atg7, Atg7, Apoe, Cdk5r1, Myo6, Mtss1, Arf6, Mycbp2, Sod1, Myo6, Atp7a, Ccdc88a, Cnp, EG665516 /// EG666036 /// EG668771 /// Phgdh, Gja1, Gja1, EG623112 /// Stmn1, Rdx, Ulk1, Pafah1b1, Vav3, Lpar1, Nrtn, Dscam, Klf7, Prkg1, B3gnt2, Arx /// LOC100044440, Kif5a /// Kif5c, Onecut1, Lima1, Isl1, Nr4a2, Dclk1, Tgfb2, Rock1, Baiap2, Ephb3, Klf5, Gtrgeo22, Ptprz1, Wasf2, Ablim1, EG665516 /// EG666036 /// EG668771 /// Phgdh, Ntn1, EG385344 /// EG627427 /// EG665516 /// EG666036 /// EG666422 /// EG666875 /// EG668506 /// EG668576 /// EG668771 /// LOC630761 /// LOC630896 /// OTTMUSG00000011498 /// Phgdh, Gli2, Pafah1b1, Nrn1, Dync2h1, Pcnt,

					Mtap2, Alkbh1, Kif5a, Nr2e1, Chl1, Apc, Dnaic2, Cc2d2a, Sema6a, Grin3a, Efna5, Bmpr1b, Sema5a, Wasf2, Bcl11b, Grin3a, Slitrk3, Ube2b, Onecut2, Dcc, Mtap2, Evl /// LOC100047333, Akt1, Dscam, Enah, Rgnef, Pcdh15, Onecut2, Nck1, Nr4a2, Ablim1, Mycbp2, Nr4a2, Fgd4, Neurl1a, Ppp1r9a, Rasgrf1, Onecut2
cellular component morphogenesis	BP	6.81E-13	9.17E-10	339	Gja1, Stmn1, Tbr1, Cap1, Chl1, Gas7, Dcx, Dcx, Lhx2, Notch1, Tnnt2, Atp7a, Drd2, Cnp, Pdpn, Rgnef, Rgnef, Ect2, Myh9, Myh9, Atp2b2, 100039963 /// Sema3a, Add1, Apc, Plxna3, Myo7a, Etv1, Shroom3, Isl1, Ift172, Ube2b, Dclk1, Dst, Slit2, Enah, Enah, Ndel1, Tnnt2, Mapk8ip3, Hnrnpab, Slc1a3, Apbb2, Ptprz1, Sox6, Egr2, Pafah1b1, Acta1, Apoe, Cdk5r1, Mycbp2, Sod1, Hmgb1, Atp7a, Cnp, Gja1, Gja1, 100042515 /// EG545555 /// EG546331 /// EG665056 /// ENSMUSG00000060128 /// Hmg1l1 /// Hmgb1 /// LOC100045972 /// LOC100046019 /// LOC637733, EG623112 /// Stmn1, Hnrnpab, Hif1a, 100039943 /// 100040234 /// 100041386 /// 100041667 /// 100042549 /// 100043683 /// 4932431P20Rik /// EG432959 /// EG545506 /// EG545555 /// EG546331 /// EG666011 /// EG666969 /// Hmg1l1 /// Hmgb1 /// Hmgb1l /// LOC100045876 /// LOC637733 /// OTTMUSG00000007611 /// OTTMUSG00000015121, Ulk1, Pafah1b1, Dscam, Klf7, B3gnt2, Arx /// LOC100044440, Kif5a /// Kif5c, Onecut1, Isl1, Nr4a2, Dclk1, Tgfb2, Ephb3, Gtrgeo22, Agfg1, Ptprz1, Hnrnpab, Ablim1, Ntn1, Gli2, Pafah1b1, Nrn1, Dync2h1, Pcnt, Kif5a, Nr2e1, Chl1, Apc, Dnaic2, Sema6a, Efna5, Bmpr1b, Sema5a, Prox1, Bcl11b, Slitrk3, Ube2b, Onecut2, Dcc, Evl /// LOC100047333, Dscam, Enah, Rgnef, Pcdh15, Onecut2, Sox6, Nr4a2, Col4a3bp, Ablim1, Mycbp2, Nr4a2, Neurl1a, Onecut2
cellular component organization	BP	6.08E-13	8.37E-10	2110	Atg5, Gja1, Gsn, Stmn1, Lcp1, Satb1, Cd24a, Flii, Ap1s1, Eif3d, Hist1h1c, 100042266 /// EG434428 /// EG636070 /// LOC100044416 /// LOC100045728 /// Tuba1a /// Tuba1b /// Tuba1c, Fbln5, Rdx, Rdx, Arpc1b, Cat, Dctpp1, Trrap, Ezh2, Acin1, Tbr1, H2afx, Trpm7, Nid1, Kpnb1, Bid, Vav3, Lpar1, Mlh1, Sertad1, Arid1a, Tacc3, Cap1, Hells, Timeless, Frap1, Limk1, Ankfy1, Unc13b, Chl1, Gas7, Vldlr, Dclre1a, Gng4, Ghr, Sh3glb1, Ndufs4, Dcx, Dcx, Lhx2, Phf21a, Kif5b, Kif5b, Kif5b, Nap1l3, Col11a1, Notch1, Tnnt2, LOC100046998 /// Opa1, Atp7a, Epc1, Nek3, Drd2, Cnp, Rgs14, Abca7, Spnb2, Tns1, Pdpn, Hook2, l7Rn6, l7Rn6, Pclo, Rgnef, Rgnef, Immp2l, Ect2, Cd47, Pttg1, Sgcb, Myo5a, Scp2, Myh9, Myh9, Atp2b2, 100039963 /// Sema3a, 100043064 /// Nap1l1, Nap1l1, Cacng2, Ttf1, Cd2ap, Add1, Apc, Plxna3, Tro, Myo7a, Cdkn1a, Col19a1, Abca1, Gria2, Inhba, LOC100047606 /// Ntrk3, Hras1, Cdk4 /// LOC640611, Cdk4 /// LOC640611, Itga6, Itga6, Lima1, H2-DMa, Etv1, Shroom3, Ache, Isl1, Eps8 /// LOC632638, Eps8, Xrn2, Tfrc, Kat2a, Dnmt3a, Ift172, Npc1, Tmod3, Ube2b, Dclk1, Rala, Taf7, Pard6b, Itsn2, Ncor1, Cap2,

Wnt7a, Rock1, Rock1, Myst4, Dst, Tubb2c, Ndufs8, Anapc4, Fgfr1, Lamb1-1, Hras1, Gprin1, Ccdc80, Elmo1, Msto1, Slit2, Rab5c, Mapt, Hip1, Enah, Enah, Nefh, Ndel1, Tnnt2, Slu7, Klc3, Anxa5, Baiap2, Tacc2, Olfm1, Sorbs1, Mapk8ip3, Cit, Hnrnpab, Slc1a3, LOC100048460 /// Lzts2, Rasa1, Lpin1, Trp53, Tesk2, Olfm1, Arhgap17, EG666036 /// EG666422 /// EG666875 /// EG668576 /// Phgdh, Apbb2, Cnn3 /// LOC100047856, Mfn1, Wasl, Smarca4, Uimc1, Ep400, Pbrm1, Ptprz1, Abi3bp, Mll3, Spg7, Mll5, Smc4, Bptf, Tubb2a, Zwint, Kdm6a, Sox6, Egr2, Pafah1b1, Acta1, Tubb2a, Spna2, Spna2, Rnf6, Dicer1, Caprin2, 2310043N10Rik, 2610039C10Rik, Atg7, Atg7, Mapre1, Hmg20a, Eny2, Dnajb6, Itsn2, Pdss1, Tekt1, Aplp2, Apoe, Cdk5r1, Anln, Nisch, Myo6, Mtss1, Arf6, Wdtc1, Ndufs8, Mycbp2, Mrpl15, Mrpl15, Mrpl15, Sod1, Kif11, Hmgb1, Fcgr2b, Myo6, Nde1, Hist3h2a, Itsn1, Fxc1, Ipo4, Kazald1, Atp7a, Gsn, Lats2, Gsn, Ccdc88a, Cnp, Rcor1, EG665516 /// EG666036 /// EG668771 /// Phgdh, Coro1c, Hexb, Gja1, Eea1, Chd4, Gja1, Fhdc1, Bptf, Cdc20, Incenp, Lats2, 100042515 /// EG545555 /// EG546331 /// EG665056 /// ENSMUSG00000060128 /// Hmg1l1 /// Hmgb1 /// LOC100045972 /// LOC100046019 /// LOC637733, Chd7, EG623112 /// Stmn1, Hnrnpab, Hif1a, Flii, 100039943 /// 100040234 /// 100041386 /// 100041667 /// 100042549 /// 100043683 /// 4932431P20Rik /// EG432959 /// EG545506 /// EG545555 /// EG546331 /// EG666011 /// EG666969 /// Hmg1l1 /// Hmgb1 /// Hmgb1l /// LOC100045876 /// LOC637733 /// OTTMUSG00000007611 /// OTTMUSG00000015121, Rdx, Hdac1, Ulk1, Eif3a, Pafah1b1, Vav3, Lpar1, Fcgr3, Smc2, Eed, Lrp1, Sept4, Hdac6, Blm, Cadps, Ino80, Ina /// LOC100047943, Ina /// LOC100047943, Rhou, Rhou, Akap2, Nrtn, Tns1, Dscam, Klf7, Mfn1, Casp3, Prkg1, Hsd17b12, Ccng1, B3gnt2, Arx /// LOC100044440, Fmn2 /// LOC100044570, Baz1b, Nolc1, Brdt, Fmnl1, Kif5a /// Kif5c, Onecut1, Nf2, Musk, Lima1, Isl1, Nr4a2, Cenpa, Stx6, Ezr, Dclk1, Tgfb2, Rock1, Baiap2, Brd8, Rerg, Mul1, Ephb3, Prkdc, Acvrl1, Ttl, Klf5, Atg12, Arid4b, Gtrgeo22, Taf11, Thrap3, Spnb2, Smc4, Agfg1, Ptprz1, Smarca2, Itsn1, Brd8, Suz12, Mll1, Hist1h2bc /// Hist1h2be /// Hist1h2bl /// Hist1h2bm /// Hist1h2bp /// LOC100046213 /// LOC665622 /// RP23-38E20.1, Tubb2b, Sfrs2ip, Gria2, 2610039C10Rik, Fxc1, Hnrnpab, Usp21, Wasf2, Ablim1, EG665516 /// EG666036 /// EG668771 /// Phgdh, Rbbp4, Ntn1, Timm13, Ndufs8, Sept4, Notch2, Olfm1, Tgfbi, Pex6, Gsn, EG385344 /// EG627427 /// EG665516 /// EG666036 /// EG666422 /// EG666875 /// EG668506 /// EG668576 /// EG668771 /// LOC630761 /// LOC630896 /// OTTMUSG00000011498 /// Phgdh, Bptf, Gli2, Lasp1, Hexb, Pafah1b1, Epb4.9, Ppp4c, Arid4b, Tspyl1, Smarcc2, Nrn1, Chd3, Fmnl2, Cep192, Lrrcc1, Dync2h1, Aqp11, Tubgcp4, Gapvd1, 4921505C17Rik, Megf10, Cd47, Chd6, Srpk2, Nrxn1, Kank1, Als2cl, Fat1, Pcnt, Ablim3, Mll3, Mtap2, Alkbh1, Kif5a, Ep300, Iqcb1, Dok7, Tdrd3, Nr2e1, Atpaf1, Cenpe, Nsd1, Tubgcp6, Lrrcc1, Lrrcc1, Chl1, Rtn4, Taf4b,

					Epas1, Apc, Mpzl3, Phf21a, Ston2, Optn, Nrxn2, Dlc1, Cdc42bpg, Dnaic2, Cc2d2a, Sema6a, Grin3a, Ermn, Itsn1, H2afv, Efna5, Nav1, Ep400, Kdm5a, Nlgn1, Rrm2b, Bmpr1b, Sgol2, Sema5a, Nek2, Nek2, Chd7, Pacsin3, Dusp18, Prox1, Epb4.9, Cdc42bpa, Wasf2, Steap2, Bcl11b, Grin3a, Rps6ka5, Mll5, Mll5, Hook1, Slitrk3, Ube2b, Ipo9, Dot1l, Ston1, Anln, Rtn4, Onecut2, Rps6ka5, Kdm6b, Cbx4, Dcc, Chrna7, Mtap2, Lrp8, Evl /// LOC100047333, Ermn, Akt1, Parp4, Dscam, Phf21a, Atg4c, Mtap9, Enah, Lrp8, Steap2, Huwe1, Rgnef, Spnb2, Pcdh15, Phf21a, Onecut2, Tubb6, Gspt1, Elmo1, Hook3, Nck1, Cep164, Ep400, Taf1, Sox6, Gng4, Hist2h2be, Nr4a2, Jmjd1c, Col4a3bp, Igf1r, Ablim1, Gapvd1, Ube2i, Cttnbp2, Ehmt1, Mycbp2, Mapt, Nr4a2, Aifm2, Smarcc1, Fgd4, Gspt2, Kdm2a, Kdm6b, Htt, Neurl1a, Adamts20, Mll3, Dot1l, Ppp1r9a, Lmna, Dclre1c, Kdm3b, Daam1, Rasgrf1, Anapc11, Palm2, Hps1, Onecut2, Dlc1
induction of positive chemotaxis	BP	9.00E-14	1.63E-10	35	Hmgb1, 100042515 /// EG545555 /// EG546331 /// EG665056 /// ENSMUSG00000060128 /// Hmg1l1 /// Hmgb1 /// LOC100045972 /// LOC100046019 /// LOC637733, 100039943 /// 100040234 /// 100041386 /// 100041667 /// 100042549 /// 100043683 /// 4932431P20Rik /// EG432959 /// EG545506 /// EG545555 /// EG546331 /// EG666011 /// EG666969 /// Hmg1l1 /// Hmgb1 /// Hmgb1l /// LOC100045876 /// LOC637733 /// OTTMUSG00000007611 /// OTTMUSG00000015121, Scg2
nervous system development	BP	1.42E-21	8.20E-17	890	Gja1, Scd2, Stmn1, Dpysl3, Cd24a, Smad1, Olig1, Nr2f2, Olig2, Glis2, Id3, Tbr1, Bcan, Sox2, Fzd6, Tacc3, Limk1, Cdkn1c, Chl1, Gas7, Neurod6, Ndufs4, Dcx, Dcx, LOC100046044 /// Nr2f1, Bhlhe22, Lhx2, Socs2, Notch1, Atp7a, En2, Drd2, Cnp, Rgnef, Rgnef, Mbp, Myo5a, Zbtb16, Atp2b2, 100039963 /// Sema3a, Mtpn, Vegfa, Atrx, Apc, Plxna3, Mef2c, Mef2c, Dab1, Nkx2-2, Atm, Myo7a, Fgfr3, LOC100045707 /// Pou3f1, Pou3f4, Slc5a3, LOC100047606 /// Ntrk3, Etv1, Shroom3, Isl1, Aldh1a2, Ift172, Dclk1, Src, Id4 /// LOC100045546, Wnt7a, Zic1, Sox5, Dst, Fgfr1, Lamb1-1, Gprin1, Rufy3, Rufy3, Slit2, Mapt, Enah, Enah, Ndel1, Lhx6, LOC676870 /// Pbx1, Tacc2, Map3k7, Dtx1, Psen2, Sema3e, Mapk8ip3, Cit, Ptprr, Slc1a3, Neurod1, Nrp2, Trp53, EG666036 /// EG666422 /// EG666875 /// EG668576 /// Phgdh, Apbb2, Smarca4, Ptprz1, Bptf, Nkx6-2, Zbtb16, Nfib, Egr2, Pafah1b1, Rnf6, Atg7, Atg7, Tcf7l2, Aplp2, Apoe, Cdk5r1, Tcf7, Myo6, Mtss1, Mycbp2, Sod1, Hmgb1, Rhoc, Myo6, Nde1, Hes6, Atp7a, Cnp, Mtpn, EG665516 /// EG666036 /// EG668771 /// Phgdh, Hexb, Gja1, Sema4a, Gja1, Bptf, Med1, 100042515 /// EG545555 /// EG546331 /// EG665056 /// ENSMUSG00000060128 /// Hmg1l1 /// Hmgb1 /// LOC100045972 /// LOC100046019 /// LOC637733, Chd7, EG623112 /// Stmn1, Ndrg2, 100039943 /// 100040234 /// 100041386 /// 100041667 /// 100042549 /// 100043683 /// 4932431P20Rik /// EG432959 /// EG545506 /// EG545555 /// EG546331 /// EG666011 /// EG666969 /// Hmg1l1

					/// Hmgb1 /// Hmgb1l /// LOC100045876 /// LOC637733 /// OTTMUSG00000007611 /// OTTMUSG00000015121, Nfib, Ulk1, Mmp14, Pafah1b1, Sept4, Sema6b, Ncor2, Ina /// LOC100047943, Ina /// LOC100047943, Socs2, Sema4g, Nrtn, Dscam, Klf7, Prkg1, B3gnt2, Arx /// LOC100044440, Atrx, Kif5a /// Kif5c, Nf2, Isl1, Nr4a2, Fabp7, Dclk1, Src, Tgfb2, Ephb3, Prkdc, Ttl, Ptprz1, Elavl3, Fmr1, Med1, Dpysl3, Timp2, Ablim1, EG665516 /// EG666036 /// EG668771 /// Phgdh, Ntn1, Sept4, Gatad2a, Hes5, Mbp, Dner, EG385344 /// EG627427 /// EG665516 /// EG666036 /// EG666422 /// EG666875 /// EG668506 /// EG668576 /// EG668771 /// LOC630761 /// LOC630896 /// OTTMUSG00000011498 /// Phgdh, Bptf, Gli2, LOC100045707 /// Pou3f1, Hexb, Pafah1b1, Ndst1, Pcsk2, Nrn1, Kndc1, Gnaq, Sox11, Dync2h1, Sema3c, Sox11, Sema3d, Nrxn1, Jag1, Nfib, Nfib, Mtap2, Zeb2, Igf1, Alkbh1, Kif5a, Nr2e1, Cntn2, Chl1, Ntrk2, Plxnb1, Rtn4, Sox8, Apc, Nrxn2, Dlc1, Rora, Sema6a, Nr2f2, Grin3a, Efna5, Nav1, Rfx4, Nlgn1, Bmpr1b, Ednrb, Sema5a, Otx1, Chd7, Hhip, Hectd1, Fzd3, Slc1a2, Rgma, Sox1, Atrx, Bcl11b, Grin3a, Gfra1, Zbtb16, Slitrk3, Rtn4, Vegfc, Ppard, Rorb, Onecut2, Pbx1, Dcc, Mtap2, Sox5, Prdm16, Lrp8, Evl /// LOC100047333, Dscam, Plxna4, Bcan, Enah, Lrp8, Pofut1, Rgnef, Pcdh15, Onecut2, Gje1, Nr4a2, Pcsk2, Igf1r, Sox11, Sema6d, Ablim1, Plxna2, Cttnbp2, Nfib, Mycbp2, Mapt, Nr4a2, Hhip, Sox5, Rorb, Prdm8, Emx2, Htt, Eya1, Ppp1r9a, Rora, Dtx1, Rasgrf1, Smad1, Onecut2, Dlc1
neurogenesis	BP	4.84E-13	7.00E-10	556	Gja1, Stmn1, Cd24a, Olig1, Nr2f2, Olig2, Id3, Tbr1, Sox2, Tacc3, Limk1, Cdkn1c, Chl1, Gas7, Dcx, Dcx, LOC100046044 /// Nr2f1, Bhlhe22, Lhx2, Socs2, Notch1, Atp7a, En2, Drd2, Cnp, Rgnef, Rgnef, Atp2b2, 100039963 /// Sema3a, Mtpn, Vegfa, Apc, Plxna3, Dab1, Nkx2-2, Myo7a, Fgfr3, LOC100045707 /// Pou3f1, Pou3f4, LOC100047606 /// Ntrk3, Etv1, Isl1, Aldh1a2, Dclk1, Id4 /// LOC100045546, Wnt7a, Sox5, Dst, Fgfr1, Lamb1-1, Gprin1, Slit2, Mapt, Enah, Enah, Ndel1, Lhx6, LOC676870 /// Pbx1, Tacc2, Dtx1, Mapk8ip3, Cit, Ptprr, Slc1a3, Trp53, EG666036 /// EG666422 /// EG666875 /// EG668576 /// Phgdh, Apbb2, Smarca4, Ptprz1, Nkx6-2, Egr2, Pafah1b1, Rnf6, Atg7, Atg7, Apoe, Cdk5r1, Myo6, Mycbp2, Sod1, Rhoc, Myo6, Nde1, Atp7a, Cnp, Mtpn, EG665516 /// EG666036 /// EG668771 /// Phgdh, Gja1, Gja1, EG623112 /// Stmn1, Ulk1, Mmp14, Pafah1b1, Socs2, Nrtn, Dscam, Klf7, Prkg1, B3gnt2, Arx /// LOC100044440, Kif5a /// Kif5c, Nf2, Isl1, Nr4a2, Fabp7, Dclk1, Tgfb2, Ephb3, Ttl, Ptprz1, Timp2, Ablim1, EG665516 /// EG666036 /// EG668771 /// Phgdh, Ntn1, Hes5, Dner, EG385344 /// EG627427 /// EG665516 /// EG666036 /// EG666422 /// EG666875 /// EG668506 /// EG668576 /// EG668771 /// LOC630761 /// LOC630896 /// OTTMUSG00000011498 /// Phgdh, Gli2, LOC100045707 /// Pou3f1, Pafah1b1, Nrn1, Kndc1, Gnaq, Jag1, Mtap2, Igf1, Alkbh1, Kif5a, Nr2e1, Cntn2, Chl1,

					Ntrk2, Plxnb1, Rtn4, Apc, Rora, Sema6a, Nr2f2, Grin3a, Efna5, Nav1, Nlgn1, Bmpr1b, Sema5a, Hhip, Sox1, Bcl11b, Grin3a, Slitrk3, Rtn4, Vegfc, Rorb, Onecut2, Pbx1, Dcc, Mtap2, Sox5, Prdm16, Evl /// LOC100047333, Dscam, Enah, Rgnef, Pcdh15, Onecut2, Nr4a2, Ablim1, Cttnbp2, Mycbp2, Mapt, Nr4a2, Hhip, Sox5, Rorb, Prdm8, Emx2, Htt, Eya1, Ppp1r9a, Rora, Dtx1, Rasgrf1, Onecut2
positive regulation of carbohydrate metabolic process	BP	2.68E-16	7.75E-13	37	Sorbs1, Hmgb1, 100042515 /// EG545555 /// EG546331 /// EG665056 /// ENSMUSG00000060128 /// Hmg1l1 /// Hmgb1 /// LOC100045972 /// LOC100046019 /// LOC637733, 100039943 /// 100040234 /// 100041386 /// 100041667 /// 100042549 /// 100043683 /// 4932431P20Rik /// EG432959 /// EG545506 /// EG545555 /// EG546331 /// EG666011 /// EG666969 /// Hmg1l1 /// Hmgb1 /// Hmgb1l /// LOC100045876 /// LOC637733 /// OTTMUSG00000007611 /// OTTMUSG00000015121, Dyrk2 /// LOC100044376, Igf1
positive regulation of catabolic process	BP	9.91E-14	1.74E-10	50	Gja1, Apc, Gclc, Apoe, Hmgb1, Gja1, Gja1, 100042515 /// EG545555 /// EG546331 /// EG665056 /// ENSMUSG00000060128 /// Hmg1l1 /// Hmgb1 /// LOC100045972 /// LOC100046019 /// LOC637733, 100039943 /// 100040234 /// 100041386 /// 100041667 /// 100042549 /// 100043683 /// 4932431P20Rik /// EG432959 /// EG545506 /// EG545555 /// EG546331 /// EG666011 /// EG666969 /// Hmg1l1 /// Hmgb1 /// Hmgb1l /// LOC100045876 /// LOC637733 /// OTTMUSG00000007611 /// OTTMUSG00000015121, Stub1, Igf1, Apc, Akt1
positive regulation of cellular carbohydrate metabolic process	BP	2.68E-16	7.75E-13	37	Sorbs1, Hmgb1, 100042515 /// EG545555 /// EG546331 /// EG665056 /// ENSMUSG00000060128 /// Hmg1l1 /// Hmgb1 /// LOC100045972 /// LOC100046019 /// LOC637733, 100039943 /// 100040234 /// 100041386 /// 100041667 /// 100042549 /// 100043683 /// 4932431P20Rik /// EG432959 /// EG545506 /// EG545555 /// EG546331 /// EG666011 /// EG666969 /// Hmg1l1 /// Hmgb1 /// Hmgb1l /// LOC100045876 /// LOC637733 /// OTTMUSG00000007611 /// OTTMUSG00000015121, Dyrk2 /// LOC100044376, Igf1
positive regulation of cellular catabolic process	BP	1.41E-17	5.83E-14	37	Gclc, Apoe, Hmgb1, 100042515 /// EG545555 /// EG546331 /// EG665056 /// ENSMUSG00000060128 /// Hmg1l1 /// Hmgb1 /// LOC100045972 /// LOC100046019 /// LOC637733, 100039943 /// 100040234 /// 100041386 /// 100041667 /// 100042549 /// 100043683 /// 4932431P20Rik /// EG432959 /// EG545506 /// EG545555 /// EG546331 /// EG666011 /// EG666969 /// Hmg1l1 /// Hmgb1 /// Hmgb1l /// LOC100045876 /// LOC637733 /// OTTMUSG00000007611 /// OTTMUSG00000015121, Stub1, Igf1, Akt1

positive regulation of glucose metabolic process	BP	6.90E-17	2.66E-13	36	Sorbs1, Hmgb1, 100042515 /// EG545555 /// EG546331 /// EG665056 /// ENSMUSG00000060128 /// Hmg1l1 /// Hmgb1 /// LOC100045972 /// LOC100046019 /// LOC637733, 100039943 /// 100040234 /// 100041386 /// 100041667 /// 100042549 /// 100043683 /// 4932431P20Rik /// EG432959 /// EG545506 /// EG545555 /// EG546331 /// EG666011 /// EG666969 /// Hmg1l1 /// Hmgb1 /// Hmgb1l /// LOC100045876 /// LOC637733 /// OTTMUSG00000007611 /// OTTMUSG00000015121, Dyrk2 /// LOC100044376, Igf1
positive regulation of glycogen catabolic process	BP	8.04E-19	4.23E-15	26	Hmgb1, 100042515 /// EG545555 /// EG546331 /// EG665056 /// ENSMUSG00000060128 /// Hmg1l1 /// Hmgb1 /// LOC100045972 /// LOC100046019 /// LOC637733, 100039943 /// 100040234 /// 100041386 /// 100041667 /// 100042549 /// 100043683 /// 4932431P20Rik /// EG432959 /// EG545506 /// EG545555 /// EG546331 /// EG666011 /// EG666969 /// Hmg1l1 /// Hmgb1 /// Hmgb1l /// LOC100045876 /// LOC637733 /// OTTMUSG00000007611 /// OTTMUSG00000015121
positive regulation of glycogen metabolic process	BP	4.50E-19	3.72E-15	31	Sorbs1, Hmgb1, 100042515 /// EG545555 /// EG546331 /// EG665056 /// ENSMUSG00000060128 /// Hmg1l1 /// Hmgb1 /// LOC100045972 /// LOC100046019 /// LOC637733, 100039943 /// 100040234 /// 100041386 /// 100041667 /// 100042549 /// 100043683 /// 4932431P20Rik /// EG432959 /// EG545506 /// EG545555 /// EG546331 /// EG666011 /// EG666969 /// Hmg1l1 /// Hmgb1 /// Hmgb1l /// LOC100045876 /// LOC637733 /// OTTMUSG00000007611 /// OTTMUSG00000015121, Dyrk2 /// LOC100044376
positive regulation of mesenchymal cell proliferation	BP	1.17E-13	1.99E-10	45	Vegfa, Foxp1, Irs1, Fgfr1, Prrx1, Foxp1, Hmgb1, Foxp1, 100042515 /// EG545555 /// EG546331 /// EG665056 /// ENSMUSG00000060128 /// Hmg1l1 /// Hmgb1 /// LOC100045972 /// LOC100046019 /// LOC637733, 100039943 /// 100040234 /// 100041386 /// 100041667 /// 100042549 /// 100043683 /// 4932431P20Rik /// EG432959 /// EG545506 /// EG545555 /// EG546331 /// EG666011 /// EG666969 /// Hmg1l1 /// Hmgb1 /// Hmgb1l /// LOC100045876 /// LOC637733 /// OTTMUSG00000007611 /// OTTMUSG00000015121
positive regulation of mitotic cell cycle	BP	1.27E-13	2.10E-10	33	Hmgb1, 100042515 /// EG545555 /// EG546331 /// EG665056 /// ENSMUSG00000060128 /// Hmg1l1 /// Hmgb1 /// LOC100045972 /// LOC100046019 /// LOC637733, 100039943 /// 100040234 /// 100041386 /// 100041667 /// 100042549 /// 100043683 /// 4932431P20Rik /// EG432959 /// EG545506 /// EG545555 /// EG546331 /// EG666011 /// EG666969 /// Hmg1l1 /// Hmgb1 /// Hmgb1l /// LOC100045876 /// LOC637733 /// OTTMUSG00000007611 /// OTTMUSG00000015121

positive regulation of myeloid cell differentiation	BP	2.54E-14	4.89E-11	51	Kitl, Acin1, Gnas, Inhba, Id2, Hmgb1, 100042515 /// EG545555 /// EG546331 /// EG665056 /// ENSMUSG00000060128 /// Hmg1l1 /// Hmgb1 /// LOC100045972 /// LOC100046019 /// LOC637733, Kitl, Hif1a, 100039943 /// 100040234 /// 100041386 /// 100041667 /// 100042549 /// 100043683 /// 4932431P20Rik /// EG432959 /// EG545506 /// EG545555 /// EG546331 /// EG666011 /// EG666969 /// Hmg1l1 /// Hmgb1 /// Hmgb1l /// LOC100045876 /// LOC637733 /// OTTMUSG00000007611 /// OTTMUSG00000015121, Gnas, Csf1, Jag1
regulation of carbohydrate catabolic process	BP	8.35E-17	2.68E-13	30	Hmgb1, 100042515 /// EG545555 /// EG546331 /// EG665056 /// ENSMUSG00000060128 /// Hmg1l1 /// Hmgb1 /// LOC100045972 /// LOC100046019 /// LOC637733, 100039943 /// 100040234 /// 100041386 /// 100041667 /// 100042549 /// 100043683 /// 4932431P20Rik /// EG432959 /// EG545506 /// EG545555 /// EG546331 /// EG666011 /// EG666969 /// Hmg1l1 /// Hmgb1 /// Hmgb1l /// LOC100045876 /// LOC637733 /// OTTMUSG00000007611 /// OTTMUSG00000015121, Igf1
regulation of carbohydrate metabolic process	BP	9.49E-15	1.96E-11	40	Sorbs1, Hmgb1, 100042515 /// EG545555 /// EG546331 /// EG665056 /// ENSMUSG00000060128 /// Hmg1l1 /// Hmgb1 /// LOC100045972 /// LOC100046019 /// LOC637733, 100039943 /// 100040234 /// 100041386 /// 100041667 /// 100042549 /// 100043683 /// 4932431P20Rik /// EG432959 /// EG545506 /// EG545555 /// EG546331 /// EG666011 /// EG666969 /// Hmg1l1 /// Hmgb1 /// Hmgb1l /// LOC100045876 /// LOC637733 /// OTTMUSG00000007611 /// OTTMUSG00000015121, Dyrk2 /// LOC100044376, Igf1
regulation of cellular carbohydrate catabolic process	BP	8.35E-17	2.68E-13	30	Hmgb1, 100042515 /// EG545555 /// EG546331 /// EG665056 /// ENSMUSG00000060128 /// Hmg1l1 /// Hmgb1 /// LOC100045972 /// LOC100046019 /// LOC637733, 100039943 /// 100040234 /// 100041386 /// 100041667 /// 100042549 /// 100043683 /// 4932431P20Rik /// EG432959 /// EG545506 /// EG545555 /// EG546331 /// EG666011 /// EG666969 /// Hmg1l1 /// Hmgb1 /// Hmgb1l /// LOC100045876 /// LOC637733 /// OTTMUSG00000007611 /// OTTMUSG00000015121, Igf1
regulation of cellular carbohydrate metabolic process	BP	9.49E-15	1.96E-11	40	Sorbs1, Hmgb1, 100042515 /// EG545555 /// EG546331 /// EG665056 /// ENSMUSG00000060128 /// Hmg1l1 /// Hmgb1 /// LOC100045972 /// LOC100046019 /// LOC637733, 100039943 /// 100040234 /// 100041386 /// 100041667 /// 100042549 /// 100043683 /// 4932431P20Rik /// EG432959 /// EG545506 /// EG545555 /// EG546331 /// EG666011 /// EG666969 /// Hmg1l1 /// Hmgb1 /// Hmgb1l /// LOC100045876 /// LOC637733 /// OTTMUSG00000007611 /// OTTMUSG00000015121, Dyrk2 /// LOC100044376,

					Igf1
regulation of generation of precursor metabolites and energy	BP	6.30E-19	4.23E-15	37	Atp7a, Sorbs1, Hmgb1, Atp7a, 100042515 /// EG545555 /// EG546331 /// EG665056 /// ENSMUSG00000060128 /// Hmg1l1 /// Hmgb1 /// LOC100045972 /// LOC100046019 /// LOC637733, 100039943 /// 100040234 /// 100041386 /// 100041667 /// 100042549 /// 100043683 /// 4932431P20Rik /// EG432959 /// EG545506 /// EG545555 /// EG546331 /// EG666011 /// EG666969 /// Hmg1l1 /// Hmgb1 /// Hmgb1l /// LOC100045876 /// LOC637733 /// OTTMUSG00000007611 /// OTTMUSG00000015121, Dyrk2 /// LOC100044376, Igf1, Cisd1
regulation of glucose metabolic process	BP	3.11E-15	6.92E-12	39	Sorbs1, Hmgb1, 100042515 /// EG545555 /// EG546331 /// EG665056 /// ENSMUSG00000060128 /// Hmg1l1 /// Hmgb1 /// LOC100045972 /// LOC100046019 /// LOC637733, 100039943 /// 100040234 /// 100041386 /// 100041667 /// 100042549 /// 100043683 /// 4932431P20Rik /// EG432959 /// EG545506 /// EG545555 /// EG546331 /// EG666011 /// EG666969 /// Hmg1l1 /// Hmgb1 /// Hmgb1l /// LOC100045876 /// LOC637733 /// OTTMUSG00000007611 /// OTTMUSG00000015121, Dyrk2 /// LOC100044376, Igf1
regulation of glycogen catabolic process	BP	8.04E-19	4.23E-15	26	Hmgb1, 100042515 /// EG545555 /// EG546331 /// EG665056 /// ENSMUSG00000060128 /// Hmg1l1 /// Hmgb1 /// LOC100045972 /// LOC100046019 /// LOC637733, 100039943 /// 100040234 /// 100041386 /// 100041667 /// 100042549 /// 100043683 /// 4932431P20Rik /// EG432959 /// EG545506 /// EG545555 /// EG546331 /// EG666011 /// EG666969 /// Hmg1l1 /// Hmgb1 /// Hmgb1l /// LOC100045876 /// LOC637733 /// OTTMUSG00000007611 /// OTTMUSG00000015121
regulation of glycogen metabolic process	BP	4.50E-19	3.72E-15	31	Sorbs1, Hmgb1, 100042515 /// EG545555 /// EG546331 /// EG665056 /// ENSMUSG00000060128 /// Hmg1l1 /// Hmgb1 /// LOC100045972 /// LOC100046019 /// LOC637733, 100039943 /// 100040234 /// 100041386 /// 100041667 /// 100042549 /// 100043683 /// 4932431P20Rik /// EG432959 /// EG545506 /// EG545555 /// EG546331 /// EG666011 /// EG666969 /// Hmg1l1 /// Hmgb1 /// Hmgb1l /// LOC100045876 /// LOC637733 /// OTTMUSG00000007611 /// OTTMUSG00000015121, Dyrk2 /// LOC100044376
regulation of mesenchymal cell proliferation	BP	2.82E-13	4.29E-10	46	Vegfa, Foxp1, Irs1, Fgfr1, Prrx1, Foxp1, Hmgb1, Foxp1, 100042515 /// EG545555 /// EG546331 /// EG665056 /// ENSMUSG00000060128 /// Hmg1l1 /// Hmgb1 /// LOC100045972 /// LOC100046019 /// LOC637733, 100039943 /// 100040234 /// 100041386 /// 100041667 /// 100042549 /// 100043683 /// 4932431P20Rik /// EG432959 /// EG545506 /// EG545555 /// EG546331 /// EG666011 /// EG666969 /// Hmg1l1 /// Hmgb1 /// Hmgb1l /// LOC100045876

					/// LOC637733 /// OTTMUSG00000007611 /// OTTMUSG00000015121
regulation of polysaccharide metabolic process	BP	4.50E-19	3.72E-15	31	Sorbs1, Hmgb1, 100042515 /// EG545555 /// EG546331 /// EG665056 /// ENSMUSG00000060128 /// Hmg1l1 /// Hmgb1 /// LOC100045972 /// LOC100046019 /// LOC637733, 100039943 /// 100040234 /// 100041386 /// 100041667 /// 100042549 /// 100043683 /// 4932431P20Rik /// EG432959 /// EG545506 /// EG545555 /// EG546331 /// EG666011 /// EG666969 /// Hmg1l1 /// Hmgb1 /// Hmgb1l /// LOC100045876 /// LOC637733 /// OTTMUSG00000007611 /// OTTMUSG00000015121, Dyrk2 /// LOC100044376
response to corticosteroid stimulus	BP	5.82E-16	1.53E-12	57	Src, Ugt1a1 /// Ugt1a10 /// Ugt1a2 /// Ugt1a5 /// Ugt1a6a /// Ugt1a6b /// Ugt1a7c /// Ugt1a9, Ugt1a1 /// Ugt1a10 /// Ugt1a2 /// Ugt1a5 /// Ugt1a6a /// Ugt1a6b /// Ugt1a7c /// Ugt1a9, Hmgb1, 100042515 /// EG545555 /// EG546331 /// EG665056 /// ENSMUSG00000060128 /// Hmg1l1 /// Hmgb1 /// LOC100045972 /// LOC100046019 /// LOC637733, 100039943 /// 100040234 /// 100041386 /// 100041667 /// 100042549 /// 100043683 /// 4932431P20Rik /// EG432959 /// EG545506 /// EG545555 /// EG546331 /// EG666011 /// EG666969 /// Hmg1l1 /// Hmgb1 /// Hmgb1l /// LOC100045876 /// LOC637733 /// OTTMUSG00000007611 /// OTTMUSG00000015121, Asl, Abcb4, Src, Gpr83
response to glucocorticoid stimulus	BP	4.00E-16	1.10E-12	54	Ugt1a1 /// Ugt1a10 /// Ugt1a2 /// Ugt1a5 /// Ugt1a6a /// Ugt1a6b /// Ugt1a7c /// Ugt1a9, Ugt1a1 /// Ugt1a10 /// Ugt1a2 /// Ugt1a5 /// Ugt1a6a /// Ugt1a6b /// Ugt1a7c /// Ugt1a9, Hmgb1, 100042515 /// EG545555 /// EG546331 /// EG665056 /// ENSMUSG00000060128 /// Hmg1l1 /// Hmgb1 /// LOC100045972 /// LOC100046019 /// LOC637733, 100039943 /// 100040234 /// 100041386 /// 100041667 /// 100042549 /// 100043683 /// 4932431P20Rik /// EG432959 /// EG545506 /// EG545555 /// EG546331 /// EG666011 /// EG666969 /// Hmg1l1 /// Hmgb1 /// Hmgb1l /// LOC100045876 /// LOC637733 /// OTTMUSG00000007611 /// OTTMUSG00000015121, Asl, Abcb4, Gpr83

YAC 13 months D1 GO Analysis

GO Term	Ontology	p value	Adjusted p value	Total genes in GO class	Genes present
extrinsic to membrane	CC	9.38E-07	0.003	87	Sytl2, Gng5, 100041120 /// Gng5 /// LOC100044719 /// OTTMUSG00000011511 /// OTTMUSG00000026148, Gng4
extrinsic to plasma membrane	CC	6.29E-08	5.12E-04	59	Sytl2, Gng5, 100041120 /// Gng5 /// LOC100044719 /// OTTMUSG00000011511 /// OTTMUSG00000026148, Gng4
heterotrimeric G-protein complex	CC	9.89E-08	5.12E-04	38	Gng5, 100041120 /// Gng5 /// LOC100044719 /// OTTMUSG00000011511 /// OTTMUSG00000026148, Gng4

YAC 23 months D2 GO Analysis

GO Term	Ontology	p value	Adjusted p value	Total genes in GO class	Genes present
heterotrimeric G-protein complex	CC	4.27E-07	0.011	38	Gng4, Gnb4, 100041120 /// Gng5 /// LOC100044719 /// OTTMUSG00000011511 /// OTTMUSG00000026148, Gna13, Gnao1, Gng4

Appendix II: IPA Analysis – pathways with Ratio p<.05

R6-2 3 weeks D1 IPA Analysis

Ingenuity Canonical Pathways	-log(p-value)	Ratio	Molecules
Inositol Phosphate Metabolism	4.77E+00	7.95E-02	PIK3C2A,CDK7,MTMR1,GRK5,PIP5K1B,BRAF,SYNJ2,PLCB4,IPMK,PIM1,PIK3CG,PRPF4B, GRK6,PRKAA2
Breast Cancer Regulation by Stathmin1	2.85E+00	6.53E-02	ARHGEF4,PIK3C2A,PPP1R14A,E2F3,GNG5,ROCK1,GNAI2,PLCB4,PPP1R10,PIK3CG,GNA13,PPP2R1B,GNG4
Nicotinate and Nicotinamide Metabolism	2.82E+00	6.62E-02	BRAF,NNT,PIM1,PRPF4B,CDK7,NT5M,PRKAA2,GRK6,GRK5
IL-8 Signaling	2.27E+00	5.91E-02	ROCK1,GNAI2,BRAF,HMOX1,CCND3,PIK3C2A,MYL12B,PIK3CG,GNA13,GNG5,GNG4
Ephrin Receptor Signaling	2.17E+00	5.61E-02	ROCK1,GNAI2,GRIN1,ITSN1,EPHB2,PIK3CG,EPHA4,GNA13,GNG5,GNG4,FGF1
Relaxin Signaling	2.17E+00	6.04E-02	GNAI2,BRAF,PDE7A,PIK3C2A,PIK3CG,GNA13,GNG5,GNG4,PDE1C
AMPK Signaling	2.04E+00	5.45E-02	CPT1A,PIK3C2A,PIK3CG,TSC2,PRKAA2,RPTOR,AK2,PPP2R1B,HLTF
Clathrin-mediated Endocytosis Signaling	2.03E+00	5.99E-02	MYO6,SH3BP4,CD2AP,SNX9 (includes EG:51429),PIK3C2A,EPHB2,PIK3CG,TFRC,HIP1,FGF1
Axonal Guidance Signaling	1.98E+00	4.47E-02	RND1,PLXNC1,PIK3C2A,ITSN1,EPHB2,EPHA4,SLIT2,GNG5,ROCK1,GNAI2,NTNG1,PLCB4,PLXNA1,MYL12B,PIK3CG,GNA13,SEMA3B,GNG4
Androgen Signaling	1.96E+00	5.56E-02	GNAI2,AR,GTF2H4,CDK7,TBP,GNA13,GNG5,GNG4
Thrombin Signaling	1.88E+00	5.39E-02	ROCK1,GNAI2,PLCB4,ARHGEF4,PIK3C2A,MYL12B,PIK3CG,TBP,GNA13,GNG5,GNG4
Sphingosine-1-phosphate Signaling	1.71E+00	6.25E-02	GNAI2,PLCB4,S1PR5,PIK3C2A,PIK3CG,GNA13,SMPD3
CXCR4 Signaling	1.67E+00	5.39E-02	ROCK1,GNAI2,PLCB4,PIK3C2A,MYL12B,PIK3CG,GNA13,GNG5,GNG4
Insulin Receptor Signaling	1.61E+00	5.71E-02	PPP1R10,PIK3C2A,PIK3CG,TSC2,RPTOR,PPP1R14A,PTPRF,GRB10
CCR3 Signaling in Eosinophils	1.57E+00	5.83E-02	ROCK1,GNAI2,PLCB4,PIK3C2A,PIK3CG,GNG5,GNG4
Aryl Hydrocarbon Receptor Signaling	1.54E+00	5.19E-02	ALDH1B1,TRIP11,CCND3,MED1,NQO2,NFIA,APAF1,GSTO1
Protein Kinase A Signaling	1.53E+00	4.44E-02	TGFBR1,PDE7A,ANAPC10,PPP1R14A,GNG5,PDE1C,BRAF,ROCK1,GNAI2,PLCB4,PPP1R10,MYL12B,GNA13,GNG4
Type II Diabetes Mellitus Signaling	1.48E+00	4.43E-02	ACSL3,PIK3C2A,PIK3CG,SOCS6,SOCS2,PRKAA2,SMPD3
Androgen and Estrogen Metabolism	1.46E+00	4.23E-02	CYP7B1,METTL2B,HSD17B7,B3GAT1,METTL6,SULF2
Prolactin Signaling	1.44E+00	6.67E-02	PIK3C2A,PIK3CG,SOCS6,SOCS2,PDK1
G Beta Gamma Signaling	1.44E+00	5.04E-02	GNAI2,PIK3CG,KCNJ3,GNA13,GNG5,GNG4
Huntington's Disease Signaling	1.44E+00	4.58E-02	PLCB4,PIK3C2A,PIK3CG,APAF1,TBP,TCERG1,HDAC9 (includes EG:9734),HIP1,GNG5,GNG4,ZDHHC17

Antiproliferative Role of Somatostatin Receptor 2	1.39E+00	6.41E-02	BRAF,PIK3C2A,PIK3CG,GNG5,GNG4
Cardiac Œ≤-adrenergic Signaling	1.36E+00	4.93E-02	PPP1R10,PDE7A,PPP1R14A,PPP2R1B,GNG5,GNG4,PDE1C
Acute Myeloid Leukemia Signaling	1.33E+00	6.41E-02	BRAF,PIK3C2A,CSF2RA (includes EG:1438),PIM1,PIK3CG
IL-9 Signaling	1.30E+00	8.11E-02	PIK3C2A,PIK3CG,SOCS2
Histidine Metabolism	1.27E+00	3.33E-02	ALDH1B1,CYP7B1,METTL2B,METTL6
G Protein Signaling Mediated by Tubby	1.23E+00	7.32E-02	PLCB4,GNG5,GNG4
Ceramide Signaling	1.23E+00	5.75E-02	S1PR5,PIK3C2A,PIK3CG,PPP2R1B,SMPD3

R6-2 3 wks D2 IPA

Ingenuity Canonical Pathways	-log(p-value)	Ratio	Molecules
Endoplasmic Reticulum Stress Pathway	2.49E+00	2.22E-01	MBTPS1,MAP3K5 (includes EG:4217),EIF2AK3,MBTPS2
Inositol Phosphate Metabolism	2.05E+00	6.25E-02	PIP5K1A,PRKX,IPMK,PIP5K1C,PDIA3,CSNK1D,PIP5KL1,GRK5,IP6K2,PLCL1,IRAK1
Glutamate Metabolism	1.97E+00	6.41E-02	GNPNAT1,GMPS,CAD,GCLM,GPT2
Keratan Sulfate Biosynthesis	1.96E+00	1.09E-01	B4GALT4,B4GALT7,HS6ST1,B3GNT2,CHST11,NDST1
Type I Diabetes Mellitus Signaling	1.93E+00	7.83E-02	TRAF6,IKBKG,ICA1,NGFR,SOCS2,MAP3K5 (includes EG:4217),MAPK11,PTPRN,IRAK1
Aminophosphonate Metabolism	1.59E+00	6.15E-02	PCYT1B,METTL1,METTL6,MEPCE
Toll-like Receptor Signaling	1.56E+00	9.26E-02	TRAF6,IKBKG,ELK1,MAPK11,IRAK1
ATM Signaling	1.46E+00	9.43E-02	TP53,GADD45B,TLK1,MDM2,MAPK11
p53 Signaling	1.38E+00	7.61E-02	TP53,KAT2B,GADD45B,STAG1,RRM2B,CSNK1D,MDM2
April Mediated Signaling	1.38E+00	9.52E-02	TRAF6,IKBKG,ELK1,MAPK11
B Cell Activating Factor Signaling	1.31E+00	9.09E-02	TRAF6,IKBKG,ELK1,MAPK11
Selenoamino Acid Metabolism	1.31E+00	5.19E-02	METTL1,SEPHS1,METTL6,MEPCE
Purine Metabolism	1.27E+00	3.87E-02	POLE4,AFG3L1,RRM2B,IDE,ADARB1,POLB,GART,NT5C,IMPDH2,MPP3,GMPS,PDE7B,CH RAC1,MYH9,HLTF,ATP6V0E1,IFNAR1
p38 MAPK Signaling	1.24E+00	7.22E-02	TRAF6,MAX,MEF2C,MAP3K5 (includes EG:4217),ELK1,MAPK11,IRAK1
IL-10 Signaling	1.21E+00	7.14E-02	TRAF6,IKBKG,TYK2,ELK1,MAPK11

Axonal Guidance Signaling	1.20E+00	4.71E-02	SEMA3E,RAP1B,PXN,PLXNC1,PAK6,ADAM15,SHANK2,SEMA5A,CRKL,WNT2B,CRK,NTRK2,NGFR,ADAM19,SMO,MYL4,SRGAP2,SEMA4B,NRP1

R6-2 8 weeks D1 IPA Analysis

Ingenuity Canonical Pathways	-log(p-value)	Ratio	Molecules
Chronic Myeloid Leukemia Signaling	3.14E+00	8.57E-02	IKBKB,E2F6,E2F4,TGFBR1,PA2G4,PIK3C2A,CRKL,CHUK,SIN3A
IL-1 Signaling	2.61E+00	7.55E-02	ADCY9,IKBKB,JUN,PRKAR2A,CHUK,GNA13,GNG2,GNG4
Relaxin Signaling	2.28E+00	6.04E-02	ADCY9,JUN,PDE7A,PIK3C2A,PRKAR2A,GNA13,GNG2,GNG4,PDE1C
cAMP-mediated Signaling	2.15E+00	6.21E-02	ADCY9,CREM,PDE7A,OPRM1,PKIB,HTR7,RGS7,PRKAR2A,ADORA2A,PDE1C
Role of CHK Proteins in Cell Cycle Checkpoint Control	2.00E+00	1.14E-01	E2F6,E2F4,HUS1,RAD50
Small Cell Lung Cancer Signaling	2.00E+00	6.74E-02	IKBKB,PA2G4,PIK3C2A,CHUK,RXRA,SIN3A
G-Protein Coupled Receptor Signaling	1.78E+00	5.00E-02	ADCY9,IKBKB,PDE7A,PIK3C2A,OPRM1,HTR7,RGS7,PRKAR2A,CHUK,ADORA2A,PDE1C
Pancreatic Adenocarcinoma Signaling	1.76E+00	6.03E-02	RAD51,E2F6,E2F4,TGFBR1,PA2G4,PIK3C2A,SIN3A
Androgen Signaling	1.58E+00	4.86E-02	JUN,PRKAR2A,POLR2B,GNA13,GNG2,GTF2A1,GNG4
p53 Signaling	1.53E+00	6.52E-02	JUN,GADD45B,PIK3C2A,SNAI2,C12ORF5,RPRM
Purine Metabolism	1.49E+00	3.19E-02	ADCY9,RSF1,ABCA2,PDE7A,PKLR,RRM2,POLR2B,POLD4,ADARB1,ATIC,PDE1C,SKIV2L,RAD51,POLR3K
Cardiac Œ≤-adrenergic Signaling	1.44E+00	4.93E-02	ADCY9,PDE7A,PKIB,PRKAR2A,GNG2,GNG4,PDE1C
4-1BB Signaling in T Lymphocytes	1.42E+00	8.82E-02	IKBKB,JUN,CHUK
CD27 Signaling in Lymphocytes	1.37E+00	7.02E-02	IKBKB,SIVA1,JUN,CHUK
ATM Signaling	1.37E+00	7.55E-02	RAD51,JUN,GADD45B,RAD50
Ovarian Cancer Signaling	1.36E+00	5.19E-02	RAD51,PA2G4,PIK3C2A,FZD3,PRKAR2A,PMS2,SIN3A
Breast Cancer Regulation by Stathmin1	1.31E+00	4.52E-02	ADCY9,E2F6,E2F4,PIK3C2A,PRKAR2A,TRPC5,GNA13,GNG2,GNG4
Hepatic Cholestasis	1.27E+00	4.19E-02	ADCY9,IKBKB,JUN,PRKAR2A,CHUK,RXRA,HSD3B7
Role of BRCA1 in DNA Damage Response	1.25E+00	6.56E-02	RAD51,E2F6,E2F4,RAD50
Cell Cycle: G1/S Checkpoint Regulation	1.25E+00	6.78E-02	E2F6,E2F4,PA2G4,SIN3A

Glutamate Receptor Signaling	1.20E+00	5.71E-02	SLC1A4,GRIK3,GNG2,HOMER1

R6-2 8 weeks D2 IPA Analysis

Ingenuity Canonical Pathways	-log(p-value)	Ratio	Molecules
LPS-stimulated MAPK Signaling	4.26E+00	1.28E-01	RAF1,IKBKG,NFKBIA,PIK3C2A,MAP3K7,PIK3C3,CREB1,MAPK8,PIK3CD,PRKCA
Role of NFAT in Cardiac Hypertrophy	3.74E+00	7.73E-02	ADCY9,RAF1,HDAC4,PIK3C2A,MAPK8,PPP3CC,PLCH2,GNG5,CABIN1,MAP3K7,PIK3C3,TGFB3,IGF1R,PIK3CD,PLCL1,PRKCA
Prostate Cancer Signaling	3.05E+00	9.38E-02	TP53,RAF1,NFKBIA,FOXO1,PA2G4,PIK3C2A,PIK3C3,CREB1,PIK3CD
VEGF Signaling	2.86E+00	9.28E-02	RAF1,EIF2S2,FOXO1,PIK3C2A,PIK3C3,PIK3CD,ACTN1,PRKCA,ARNT
IL-3 Signaling	2.86E+00	1.11E-01	STAT6,RAF1,FOXO1,PIK3C2A,PIK3C3,PIK3CD,PPP3CC,PRKCA
Cardiac Hypertrophy Signaling	2.77E+00	6.58E-02	ADCY9,RAF1,PIK3C2A,MYL2,GNA12,MAPK8,PPP3CC,PLCH2,GNG5,MAP3K7,PIK3C3,CREB1,IGF1R,TGFB3,PIK3CD,PLCL1
RANK Signaling in Osteoclasts	2.76E+00	9.38E-02	RAF1,IKBKG,NFKBIA,PIK3C2A,MAP3K7,PIK3C3,MAPK8,PIK3CD,PPP3CC
Molecular Mechanisms of Cancer	2.70E+00	5.65E-02	TP53,ADCY9,RAF1,TCF4,PIK3C2A,PA2G4,GNA12,MAPK8,ARHGEF17,AURKA,NFKBIA,FOXO1,MAP3K7,SUFU,BMPR1A,PIK3C3,FZD3,TGFB3,PIK3CD,FZD2,PRKCA
EGF Signaling	2.67E+00	1.22E-01	RAF1,PIK3C2A,PIK3C3,MAPK8,PIK3CD,PRKCA
14-3-3-mediated Signaling	2.62E+00	8.77E-02	RAF1,FOXO1,PIK3C2A,PIK3C3,MAPK8,VIM,PIK3CD,PLCH2,PLCL1,PRKCA
IL-9 Signaling	2.59E+00	1.35E-01	PIK3C2A,PIK3C3,CISH,SOCS2,PIK3CD
CD40 Signaling	2.58E+00	1.04E-01	IKBKG,NFKBIA,PIK3C2A,MAP3K7,PIK3C3,MAPK8,PIK3CD
Chronic Myeloid Leukemia Signaling	2.56E+00	8.57E-02	TP53,RAF1,IKBKG,HDAC4,PA2G4,PIK3C2A,PIK3C3,TGFB3,PIK3CD
JAK/Stat Signaling	2.54E+00	1.09E-01	STAT6,RAF1,PIK3C2A,PIK3C3,CISH,SOCS2,PIK3CD
GŒ±12/13 Signaling	2.45E+00	8.00E-02	RAF1,IKBKG,CDH4 (includes EG:1002),NFKBIA,MYL2,PIK3C2A,GNA12,PIK3C3,MAPK8,PIK3CD
Non-Small Cell Lung Cancer Signaling	2.38E+00	8.86E-02	TP53,RAF1,PA2G4,PIK3C2A,PIK3C3,PIK3CD,PRKCA
Neurotrophin/TRK Signaling	2.31E+00	9.33E-02	RAF1,PIK3C2A,PIK3C3,CREB1,MAPK8,SORCS1,PIK3CD
ATM Signaling	2.29E+00	1.13E-01	TP53,NFKBIA,CREB1,MAPK8,MRE11A,SMC1A
Prolactin Signaling	2.27E+00	9.33E-02	RAF1,PIK3C2A,PIK3C3,SOCS2,PIK3CD,PDK1,PRKCA
PDGF Signaling	2.27E+00	9.21E-02	RAF1,PIK3C2A,PIK3C3,ACP1,MAPK8,PIK3CD,PRKCA
Ovarian Cancer Signaling	2.22E+00	7.41E-02	TP53,RAF1,GJA1,MSH2,PA2G4,PIK3C2A,PIK3C3,FZD3,PIK3CD,FZD2

Glioblastoma Multiforme Signaling	2.22E+00	6.75E-02	TP53,RAF1,FOXO1,PIK3C2A,PIK3C3,IGF1R,FZD3,PIK3CD,PLCH2,PLCL1,FZD2
Small Cell Lung Cancer Signaling	2.17E+00	7.87E-02	TP53,IKBKG,NFKBIA,PA2G4,PIK3C2A,PIK3C3,PIK3CD
NF-ŒʃB Activation by Viruses	2.13E+00	8.64E-02	RAF1,IKBKG,NFKBIA,PIK3C2A,PIK3C3,PIK3CD,PRKCA
Role of NANOG in Mammalian Embryonic Stem Cell Pluripotency	2.13E+00	7.89E-02	TP53,RAF1,PIK3C2A,BMPR1A,PIK3C3,FZD3,PIK3CD,FZD2,IL11RA
SAPK/JNK Signaling	2.11E+00	8.16E-02	TP53,PIK3C2A,MAP3K7,GNA12,PIK3C3,MAPK8,PIK3CD,GNG5
Leptin Signaling in Obesity	2.10E+00	8.54E-02	ADCY9,FOXO1,PIK3C2A,PIK3C3,PIK3CD,PLCH2,PLCL1
IL-12 Signaling and Production in Macrophages	2.08E+00	6.72E-02	STAT6,IKBKG,PIK3C2A,PIK3C3,MAF,MAPK8,TGFB3,PIK3CD,PRKCA
IGF-1 Signaling	2.08E+00	8.00E-02	RAF1,FOXO1,PIK3C2A,PIK3C3,IGF1R,MAPK8,IGFBP5,PIK3CD
HER-2 Signaling in Breast Cancer	2.04E+00	8.86E-02	TP53,FOXO1,PIK3C2A,PIK3C3,PIK3CD,PARD3,PRKCA
Type II Diabetes Mellitus Signaling	2.03E+00	5.70E-02	IKBKG,NFKBIA,PIK3C2A,MAP3K7,PIK3C3,SOCS2,MAPK8,PIK3CD,PRKCA
Melanoma Signaling	2.01E+00	1.09E-01	TP53,RAF1,PIK3C2A,PIK3C3,PIK3CD
Neuropathic Pain Signaling In Dorsal Horn Neurons	2.00E+00	7.77E-02	PIK3C2A,GRIN2D,PIK3C3,CREB1,PIK3CD,PLCH2,PLCL1,PRKCA
Glioma Signaling	2.00E+00	7.14E-02	TP53,RAF1,PA2G4,PIK3C2A,PIK3C3,IGF1R,PIK3CD,PRKCA
T Cell Receptor Signaling	2.00E+00	7.48E-02	RAF1,IKBKG,NFKBIA,PIK3C2A,PIK3C3,MAPK8,PIK3CD,PPP3CC
Inositol Phosphate Metabolism	1.99E+00	5.68E-02	SYNJ2,PIK3C2A,PIK3C3,SEC16A,CDK7,GRK6,MAPK8,PIK3CD,PLCH2,PLCL1
Aldosterone Signaling in Epithelial Cells	1.95E+00	7.37E-02	RAF1,PIK3C2A,PIK3C3,PIK3CD,PLCH2,PLCL1,PRKCA
Myc Mediated Apoptosis Signaling	1.92E+00	9.52E-02	TP53,PIK3C2A,PIK3C3,IGF1R,MAPK8,PIK3CD
GM-CSF Signaling	1.89E+00	8.96E-02	RAF1,PIK3C2A,PIK3C3,CISH,PIK3CD,PPP3CC
Factors Promoting Cardiogenesis in Vertebrates	1.87E+00	7.87E-02	MYL2,BMPR1A,MAP3K7,FZD3,TGFB3,FZD2,PRKCA
Growth Hormone Signaling	1.85E+00	8.57E-02	PIK3C2A,PIK3C3,SOCS2,IGF1R,PIK3CD,PRKCA
Sphingosine-1-phosphate Signaling	1.85E+00	7.14E-02	ADCY9,PIK3C2A,GNA12,PIK3C3,PIK3CD,PLCH2,PLCL1,ASAH2
B Cell Receptor Signaling	1.85E+00	6.49E-02	RAF1,IKBKG,NFKBIA,PIK3C2A,MAP3K7,PIK3C3,CREB1,MAPK8,PIK3CD,PPP3CC
FGF Signaling	1.84E+00	7.95E-02	RAF1,PIK3C2A,PIK3C3,CREB1,MAPK8,PIK3CD,PRKCA
Thrombin Signaling	1.80E+00	5.88E-02	ADCY9,RAF1,MYL2,PIK3C2A,GNA12,PIK3C3,CREB1,PIK3CD,PLCH2,PLCL1,GNG5,PRKCA
Pancreatic Adenocarcinoma	1.80E+00	6.90E-02	TP53,RAF1,PA2G4,PIK3C2A,PIK3C3,MAPK8,TGFB3,PIK3CD

Signaling			
CREB Signaling in Neurons	1.80E+00	5.61E-02	ADCY9,RAF1,PIK3C2A,GNA12,PIK3C3,CREB1,PIK3CD,PLCH2,PLCL1,GNG5,PRKCA
Erythropoietin Signaling	1.79E+00	7.89E-02	RAF1,NFKBIA,PIK3C2A,PIK3C3,PIK3CD,PRKCA
Angiopoietin Signaling	1.79E+00	8.11E-02	IKBKG,NFKBIA,FOXO1,PIK3C2A,PIK3C3,PIK3CD
Apoptosis Signaling	1.79E+00	7.78E-02	ACIN1,TP53,RAF1,IKBKG,NFKBIA,MAPK8,PRKCA
Relaxin Signaling	1.77E+00	6.04E-02	ADCY9,NFKBIA,PIK3C2A,GNA12,PIK3C3,CREB1,PIK3CD,GNG5,NPR2
fMLP Signaling in Neutrophils	1.76E+00	6.40E-02	RAF1,NFKBIA,PIK3C2A,PIK3C3,PIK3CD,PPP3CC,GNG5,PRKCA
Cardiomyocyte Differentiation via BMP Receptors	1.75E+00	1.50E-01	MYL2,BMPR1A,MAP3K7
NRF2-mediated Oxidative Stress Response	1.71E+00	6.01E-02	DNAJC21,RAF1,DNAJC17,PIK3C2A,MAP3K7,PIK3C3,MAF,MAPK8,SLC35A2,PIK3CD,PRKCA
Renal Cell Carcinoma Signaling	1.70E+00	8.33E-02	RAF1,PIK3C2A,PIK3C3,PIK3CD,FH,ARNT
CXCR4 Signaling	1.68E+00	5.99E-02	ADCY9,RAF1,MYL2,PIK3C2A,GNA12,PIK3C3,MAPK8,PIK3CD,GNG5,PRKCA
Hypoxia Signaling in the Cardiovascular System	1.68E+00	8.57E-02	TP53,NFKBIA,CREB1,UBE2V2,UBE2E3,ARNT
Thrombopoietin Signaling	1.67E+00	8.47E-02	RAF1,PIK3C2A,PIK3C3,PIK3CD,PRKCA
Antiproliferative Role of Somatostatin Receptor 2	1.65E+00	7.69E-02	ADCY9,PIK3C2A,PIK3C3,PIK3CD,GNG5,NPR2
p53 Signaling	1.64E+00	7.61E-02	TP53,PIK3C2A,JMY,PIK3C3,MAPK8,C12ORF5,PIK3CD
Endometrial Cancer Signaling	1.63E+00	8.77E-02	TP53,RAF1,PIK3C2A,PIK3C3,PIK3CD
Role of Pattern Recognition Receptors in Recognition of Bacteria and Viruses	1.62E+00	7.50E-02	PIK3C2A,PIK3C3,DDX58,CREB1,PIK3CD,IRF3
IL-1 Signaling	1.61E+00	6.60E-02	ADCY9,IKBKG,NFKBIA,MAP3K7,GNA12,MAPK8,GNG5
IL-2 Signaling	1.60E+00	8.62E-02	RAF1,PIK3C2A,PIK3C3,MAPK8,PIK3CD
FLT3 Signaling in Hematopoietic Progenitor Cells	1.59E+00	8.11E-02	STAT6,RAF1,PIK3C2A,PIK3C3,CREB1,PIK3CD
Aryl Hydrocarbon Receptor Signaling	1.59E+00	5.84E-02	NR2F1,TP53,NCOA2,ALDH3A2,MAPK8,TGFB3,SLC35A2,ALDH7A1,ARNT
Lymphotoxin Œ≤ Receptor Signaling	1.57E+00	8.20E-02	IKBKG,NFKBIA,PIK3C2A,PIK3C3,PIK3CD
G-Protein Coupled Receptor Signaling	1.57E+00	5.45E-02	ADCY9,HRH1,RAF1,IKBKG,NFKBIA,PIK3C2A,PIK3C3,CREB1,HTR1F,PIK3CD,RGS12,PRKCA
Colorectal Cancer Metastasis Signaling	1.52E+00	5.22E-02	ADCY9,TP53,SIAH1,PIK3C2A,MAPK8,GNG5,APPL1,MSH2,PIK3C3,FZD3,TGFB3,PIK3CD,FZD2

FcŒ≥RIIB Signaling in B Lymphocytes	1.51E+00	7.14E-02	PIK3C2A,PIK3C3,MAPK8,PIK3CD
Docosahexaenoic Acid (DHA) Signaling	1.51E+00	8.33E-02	FOXO1,PIK3C2A,PIK3C3,PIK3CD
Hereditary Breast Cancer Signaling	1.51E+00	6.20E-02	TP53,HDAC4,MSH2,PIK3C2A,PIK3C3,FANCF,MRE11A,PIK3CD
Role of Osteoblasts, Osteoclasts and Chondrocytes in Rheumatoid Arthritis	1.50E+00	5.26E-02	IKBKG,NFKBIA,FOXO1,PIK3C2A,BMPR1A,MAP3K7,PIK3C3,FZD3,MAPK8,PIK3CD,PPP3CC,FZD2
HGF Signaling	1.48E+00	6.80E-02	RAF1,PIK3C2A,MAP3K7,PIK3C3,MAPK8,PIK3CD,PRKCA
PPARŒ±/RXRŒ± Activation	1.45E+00	5.49E-02	ADCY9,RAF1,IKBKG,NFKBIA,MAP3K7,MAPK8,TGFB3,PLCH2,PLCL1,PRKCA
Role of PKR in Interferon Induction and Antiviral Response	1.44E+00	8.70E-02	TP53,IKBKG,NFKBIA,MAP3K7
IL-8 Signaling	1.43E+00	5.38E-02	RAF1,IKBKG,MYL2,PIK3C2A,GNA12,PIK3C3,MAPK8,PIK3CD,GNG5,PRKCA
Endothelin-1 Signaling	1.42E+00	5.41E-02	ADCY9,RAF1,PIK3C2A,GNA12,PIK3C3,MAPK8,PIK3CD,PLCH2,PLCL1,PRKCA
Regulation of IL-2 Expression in Activated and Anergic T Lymphocytes	1.40E+00	6.67E-02	RAF1,IKBKG,NFKBIA,MAPK8,TGFB3,PPP3CC
IL-10 Signaling	1.40E+00	7.14E-02	IKBKG,NFKBIA,BLVRA,MAP3K7,MAPK8
Estrogen-Dependent Breast Cancer Signaling	1.40E+00	7.14E-02	PIK3C2A,PIK3C3,CREB1,IGF1R,PIK3CD
Axonal Guidance Signaling	1.40E+00	4.47E-02	RAF1,PIK3C2A,MYL2,GNA12,SEMA6A,PPP3CC,DPYSL5,GNG5,SUFU,SEMA6D,PIK3C3,FZD3,PIK3CD,SEMA3B,SEMA4A,FZD2,VASP,PRKCA
Melanocyte Development and Pigmentation Signaling	1.38E+00	6.82E-02	ADCY9,RAF1,PIK3C2A,PIK3C3,CREB1,PIK3CD
Role of NFAT in Regulation of the Immune Response	1.37E+00	5.10E-02	RAF1,IKBKG,NFKBIA,PIK3C2A,GNA12,PIK3C3,PIK3CD,PPP3CC,GNG5,CABIN1
IL-15 Signaling	1.37E+00	7.46E-02	STAT6,RAF1,PIK3C2A,PIK3C3,PIK3CD
Renin-Angiotensin Signaling	1.36E+00	5.83E-02	ADCY9,RAF1,PIK3C2A,PIK3C3,MAPK8,PIK3CD,PRKCA
EIF2 Signaling	1.33E+00	6.00E-02	RAF1,EIF2S2,EIF2C4,PIK3C2A,PIK3C3,PIK3CD
Regulation of eIF4 and p70S6K Signaling	1.32E+00	5.38E-02	RAF1,EIF2S2,EIF2C4,EIF4EBP2,PIK3C2A,PIK3C3,PIK3CD
Glycerolipid Metabolism	1.32E+00	4.49E-02	AGPAT4,PPAP2A,ALDH3A2,DAGLB,DGKG,AGPAT3,ALDH7A1
Macropinocytosis Signaling	1.30E+00	6.94E-02	PIK3C2A,PIK3C3,USP6NL,PIK3CD,PRKCA
Production of Nitric Oxide	1.30E+00	4.86E-02	IKBKG,NFKBIA,PIK3C2A,MAP3K7,PIK3C3,MAPK8,IFNGR2,PIK3CD,PRKCA

and Reactive Oxygen Species in Macrophages			
Cleavage and Polyadenylation of Pre-mRNA	1.28E+00	1.67E-01	PAPOLA,NUDT21
TR/RXR Activation	1.27E+00	6.19E-02	PIK3C2A,PIK3C3,STRBP,PIK3CD,ME1,TBL1XR1
PAK Signaling	1.27E+00	5.88E-02	RAF1,MYL2,PIK3C2A,PIK3C3,MAPK8,PIK3CD

R6-2 12 wk D1 IPA Analysis

Ingenuity Canonical Pathways	-log (p-value)	Ratio	Molecules
Polyamine Regulation in Colon Cancer	2.88E+00	2.27E-01	TCF4,MAX,SAT2,CTNNB1,ODC1
Axonal Guidance Signaling	2.47E+00	8.68E-02	NTF3,RND1,ITSN1,EPHB2,LIMK2,CRK,WNT8B,LIMK1,EFNB2,WNT7A,NFAT5,GLI3,ADAM28,NGFR,PFN4,SMO,ADAM23,GNA13,RASA1,SEMA3E,SEMA3G,PAK6,NFATC1,PPP3CC,MYL6B,GNG5,EFNA1,EPHA6,SDCBP,PAK3,NTRK3,SEMA6D,PRKCD,SEMA7A,NTN3
Actin Cytoskeleton Signaling	2.17E+00	9.44E-02	MYH4,MYH6,PAK6,RDX,LIMK2,CRK,MYL6B,SSH1,LIMK1,FGF17,PIP5K1A,PAK3,PFN4,PPP1R12B,FGF3,VCL,GNA13,NCKAP1L,PIP4K2A,ACTN1,IQGAP3,MYH1
Semaphorin Signaling in Neurons	1.96E+00	1.54E-01	RND1,PAK6,PAK3,RHOT1,LIMK2,FNBP1,SEMA7A,LIMK1
Nicotinate and Nicotinamide Metabolism	1.82E+00	8.82E-02	DAPK1,ADH7,NEK2,MAP3K6,PAK3,PIM1,PRKCD,PRKAA2,PNP,LIMK2,LIMK1,DYRK1A
Tight Junction Signaling	1.57E+00	9.58E-02	MYH4,MYH6,TGFBR1,MLLT4,CASK,MYL6B,CPSF6,EPB41,NGFR,PPM1L,TGFB2,VCL,TNFRSF1B,CTNNB1,CSTF3,MYH1
Regulation of Actin-based Motility by Rho	1.55E+00	1.09E-01	PIP5K1A,PAK6,PAK3,RHOT1,PFN4,PPP1R12B,MYL6B,PIP4K2A,FNBP1,LIMK1
Cleavage and Polyadenylation of Pre-mRNA	1.51E+00	2.50E-01	PAPOLA,CPSF6,CSTF3
Germ Cell-Sertoli Cell Junction Signaling	1.51E+00	9.49E-02	TGFBR1,PAK6,MAP3K6,MLLT4,LIMK2,LIMK1,CDH2,PAK3,RHOT1,SORBS1,PPAP2B,TGFB2,CTNNB1,ACTN1,FNBP1
Wnt/Œ≤-catenin Signaling	1.47E+00	9.52E-02	SOX4,TCF4,TGFBR1,ACVR1,TLE1,MDM2,SOX11,WNT8B,CSNK2A2,CDH2,WNT7A,PPM1L,SMO,TGFB2,CTNNB1,TCF7L2
Type I Diabetes Mellitus Signaling	1.36E+00	9.57E-02	IL12A,NFKBIA,CD80,HLA-E,NGFR,SOCS2,APAF1,TNFRSF1B,STAT1,PTPRN,HLA-C
Protein Kinase A Signaling	1.34E+00	7.94E-02	MYH4,TGFBR1,CREM,PDE7A,NFKBIA,NFAT5,GLI3,PDE3B,NGFR,TGFB2,SMO,RYR1,YWHAQ (includes EG:22630),GNA13,CTNNB1,YWHAG,HIST1H1E,PDE10A,NFATC1,PPP3CC,GNG5,MYL

			6B,PRKCD,ADCY1,AKAP9
Calcium Signaling	1.31E+00	7.80E-02	MYH4,MYH6,CHRNA4,ATP2C1,TNNT2,TRDN,NFATC1,PPP3CC,MYL6B,ATP2A2,NFAT5,HDAC7,RYR1,RCAN3,CAMKK2,MYH1
Inositol Phosphate Metabolism	1.24E+00	7.39E-02	DAPK1,MAP3K6,LIMK2,LIMK1,PIP5K1A,INPP4B,NEK2,PAK3,PIM1,PRKCD,PRKAA2,PIP4K2A,DYRK1A

R6-2 12 wk D2 IPA Analysis

Ingenuity Canonical Pathways	-log(p-value)	Ratio	Molecules
Molecular Mechanisms of Cancer	6.51E+00	2.39E-01	GAB2,JAK1,MAPK1,HRAS,CCND1,E2F6,CAMK2A,CAMK2D,PLCB1,GSK3B,GNA13,HIPK2,SMAD1,RASA1,PRKD1,ATM,TP53,AKT2,CCNE2,PRKCQ,CASP3,CDK6,RAPGEF3,GNAZ,APC,PIK3R3,BMPR1B,CBL,MAX,RND3,IRS1,CDK4,FZD6,FZD3,PRKCH,MAP2K3,PAK7,CFLAR,NOTCH1,GNAL,CAMK2G,TCF4,PIK3CA,RALA,PA2G4,CRK,PSEN2,PSENEN,FZD1,HIF1A,SMAD5,EP300,BRAF,AKT1,NFKBIA,MAP3K7,RHOU,TGFB2,BID,ADCY8,CAMK2B,SRC,PRKDC,ADCY2,PAK2,RHOC,ADCY6,MAPK8,SMAD7,GNAQ,XIAP,GNAI2,GNAS,PLCB4,ARHGEF10,RRAS2,FOXO1,PAK3,RASGRP1,CDKN1A,ADCY1,RASGRF1,ADCY7,ATR,BCL2L11,LRP1,CTNND1,RAPGEF1,PRKCB
Axonal Guidance Signaling	6.06E+00	2.33E-01	GLI2,MAPK1,ITSN1,NFATC3,GNB5,HRAS,SEMA6B,NCK1,WNT9A,NTN1,LIMK1,VEGFA,GNB4,MICAL1,SEMA3D,ABLIM3,BAIAP2,PLCB1,ADAM23,SRGAP2,GNA13,GSK3B,PLXNB3,RASA1,PRKD1,AKT2,PRKCQ,SEMA5A,VEGFC,HHIP,PPP3CC,GNAZ,MYL9 (includes EG:10398),PIK3R3,SRGAP3,MYL12B,SEMA6D,FZD6,FZD3,RTN4,PRKCH,PAK7,GNG2,GNAL,ADAM17,PIK3CA,PLXNA3,UNC5A,ARPC1B,SEMA6A,EGF,CRK,PLXNA2,FZD1,WNT8B,ABLIM1,EIF4E,WNT7A,AKT1,WASL (includes EG:8976),GNG11,PPP3CB,IGF1,SDC2,EFNA5,DCC,SEMA4A,GNG4,ITGB1,SEMA3E,PAK2,PLXNC1,NRP2,SHANK2,GNAQ,SLIT2,EPHA3,ROCK1,GNAI2,GNAS,SEMA3A,PLCB4,NTRK2,RRAS2,GLIS2,MAG,PAK3,NTRK3,PLXNB1,EPHA5,SEMA4G,EPHB3,SEMA3C,PRKCB
Role of NFAT in Cardiac Hypertrophy	5.43E+00	2.56E-01	CAMK1D,MAPK1,GNB5,HRAS,CABIN1,HDAC6,GNB4,CAMK2A,CAMK2D,PLCB1,GSK3B,PLCL1,PRKD1,AKT2,PRKCQ,PPP3CC,PIK3R3,RCAN3,MAP2K3,PRKCH,GNG2,CAMK2G,IL6ST,PIK3CA,CAMK4,PDIA3,EP300,AKT1,GNG11,IGF1,PPP3CB,MAP3K7,TGFB2,CAMK1G,IGF1R,ADCY8,GNG4,CAMK2B,SRC,ADCY2,HDAC1,GNAQ,MAPK8,ADCY6,PLCG1,GNAI2,GNAS,PLCB4,RRAS2,ADCY1,MEF2C,ADCY7,PRKCB
Breast Cancer Regulation by Stathmin1	5.20E+00	2.66E-01	CAMK1D,MAPK1,GNB5,HRAS,LIMK1,E2F6,GNB4,STMN1,CAMK2A,CAMK2D,PPM1L,PLCB1,TUBA1C,GNA13,PRKD1,TP53,PPP1R14C,CCNE2,PRKCQ,TUBB2A,PPP1R14A,PIK3R3,PPP2R3A,PPP1R12A,PRKCH,GNG2,CAMK2G,PIK3CA,CAMK4,PPP1R3C,PPP1CB,GNG11,CAMK1G,PPP2R2C,ADCY8,GNG4,CAMK2B,ADCY2,PPP2R5C,TUBB2C,GNAQ,ADCY6,ROCK1,GNAI2,GNAS,PLCB4,ARHGEF10,RRAS2,ADCY1,CDKN1A,ADCY7,PPP2R1B,PRKCB

Thrombin Signaling	5.17E+00	2.65E-01	CAMK1D,MAPK1,GNB5,HRAS,MYLK,IKBKB,GNB4,CAMK2A,CAMK2D,PLCB1,GNA13,PLCL1,PRKD1,AKT2,PRKCQ,GNAZ,MYL9 (includes EG:10398),PIK3R3,RND3,MYL12B,PPP1R12B,PPP1R12A,PRKCH,GNG2,ARHGEF9,GNAL,CAMK2G,PIK3CA,CAMK4,PDIA3,EGF,AKT1,GNG11,CAMK1G,RHOU,GATA6,ADCY8,GNG4,CAMK2B,SRC,ADCY2,RHOC,GNAQ,ADCY6,PLCG1,ROCK1,GNAI2,GNAS,PLCB4,RRAS2,ARHGEF10,ADCY1,ADCY7,PRKCB
Reelin Signaling in Neurons	4.72E+00	3.46E-01	APOE,PIK3CA,MAPT,DAB1,CDK5R1,MAP3K10,YES1,AKT1,GSK3B,ITGB1,SRC,MAP3K9,CNR1,MAPK8IP2,MAPK8,ITGA6,MAPK8IP3,VLDLR,MAPK8IP1,PIK3R3,ARHGEF10,NDEL1,LRP8,PAFAH1B1,DCX,ARHGEF9,PAFAH1B3
CXCR4 Signaling	4.50E+00	2.63E-01	PIK3CA,MAPK1,CD4,GNB5,HRAS,CRK,GNB4,GNG11,AKT1,RHOU,PLCB1,GNA13,ADCY8,GNG4,PRKD1,SRC,ADCY2,AKT2,PAK2,PRKCQ,RHOC,EGR1,GNAQ,MAPK8,ADCY6,GNAZ,GNAI2,ROCK1,PIK3R3,MYL9 (includes EG:10398),GNAS,PLCB4,RRAS2,RND3,PAK3,MYL12B,ADCY1,PAK7,PRKCH,GNG2,ELMO1,ADCY7,GNAL,PRKCB
Synaptic Long Term Potentiation	4.41E+00	2.92E-01	CAMK4,MAPK1,GRM3,PPP1R1A,PPP1R3C,HRAS,PPP1CB,EP300,CAMK2D,CAMK2A,PPP3CB,PLCB1,ADCY8,PRKD1,CAMK2B,GRIN2B,PPP1R14C,PRKCQ,GNAQ,GRIA2,PPP1R14A,RAPGEF3,GRM4,PPP3CC,GRIN3A,ATF2,PLCB4,RRAS2,ADCY1,PPP1R12A,PRKCH,PRKCB,CAMK2G
CREB Signaling in Neurons	4.41E+00	2.40E-01	PIK3CA,POLR2F,POLR2D,CAMK4,MAPK1,PDIA3,GRM3,GNB5,HRAS,EP300,GNB4,CAMK2D,CAMK2A,AKT1,POLR2A,GNG11,PLCB1,GNA13,GRIK2,PLCL1,ADCY8,GNG4,PRKD1,CAMK2B,AKT2,ADCY2,PRKCQ,ADCY6,GRIA2,GNAQ,PLCG1,GRM4,GNAZ,ATF2,GNAI2,PIK3R3,GNAS,PLCB4,RRAS2,ADCY1,PRKCH,GNG2,POLR2I,ADCY7,GNAL,CAMK2G,PRKCB
Ephrin Receptor Signaling	4.38E+00	2.45E-01	ARPC1B,ITSN1,MAPK1,PTPN13,GNB5,EGF,HRAS,MAP4K4,CRK,NCK1,LIMK1,VEGFA,GNB4,GNG11,WASL (includes EG:8976),AKT1,SORBS1,SDC2,EFNA5,GNA13,RASA1,GNG4,ITGB1,SRC,GRIN2B,AKT2,PAK2,ANGPT1,GNAQ,VEGFC,GNAZ,EPHA3,FGF1,GRIN3A,ATF2,ROCK1,GNAI2,GNAS,RRAS2,ABI1,PAK3,ACP1,EPHA5,EPHB3,PAK7,GNG2,GNAL,RAPGEF1
Glioma Signaling	4.36E+00	2.77E-01	PIK3CA,CAMK4,MAPK1,CAMK1D,PA2G4,EGF,HRAS,CCND1,E2F6,MTOR,AKT1,CAMK2D,CAMK2A,IGF1,CAMK1G,IGF1R,PRKD1,CAMK2B,PDGFRB,TP53,AKT2,PRKCQ,CDK6,PLCG1,PIK3R3,RRAS2,CDK4,CDKN1A,PRKCH,PRKCB,CAMK2G
Protein Kinase A Signaling	4.23E+00	2.32E-01	CREM,MAPK1,NFATC3,GNB5,NTN1,TCF7,MYLK,GNB4,CAMK2A,CAMK2D,PDE7B,PLCB1,GNA13,GSK3B,ANAPC11,PLCL1,PRKD1,PPP1R14C,PRKCQ,ADD2,PDE10A,PPP1R1B,YWHAB,YWHAZ,PPP1R14A,PPP3CC,ATF2,PDE8A,MYL9 (includes EG:10398),AKAP13,ANAPC4,MYL12B,PDE1B,PPP1R12A,PRKCH,GNG2,CAMK2G,AKAP12,HIST1H1C,FLNB,CAMK4,PDE7A,PDIA3,PPP1R3C,PPP1CB,PDE1A,BRAF,NFKBIA,GNG11,PPP3CB,DCC,TGFB2,RYR1,CHUK,ADCY8,GNG4,CAMK2B,ADCY2,ADCY6,GNAQ,PLCG1,PYGL,AKAP6,PYGB,GNAI2,ROCK1,GNAS,AKAP2,PLCB4,ADCY1,ADD1,ADCY7,PRKCB
cAMP-mediated Signaling	4.20E+00	2.73E-01	AKAP12,CAMK4,CREM,CAMK1D,PDE7A,HTR4,MAPK1,GRM3,DUSP6,HTR1D,PDE1A,BRAF,CAMK2A,CAMK2D,PPP3CB,PDE7B,CAMK1G,ADORA2B,RGS14,ADCY8,CAMK2

			B,SRC,ADCY2,PDE10A,ADCY6,RGS4,AKAP6,RAPGEF3,GRM4,PPP3CC,DRD2,ATF2,GNAI2,PDE8A,GNAS,AKAP13,AKAP2,DUSP1,PKIB,ADCY1,PDE1B,ADCY7,AGTR1,CAMK2G
PPARŒ±/RXRŒ± Activation	4.15E+00	2.53E-01	PPARA,GPD1,MAPK1,PDIA3,HRAS,MAP4K4,CYP2C44,ACVR2B,ABCA1,EP300,IKBKB,NFKBIA,HSP90AB1,MAP3K7,GPD2,LPL,TGFB2,PRKAA2,PLCB1,NCOR1,CHUK,PLCL1,ADCY8,ACVR1C,ITGB5,ADCY2,ACAA1,MED1,MAPK8,ADCY6,GNAQ,PLCG1,MED12,GNAS,PLCB4,ACADL,GHR,RRAS2,IRS1,ADCY1,MAP2K3,NCOR2,ADCY7,TGS1,PPARGC1A,PRKCB
RAR Activation	4.15E+00	2.54E-01	NSD1,PIK3CA,NR2F2,SMAD5,RBP1,SMARCA4,EP300,VEGFA,NR2F1,AKT1,ALDH1A1,RARB,TGFB2,CSNK2A1,GTF2H5,NCOR1,ADCY8,MAPKAPK2,ZBTB16,SMAD1,RDH13,PRKD1,SRC,ADCY2,AKT2,PRKCQ,MED1,CDK7,SMAD7,MAPK8,ADCY6,PIK3R3,CSNK2A2,RXRG,DUSP1,SMARCA2,ALDH1A2,ADCY1,PRKCH,NCOR2,NRIP1,ADCY7,SCAND1,PPARGC1A,RBP4,PRKCB
Aryl Hydrocarbon Receptor Signaling	4.05E+00	2.53E-01	TRIP11,NFIX,GSTM5,MAPK1,ALDH1L1,CCND1,SMARCA4,EP300,ARNT,NR2F1,ALDH1A1,SP1,HSP90AB1,GSTA4,ALDH3A2,RARB,TGFB2,NFE2L2,GSTK1,ATM,TP53,SRC,MGST1,CCNE2,MED1,CDK6,MAPK8,ALDH9A1,RXRG,NFIA,CDK4,CDKN1A,ALDH1A2,ALDH18A1,NFIB,NCOR2,NRIP1,ATR,MGST3
Wnt/Œ≤-catenin Signaling	3.90E+00	2.68E-01	TCF4,CSNK1G1,SOX1,ACVR2B,FZD1,BCL9,WNT9A,WNT8B,CCND1,EP300,SOX2,WNT7A,AKT1,MAP3K7,DKK3,RARB,PPM1L,TGFB2,CSNK2A1,PPP2R2C,GSK3B,ACVR1C,SOX5 (includes EG:6660),TP53,SOX4,SRC,GJA1,AKT2,PPP2R5C,PPARD,HDAC1,GNAQ,SOX11,APC,CSNK2A2,SOX6,PPP2R3A,TLE3,FZD3,FZD6,SOX8,SFRP1,PPP2R1B,LRP1,TCF7L2
CDK5 Signaling	3.88E+00	3.01E-01	MAPK1,PPP1R3C,MAPT,HRAS,PPP1CB,CDK5R1,PPM1L,LAMB1,PPP2R2C,ADCY8,ITGB1,PPP1R14C,ADCY2,PPP2R5C,PPP1R1B,EGR1,ITGA6,ADCY6,PPP1R14A,GNAS,NTRK2,RRAS2,PPP2R3A,ADCY1,PPP1R12A,PPP2R1B,ADCY7,GNAL
B Cell Receptor Signaling	3.80E+00	2.60E-01	GAB2,PIK3CA,CAMK4,MAPK1,NFATC3,HRAS,INPPL1,FCGR2B,PTPRC,IKBKB,MAP3K10,MTOR,CAMK2A,NFKBIA,CAMK2D,AKT1,PPP3CB,MAP3K7,RPS6KB2,GSK3B,CHUK,CAMK2B,MAP3K9,PTPN6,AKT2,PRKCQ,FCGR2A,EGR1,MAPK8,PPP3CC,MALT1,ATF2,PIK3R3,RRAS2,DAPP1,VAV3,MAP2K3,MAP3K3,CAMK2G,PRKCB
NRF2-mediated Oxidative Stress Response	3.75E+00	2.51E-01	FTL,PIK3CA,GSTM5,MAPK1,MAF,HSPB8,GCLC,HRAS,EP300,AKT1,GSTA4,MAP3K7,ABCC1,DNAJC8,DNAJC1,UBE2K,DNAJA2,FMO1,GCLM,TXN,GSK3B,NFE2L2,PRKD1,ACTA1,GSTK1,MGST1,PRKCQ,DNAJB12,SOD1,ACTB,DNAJC19,MAPK8,DNAJB14,TXNRD1,BACH1,PIK3R3,RRAS2,CAT,MAP2K3,PRKCH,AOX1,DNAJB6,MAP2K5,MGST3,EPHX1,PRKCB
Huntington's Disease Signaling	3.72E+00	2.33E-01	POLR2F,POLR2D,MAPK1,GNB5,HRAS,CDK5R1,HDAC6,NSF,MAP3K10,GNB4,CPLX2,PLCB1,TCERG1,RASA1,PRKD1,CAPN5,TP53,AKT2,PRKCQ,CASP3,RPH3A,ATF2,PIK3R3,CACNA1B,PENK,HTT,PRKCH,CAPN2,CAPN7,GNG2,POLR2I,PIK3CA,EGF,EP300,MTOR,AKT1,GNG11,POLR2A,SP1,IGF1,IGF1R,NCOR1,GOSR1,GNG4,NEUROD1,GRIN2B,YKT6,HDAC1,GNAQ,MAPK8,HIP1,RCOR1,PLCB4,HAP1,NCOR2,PRKCB
Melatonin Signaling	3.54E+00	2.99E-01	CAMK4,PRKCQ,MAPK1,PDIA3,GNAQ,PLCG1,BRAF,GNAI2,PLCB4,CAMK2A,CAMK2D,ARAF,RORA,PLCB1,MAP2K3,PRKCH,PLCL1,RORB,MAP2K5,PRKD1,CAMK2G,CAMK2B

			,PRKCB
IL-8 Signaling	3.46E+00	2.37E-01	PIK3CA,MAPK1,GNB5,EGF,HRAS,MAP4K4,CCND1,LIMK1,IRAK1,VEGFA,BRAF,IKBKB,GNB4,MTOR,AKT1,GNG11,RHOU,GNA13,CHUK,GNG4,PRKD1,SRC,VCAM1,AKT2,PRKCQ,PAK2,ANGPT1,RHOC,MAPK8,VEGFC,PLD1,CSTB,GNAI2,ROCK1,PIK3R3,GNAS,RRAS2,ARAF,RND3,MYL12B,PRKCH,PTGS2,GNG2,PRKCB
Cardiac Œ≤-adrenergic Signaling	3.37E+00	2.39E-01	AKAP12,PDE7A,PPP1R1A,PPP1R3C,GNB5,PPP1CB,PDE1A,GNB4,GNG11,PDE7B,PPM1L,PPP2R2C,ADCY8,GNG4,PPP1R14C,ADCY2,PPP2R5C,PDE10A,ADRBK2,ADCY6,PPP1R14A,AKAP6,PDE8A,AKAP13,GNAS,AKAP2,PPP2R3A,PKIB,ADCY1,PDE1B,PPP1R12A,GNG2,PPP2R1B,ADCY7
G-Protein Coupled Receptor Signaling	3.30E+00	2.32E-01	MAPK1,GRM3,HRAS,IKBKB,CAMK2D,CAMK2A,PDE7B,PLCB1,RGS14,ADORA2B,RASA1,AKT2,PDE10A,RGS4,RAPGEF3,GRM4,DRD2,ATF2,PIK3R3,PDE8A,DUSP1,PDE1B,AGTR1,CAMK2G,PIK3CA,CAMK4,GPR12,PDE7A,HTR4,DUSP6,HTR1D,PDE1A,BRAF,AKT1,NFKBIA,CHUK,ADCY8,CAMK2B,SRC,ADCY2,EDNRB,ADCY6,GNAQ,GNAI2,GNAS,PLCB4,RRAS2,RASGRP1,ADCY1,ADCY7,PRKCB
GNRH Signaling	3.23E+00	2.36E-01	MAPK1,EGF,HRAS,MAP3K10,CAMK2D,CAMK2A,MAP3K7,PLCB1,ADCY8,PRKD1,CAMK2B,SRC,MAP3K9,ADCY2,PRKCQ,PAK2,EGR1,GNAQ,MAPK8,ADCY6,ATF2,GNAI2,GNAS,PLCB4,RRAS2,PAK3,ADCY1,MAP2K3,PAK7,PRKCH,ADCY7,MAP3K3,PRKCB,CAMK2G
Neuropathic Pain Signaling In Dorsal Horn Neurons	3.17E+00	2.72E-01	PIK3CA,CAMK4,MAPK1,CAMK1D,GRM3,PDIA3,CAMK2D,CAMK2A,GPR37,CAMK1G,PLCB1,KCNQ3,PLCL1,PRKD1,CAMK2B,GRIN2B,SRC,PRKCQ,GRIA2,PLCG1,GRM4,GRIN3A,PIK3R3,PLCB4,NTRK2,PRKCH,PRKCB,CAMK2G
Nicotinate and Nicotinamide Metabolism	3.14E+00	2.13E-01	MAPK1,IRAK1,LIMK1,BRAF,PRKX,NEK2,PRPF4B,PRKAA2,MAP3K9,CDK18,AKT2,DAPK1,ENPP1,PAK2,PRKCQ,CDK7,MAPK8,CDK6,PAK3,ARAF,NT5E,CDK4,MAP2K3,PRKCH,PAK7,DUSP18,AOX1,NMNAT3 (includes EG:349565),DUSP16
FcŒ≥ Receptor-mediated Phagocytosis in Macrophages and Monocytes	3.05E+00	2.67E-01	GAB2,MAPK1,ARPC1B,DGKB,CRK,NCK1,ARF6,YES1,AKT1,EZR,RPS6KB2,PRKD1,ACTA1,SRC,AKT2,PRKCQ,FCGR2A,ACTB,PLCG1,PLD1,MYO5A,PIK3R3,PIP5K1A,CBL,VAV3,PRKCH,PRKCB
Inositol Phosphate Metabolism	2.99E+00	2.05E-01	MINPP1,PIK3CA,MAPK1,PDIA3,INPPL1,LIMK1,IRAK1,BRAF,PRKX,NEK2,PRPF4B,PRKAA2,PLCB1,PLCL1,ATM,CDK18,MAP3K9,DAPK1,AKT2,PAK2,PRKCQ,CDK7,MAPK8,CDK6,PLCG1,ITPKA,PIK3R3,PIP5K1A,PLCB4,ARAF,PAK3,CDK4,PAK7,MAP2K3,PRKCH,PIP4K2A
HER-2 Signaling in Breast Cancer	2.96E+00	2.91E-01	TP53,ITGB1,PIK3CA,CCNE2,AKT2,PRKCQ,CDK6,HRAS,EGF,PLCG1,PARD6B,CCND1,PIK3R3,AKT1,RRAS2,FOXO1,CDKN1A,PRKCH,GSK3B,PARD3,ITGB5,PRKD1,PRKCB
RhoA Signaling	2.96E+00	2.73E-01	ARPC1B,SEPT3,LIMK1,MYLK,IGF1,EZR,CIT,BAIAP2,IGF1R,CDC42EP1,GNA13,ACTA1,SEPT8,ACTB,RDX,SEPT4,ANLN,DLC1,PLD1,ROCK1,MYL9 (includes EG:10398),KTN1,PIP5K1A,RHPN2,LPAR1,MYL12B,PPP1R12B,PPP1R12A,PIP4K2A,MSN
Small Cell Lung Cancer Signaling	2.93E+00	2.47E-01	TP53,TRAF3,PIK3CA,CCNE2,FHIT,AKT2,PA2G4,CDK6,CCND1,SKP2,PIK3R3,RXRG,IKBKB,AKT1,MAX,NFKBIA,CDK4,RARB,CKS1B,BID,CHUK,PTGS2
Chemokine Signaling	2.93E+00	2.93E-01	SRC,CAMK4,MAPK1,CAMK1D,GNAQ,MAPK8,PPP1CB,HRAS,PLCG1,LIMK1,GNAI2,PL

			CB4,RRAS2,CAMK2D,CAMK2A,PPP1R12B,CAMK1G,PLCB1,PPP1R12A,CAMK2B,CAMK2G,PRKCB
PTEN Signaling	2.93E+00	2.52E-01	PIK3CA,MAPK1,HRAS,INPPL1,CCND1,IKBKB,AKT1,CSNK2A1,RPS6KB2,CHUK,GSK3B,PDGFRB,ITGB1,AKT2,CASP3,PIK3R3,CSNK2A2,BMPR1B,GHR,MAGI1,RRAS2,CBL,FOXO1,CDKN1A,MAGI2,BCL2L11
Cardiac Hypertrophy Signaling	2.91E+00	2.18E-01	MAPK1,GNB5,HRAS,MAP3K10,GNB4,PLCB1,GNA13,GSK3B,PLCL1,MAP3K9,GNAZ,PPP3CC,ATF2,MYL9 (includes EG:10398),PIK3R3,RND3,MYL12B,IRS1,MAP2K3,GNG2,GNAL,PIK3CA,CAMK4,PDIA3,EIF4E,EP300,MTOR,AKT1,GNG11,IGF1,PPP3CB,MAP3K7,IGF1R,RHOU,TGFB2,MAPKAPK2,ADCY8,GNG4,ADCY2,RHOC,GNAQ,MAPK8,ADCY6,PLCG1,ROCK1,GNAI2,GNAS,PLCB4,RRAS2,ADCY1,MEF2C,ADCY7,MAP3K3
14-3-3-mediated Signaling	2.76E+00	2.63E-01	PIK3CA,MAPK1,PDIA3,MAPT,HRAS,AKT1,PLCB1,GFAP,TUBA1C,GSK3B,PLCL1,PRKD1,SRC,AKT2,PRKCQ,TUBB2C,YWHAB,TUBB2A,YWHAZ,MAPK8,PLCG1,VIM,PIK3R3,PLCB4,CBL,RRAS2,FOXO1,YAP1,PRKCH,PRKCB
Colorectal Cancer Metastasis Signaling	2.73E+00	2.17E-01	JAK1,MAPK1,MMP16,GNB5,HRAS,WNT9A,CCND1,TCF7,VEGFA,GNB4,GSK3B,TP53,AKT2,CASP3,ADRBK2,VEGFC,APC,PIK3R3,RND3,FZD3,FZD6,GNG2,PTGER2,IL6ST,SIAH1,PIK3CA,MMP14,EGF,FZD1,WNT8B,MLH1,BRAF,APPL1,WNT7A,AKT1,GNG11,DCC,RHOU,TGFB2,ADCY8,STAT1,GNG4,SRC,ADCY2,RHOC,MAPK8,ADCY6,GNAS,RRAS2,ADCY1,MSH6,PTGS2,ADCY7,LRP1
Synaptic Long Term Depression	2.69E+00	2.25E-01	MAPK1,GRM3,HRAS,PRKG1,IGF1,PPM1L,IGF1R,RYR1,PLCB1,PPP2R2C,GNA13,ADCY8,PRKD1,TMEM87B,ADCY2,PRKCQ,PPP2R5C,GUCY1A3,GNAQ,GRIA2,YWHAZ,ADCY6,GNAZ,GRM4,GNAI2,PLA2G4A,GNAS,PLCB4,RRAS2,PPP2R3A,PRKCH,PPP2R1B,ADCY7,NPR2,GNAL,PRKCB
Glioblastoma Multiforme Signaling	2.69E+00	2.27E-01	PIK3CA,MAPK1,PDIA3,NF2,EGF,HRAS,FZD1,WNT9A,WNT8B,CCND1,E2F6,MTOR,AKT1,WNT7A,IGF1,RHOU,IGF1R,PLCB1,GSK3B,PLCL1,PDGFRB,TP53,SRC,AKT2,RHOC,CDK6,PLCG1,APC,PIK3R3,PLCB4,RRAS2,FOXO1,RND3,CDK4,CDKN1A,FZD3,FZD6
p70S6K Signaling	2.66E+00	2.44E-01	PIK3CA,JAK1,MAPK1,PDIA3,MAPT,HRAS,MTOR,AKT1,PPM1L,PLCB1,PPP2R2C,PLCL1,PRKD1,SRC,AKT2,PRKCQ,PPP2R5C,YWHAB,GNAQ,YWHAZ,PLCG1,PLD1,GNAI2,PIK3R3,PLCB4,RRAS2,PPP2R3A,IRS1,PRKCH,PPP2R1B,AGTR1,PRKCB
Antiproliferative Role of Somatostatin Receptor 2	2.63E+00	2.69E-01	SRC,PTPN6,ADCY2,PIK3CA,MAPK1,GUCY1A3,GNB5,ADCY6,HRAS,BRAF,PIK3R3,GNB4,RRAS2,GNG11,CDKN1A,SST,GNG2,ADCY8,GNG4,ADCY7,NPR2
Production of Nitric Oxide and Reactive Oxygen Species in Macrophages	2.57E+00	2.05E-01	PPARA,PIK3CA,JAK1,MAPK1,PPP1R3C,PPP1CB,ARG2,IKBKB,MAP3K10,AKT1,NFKBIA,MAP3K7,PPM1L,RHOU,PPP2R2C,CHUK,STAT1,PRKD1,PPP1R14C,MAP3K9,PTPN6,AKT2,PRKCQ,PPP2R5C,RHOC,IFNGR2,MAPK8,PLCG1,PPP1R14A,PIK3R3,RND3,PPP2R3A,CAT,PPP1R12A,PRKCH,PPP2R1B,MAP3K3,PRKCB
CCR3 Signaling in Eosinophils	2.57E+00	2.42E-01	PIK3CA,CAMK4,MAPK1,GNB5,HRAS,PPP1CB,LIMK1,MYLK,GNB4,GNG11,PLCB1,GNG4,PRKD1,PAK2,PRKCQ,ROCK1,GNAI2,PIK3R3,PLA2G4A,GNAS,PLCB4,RRAS2,PAK3,PPP1R12B,PPP1R12A,PAK7,PRKCH,GNG2,PRKCB
PI3K/AKT Signaling	2.49E+00	2.26E-01	GAB2,PIK3CA,JAK1,MAPK1,HRAS,INPPL1,CCND1,EIF4E,IKBKB,MTOR,AKT1,NFKBIA,HSP90AB1,PPM1L,RPS6KB2,PPP2R2C,GSK3B,CHUK,TP53,ITGB1,AKT2,PPP2R5C,YWHAB,YWHAZ,MAPK8IP1,PIK3R3,RRAS2,FOXO1,PPP2R3A,CDKN1A,PPP2R1B

Germ Cell-Sertoli Cell Junction Signaling	2.47E+00	2.34E-01	PIK3CA,MAPK1,MYO7A,PVRL3,HRAS,IQGAP1,LIMK1,MAP3K10,WASL (includes EG:8976),AKT1,MAP3K7,SORBS1,PPAP2B,TGFB2,RHOU,TUBA1C,ACTA1,ITGB1,MAP3K9,SRC,PAK2,RHOC,TUBB2C,ACTB,TUBB2A,ITGA6,MAPK8,GSN,PIK3R3,RRAS2,RND3,PAK3,ZYX,MAP2K3,PAK7,MAP3K3,CTNND1
Growth Hormone Signaling	2.46E+00	2.71E-01	PTPN6,PIK3CA,PRKCQ,MAPK1,SOCS2,PLCG1,ONECUT1,PIK3R3,GHR,IGF1,IRS1,IGF1R,RPS6KB2,RPS6KA4,RPS6KA5,PRKCH,STAT1,PRKD1,PRKCB
G Beta Gamma Signaling	2.44E+00	2.10E-01	MAPK1,GNB5,HRAS,GNB4,GNG11,AKT1,GNA13,GNG4,PRKD1,SRC,ADCY2,AKT2,PRKCQ,GNAQ,PLCG1,KCNJ3,GNAZ,GNAI2,GNAS,RRAS2,ADCY1,PRKCH,GNG2,GNAL,PRKCB
Relaxin Signaling	2.43E+00	2.15E-01	PIK3CA,PDE7A,MAPK1,GNB5,PDE1A,VEGFA,BRAF,GNB4,GNG11,AKT1,NFKBIA,PDE7B,GNA13,ADCY8,GNG4,ADCY2,AKT2,GUCY1A3,PDE10A,GNAQ,ADCY6,GNAZ,PDE8A,GNAI2,PIK3R3,GNAS,ADCY1,PDE1B,GNG2,NPR2,ADCY7,GNAL
Ovarian Cancer Signaling	2.43E+00	2.37E-01	PIK3CA,MAPK1,PA2G4,EGF,HRAS,FZD1,WNT9A,WNT8B,CCND1,TCF7,MLH1,VEGFA,BRAF,MTOR,WNT7A,AKT1,RPS6KB2,GSK3B,TP53,SRC,GJA1,AKT2,PTGS1,VEGFC,APC,PIK3R3,RRAS2,CDK4,FZD3,MSH6,FZD6,PTGS2
Sphingosine-1-phosphate Signaling	2.41E+00	2.41E-01	PIK3CA,MAPK1,PDIA3,AKT1,RHOU,PLCB1,GNA13,PLCL1,ADCY8,SMPD3,PDGFRB,ADCY2,AKT2,CASP3,S1PR5,RHOC,GNAQ,ADCY6,PLCG1,SMPD2,GNAI2,PIK3R3,S1PR3,PLCB4,RND3,ADCY1,ADCY7
Macropinocytosis Signaling	2.37E+00	2.64E-01	ITGB1,SRC,PIK3CA,PRKCQ,USP6NL,HRAS,EGF,PLCG1,CSF1R,PIK3R3,ANKFY1,ARF6,RRAS2,ABI1,CSF1,PRKCH,ITGB5,PRKD1,PRKCB
Valine, Leucine and Isoleucine Degradation	2.34E+00	1.80E-01	ACAA1,ECH1,ACAD9,ALDH9A1,ELOVL6,ACAA1B,HIBCH,HADHB,ACADL,ALDH1A1,PCCA,ACADVL,ALDH3A2,ALDH1A2,DBT,OXCT1,MCCC1,AOX1,ACADM,HADH
Endothelin-1 Signaling	2.33E+00	2.16E-01	PIK3CA,MAPK1,PDIA3,HRAS,SHC3,BRAF,PLCB1,GNA13,ADCY8,PLCL1,PRKD1,TMEM87B,SRC,ADCY2,PRKCQ,EDNRB,CASP3,GUCY1A3,PTGS1,GNAQ,YWHAZ,MAPK8,ADCY6,PLCG1,GNAZ,PLD1,GNAI2,PIK3R3,PLA2G4A,GNAS,PLCB4,RRAS2,ARAF,ADCY1,PRKCH,PTGS2,PTGER2,ADCY7,GNAL,PRKCB
Œ±-Adrenergic Signaling	2.32E+00	2.26E-01	ADCY2,CAMK4,PRKCQ,MAPK1,GNAQ,ADCY6,GNB5,HRAS,PLCG1,PYGB,PYGL,GNAI2,GNAS,GNB4,GNG11,RRAS2,ADCY1,PRKCH,GNG2,ADCY8,GNG4,ADCY7,PRKD1,PRKCB
mTOR Signaling	2.31E+00	2.18E-01	PIK3CA,MAPK1,FKBP1A,HRAS,HIF1A,RICTOR,EIF4E,VEGFA,MTOR,AKT1,EIF3D,PPM1L,PRKAA2,RPS6KB2,EIF3A,RHOU,PPP2R2C,PRKD1,AKT2,PRKCQ,PPP2R5C,RHOC,VEGFC,PLD1,PIK3R3,RRAS2,RND3,PPP2R3A,IRS1,RPS6KA4,RPS6KA5,PRKCH,PPP2R1B,PRKCB
Angiopoietin Signaling	2.29E+00	2.57E-01	PIK3CA,AKT2,PAK2,ANGPT1,HRAS,CRK,NCK1,PIK3R3,IKBKB,TNIP1,NFKBIA,AKT1,RRAS2,FOXO1,PAK3,IKBKAP,PAK7,CHUK,RASA1
Role of NFAT in Regulation of the Immune Response	2.19E+00	2.04E-01	PIK3CA,CAMK4,CSNK1G1,MAPK1,NFATC3,CD4,GNB5,HRAS,FCGR2B,CABIN1,IKBKB,GNB4,NFKBIA,GNG11,AKT1,PPP3CB,PLCB1,GSK3B,GNA13,CHUK,GNG4,HLA-DMA,AKT2,PRKCQ,FCGR2A,GNAQ,PLCG1,GNAZ,PPP3CC,ATF2,GNAI2,PIK3R3,GNAS,PLCB4,RRAS2,RCAN3,IKBKAP,MEF2C,GNG2,GNAL
p53 Signaling	2.19E+00	2.61E-01	TP53,WT1,PRKDC,PIK3CA,AKT2,JMY,MED1,RRM2B,HDAC1,MAPK8,C12ORF5,RPRM,CCND1,EP300,CCNG1,PIK3R3,PCNA,AKT1,CDK4,CDKN1A,GSK3B,HIPK2,ATR,ATM

Integrin Signaling	2.18E+00	2.20E-01	PIK3CA,RALA,ARPC1B,MAPK1,HRAS,PPP1CB,MYLK,BRAF,ARF6,WASL (includes EG:8976),AKT1,ITGA9,RHOU,GSK3B,ITGB5,ACTA1,ITGB1,CAPN5,SRC,PARVA,AKT2,PAK2,RHOC,ASAP1,ACTB,ITGA6,MAPK8,PLCG1,TNK2,ROCK1,PIK3R3,RRAS2,RND3,PAK3,ARF3,MYL12B,PPP1R12B,PPP1R12A,ZYX,PAK7,CAPN2,CAPN7,TSPAN6,RAPGEF1
Estrogen Receptor Signaling	2.16E+00	2.35E-01	TAF4B,POLR2F,TAF11,POLR2D,MAPK1,HRAS,TAF7,SMARCA4,EP300,PGR,SPEN,POLR2A,PCK2,CTBP2,GTF2H5,NCOR1,PRKDC,SRC,MED1,TAF15,CDK7,TAF1,RRAS2,NCOR2,NRIP1,TRRAP,POLR2I,PPARGC1A
Melanocyte Development and Pigmentation Signaling	2.15E+00	2.50E-01	SRC,PTPN6,ADCY2,PIK3CA,MAPK1,MITF,ADCY6,HRAS,PLCG1,CRK,ATF2,EP300,PIK3R3,KITLG,GNAS,RRAS2,ADCY1,RPS6KB2,RPS6KA4,RPS6KA5,ADCY8,ADCY7
Role of PKR in Interferon Induction and Antiviral Response	2.13E+00	2.83E-01	TP53,TRAF3,CASP3,RNASEL,ATF2,IKBKB,AKT1,NFKBIA,MAP3K7,BID,MAP2K3,CHUK,STAT1
IL-1 Signaling	2.12E+00	2.26E-01	ADCY2,GNAQ,ADCY6,MAPK8,GNB5,GNAZ,IRAK1,GNAI2,GNB4,IKBKB,GNAS,NFKBIA,GNG11,MAP3K7,ADCY1,MAP2K3,CHUK,GNA13,GNG2,ADCY8,IL1RAP,GNG4,ADCY7,GNAL
SAPK/JNK Signaling	2.12E+00	2.45E-01	TP53,MAP3K9,PIK3CA,NFATC3,MAPK8IP2,MAPK8,HRAS,CRK,MAP4K4,MAPK8IP3,MAPK8IP1,ATF2,MAP4K3,PIK3R3,TRADD,MAP3K10,GNG11,RRAS2,MAP3K7,IRS1,ZAK,GNA13,GNG2,MAP3K3
Renal Cell Carcinoma Signaling	2.06E+00	2.64E-01	PIK3CA,AKT2,PAK2,MAPK1,HRAS,CRK,HIF1A,ARNT,EP300,PIK3R3,VEGFA,TCEB2,RRAS2,AKT1,PAK3,TGFA,EGLN3,PAK7,RAPGEF1
Androgen Signaling	2.04E+00	1.94E-01	POLR2F,POLR2D,CAMK4,MAPK1,GNB5,CCND1,EP300,GNB4,TGFB1I1,AR,GNG11,POLR2A,GTF2H5,GNA13,GNG4,PRKD1,SRC,PRKCQ,CDK7,GNAQ,GNAZ,GNAI2,GNAS,PRKCH,GNG2,POLR2I,GNAL,PRKCB
Phospholipase C Signaling	2.00E+00	1.98E-01	MAPK1,NFATC3,GNB5,HRAS,HDAC6,GNB4,PLCB1,GNA13,PRKD1,PRKCQ,PPP1R14A,RAPGEF3,PPP3CC,PLD1,ATF2,MYL9 (includes EG:10398),RND3,MYL12B,PPP1R12B,PPP1R12A,PRKCH,GNG2,RALA,CAMK4,PPP1CB,FCGR2B,EP300,GNG11,PPP3CB,RHOU,ADCY8,GNG4,ITGB1,SRC,ADCY2,RHOC,FCGR2A,HDAC1,ADCY6,GNAQ,PLCG1,PLA2G4A,GNAS,PLCB4,ARHGEF10,RRAS2,ADCY1,MEF2C,ADCY7,PRKCB
Renin-Angiotensin Signaling	1.99E+00	2.17E-01	PIK3CA,MAPK1,SHC3,HRAS,ADCY8,STAT1,PRKD1,PTPN6,ADCY2,PAK2,PRKCQ,MAPK8,ADCY6,GNAQ,PLCG1,ATF2,PIK3R3,RRAS2,PAK3,ADCY1,PRKCH,PAK7,PTGER2,ADCY7,AGTR1,PRKCB
IL-3 Signaling	1.99E+00	2.64E-01	GAB2,PTPN6,PIK3CA,AKT2,JAK1,PRKCQ,MAPK1,HRAS,PPP3CC,PIK3R3,AKT1,RRAS2,FOXO1,PPP3CB,PRKCH,STAT1,PRKD1,RAPGEF1,PRKCB
Non-Small Cell Lung Cancer Signaling	1.94E+00	2.28E-01	TP53,PIK3CA,FHIT,AKT2,PA2G4,MAPK1,CDK6,HRAS,EGF,PLCG1,CCND1,PIK3R3,RXRG,RRAS2,AKT1,CDK4,RARB,TGFA
Melanoma Signaling	1.94E+00	2.83E-01	TP53,PIK3CA,AKT2,MAPK1,MITF,HRAS,CCND1,PIK3R3,BRAF,AKT1,RRAS2,CDK4,CDKN1A
Role of BRCA1 in DNA	1.91E+00	2.62E-01	TP53,RBBP8,RFC1,RFC5,SMARCA4,MLH1,BACH1,E2F6,POU2F1,SMARCA2,CDKN1A,

Damage Response			MSH6,BLM,STAT1,ATR,ATM
Cell Cycle: G1/S Checkpoint Regulation	1.91E+00	2.71E-01	TP53,CCNE2,PA2G4,HDAC1,CDK6,CCND1,SKP2,HDAC6,E2F6,MAX,CDK4,CDKN1A, TGFB2,GSK3B,ATR,ATM
Prostate Cancer Signaling	1.90E+00	2.19E-01	TP53,PIK3CA,CCNE2,AKT2,PA2G4,MAPK1,HRAS,CCND1,ATF2,PIK3R3,MTOR,AR,RRAS2,NFKBIA,AKT1,FOXO1,HSP90AB1,CDKN1A,NKX3-1,CHUK,GSK3B
Notch Signaling	1.90E+00	2.79E-01	ADAM17,NOTCH2,CNTN1,DTX1,DTX4,MAG,HES5,PSEN2,PSENEN,JAG1,NOTCH1,HEY1
Regulation of Actin-based Motility by Rho	1.89E+00	2.39E-01	PAK2,ARPC1B,RHOC,ACTB,PPP1CB,GSN,LIMK1,MYL9 (includes EG:10398),ROCK1,MYLK,PIP5K1A,WASL (includes EG:8976),RND3,PAK3,MYL12B,BAIAP2,PPP1R12B,RHOU,PPP1R12A,PAK7,PIP4K2A, ACTA1
Xenobiotic Metabolism Signaling	1.89E+00	2.02E-01	FTL,MAPK1,CAMK1D,MAF,HRAS,GCLC,CHST15,ARNT,MAP3K10,CAMK2A,CAMK2D, ALDH1A1,ALDH3A2,PPM1L,PRKD1,GSTK1,MAP3K9,MGST1,PRKCQ,MED1,GRIP1,UGT1A1,ALDH9A1,PIK3R3,PPP2R3A,ALDH1A2,PRKCH,ALDH18A1,MAP2K3,CYP2B6,NDST1,MGST3,MAP2K5,CAMK2G,GAL3ST2,PIK3CA,CAMK4,GSTM5,ALDH1L1,EP300,HSP90AB1,GSTA4,MAP3K7,CAMK1G,FMO1,PPP2R2C,NFE2L2,CAMK2B,PPP2R5C,MAPK8,RRAS2,CAT,NRIP1,NCOR2,PPP2R1B,MAP3K3,SCAND1,PRKCB,PPARGC1A
Factors Promoting Cardiogenesis in Vertebrates	1.84E+00	2.36E-01	CCNE2,PRKCQ,SMAD5,FZD1,ACVR2B,TCF7,APC,ATF2,BMPR1B,MAP3K7,FZD6,TGFB2,FZD3,MEF2C,PRKCH,GSK3B,ACVR1C,SMAD1,LRP1,PRKD1,PRKCB
TR/RXR Activation	1.83E+00	2.27E-01	AKT2,PIK3CA,CAMK4,MED1,GRIP1,ME1,HIF1A,DIO2,NRGN,EP300,PIK3R3,RXRG,KLF9,MTOR,AKT1,SLC16A2,SYT2,ACACA,NCOR1,STRBP,NCOR2,PPARGC1A
FAK Signaling	1.83E+00	2.24E-01	ITGB1,CAPN5,SRC,PIK3CA,AKT2,PAK2,MAPK1,ASAP1,ACTB,HRAS,EGF,PLCG1,CRK, PIK3R3,AKT1,RRAS2,PAK3,PAK7,CAPN2,CAPN7,TNS1,ACTA1
PAK Signaling	1.83E+00	2.16E-01	ITGB1,PIK3CA,PAK2,MAPK1,CASP3,PAK1IP1,MAPK8,HRAS,EPHA3,NCK1,LIMK1,MYLK,MYL9 (includes EG:10398),PIK3R3,WASL (includes EG:8976),RRAS2,PAK3,MYL12B,EPHB3,DSCAM,PAK7,PDGFRB
NF-ŒʃB Activation by Viruses	1.79E+00	2.35E-01	ITGB1,PIK3CA,AKT2,PRKCQ,MAPK1,CD4,ITGA6,HRAS,PIK3R3,IKBKB,NFKBIA,AKT1,RRAS2,IKBKAP,PRKCH,CHUK,ITGB5,PRKD1,PRKCB
Hereditary Breast Cancer Signaling	1.79E+00	2.17E-01	POLR2F,PIK3CA,POLR2D,HRAS,CCND1,MLH1,SMARCA4,EP300,HDAC6,POLR2A,AKT1,BLM,ATM,TP53,AKT2,HDAC1,CDK6,RFC1,RFC5,PIK3R3,RRAS2,SMARCA2,H2AFX,CDK4,CDKN1A,MSH6,ATR,POLR2I
Œ≤-alanine Metabolism	1.78E+00	1.53E-01	DPYD,DPYSL3,ECH1,ACAD9,ALDH9A1,UPB1,HIBCH,HADHB,ACADL,ALDH1A1,ACADVL,ALDH3A2,ALDH1A2,MYO5B,ACADM
VDR/RXR Activation	1.78E+00	2.50E-01	WT1,PRKCQ,CCNC,PPARD,MED1,KLF4,EP300,RXRG,SP1,FOXO1,CDKN1A,TGFB2,CSNK2A1,NCOR1,PRKCH,NCOR2,CALB1,CST6,PRKD1,PRKCB
ERK5 Signaling	1.74E+00	2.54E-01	IL6ST,SRC,YWHAB,GNAQ,YWHAZ,HRAS,EGF,ATF2,AKT1,RRAS2,RPS6KB2,WNK1,MEF2C,RPS6KA4,RPS6KA5,GNA13,MAP3K3,MAP2K5
PDGF Signaling	1.74E+00	2.37E-01	SRC,PIK3CA,JAK1,MAPK1,MAPK8,HRAS,PLCG1,CRK,INPPL1,PIK3R3,CSNK2A2,RRAS2,ACP1,CSNK2A1,STAT1,RASA1,PDGFRB,PRKCB
CNTF Signaling	1.73E+00	2.69E-01	IL6ST,PIK3CA,JAK1,MAPK1,HRAS,PIK3R3,LIFR,MTOR,AKT1,RRAS2,RPS6KB2,RPS6

Hypoxia Signaling in the Cardiovascular System	1.67E+00	2.57E-01	KA5,RPS6KA4,STAT1 TP53,UBE2A,UBE2L3,UBE2V2,HIF1A,UBE2D1,ATF2,ARNT,EP300,VEGFA,NFKBIA,AKT1,UBE2B,HSP90AB1,UBE2G1,UBE2E3,UBE2I,ATM
Protein Ubiquitination Pathway	1.67E+00	2.04E-01	USP21 (includes EG:27005),USP24,USP18,UBE2A,PSMD7,CDC20,PSMB10,UBE2L3,PSMD9,FBXW7,UBE2V2,USP54,USP2,USP8,TCEB2,UBE2B,STUB1,UBE2E3,USP40,NEDD4L,ANAPC11,HLA-C,PSMD13,USP36,USP1,UBE3A,UBE2D1,XIAP,PSMD8,SKP2,ANAPC4,PSME1,CBL,PSMB2,UBE2G1,PSMD1,USP46,SMURF2,PSMD4,USP34,UBE2I
Cholecystokinin/Gastrin-mediated Signaling	1.67E+00	2.31E-01	SRC,CREM,PRKCQ,MAPK1,RHOC,GNAQ,MAPK8,HRAS,ATF2,ROCK1,PLCB4,RRAS2,RND3,IL1F5,RHOU,PLCB1,SST,MAP2K3,MEF2C,PRKCH,GNA13,MAP2K5,PRKD1,PRKCB
Neuregulin Signaling	1.66E+00	2.18E-01	ITGB1,SRC,ADAM17,AKT2,PRKCQ,MAPK1,HRAS,EGF,PLCG1,CRK,CDK5R1,PIK3R3,MTOR,AKT1,RRAS2,HSP90AB1,NRG3,RPS6KB2,TGFA,PRKCH,PRKD1,PRKCB
Apoptosis Signaling	1.66E+00	2.33E-01	TP53,CAPN5,PRKCQ,MAPK1,CASP3,MAPK8,HRAS,PLCG1,LMNA,MAP4K4,XIAP,ACIN1,ROCK1,IKBKB,RRAS2,NFKBIA,BID,CAPN2,CHUK,SPTAN1,CAPN7
Pantothenate and CoA Biosynthesis	1.66E+00	1.25E-01	PANK1,ENPP1,DPYD,DPYSL3,COASY,PANK4,UPB1,ILVBL
Glycerophospholipid Metabolism	1.62E+00	1.56E-01	DGKD,GPD1,PDIA3,DGKB,PGS1,LPIN1,PCYT1B,GPD2,PPAP2B,PLCB1,MGLL,LPIN2,PLCL1,TMEM87B,YWHAZ,DGKE,PLCG1,ACHE,ETNK1,CERK,CDS2,PLD1,ELOVL6,AGPAT4,PLA2G4A,PLCB4,LPCAT1,DGKK,DBT,CHKB
Propanoate Metabolism	1.56E+00	1.31E-01	ACAA1,SUCLG2,ACSS1,ECH1,ACAD9,ALDH9A1,HIBCH,HADHB,ACADL,ALDH1A1,PCCA,ACADVL,ALDH3A2,ALDH1A2,ACACA,ACADM,ACSL1
Role of Osteoblasts, Osteoclasts and Chondrocytes in Rheumatoid Arthritis	1.54E+00	1.93E-01	PIK3CA,ADAM17,CAMK4,MAPK1,NFATC3,MMP14,FZD1,SMAD5,WNT9A,WNT8B,TCF7,IKBKB,TRADD,NFKBIA,AKT1,WNT7A,PPP3CB,IGF1,MAP3K7,DKK3,GSK3B,CHUK,SMAD1,ADAMTS4,ITGB1,SRC,AKT2,MAPK8,PPP3CC,GSN,CSF1R,XIAP,APC,PIK3R3,BMPR1B,CBL,FOXO1,CSF1,IL1F5,FZD3,FZD6,MAP2K3,SFRP1,LRP1
G Protein Signaling Mediated by Tubby	1.54E+00	2.44E-01	GNAS,GNB4,PLCB4,GNG11,GNB5,GNAQ,PLCG1,PLCB1,GNG2,GNG4
ERK/MAPK Signaling	1.53E+00	1.98E-01	PIK3CA,MAPK1,PPP1R3C,DUSP6,HRAS,PPP1CB,CRK,EIF4E,BRAF,PPM1L,PPP2R2C,STAT1,ITGB1,PPP1R14C,SRC,PAK2,PPP2R5C,YWHAB,YWHAZ,PLCG1,PPP1R14A,RAPGEF3,ATF2,PIK3R3,PLA2G4A,RRAS2,ARAF,PAK3,DUSP1,PPP2R3A,PPP1R12A,RPS6KA4,PAK7,RPS6KA5,PPP2R1B,ELK3,RAPGEF1,PRKCB
DNA Methylation and Transcriptional Repression Signaling	1.52E+00	3.04E-01	CHD3,DNMT3A,CHD4,HDAC1,SAP130,ARID4B,RBBP4
HGF Signaling	1.52E+00	2.23E-01	MAP3K9,PIK3CA,AKT2,PRKCQ,MAPK1,MAPK8,HRAS,PLCG1,CCND1,ATF2,PIK3R3,MAP3K10,RRAS2,AKT1,MAP3K7,CDKN1A,PRKCH,PTGS2,MAP3K3,ELK3,PRKD1,RAPGEF1,PRKCB
Amyotrophic Lateral Sclerosis Signaling	1.51E+00	1.96E-01	TP53,CAPN5,GRIN2B,PIK3CA,SOD1,CASP3,GRIA2,VEGFC,NEFH,XIAP,GRIN3A,PIK3R3,VEGFA,IGF1,HECW1,RAB5C,CAT,SLC1A2,BID,CAPN2,GRIK2,CAPN7

Clathrin-mediated Endocytosis Signaling	1.51E+00	2.04E-01	PIK3CA,EPS15,STON2,ARPC1B,SH3GLB1,EGF,VEGFA,CD2AP,ARF6,WASL (includes EG:8976),IGF1,PPP3CB,RAB5C,CSNK2A1,STAM,FGF3,AAK1,ITGB5,ACTA1,ITGB1,MYO6,SRC,ACTB,FGF14,VEGFC,PPP3CC,HIP1,FGF1,PIK3R3,CSNK2A2,CBL,CLTA,TFRC,MYO1E
PPAR Signaling	1.50E+00	2.14E-01	PPARA,MAPK1,PPARD,MED1,HRAS,MAP4K4,EP300,NR2F1,IKBKB,NFKBIA,RRAS2,HSP90AB1,MAP3K7,IL1F5,NCOR1,CHUK,NCOR2,NRIP1,SCAND1,PPARGC1A,PDGFRB
Butanoate Metabolism	1.50E+00	1.21E-01	ACAA1,NLGN1,SUCLG2,ECH1,ALDH9A1,ELOVL6,HADHB,BDH1,ALDH1A1,ALDH3A2,ALDH1A2,OXCT1,DBT,MYO5B,HADH,ILVBL
GM-CSF Signaling	1.50E+00	2.39E-01	PIK3CA,AKT2,MAPK1,HRAS,PPP3CC,CCND1,PIK3R3,CAMK2A,CAMK2D,AKT1,RRAS2,PPP3CB,STAT1,PRKCB,CAMK2G,CAMK2B
Cdc42 Signaling	1.49E+00	2.03E-01	RALA,ARPC1B,PPP1CB,IQGAP1,LIMK1,MYLK,WASL (includes EG:8976),BAIAP2,GSK3B,RASA1,ITGB1,SRC,PAK2,MAPK8,TNK2,APC,ATF2,MYL9 (includes EG:10398),CDC42BPA,EXOC4,PAK3,MYL12B,PPP1R12A,PRKCH,PARD3
EGF Signaling	1.48E+00	2.45E-01	PIK3R3,CSNK2A2,PIK3CA,JAK1,MAPK1,MAPK8,CSNK2A1,PLCG1,EGF,HRAS,STAT1,RASA1
ILK Signaling	1.46E+00	2.04E-01	FLNB,PIK3CA,MAPK1,HIF1A,CCND1,VEGFA,TGFB1I1,MTOR,AKT1,PPAP2B,PPM1L,RHOU,PPP2R2C,GSK3B,DSP,ITGB5,ACTA1,ITGB1,PARVA,AKT2,FBLIM1,PPP2R5C,RHOC,ACTB,MAPK8,VIM,VEGFC,ATF2,PIK3R3,MYL9 (includes EG:10398),RND3,PPP2R3A,IRS1,MYH9,RPS6KA4,RPS6KA5,PTGS2,PPP2R1B
RANK Signaling in Osteoclasts	1.45E+00	2.19E-01	SRC,MAP3K9,PIK3CA,AKT2,CAMK4,MAPK1,MITF,MAPK8,PPP3CC,GSN,XIAP,PIK3R3,IKBKB,MAP3K10,AKT1,CBL,NFKBIA,PPP3CB,MAP3K7,CHUK,MAP3K3
Glutamate Receptor Signaling	1.44E+00	2.14E-01	GRIN2B,CAMK4,HOMER2,GRM3,GRIA2,SLC1A3,SLC1A1,GRIP1,GRM4,GRIN3A,GNG11,SLC1A2,GRIK2,GNG2,HOMER1
Cell Cycle: G2/M DNA Damage Checkpoint Regulation	1.42E+00	2.56E-01	TP53,PRKDC,YWHAB,CDK7,CDKN1A,YWHAZ,RPRM,ATR,SKP2,ATM,EP300
Chronic Myeloid Leukemia Signaling	1.41E+00	2.10E-01	TP53,GAB2,PIK3CA,AKT2,PA2G4,MAPK1,HDAC1,CDK6,HRAS,CRK,CCND1,PIK3R3,HDAC6,IKBKB,E2F6,AKT1,RRAS2,CDK4,CDKN1A,CTBP2,TGFB2,CHUK
Cellular Effects of Sildenafil (Viagra)	1.41E+00	1.92E-01	CAMK4,PDIA3,PPP1CB,PDE1A,PRKG1,CACNG2,MYLK,GPR37,PLCB1,KCNQ3,PLCL1,CACNG8,ADCY8,ACTA1,ADCY2,GUCY1A3,ACTB,ADCY6,PLCG1,MYL9 (includes EG:10398),GNAS,PLCB4,MYL12B,PDE1B,ADCY1,PPP1R12B,MYH9,PPP1R12A,ADCY7
Interferon Signaling	1.40E+00	3.00E-01	IFIT3,JAK1,PTPN2,PIAS1,IFNGR2,IFI35,STAT1,IFNAR2,IFNAR1
fMLP Signaling in Neutrophils	1.39E+00	1.92E-01	PIK3CA,CAMK4,PRKCQ,MAPK1,ARPC1B,NFATC3,GNB5,HRAS,PPP3CC,PIK3R3,GNAI2,GNB4,GNAS,PLCB4,GNG11,RRAS2,NFKBIA,PPP3CB,PLCB1,PRKCH,GNG2,GNG4,PRKD1,PRKCB
Dopamine Receptor Signaling	1.39E+00	1.94E-01	PPP1R14C,ADCY2,PPP2R5C,PPP1R1B,DDC,PPP1R3C,ADCY6,PPP1CB,PPP1R14A,DRD2,PPP2R3A,ADCY1,PPM1L,PPP1R12A,PPP2R2C,ADCY8,ADCY7,PPP2R1B
Lymphotoxin Œ≤ Receptor Signaling	1.39E+00	2.30E-01	TRAF3,PIK3CA,AKT2,VCAM1,CASP3,MAPK1,RELB,EP300,PIK3R3,IKBKB,AKT1,NFKBIA,IKBKAP,CHUK
Cell Cycle Regulation by	1.37E+00	2.78E-01	E2F6,CCNE2,PPP2R5C,PPP2R3A,CDK4,PPM1L,PPP2R2C,PPP2R1B,CCND1,CCRN4L

BTG Family Proteins			
T Cell Receptor Signaling	1.37E+00	2.06E-01	PIK3CA,CAMK4,PRKCQ,MAPK1,NFATC3,CD4,MAPK8,HRAS,PLCG1,PPP3CC,MALT1,PIK3R3,PTPRC,IKBKB,RRAS2,CBL,NFKBIA,PPP3CB,VAV3,RASGRP1,CHUK,RASA1
Erythropoietin Signaling	1.33E+00	2.11E-01	SRC,PIK3CA,AKT2,PTPN6,PRKCQ,MAPK1,HRAS,PLCG1,PIK3R3,NFKBIA,AKT1,RRAS2,CBL,PRKCH,PRKD1,PRKCB
Virus Entry via Endocytic Pathways	1.30E+00	2.08E-01	ITGB1,FLNB,SRC,PIK3CA,PRKCQ,ITSN1,ACTB,ITGA6,HRAS,PLCG1,PIK3R3,RRAS2,CLTA,TFRC,PRKCH,ACTA1,ITGB5,PRKD1,HLA-C,PRKCB
CD27 Signaling in Lymphocytes	1.27E+00	2.28E-01	MAP3K9,CASP3,MAPK8,IKBKB,MAP3K10,NFKBIA,MAP3K7,BID,IKBKAP,MAP2K3,CHUK,MAP3K3,MAP2K5
Pancreatic Adenocarcinoma Signaling	1.25E+00	1.98E-01	TP53,PIK3CA,AKT2,RALA,JAK1,PA2G4,MAPK1,MAPK8,EGF,VEGFC,CCND1,PLD1,VEGFA,PIK3R3,E2F6,AKT1,CDK4,CDKN1A,TGFA,TGFB2,PTGS2,STAT1,NOTCH1
FGF Signaling	1.25E+00	2.16E-01	PTPN6,PIK3CA,AKT2,MAPK1,FGFR1,FGF14,MAPK8,HRAS,PLCG1,CRK,ATF2,FGF1,PIK3R3,FGFR3,AKT1,MAP2K3,RPS6KA5,FGF3,MAPKAPK2
Insulin Receptor Signaling	1.24E+00	2.00E-01	PIK3CA,JAK1,MAPK1,PPP1R3C,HRAS,PPP1CB,INPPL1,CRK,STXBP4,NCK1,EIF4E,MTOR,AKT1,RPS6KB2,STX4,GSK3B,PPP1R14C,AKT2,MAPK8,PPP1R14A,PIK3R3,RRAS2,CBL,FOXO1,IRS1,PPP1R12A,PRKCH,RAPGEF1
Role of NANOG in Mammalian Embryonic Stem Cell Pluripotency	1.22E+00	2.11E-01	TP53,PIK3CA,AKT2,JAK1,MAPK1,HRAS,SMAD5,FZD1,WNT9A,WNT8B,APC,SOX2,LIFR,PIK3R3,BMPR1B,WNT7A,AKT1,RIF1,RRAS2,FZD3,FZD6,GATA6,GSK3B,SMAD1
Semaphorin Signaling in Neurons	1.21E+00	2.50E-01	ITGB1,PAK2,MAPK1,DPYSL3,RHOC,LIMK1,ROCK1,SEMA3A,RND3,PAK3,PLXNB1,RHOU,PAK7

YAC 13 month D1 IPA Analysis

Ingenuity Canonical Pathways	-log(p-value)	Ratio	Molecules
Leukocyte Extravasation Signaling	2.96E+00	3.09E-02	WIPF1,CLDN23,ACTN2,VAV3,RAPGEF3,DLC1
Integrin Signaling	2.15E+00	2.50E-02	WIPF1,RND3,ARF3,ACTN2,TSPAN6
G Protein Signaling Mediated by Tubby	1.74E+00	4.88E-02	GNG5,GNG4
Serotonin Receptor Signaling	1.74E+00	4.35E-02	MAOB,DDC
Phenylalanine Metabolism	1.67E+00	1.83E-02	MAOB,DDC
Notch Signaling	1.62E+00	4.65E-02	APH1B,JAG1
Axonal Guidance Signaling	1.56E+00	1.49E-02	NTNG1,WIPF1,BMP2,WNT8B,GNG5,GNG4
Histidine Metabolism	1.36E+00	1.67E-02	MAOB,DDC
Aryl Hydrocarbon Receptor Signaling	1.28E+00	1.95E-02	NR2F1,MGST1,GSTA4
Phospholipase C Signaling	1.26E+00	1.58E-02	RND3,RAPGEF3,GNG5,GNG4
Colorectal Cancer Metastasis Signaling	1.24E+00	1.61E-02	RND3,WNT8B,GNG5,GNG4
Molecular Mechanisms of Cancer	1.23E+00	1.34E-02	APH1B,RND3,BMP2,BID,RAPGEF3
Basal Cell Carcinoma Signaling	1.20E+00	2.94E-02	BMP2,WNT8B
Glutathione Metabolism	1.20E+00	2.04E-02	MGST1,GSTA4

YAC 13 month D2 IPA Analysis

Ingenuity Canonical Pathways	-log(p-value)	Ratio	Molecules
LPS/IL-1 Mediated Inhibition of RXR Function	3.50E+00	2.33E-02	MGST1,JUN,FABP7,HS3ST3A1,ABCA1
IGF-1 Signaling	2.55E+00	3.00E-02	IGFBP4,IGFBP6,JUN
Aryl Hydrocarbon Receptor Signaling	2.09E+00	1.95E-02	NR2F1,MGST1,JUN
GABA Receptor Signaling	2.05E+00	3.64E-02	GABRA5,GABRG1
PPAR Signaling	1.53E+00	2.04E-02	NR2F1,JUN
Corticotropin Releasing Hormone Signaling	1.34E+00	1.47E-02	JUN,CNR1
Relaxin Signaling	1.25E+00	1.34E-02	JUN,PDE10A

YAC 23 month D1 IPA Analysis

Ingenuity Canonical Pathways	-log(p-value)	Ratio	Molecules
Molecular Mechanisms of Cancer	4.36E+00	5.91E-02	PRKDC,TCF4,STK36,TGFBR1,RHOC,BMP2,RALB,FZD1,RASGRF2,CAMK2D, CBL,RND3,SUFU,GNAO1,RHOU,E2F5,TGFB2,PAK7,GNA13,CDKN1B,HIPK2, BRCA1
Semaphorin Signaling in Neurons	3.49E+00	1.35E-01	RND3,DPYSL3,RHOC,RHOU,PAK7,SEMA7A,NRP1
Axonal Guidance Signaling	2.96E+00	4.96E-02	SEMA3E,SLIT3,PLXNC1,STK36,BMP2,UNC5B,FZD1,ABLIM1,GNG5,GNB4, WIPF1,NFAT5,SUFU,GNAO1,PAK7,SEMA4A,GNA13,GNG4,SEMA7A,NRP1
Cardiac Hypertrophy Signaling	2.80E+00	5.76E-02	TGFBR1,RHOC,PLCH2,GNG5,CACNA1A,GNB4,PLCE1,RND3,GNAO1,RHOU, TGFB2,GNA13,GNG4,ADRA1A
ILK Signaling	2.70E+00	6.45E-02	FLNB,PARVA,RND3,PPP2R3A,RHOC,ACTN2,PPAP2B,RHOU,MYH3,RPS6KA4 ,RPS6KA5,DSP
mTOR Signaling	2.58E+00	6.41E-02	MAPKAP1,PLD2,EIF4G2,RND3,PPP2R3A,RHOC,RHOU,RPS6KA4,RPS6KA5, RICTOR
Glycine, Serine and	2.57E+00	4.67E-02	MAOB,PLCE1,CHDH,GLYCTK,PDPR,PLCH2,GATM

Threonine Metabolism			
Phospholipase C Signaling	2.27E+00	5.14E-02	PLD2,HDAC8,RHOC,RALB,PPP1R14A,GNG5,GNB4,NFAT5,PLCE1,RND3,RHOU,GNA13,GNG4
Protein Kinase A Signaling	2.07E+00	4.76E-02	FLNB,HIST1H1C,TGFBR1,PPP1R14A,PLCH2,PDE1A,GNG5,GNB4,NFAT5,PLCE1,CAMK2D,TGFB2,RYR1,GNA13,GNG4
Thrombin Signaling	2.06E+00	5.39E-02	GNB4,PLCE1,CAMK2D,RND3,RHOC,GNAO1,RHOU,GNA13,PLCH2,GNG5,GNG4
Integrin Signaling	2.01E+00	5.50E-02	PARVA,WIPF1,RND3,ITGA9,RHOC,ACTN2,RALB,RHOU,PAK7,LIMS1,TSPAN6
CXCR4 Signaling	1.82E+00	5.39E-02	GNB4,RND3,RHOC,GNAO1,RHOU,PAK7,GNA13,GNG5,GNG4
Aminoacyl-tRNA Biosynthesis	1.74E+00	4.82E-02	WARS2,IARS2,LARS2,HARS2
Growth Hormone Signaling	1.66E+00	7.14E-02	IGFBP3,RPS6KA4,SOCS4,RPS6KA5,ONECUT1
Wnt/Œ≤-catenin Signaling	1.61E+00	5.36E-02	TCF4,TGFBR1,PPP2R3A,GNAO1,TLE3,TGFB2,KREMEN1,FZD1,TCF7L2
IL-1 Signaling	1.55E+00	5.66E-02	GNB4,GNAO1,GNA13,GNG5,GNG4,IL1RAP
Glioblastoma Multiforme Signaling	1.50E+00	4.91E-02	PLCE1,RND3,RHOC,E2F5,RHOU,FZD1,CDKN1B,PLCH2
Cardiac Œ≤-adrenergic Signaling	1.48E+00	4.93E-02	GNB4,PPP2R3A,PPP1R14A,PDE1A,GNG5,GNG4,CACNA1A
Germ Cell-Sertoli Cell Junction Signaling	1.44E+00	5.06E-02	TGFBR1,RND3,RHOC,ACTN2,PPAP2B,RHOU,TGFB2,PAK7
Role of NFAT in Cardiac Hypertrophy	1.39E+00	4.35E-02	GNB4,PLCE1,TGFBR1,CAMK2D,HDAC8,TGFB2,PLCH2,GNG5,GNG4
Valine, Leucine and Isoleucine Biosynthesis	1.38E+00	4.55E-02	IARS2,LARS2
Chondroitin Sulfate Biosynthesis	1.37E+00	5.97E-02	B3GAT1,CSGALNACT1,HS3ST3A1,SULT2B1
Sphingosine-1-phosphate Signaling	1.36E+00	5.36E-02	PLCE1,RND3,RHOC,RHOU,GNA13,PLCH2
Breast Cancer Regulation by Stathmin1	1.35E+00	4.52E-02	GNB4,CAMK2D,PPP2R3A,E2F5,PPP1R14A,GNA13,CDKN1B,GNG5,GNG4
Histidine Metabolism	1.34E+00	3.33E-02	PRPS2,MAOB,METTL1,HARS2
G Protein Signaling Mediated by Tubby	1.30E+00	7.32E-02	GNB4,GNG5,GNG4
Cell Cycle: G1/S Checkpoint Regulation	1.27E+00	6.78E-02	HDAC8,E2F5,TGFB2,CDKN1B
IL-8 Signaling	1.21E+00	4.30E-02	GNB4,PLD2,RND3,RHOC,RHOU,GNA13,GNG5,GNG4

CREB Signaling in Neurons	1.21E+00	4.08E-02	GNB4,PLCE1,CAMK2D,GNAO1,GNA13,PLCH2,GNG5,GNG4

YAC 23 months D2 IPA Analysis

Ingenuity Canonical Pathways	-log(p-value)	Ratio	Molecules
PPARŒ±/RXRŒ± Activation	3.71E+00	7.14E-02	GPD1,SMAD3,PRKAR2A,NR2C2,PLCH2,IKBKG,ACADL,JUN,NFKBIA,ADCY5,SOS1,TGFB2,INSR
CD27 Signaling in Lymphocytes	2.86E+00	1.05E-01	TRAF2,IKBKG,JUN,CASP9,NFKBIA,MAP3K3
Small Cell Lung Cancer Signaling	2.79E+00	7.87E-02	PTK2,NOS1,TRAF2,IKBKG,CASP9,NFKBIA,SIN3A
IGF-1 Signaling	2.76E+00	8.00E-02	PTK2,IGFBP4,JUN,CASP9,SOS1,PRKAR2A,IGFBP5,NEDD4
Role of PKR in Interferon Induction and Antiviral Response	2.57E+00	1.09E-01	FADD,TRAF2,IKBKG,CASP9,NFKBIA
Death Receptor Signaling	2.57E+00	9.38E-02	FADD,TRAF2,IKBKG,CASP9,NFKBIA,XIAP
Induction of Apoptosis by HIV1	2.53E+00	9.23E-02	FADD,TRAF2,IKBKG,CASP9,NFKBIA,XIAP
4-1BB Signaling in T Lymphocytes	2.30E+00	1.18E-01	TRAF2,IKBKG,JUN,NFKBIA
RANK Signaling in Osteoclasts	2.26E+00	7.29E-02	TRAF2,IKBKG,JUN,NFKBIA,GSN,MAP3K3,XIAP
IL-1 Signaling	2.18E+00	6.60E-02	IKBKG,JUN,NFKBIA,ADCY5,PRKAR2A,GNG5,GNG4
April Mediated Signaling	1.92E+00	9.52E-02	TRAF2,IKBKG,JUN,NFKBIA
Role of NFAT in Cardiac Hypertrophy	1.90E+00	4.83E-02	HDAC4,ADCY5,SOS1,PRKAR2A,TGFB2,SLC8A2,ITPR1,PLCH2,GNG5,GNG4
Regulation of IL-2 Expression in Activated and Anergic T Lymphocytes	1.89E+00	6.67E-02	IKBKG,JUN,NFKBIA,SMAD3,SOS1,TGFB2
B Cell Activating Factor Signaling	1.84E+00	9.09E-02	TRAF2,IKBKG,JUN,NFKBIA
Hepatic Cholestasis	1.84E+00	4.79E-02	TRAF2,IKBKG,CYP7B1,JUN,NFKBIA,ADCY5,PRKAR2A,INSR
Molecular	1.79E+00	4.03E-02	SMAD3,PRKAR2A,ARHGEF1,AURKA,XIAP,SIN3A,FADD,PTK2,JUN,CASP9,NFK

Mechanisms of Cancer			BIA,RND3,ADCY5,SOS1,TGFB2
PPAR Signaling	1.72E+00	6.12E-02	TRAF2,IKBKG,JUN,NFKBIA,SOS1,INSR
Œ±-Adrenergic Signaling	1.70E+00	5.66E-02	ADCY5,PRKAR2A,SLC8A2,ITPR1,GNG5,GNG4
Angiopoietin Signaling	1.69E+00	6.76E-02	PTK2,IKBKG,CASP9,NFKBIA,SOS1
SAPK/JNK Signaling	1.64E+00	6.12E-02	FADD,TRAF2,JUN,SOS1,GNG5,MAP3K3
Chronic Myeloid Leukemia Signaling	1.57E+00	5.71E-02	IKBKG,HDAC4,SMAD3,SOS1,TGFB2,SIN3A
Role of RIG1-like Receptors in Antiviral Innate Immunity	1.57E+00	7.69E-02	FADD,TRAF2,IKBKG,NFKBIA
Antiproliferative Role of Somatostatin Receptor 2	1.56E+00	6.41E-02	NOS1,SSTR2,ADCY5,GNG5,GNG4
Protein Kinase A Signaling	1.55E+00	4.13E-02	PPP1R14C,CREM,SMAD3,PRKAR2A,ITPR1,PLCH2,GNG5,PTK2,NFKBIA,ADCY5,TGFB2,GNG4,ANAPC1
GNRH Signaling	1.54E+00	4.86E-02	PTK2,JUN,ADCY5,SOS1,PRKAR2A,ITPR1,MAP3K3
Cholecystokinin/Gastrin-mediated Signaling	1.48E+00	5.77E-02	PTK2,CREM,JUN,RND3,SOS1,ITPR1
Reelin Signaling in Neurons	1.45E+00	6.41E-02	YES1,HCK,ARHGEF1,LRP8,DCX
Renin-Angiotensin Signaling	1.41E+00	5.00E-02	PTK2,JUN,ADCY5,SOS1,PRKAR2A,ITPR1
Pancreatic Adenocarcinoma Signaling	1.41E+00	5.17E-02	CASP9,SMAD3,TGFB2,BRCA2,HBEGF,SIN3A
Thrombin Signaling	1.40E+00	4.41E-02	PTK2,RND3,ADCY5,SOS1,ARHGEF1,ITPR1,PLCH2,GNG5,GNG4
Type I Diabetes Mellitus Signaling	1.39E+00	5.22E-02	FADD,TRAF2,IKBKG,CASP9,NFKBIA,ICA1
Lymphotoxin Œ≤ Receptor Signaling	1.38E+00	6.56E-02	TRAF2,IKBKG,CASP9,NFKBIA
Glioma Invasiveness Signaling	1.38E+00	7.02E-02	PTK2,TIMP3,RND3,CD44
Cardiac Hypertrophy Signaling	1.36E+00	4.12E-02	JUN,RND3,ADCY5,SOS1,PRKAR2A,TGFB2,PLCH2,GNG5,GNG4,MAP3K3
G Protein Signaling Mediated by Tubby	1.35E+00	7.32E-02	INSR,GNG5,GNG4
Cell Cycle: G1/S Checkpoint Regulation	1.33E+00	6.78E-02	HDAC4,SMAD3,TGFB2,SIN3A

Colorectal Cancer Metastasis Signaling	1.27E+00	4.02E-02	JUN,CASP9,RND3,ADCY5,SMAD3,SOS1,PRKAR2A,TGFB2,GNG5,GNG4
Methane Metabolism	1.25E+00	3.03E-02	CYP7B1,SHMT1
CD40 Signaling	1.24E+00	5.97E-02	TRAF2,IKBKG,JUN,NFKBIA
Calcium Signaling	1.23E+00	3.90E-02	TNNT1,HDAC4,TPM3,PRKAR2A,TPM2,SLC8A2,TRPC6,ITPR1
IL-6 Signaling	1.22E+00	5.38E-02	TRAF2,IKBKG,JUN,NFKBIA,SOS1
GŒ±12/13 Signaling	1.20E+00	4.80E-02	PTK2,CDH2,IKBKG,JUN,NFKBIA,ARHGEF1

Appendix III: qPCR

Confirmed Genes

Date	Model	Cell Type	Age	Method	Sample size?	Gene	Array Fold Change	qPCR Fold Change	Confirmed?	Reference Gene
4/14/09	R6-2	D2	14 weeks	Pooled	n=1	Ppap2b	0.769230769	0.89	Y	Map2
4/14/09	R6-2	D2	14 weeks	Pooled	n=1	SGPL1	1.1	4.2	Y	Map2
4/14/09	R6-2	D2	14 weeks	Pooled	n=1	Sulf2	1.05	2.4	Y	Map2
4/17/09	R6-2	D2	14 weeks	Pooled	n=1	Smpd1	1.082159664	1.399729693	Y	Map2
4/17/09	R6-2	D2	14 weeks	Pooled	n=1	Ugt8a	1.166292442	0.935350022	Y	Map2
4/17/09	R6-2	D2	14 weeks	Pooled	n=1	Ddost	0.571428571	0.413476431	Y	Map2
4/17/09	R6-2	D2	14 weeks	Pooled	n=1	Rpn2	0.80705191	0.710149782	Y	Map2
5/7/09	R6-2	D2	14 weeks	Pooled	n=1	Actb	0.806451613	0.623206672	Y	Atp5b
5/7/09	R6-2	D2	14 weeks	Pooled	n=1	Ubc	0.555555556	0.127560229	Y	Atp5b
5/7/09	R6-2	D2	14 weeks	Pooled	n=1	Atp5b	0.980392157	1	Y	Atp5b
5/7/09	R6-2	D2	14 weeks	Pooled	n=1	Acin1	1.7	1.717002234	Y	Atp5b
5/7/09	R6-2	D2	14 weeks	Pooled	n=1	Casp3	2.24	1.805956947	Y	Atp5b
5/7/09	R6-2	D2	14 weeks	Pooled	n=1	Garnl1	1.2	1.794057442	Y	Atp5b
5/7/09	R6-2	D2	14 weeks	Pooled	n=1	Penk1	0.476190476	0.213401381	Y	Atp5b
5/11/09	R6-2	D1	4 weeks	Pooled	n=2	SGPL1 (20ng)	1.2	3.548383843	Y	Eif4a2/Atp5b
5/11/09	R6-2	D1	4 weeks	Pooled	n=2	Ugt8	1.08	1.199675068	Y	Eif4a2/Atp5b
5/11/09	R6-2	D1	4 weeks	Pooled	n=2	Ddost	1.14	2.416403414	Y	Eif4a2/Atp5b
5/11/09	R6-2	D1	4	Pooled	n=2	Rpn1	1.2	1.304021883	Y	Eif4a2/Atp5b

			weeks 4							
5/11/09	R6-2	D1	weeks 4	Pooled	n=2	Rpn2	1.2	1.214125941	Y	Eif4a2/Atp5b
5/11/09	R6-2	D1	weeks 4	Pooled	n=2	TUSC3	1.18	1.230570088	Y	Eif4a2/Atp5b
5/11/09	R6-2	D1	weeks 4	Pooled	n=2	CHUK	0.917431193	0.589830193	Y	Eif4a2/Atp5b
5/12/09	R6-2	D1	weeks 4	Pooled	n=2	Acin1	0.925925926	0.766674054	Y	Eif4a2/Atp5b
5/12/09	R6-2	D1	weeks 4	Pooled	n=2	CyclinD1	0.925925926	0.692784598	Y	Eif4a2/Atp5b
5/12/09	R6-2	D1	weeks 4	Pooled	n=2	Garnl1	1	0.947672686	Y	Eif4a2/Atp5b
5/12/09	R6-2	D1	weeks 4	Pooled	n=2	Gsn	1.08	1.450764664	Y	Eif4a2/Atp5b
5/12/09	R6-2	D1	weeks 4	Pooled	n=2	Aplp2	1.2	1.277988861	Y	Eif4a2/Atp5b
5/11/09	R6-2	D2	weeks 4	Pooled	n=1	SGPL1 (20ng)	1.2	4.152241957	Y	Eif4a2/Atp5b
5/11/09	R6-2	D2	weeks 4	Pooled	n=1	Ugt8	1.4	1.704230545	Y	Eif4a2/Atp5b
5/11/09	R6-2	D2	weeks 4	Pooled	n=1	TUSC3	1.3	1.218353693	Y	Eif4a2/Atp5b
5/11/09	R6-2	D2	weeks 4	Pooled	n=1	PPARalpha	1.2	4.024697949	Y	Eif4a2/Atp5b
5/11/09	R6-2	D2	weeks 4	Pooled	n=1	CHUK	1.3	2.106307782	Y	Eif4a2/Atp5b
5/12/09	R6-2	D2	weeks 4	Pooled	n=2	Acin1	0.769230769	0.639953167	Y	Eif4a2/Atp5b
5/12/09	R6-2	D2	weeks 4	Pooled	n=2	CyclinD1	1	1.178844956	Y	Eif4a2/Atp5b
5/12/09	R6-2	D2	weeks 4	Pooled	n=2	Garnl1	1	1.586486489	Y	Eif4a2/Atp5b
5/12/09	R6-2	D2	weeks 4	Pooled	n=2	PPARGC1alpha	1	0.870973503	Y	Eif4a2/Atp5b
5/12/09	R6-2	D2	weeks 4	Pooled	n=2	Aplp2	1.07	1.064202158	Y	Eif4a2/Atp5b
5/12/09	R6-2	D2	weeks 4	Pooled	n=2	Hnrnpu	1	1.099359307	Y	Eif4a2/Atp5b
5/12/09	R6-2	D1	weeks	Pooled	n=2	Ubc	1.2	5.880303971	Y	Eif4a2/Atp5b

5/8/09	R6-2	D1	4 weeks	Pooled	n=2	SGPL1		1.16	3.715273471	Y	Eif4a2/Atp5b
5/8/09	R6-2	D1	4 weeks	Pooled	n=2	Akt2		1	1.167330258	Y	Eif4a2/Atp5b
5/8/09	R6-2	D1	4 weeks	Pooled	n=2	GBA		1.1	2.391942829	Y	Eif4a2/Atp5b
5/8/09	R6-2	D1	4 weeks	Pooled	n=2	SMPD1		1.1	1.501846543	Y	Eif4a2/Atp5b
5/8/09	R6-2	D2	4 weeks	Pooled	n=1	SGPL1		1.2	5.114830301	Y	Eif4a2/Atp5b
5/8/09	R6-2	D2	4 weeks	Pooled	n=1	SMPD1		1.27	1.078988789	Y	Eif4a2/Atp5b
12/3/09	R6-2	D1	4 weeks	Single	n=4	Sphk1		1	#DIV/0!	Y	Eif4a2
12/3/09	R6-2	D2	4 weeks	Single	n=4	Sphk1		1.1	#DIV/0!	Y	Eif4a2
2/26/10	YAC128	D1	13 months	Single	n=3	Sphk2		1	1.349454344	Y	Eif4a2
2/26/10	YAC128	D2	13 months	Single	n=3	Sphk1	0.943396226		#DIV/0!	Y	Eif4a2
11/11/09	YAC128	D1	13 months	Single	n=3	IGFBP4	0.384615385		0.384592669	Y	Eif4a2
11/11/09	YAC128	D1	13 months	Single	n=3	TTR		1.06	1.152349825	Y	Eif4a2
11/11/09	YAC128	D2	13 months	Single	n=3	IGFBP4	0.37037037		0.236194073	Y	Eif4a2
11/11/09	YAC128	D2	13 months	Single	n=3	TTR	0.666666667		0.303815806	Y	Eif4a2
8/30/10	R6-2	D2	4.5 weeks	Single	n=3 or 4	PENK1	0.980392157		0.935672084	Y	Eif4a2
8/30/10	R6-2	D2	4.5 weeks	Single	n=3 or 4	Sphk1 "41"		1.08	#DIV/0!	Y	Eif4a2
8/30/10	R6-2	D2	4.5 weeks	Single	n=3 or 4	Sphk2 Mm00445020_m1		1.3	2.068550363	Y	Eif4a2
8/30/10	R6-2	D2	4.5 weeks	Single	n=3 or 4	Sphk2 Mm00445021_m1		1.3	2.55828979	Y	Eif4a2
11/15/10	YAC128	D1	13 months	Single	n=4	Rprm		2.86	16.58424868	Y	Eif4a2
11/15/10	YAC128	D1	13 months	Single	n=4	Igfbp4	0.333333333		0.410214767	Y	Eif4a2
11/15/10	YAC128	D1	13	Single	n=4	Sox11		1.3	4.420514111	Y	Eif4a2

			months 13							
11/15/10	YAC128	D1	months 13	Single	n=4	Mprl13	1.15	1.098504541	Y	Eif4a2
11/15/10	YAC128	D1	months 13	Single	n=4	Pcdh20	2.1	11.33039564	Y	Eif4a2
11/15/10	YAC128	D1	months 13	Single	n=4	Pkp2	0.344827586	0.345732947	Y	Eif4a2
11/15/10	YAC128	D1	months 13	Single	n=4	Ppp1r9a	0.588235294	0.557679251	Y	Eif4a2
11/15/10	YAC128	D1	months 13	Single	n=4	Actn2	0.571428571	0.402287714	Y	Eif4a2
11/15/10	YAC128	D1	months 13	Single	n=4	Mapkbp1	0.952380952	0.772060379	Y	Eif4a2
11/15/10	YAC128	D1	months 13	Single	n=4	Ntrk3	0.833333333	0.840539972	Y	Eif4a2
11/15/10	YAC128	D1	months 13	Single	n=4	Igfbp5	0.909090909	0.944631576	Y	Eif4a2
11/14/10	YAC128	D2	months 13	Single	n=4	Tmem183a	1.08	1.118417753	Y	Eif4a2
11/14/10	YAC128	D2	months 13	Single	n=4	Pea15a	0.8	0.861685463	Y	Eif4a2
11/14/10	YAC128	D2	months 13	Single	n=4	Rprm	1.4	1.735154647	Y	Eif4a2
11/14/10	YAC128	D2	months 13	Single	n=4	B3gat1	1.1	1.459853991	Y	Eif4a2
11/14/10	YAC128	D2	months 13	Single	n=4	Thtpa	0.996412914	0.91093704	Y	Eif4a2
11/14/10	YAC128	D2	months 13	Single	n=4	Agfg2	0.854700855	0.954266743	Y	Eif4a2
11/14/10	YAC128	D2	months 13	Single	n=4	Igfbp4	0.35971223	0.266217303	Y	Eif4a2
11/14/10	YAC128	D2	months 13	Single	n=4	Sox11	1.3	3.73540995	Y	Eif4a2
11/14/10	YAC128	D2	months 13	Single	n=4	Bcl11a	1.15	1.011950578	Y	Eif4a2
11/14/10	YAC128	D2	months 13	Single	n=4	Mgst1	2.2	1.32267245	Y	Eif4a2
11/14/10	YAC128	D2	months 13	Single	n=4	Jun	0.454545455	0.352470499	Y	Eif4a2
11/14/10	YAC128	D2	months	Single	n=4	Pkp2	0.588235294	0.018121244	Y	Eif4a2

11/14/10	YAC128	D2	13 months	Single	n=4	WT1	0.980392157	#DIV/0!	Y	Eif4a2
11/14/10	YAC128	D2	13 months	Single	n=4	Ppp1r9a	0.740740741	0.595880077	Y	Eif4a2
11/14/10	YAC128	D2	13 months	Single	n=4	Actn2	0.714285714	0.557737011	Y	Eif4a2
11/14/10	YAC128	D2	13 months	Single	n=4	Mapkbp1	0.925925926	0.647535301	Y	Eif4a2
11/14/10	YAC128	D2	13 months	Single	n=4	Igfbp5	1.08	3.832218754	Y	Eif4a2

qPCR: Unconfirmed Genes

Date	Model	Cell Type	Age	Method	Sample size?	Gene	Array Fold Change	qPCR Fold Change	Confirmed?	Reference Gene
4/14/09	R6-2	D2	14 weeks	Pooled	n=1	GBA	1.07	0.670216217	N	Map2
4/17/09	R6-2	D2	14 weeks	Pooled	n=1	Rpn1	0.887519484	1.103251149	N	Map2
4/17/09	R6-2	D2	14 weeks	Pooled	n=1	Tusc3	1.106960555	0.837248766	N	Map2
5/7/09	R6-2	D2	14 weeks	Pooled	n=1	Eif4a	0.970873786	1.116182552	N	Atp5b
5/7/09	R6-2	D2	14 weeks	Pooled	n=1	CyclinD1	Var	3.441397602	N	Atp5b
5/7/09	R6-2	D2	14 weeks	Pooled	n=1	Gsn	0.666666667	1.022378687	N	Atp5b
5/7/09	R6-2	D2	14 weeks	Pooled	n=1	PPARGC1alpha	1.5	0.64015278	N	Atp5b
5/11/09	R6-2	D1	4 weeks	Pooled	n=2	PPARalpha	0.980392157	152.5044685	N	Eif4a2/Atp5b
5/11/09	R6-2	D1	4 weeks	Pooled	n=2	CASP3	0.952380952	7.486508046	N	Eif4a2/Atp5b
5/12/09	R6-2	D1	4 weeks	Pooled	n=2	PPARGC1alpha	0.980392157	1.330167347	N	Eif4a2/Atp5b
5/12/09	R6-2	D1	4 weeks	Pooled	n=2	Calpain2	0.862068966	1.568453775	N	Eif4a2/Atp5b
5/12/09	R6-2	D1	4 weeks	Pooled	n=2	Hnrnpu	0.980392157	1.358907623	N	Eif4a2/Atp5b
5/12/09	R6-2	D1	4 weeks	Pooled	n=2	Ubc	1	36.2454797	N	Eif4a2/Atp5b
5/11/09	R6-2	D2	4 weeks	Pooled	n=1	Ddost	1.3	0.830498671	N	Eif4a2/Atp5b
5/11/09	R6-2	D2	4 weeks	Pooled	n=1	Rpn1	1.5	0.872429231	N	Eif4a2/Atp5b
5/11/09	R6-2	D2	4 weeks	Pooled	n=1	Rpn2	1.3	0.293014358	N	Eif4a2/Atp5b
5/11/09	R6-2	D2	4 weeks	Pooled	n=1	CASP3	1	0.232427111	N	Eif4a2/Atp5b
5/12/09	R6-2	D2	4 weeks	Pooled	n=2	Gsn	1.4	0.491110725	N	Eif4a2/Atp5b
5/12/09	R6-2	D2	4	Pooled	n=2	Calpain2	1.07	0.86241907	N	Eif4a2/Atp5b

			weeks 4							
5/8/09	R6-2	D1	weeks 4	Pooled	n=2	SULF2	1	0.606060945	N	Eif4a2/Atp5b
5/8/09	R6-2	D1	weeks 4	Pooled	n=2	PPAP2b	1.2	0.774489874	N	Eif4a2/Atp5b
5/8/09	R6-2	D1	weeks 4	Pooled	n=2	Penk1	0.909090909	1.03065655	N	Eif4a2/Atp5b
5/8/09	R6-2	D2	weeks 4	Pooled	n=1	SULF2	1.2	0.47270028	N	Eif4a2/Atp5b
5/8/09	R6-2	D2	weeks 4	Pooled	n=1	PPAP2b	1.25	0.351235452	N	Eif4a2/Atp5b
5/8/09	R6-2	D2	weeks 4	Pooled	n=1	Akt2	1	0.670351243	N	Eif4a2/Atp5b
5/8/09	R6-2	D2	weeks 4	Pooled	n=1	Penk1	1.2	0.911081409	N	Eif4a2/Atp5b
5/8/09	R6-2	D2	weeks 4	Pooled	n=1	Htt		#DIV/0!	N	Eif4a2/Atp5b
5/8/09	R6-2	D2	weeks 4	Pooled	n=1	GBA	1.2	0.291528559	N	Eif4a2/Atp5b
12/3/09	R6-2	D1	weeks 4	Single	n=4	SGPL1	1	50.73284812	N	Eif4a2
12/3/09	R6-2	D1	weeks 4	Single	n=4	Sphk2	1.3	0.448867505	N	Eif4a2
12/3/09	R6-2	D2	weeks 4	Single	n=4	SGPL1	1	64.04803093	N	Eif4a2
12/3/09	R6-2	D2	weeks 4	Single	n=4	Sphk2	1.15	0.029226435	N	Eif4a2
2/26/10	YAC128	D1	months 13	Single	n=3	Sphk1	1.01	#DIV/0!	N	Eif4a2
2/26/10	YAC128	D2	months 13	Single	n=3	SGPL1	1	2.44701792	N	Eif4a2
2/26/10	YAC128	D2	months 13	Single	n=3	Sphk2	1.01	0.619613794	N	Eif4a2
2/26/10	YAC128	D2	months 13	Single	n=3	SGPL1	1.07	0.490449056	N	Eif4a2
11/11/09	YAC128	D1	months 13	Single	n=3	SGPL1	1	0.202129435	N	Eif4a2
11/11/09	YAC128	D2	months 13	Single	n=3	SGPL1	1	1.564710131	N	Eif4a2
8/30/10	R6-2	D2	4.5 weeks	Single	n=3 or 4	SGPL1 Mm1149898_m1	1	0.64569466	N	Eif4a2

11/15/10	YAC128	D1	13 months	Single	n=4	Tmem183a	1.1	0.934857849	N	Eif4a2
11/15/10	YAC128	D1	13 months	Single	n=4	Pea15a	1.05	0.838178933	N	Eif4a2
11/15/10	YAC128	D1	13 months	Single	n=4	B3gat1	1.03	0.894291457	N	Eif4a2
11/15/10	YAC128	D1	13 months	Single	n=4	Thtpa	1.06	0.546563333	N	Eif4a2
11/15/10	YAC128	D1	13 months	Single	n=4	Agfg2	0.869565217	1.291687206	N	Eif4a2
11/15/10	YAC128	D1	13 months	Single	n=4	Gpr56	0.952380952	4.279516569	N	Eif4a2
11/15/10	YAC128	D1	13 months	Single	n=4	Bcl11a	1.2	0.815485521	N	Eif4a2
11/15/10	YAC128	D1	13 months	Single	n=4	Mrpl22	1.1	0.940328935	N	Eif4a2
11/15/10	YAC128	D1	13 months	Single	n=4	hexb	1.2	0.734682933	N	Eif4a2
11/15/10	YAC128	D1	13 months	Single	n=4	Spata5	(up 1.7 in one probe, down 1.7 in another)	0.479906192	N	Eif4a2
11/15/10	YAC128	D1	13 months	Single	n=4	Mgst1	1.5	0.585286943	N	Eif4a2
11/15/10	YAC128	D1	13 months	Single	n=4	Jun	0.769230769	1.62525743	N	Eif4a2
11/15/10	YAC128	D1	13 months	Single	n=4	Lsm10	0.970873786	2.36144879	N	Eif4a2
11/15/10	YAC128	D1	13 months	Single	n=4	Fxc1	1.05	0.862545669	N	Eif4a2
11/15/10	YAC128	D1	13 months	Single	n=4	Mtap1a	0.833333333	1.524723791	N	Eif4a2
11/14/10	YAC128	D2	13 months	Single	n=4	Gpr56	0.991080278	0.130614601	N	Eif4a2
11/14/10	YAC128	D2	13 months	Single	n=4	Mprl13	1.06	0.844212883	N	Eif4a2
11/14/10	YAC128	D2	13 months	Single	n=4	Mrpl22	1.06	0.596827017	N	Eif4a2
11/14/10	YAC128	D2	13 months	Single	n=4	hexb	1.2	0.873986257	N	Eif4a2
11/14/10	YAC128	D2	13	Single	n=4	Spata5	varies	0.441653878	N	Eif4a2

			months 13							
11/14/10	YAC128	D2	months 13	Single	n=4	Lsm10	1.1	0.595337461	N	Eif4a2
11/14/10	YAC128	D2	months 13	Single	n=4	Ntrk3	1.05	0.684477805	N	Eif4a2
11/14/10	YAC128	D2	months 13	Single	n=4	Fxc1	1.06	0.970738029	N	Eif4a2
11/14/10	YAC128	D2	months 13	Single	n=4	Mtap1a	1.01	0.629813535	N	Eif4a2

Works Cited

Albin, R. L., A. Reiner, et al. (1992). "Preferential loss of striato-external pallidal projection neurons in presymptomatic Huntington's disease." Ann Neurol **31**(4): 425-30.

Alvarez, S. E., K. B. Harikumar, et al. "Sphingosine-1-phosphate is a missing cofactor for the E3 ubiquitin ligase TRAF2." Nature **465**(7301): 1084-8.

Andreassen, O. A., A. Dedeoglu, et al. (2002). "Huntington's disease of the endocrine pancreas: insulin deficiency and diabetes mellitus due to impaired insulin gene expression." Neurobiol Dis **11**(3): 410-24.

Bae, B. I., H. Xu, et al. (2005). "p53 mediates cellular dysfunction and behavioral abnormalities in Huntington's disease." Neuron **47**(1): 29-41.

Bates, G., P. S. Harper, et al. (2002). Huntington's disease. Oxford ; New York, Oxford University Press.

Bateup, H. S., P. Svenningsson, et al. (2008). "Cell type-specific regulation of DARPP-32 phosphorylation by psychostimulant and antipsychotic drugs." Nat Neurosci **11**(8): 932-9.

Becanovic, K., M. A. Pouladi, et al. "Transcriptional changes in Huntington disease identified using genome-wide expression profiling and cross-platform analysis." Hum Mol Genet **19**(8): 1438-52.

Benn, C. L., C. Landles, et al. (2005). "Contribution of nuclear and extranuclear polyQ to neurological phenotypes in mouse models of Huntington's disease." Hum Mol Genet **14**(20): 3065-78.

Benn, C. L., E. J. Slow, et al. (2007). "Glutamate receptor abnormalities in the YAC128 transgenic mouse model of Huntington's disease." Neuroscience **147**(2): 354-72.

Benn, C. L., T. Sun, et al. (2008). "Huntingtin modulates transcription, occupies gene promoters in vivo, and binds directly to DNA in a polyglutamine-dependent manner." J Neurosci **28**(42): 10720-33.

Bibb, J. A., Z. Yan, et al. (2000). "Severe deficiencies in dopamine signaling in presymptomatic Huntington's disease mice." Proc Natl Acad Sci U S A **97**(12): 6809-14.

Cahoy, J. D., B. Emery, et al. (2008). "A transcriptome database for astrocytes, neurons, and oligodendrocytes: a new resource for understanding brain development and function." J Neurosci **28**(1): 264-78.

Cattaneo, E. and L. Conti (1998). "Generation and characterization of embryonic striatal conditionally

immortalized ST14A cells." J Neurosci Res **53**(2): 223-34.
Cepeda, C., R. S. Hurst, et al. (2003). "Transient and progressive electrophysiological alterations in the corticostriatal pathway in a mouse model of Huntington's disease." J Neurosci **23**(3): 961-9.
Cha, J. H. (2000). "Transcriptional dysregulation in Huntington's disease." Trends Neurosci **23**(9): 387-92.
Cha, J. H. (2007). "Transcriptional signatures in Huntington's disease." Prog Neurobiol **83**(4): 228-48.
Chan, E. Y., R. Luthi-Carter, et al. (2002). "Increased huntingtin protein length reduces the number of polyglutamine-induced gene expression changes in mouse models of Huntington's disease." Hum Mol Genet **11**(17): 1939-51.
Chen, W. V., J. Delrow, et al. (2004). "Identification and validation of PDGF transcriptional targets by microarray-coupled gene-trap mutagenesis." Nat Genet **36**(3): 304-12.
Cohen-Cory, S. and S. E. Fraser (1995). "Effects of brain-derived neurotrophic factor on optic axon branching and remodelling in vivo." Nature **378**(6553): 192-6.
Coyle, K. and R. Schwarcz (1976). "Lesions of striatal neurons with kainic acid provides a model for Huntington's chorea." Nature **263**: 244-246
Crabbe, J. C., D. Wahlsten, et al. (1999). "Genetics of mouse behavior: interactions with laboratory environment." Science **284**(5420): 1670-2.
Crabbe, T., M. Donmall, et al. (1999). "Validation of the University of Manchester Drug Misuse Database." J Epidemiol Community Health **53**(3): 159-64.
Crawley, J. N. (2000). What's wrong with my mouse? : behavioral phenotyping of transgenic and knockout mice. New York, Wiley-Liss.
Cui, L., H. Jeong, et al. (2006). "Transcriptional repression of PGC-1alpha by mutant huntingtin leads to mitochondrial dysfunction and neurodegeneration." Cell **127**(1): 59-69.
Davies, S. W., M. Turmaine, et al. (1997). "Formation of neuronal intranuclear inclusions underlies the neurological dysfunction in mice transgenic for the HD mutation." Cell **90**(3): 537-48.
Deyts, C., B. Galan-Rodriguez, et al. (2009). "Dopamine D2 receptor stimulation potentiates PolyQ-Huntingtin-induced mouse striatal neuron dysfunctions via Rho/ROCK-II activation." PLoS One **4**(12): e8287.
DiFiglia, M., E. Sapp, et al. (1997). "Aggregation of huntingtin in neuronal intranuclear inclusions and

dystrophic neurites in brain." Science **277**(5334): 1990-3.
Dragatsis, I., D. Goldowitz, et al. (2009). "CAG repeat lengths > or =335 attenuate the phenotype in the R6/2 Huntington's disease transgenic mouse." Neurobiol Dis **33**(3): 315-30.
Dragileva, E., A. Hendricks, et al. (2009). "Intergenerational and striatal CAG repeat instability in Huntington's disease knock-in mice involve different DNA repair genes." Neurobiol Dis **33**(1): 37-47.
Edsall, L. C., G. G. Pirianov, et al. (1997). "Involvement of sphingosine 1-phosphate in nerve growth factor-mediated neuronal survival and differentiation." J Neurosci **17**(18): 6952-60.
Ehrlich, M. E., L. Conti, et al. (2001). "ST14A cells have properties of a medium-size spiny neuron." Exp Neurol **167**(2): 215-26.
Enokido, Y., T. Tamura, et al. "Mutant huntingtin impairs Ku70-mediated DNA repair." J Cell Biol **189**(3): 425-43.
Farrer, L. A. (1985). "Diabetes mellitus in Huntington disease." Clin Genet **27**(1): 62-7.
Ferrante, R. J., J. K. Kubilus, et al. (2003). "Histone deacetylase inhibition by sodium butyrate chemotherapy ameliorates the neurodegenerative phenotype in Huntington's disease mice." J Neurosci **23**(28): 9418-27.
Frederick, J. P., D. Mattiske, et al. (2005). "An essential role for an inositol polyphosphate multikinase, Ipk2, in mouse embryogenesis and second messenger production." Proc Natl Acad Sci U S A **102**(24): 8454-9.
Frey, U. H., H. S. Bachmann, et al. (2008). "PCR-amplification of GC-rich regions: 'slowdown PCR'." Nat Protoc **3**(8): 1312-7.
Fuller, M. "Sphingolipids: the nexus between Gaucher disease and insulin resistance." Lipids Health Dis **9**: 113.
Gatchel, J. R. and H. Y. Zoghbi (2005). "Diseases of unstable repeat expansion: mechanisms and common principles." Nat Rev Genet **6**(10): 743-55.
Gerfen, CR. (1992). "The neostriatal mosaic: multiple levels of compartmental organization." Trends Neurosci **15**(4): 133-9.
Gong, S., C. Zheng, et al. (2003). "A gene expression atlas of the central nervous system based on bacterial artificial chromosomes." Nature **425**(6961): 917-25.
Gray, M., D. I. Shirasaki, et al. (2008). "Full-length human mutant huntingtin with a stable polyglutamine

repeat can elicit progressive and selective neuropathogenesis in BACHD mice." J Neurosci **28**(24): 6182-95.

Group, H. s. D. C. R. (1993). "A novel gene containing a trinucleotide repeat that is expanded and unstable on Huntington's disease chromosomes. The Huntington's Disease Collaborative Research Group." Cell **72**(6): 971-83.

Gusella, J. F., N. S. Wexler, et al. (1983). "A polymorphic DNA marker genetically linked to Huntington's disease." Nature **306**(5940): 234-8.

Gutekunst, C. A., S. H. Li, et al. (1999). "Nuclear and neuropil aggregates in Huntington's disease: relationship to neuropathology." J Neurosci **19**(7): 2522-34.

Hait, N. C., J. Allegood, et al. (2009). "Regulation of histone acetylation in the nucleus by sphingosine-1-phosphate." Science **325**(5945): 1254-7.

Han, I., Y. You, et al. (2010) "Differential vulnerability of neurons in Huntington's disease: the role of cell type-specific features." J Neurochem **113**(5): 1073-91.

Han, S., M. A. Lone, et al. "Orm1 and Orm2 are conserved endoplasmic reticulum membrane proteins regulating lipid homeostasis and protein quality control." Proc Natl Acad Sci U S A **107**(13): 5851-6.

Hannun, Y. A. and L. M. Obeid (2008). "Principles of bioactive lipid signalling: lessons from sphingolipids." Nat Rev Mol Cell Biol **9**(2): 139-50.

Hebb, A. L., H. A. Robertson, et al. (2004). "Striatal phosphodiesterase mRNA and protein levels are reduced in Huntington's disease transgenic mice prior to the onset of motor symptoms." Neuroscience **123**(4): 967-81.

Heiman, M., A. Schaefer, et al. (2008). "A translational profiling approach for the molecular characterization of CNS cell types." Cell **135**(4): 738-48.

Hodges, A., A. D. Strand, et al. (2006). "Regional and cellular gene expression changes in human Huntington's disease brain." Hum Mol Genet **15**(6): 965-77.

Holschneider, D. P., J. Yang, et al. (2007). "Reorganization of functional brain maps after exercise training: Importance of cerebellar-thalamic-cortical pathway." Brain Res **1184**: 96-107.

Hu, H., E. A. McCaw, et al. (2004). "Mutant huntingtin affects the rate of transcription of striatum-specific isoforms of phosphodiesterase 10A." Eur J Neurosci **20**(12): 3351-63.

Humbert, S., E. A. Bryson, et al. (2002). "The IGF-1/Akt pathway is neuroprotective in Huntington's disease and

involves Huntingtin phosphorylation by Akt." Dev Cell **2**(6): 831-7.
Jeanneteau, F., K. Deinhardt, et al. (2010). "The MAP kinase phosphatase MKP-1 regulates BDNF-induced axon branching. Nat. Neuroscience 13**(11):**1373-9
Kovtun, I. V., Y. Liu, et al. (2007). "OGG1 initiates age-dependent CAG trinucleotide expansion in somatic cells." Nature **447**(7143): 447-52.
Kravitz, A. V., B. S. Freeze, et al. "Regulation of parkinsonian motor behaviours by optogenetic control of basal ganglia circuitry." Nature **466**(7306): 622-6.
Kuhn, A., D. R. Goldstein, et al. (2007). "Mutant huntingtin's effects on striatal gene expression in mice recapitulate changes observed in human Huntington's disease brain and do not differ with mutant huntingtin length or wild-type huntingtin dosage." Hum Mol Genet **16**(15): 1845-61.
Lalonde, R., M. Filali, et al. (1996). "Sensorimotor learning in three cerebellar mutant mice." Neurobiol Learn Mem **65**(2): 113-20.
Lin, L., T. G. Lesnick, et al. (2009). "Axon guidance and synaptic maintenance: preclinical markers for neurodegenerative disease and therapeutics." Trends Neurosci **32**(3): 142-9.
Lobo , M.K., Y. Cui et al. (2006). "FACS-array profiling of striatal projection neuron subtypes in juvenile and adult brains." Nat. Neuroscience. **9**(3):1395-7.
Luthi-Carter, R., A. Strand, et al. (2000). "Decreased expression of striatal signaling genes in a mouse model of Huntington's disease." Hum Mol Genet **9**(9): 1259-71.
Lucke, S and Levakau, B. (2010). "Endothelial Functions of Sphingosine-1-Phosphate." Cellular Physiology and Biochemistry **26:**87-96.
Maceyka, M., S. Milstien, et al. (2007). "Shooting the messenger: oxidative stress regulates sphingosine-1-phosphate." Circ Res **100**(1): 7-9.
Mangiarini, L., K. Sathasivam, et al. (1997). "Instability of highly expanded CAG repeats in mice transgenic for the Huntington's disease mutation." Nat Genet **15**(2): 197-200.
Mangiarini, L., K. Sathasivam, et al. (1996). "Exon 1 of the HD gene with an expanded CAG repeat is sufficient to cause a progressive neurological phenotype in transgenic mice." Cell **87**(3): 493-506.
McGeer, P. L. and E. G. McGeer (1976). "Enzymes associated with the metabolism of catecholamines, acetylcholine and gaba in human controls and patients with

Parkinson's disease and Huntington's chorea." J Neurochem **26**(1): 65-76.
Menalled, L., B. F. El-Khodor, et al. (2009). "Systematic behavioral evaluation of Huntington's disease transgenic and knock-in mouse models." Neurobiol Dis **35**(3): 319-36.
Menalled, L., H. Zanjani, et al. (2000). "Decrease in striatal enkephalin mRNA in mouse models of Huntington's disease." Exp Neurol **162**(2): 328-42.
Meriin, A. B., X. Zhang, et al. (2002). "Huntington toxicity in yeast model depends on polyglutamine aggregation mediated by a prion-like protein Rnq1." J Cell Biol **157**(6): 997-1004.
Milstien, S., D. Gude, et al. (2007). "Sphingosine 1-phosphate in neural signalling and function." Acta Paediatr Suppl **96**(455): 40-3.
Morfini, G. A., M. Burns, et al. (2009). "Axonal transport defects in neurodegenerative diseases." J Neurosci **29**(41): 12776-86.
Morton, A. J., D. Glynn, et al. (2009). "Paradoxical delay in the onset of disease caused by super-long CAG repeat expansions in R6/2 mice." Neurobiol Dis **33**(3): 331-41.
Muchowski, P. J., G. Schaffar, et al. (2000). "Hsp70 and hsp40 chaperones can inhibit self-assembly of polyglutamine proteins into amyloid-like fibrils." Proc Natl Acad Sci U S A **97**(14): 7841-6.
Okada, T., T. Kajimoto, et al. (2009). "Sphingosine kinase/sphingosine 1-phosphate signalling in central nervous system." Cell Signal **21**(1): 7-13.
Olivera, A., T. Kohama, et al. (1999). "Sphingosine kinase expression increases intracellular sphingosine-1-phosphate and promotes cell growth and survival." J Cell Biol **147**(3): 545-58.
Pouladi, M. A., Y. Xie, et al. "Full-length huntingtin levels modulate body weight by influencing insulin-like growth factor 1 expression." Hum Mol Genet **19**(8): 1528-38.
Rauskolb, S., M. Zagrebelsky, et al. "Global deprivation of brain-derived neurotrophic factor in the CNS reveals an area-specific requirement for dendritic growth." J Neurosci **30**(5): 1739-49.
Reiner, A., R. L. Albin, et al. (1988). "Differential loss of striatal projection neurons in Huntington disease." Proc Natl Acad Sci U S A **85**(15): 5733-7.
Reiner A, A. R., Anderson KD, D'Amato C, and Young, A. (1988). "Differential loss of striatal projection neurons in Huntington disease." PNAS **85**: 5733-5737.

Ridley, R. M., C. D. Frith, et al. (1988). "Anticipation in Huntington's disease is inherited through the male line but may originate in the female." J Med Genet **25**(9): 589-95.
Rigamonti, D., J. H. Bauer, et al. (2000). "Wild-type huntingtin protects from apoptosis upstream of caspase-3." J Neurosci **20**(10): 3705-13.
Rosas, H. D., A. K. Liu, et al. (2002). "Regional and progressive thinning of the cortical ribbon in Huntington's disease." Neurology **58**(5): 695-701.
Rosas, H. D. S., David H.; Lee Stephanie Y; Zaleta Alexandra K; Pappu Vasanth, Fischl, Bruce; Greve D, Hevelone N, and Hersch, S. (2008). "Cerebral cortex and the clinical expression of Huntington's disease: complexity and heterogeneity." Brain **131**: 1057-1068.
Rutkowski, D. T. and R. S. Hegde "Regulation of basal cellular physiology by the homeostatic unfolded protein response." J Cell Biol **189**(5): 783-94.
Sapp, E., P. Ge, et al. (1995). "Evidence for a preferential loss of enkephalin immunoreactivity in the external globus pallidus in low grade Huntington's disease using high resolution image analysis." Neuroscience **64**(2): 397-404.
Schaefer, A., D. O'Carroll, et al. (2007). "Cerebellar neurodegeneration in the absence of microRNAs." J Exp Med **204**(7): 1553-8.
Shelbourne, P. F., C. Keller-McGandy, et al. (2007). "Triplet repeat mutation length gains correlate with cell-type specific vulnerability in Huntington disease brain." Hum Mol Genet **16**(10): 1133-42.
Sim-Selley, L. J., P. B. Goforth, et al. (2009). "Sphingosine-1-phosphate receptors mediate neuromodulatory functions in the CNS." J Neurochem **110**(4): 1191-202.
Sipione, S., D. Rigamonti, et al. (2002). "Early transcriptional profiles in huntingtin-inducible striatal cells by microarray analyses." Hum Mol Genet **11**(17): 1953-65.
Slow, E. J., J. van Raamsdonk, et al. (2003). "Selective striatal neuronal loss in a YAC128 mouse model of Huntington disease." Hum Mol Genet **12**(13): 1555-67.
Sonnino, S. and V. Chigorno (2000). "Ganglioside molecular species containing C18- and C20-sphingosine in mammalian nervous tissues and neuronal cell cultures." Biochim Biophys Acta **1469**(2): 63-77.
Starr, P. A., G. A. Kang, et al. (2008). "Pallidal neuronal discharge in Huntington's disease: support for

selective loss of striatal cells originating the indirect pathway." Exp Neurol **211**(1): 227-33.
Steiner H, a. G. C. (1998). "Role of dynorphin and enkephalin in the regulation of striatal output pathways and behavior." Exp Brain Res **123**: 60-76.
Studer, L. (2001). "Culture of substantia nigra neurons." Curr Protoc Neurosci **Chapter 3**: Unit 3 3.
Subramaniam, S., K. M. Sixt, et al. (2009). "Rhes, a striatal specific protein, mediates mutant-huntingtin cytotoxicity." Science **324**(5932): 1327-30.
Swami, M., A. E. Hendricks, et al. (2009). "Somatic expansion of the Huntington's disease CAG repeat in the brain is associated with an earlier age of disease onset." Hum Mol Genet **18**(16): 3039-47.
Tabrizi, S. J., R. I. Scahill, et al. "Biological and clinical changes in premanifest and early stage Huntington's disease in the TRACK-HD study: the 12-month longitudinal analysis." Lancet Neurol **10**(1): 31-42.
Taketo, M., A. C. Schroeder, et al. (1991). "FVB/N: an inbred mouse strain preferable for transgenic analyses." Proc Natl Acad Sci U S A **88**(6): 2065-9.
Tauber, E., L. Miller-Fleming, et al. "Functional gene expression profiling in yeast implicates translational dysfunction in mutant huntingtin toxicity." J Biol Chem.
Thathiah, A., K. Spittaels, et al. (2009). "The orphan G protein-coupled receptor 3 modulates amyloid-beta peptide generation in neurons." Science **323**(5916): 946-51.
Thompson, L. M., C. T. Aiken, et al. (2009). "IKK phosphorylates Huntingtin and targets it for degradation by the proteasome and lysosome." J Cell Biol **187**(7): 1083-99.
Turmaine, M., A. Raza, et al. (2000). "Nonapoptotic neurodegeneration in a transgenic mouse model of Huntington's disease." Proc Natl Acad Sci U S A **97**(14): 8093-7.
Van Raamsdonk, J. M., M. Metzler, et al. (2007). "Phenotypic abnormalities in the YAC128 mouse model of Huntington disease are penetrant on multiple genetic backgrounds and modulated by strain." Neurobiol Dis **26**(1): 189-200.
Van Raamsdonk, J. M., J. Pearson, et al. (2005). "Cognitive dysfunction precedes neuropathology and motor abnormalities in the YAC128 mouse model of Huntington's disease." J Neurosci **25**(16): 4169-80.

Varma, H., R. Cheng, et al. (2007). "Inhibitors of metabolism rescue cell death in Huntington's disease models." Proc Natl Acad Sci U S A **104**(36): 14525-30.

Voisine, C., H. Varma, et al. (2007). "Identification of potential therapeutic drugs for huntington's disease using Caenorhabditis elegans." PLoS ONE **2**(6): e504.

Vonsattel, J.-P., Myers, Richard, Stevens, Thomas, Ferrante Robert J, Bird, Edward, Richardson, Edward (1985). "Neuropathological Classification of Huntington's Disease." Journal of Neuropathology and Experimental Neurology **44**(6): 559-577.

Wang, X., S. Zhu, et al. (2003). "Minocycline inhibits caspase-independent and -dependent mitochondrial cell death pathways in models of Huntington's disease." Proc Natl Acad Sci U S A **100**(18): 10483-7.

Weydt, P., S. M. Soyal, et al. (2009). "The gene coding for PGC-1alpha modifies age at onset in Huntington's Disease." Mol Neurodegener **4**: 3.

Wheeler, V. C., L. A. Lebel, et al. (2003). "Mismatch repair gene Msh2 modifies the timing of early disease in Hdh(Q111) striatum." Hum Mol Genet **12**(3): 273-81.

Willingham, S., T. F. Outeiro, et al. (2003). "Yeast genes that enhance the toxicity of a mutant huntingtin fragment or alpha-synuclein." Science **302**(5651): 1769-72.

Xie, Y., M. R. Hayden, et al. "BDNF overexpression in the forebrain rescues Huntington's disease phenotypes in YAC128 mice." J Neurosci **30**(44): 14708-18.

Zuccato, C., A. Ciammola, et al. (2001). "Loss of huntingtin-mediated BDNF gene transcription in Huntington's disease." Science **293**(5529): 493-8.